UNIVERSITY OF SOUTHAMPTON

FACULTY OF ENGINEERING AND THE ENVIRONMENT
INSTITUTE OF SOUND AND VIBRATION RESEARCH

Nonlinear System Analysis of Local Reflex Control of Locust Hind Limbs

by
Oliver Paul Dewhirst

Thesis for the degree of Doctor of Philosophy

October 2012

UNIVERSITY OF SOUTHAMPTON

ABSTRACT

FACULTY OF ENGINEERING AND THE ENVIRONMENT
INSTITUTE OF SOUND AND VIBRATION RESEARCH

Doctor of Philosophy

NONLINEAR SYSTEM ANALYSIS OF LOCAL REFLEX CONTROL OF LOCUST HIND LIMBS

by Oliver Paul Dewhirst

Nonlinear Volterra type system identification models coupled with a Gaussian White Noise (GWN) stimulation signal provide an experimentally convenient and quick way to investigate the often complex and nonlinear interactions between the mechanical and neural elements of invertebrate reflex limb control systems. Previous steady state analysis has allowed the neurons in such systems to be categorised by their sensitivity to position, velocity or acceleration (system dynamics) and has improved understanding of network function.

These neurons, however, are known to adapt their output amplitude or spike firing rate during repetitive stimulation and this transient response may be more important than the steady state response for reflex limb control. Furthermore, whilst the use of GWN for system identification can be theoretically and experimentally justified, the properties of this signal are very different from those received by the sensory, inter and motor neurons in the neural networks which monitor the position of the locusts leg under natural operating conditions.

The current study provides improvements to the previously used experimental methods, equipment and nonlinear system identification methods. Validation of the models using biologically more realistic stimulation signals has been carried out to determine where they perform well and to identify their limitations. The use of the parsimonious cascade model structure, applied in a quasi stationary fashion coupled with Monte Carlo (MC) simulations, has been shown to provide a useful tool for the characterisation of the dynamics and nonlinear responses of the neuromuscular elements in a locust's reflex limb control system during both transient and steady state response sections. This method been applied to test the null hypothesis that the dynamics and nonlinear responses of the locust's Fast Extensor Tibia (FETi) motor neuron system are the same during transient and steady state sections. It can be concluded that key FETi system dynamics remain relatively unchanged during repetitive stimulation while output amplitude adaptation is occurring. Whilst some evidence of a significant change was found in parts of the system's nonlinear response, the effect was small and probably of little physiological relevance. Analysis using biologically more realistic stimulation reinforces this conclusion.

Contents

List of Figures

List of Tables

List of Abbreviations

AD	Analogue to Digital
AR	autoregressive
BLP	base line power
BMN	baseline measurement noise
BW	block wise
DA	Digital to Analogue
DDE	Down-sampled Differential Evolution
DE	Differential Evolution
DKH	Down-sampled Korenberg Hunter
DLF	Discrete Laguerre Filter
FeCO	Femoral Chordotonal Organ
FETi	Fast Extensor Tibia
FIR	Finite Impulse Response
GWN	Gaussian White Noise
IP	ideal position
IQR	Inter-Quartile Range
IRF	Impulse Response Function
IV	ideal velocity
KH	Korenberg Hunter
LM	Levenberg Marquardt

LMS	Least Mean Squares
LN	Linear Nonlinear
LNL	Linear Nonlinear Linear
LTI	Linear Time Invariant
MC	Monte Carlo
MCA	mean coherent average
MDP	Maximum Deterministic Performance
MMSE	Minimum Mean Square Error
MSE	Mean Square Error
NL	Nonlinear Linear
PlFITi	Posterior Intermediate Flexor Tibiae
RLS	Recursive Least Squares
SETi	Slow Extensor Tibia
SKH	Smoothed Korenberg Hunter
SNR	Signal to Noise ratio
SS	steady state
SSμ	steady state mean
SSCAμ	steady state response coherent average mean
SSM	simulated system model
SSMN	steady state measurement noise
SVD	Singular Value Decomposition
TR	transient
TRCA	transient response coherent average

List of Symbols

$E[\cdot]$	Expected (average) value
G	Wiener operators
J	MMSE cost function
$\boldsymbol{J_{ac}}$	Gradient descent Jacobian
J_{WL}	Number of Wiener Laguerre functions in the decomposition
L_j	Laguerre function
N	Recording sample number
N_{DS}	Deterministic model of FETi
N_h	Number of Volterra kernels
Q	Polynomial order
$\mathbf{S}$	SVD diagonal matrix
T	Number of IRF model parameters
$\mathbf{U}$	Matrix of time delayed input signals
$\mathbf{V}$	SVD orthogonal matrix
c	Wiener Laguerre coefficients of Volterra kernels
c^q	Polynomial coefficients
$\boldsymbol{d_k}$	Gradient descent update factor
$g(\sigma)$	Second linear element of LNL model
$h(\tau)$	IRF
h_0	Zero order Volterra kernel
h_1	First order Volterra kernel
h_2	Second order Volterra kernel

$m()$	Static nonlinearity
$\mathbf{s}$	Singular values
$u(t)$	Input signal
v_0	Zero order residual
$v(t)$	Measurement noise
v_1	First order residual
$x^q(t)$	Polynomial input
$y(t)$	Output signal
$\hat{y}(t)$	Estimated model output
$z(t)$	Measured output
$\Phi_{uu}(\tau)$	Auto correlation function
$\boldsymbol{\epsilon}$	Gradient descent error signal vector
μ_k	Gradient descent step size
ϕ_{uy}	Cross correlation function
σ_v^2	Measurement noise variance
σ_u^2	Input power
θ	Model parameters (MMSE estimation)
$\vartheta_j(t)$	Wiener Laguerre output

Declaration of Authorship

I, Oliver Paul Dewhirst, declare that the thesis entitled 'Nonlinear System Analysis of Local Reflex Control of Locust Hind Limbs' and the work presented in the thesis are both my own, and have been generated by me as the result of my own original research. I confirm that:

- this work was done wholly or mainly while in candidature for a research degree at this University;
- where any part of this thesis has previously been submitted for a degree or any other qualification at this University or any other institution, this has been clearly stated;
- where I have consulted the published work of others, this is always clearly attributed;
- where I have quoted from the work of others, the source is always given. With the exception of such quotations, this thesis is entirely my own work;
- I have acknowledged all main sources of help;
- where the thesis is based on work done by myself jointly with others, I have made clear exactly what was done by others and what I have contributed myself;
- Parts of this work have been published as

1. O.P. Dewhirst, D.M. Simpson, R. Allen and P.L. Newland. Neuromuscular reflex control of limb movement - validating models of the locust's hind leg control system using physiological input signals. In *Proceedings of the 4th International IEEE EMBS Conference on Neural Engineering, Antalya, Turkey*, pages 689-692, 2009.
2. O.P. Dewhirst, D.M. Simpson, N. Angarita, R. Allen and P.L. Newland. Wiener-Hammerstein parameter estimation using differential evolution - application to limb reflex dynamics. In *Proceedings of Biosignals 2010 International Conference on Bio-inspired Systems and Signal Processing, Valencia, Spain*, pages 271-276, 2010.
3. O.P. Dewhirst, N. Angarita-Jaimes, D.M. Simpson, R. Allen and P.L. Newland. The dynamics of locust non-spiking local interneurons - responses to imposed-limb movements. In *Proceedings of Biosignals 2011 International Conference on Bio-inspired Systems and Signal Processing, Rome, Italy*, pages 270-275, 2011.
4. O.P. Dewhirst, N. Angarita-Jaimes, D.M. Simpson, R. Allen, C.D. Maciel and P.L. Newland. Neural adaptation in local reflex control of limb movements. In *Proceedings of*

Biosignals 2012 International Conference on Bio-inspired Systems and Signal Processing, Vilamoura, Algarve, Portugal, pages 398-401, 2012.

5. O.P. Dewhirst, N. Angarita-Jaimes, D.M. Simpson, R. Allen and P.L. Newland. A system identification analysis of neural adaptation dynamics and nonlinear responses in the local reflex control of locust hind limbs. *Journal of Computational Neuroscience*. In Press.

Signed: .....

Date: .....

Acknowledgements

I wish to thank my supervisors Dr David Simpson, Professor Philip Newland and Professor Robert Allen for providing me with support, motivation and, most importantly, inspiration, throughout my PhD. Dr Simpson's help with signal processing and Professor Newland's skills in collecting and interpreting data from the locusts have been invaluable.

I am grateful for all the assistance I have received from the students and staff in the ISVR and the School of Biological Sciences. Many thanks to Mark Hadley, Jens Rolfing, Charmaine Demanuele, Scott Notley, Oliver Bauman and Natalia Angarita-Jaimes for their help and friendship.

I would like to thank Professor Paul White for suggesting the use of Differential Evolution to estimate the parameters of the LNL model.

I wish to give special thanks to John Barrett for his advice and encouragement.

The financial support provided for this project by the Gerald Kerkut Trust, the Life Sciences Interfaces Forum and the ISVR Rayleigh Scholarship is gratefully acknowledged.

My thanks go to my parents for always being there to support, love, help and encourage me - and to do a spot of proof reading.

I especially wish to thank my girlfriend Helga Groll for her support, encouragement and belief in me.

Finally, I dedicate this thesis to my two sons, Joseph and Charlie Dewhirst, the brightest and most wonderful people in my life.

Chapter 1

Introduction

1.1 Motivation

Greater understanding of neuromuscular control of limb movements is a key aim in neuroscience and is vital for optimising the treatment of patients with neuromuscular dysfunction. It may also allow features of such biological systems to be exploited to improve the design of engineering control systems used in robotic applications (bio-inspired design [8]).

Reflexes tune the contraction of muscles that operate around joints to enable locomotion and posture to be adapted to suit changes in the external environment [12]. In vertebrates and invertebrates, sensory receptors in the limb activate sensory neurons which excite interneurons and motor neurons (in the spinal cord in vertebrates) and these activate muscle contraction or relaxation. Reflex arcs bypass the brain and hence allow movement to occur more quickly than when it is under voluntary control.

Invertebrates in general and arthropods in particular (specifically locusts), provide the opportunity to develop new investigative techniques and gain physiological insight into the local reflex control of limbs in systems which are more accessible than their vertebrate counterparts [10, 39, 76] yet share many common operating principles [10, 101]. The system of nerve cells (neurons) which control the hind legs of a locust, for example, is robust, flexible, efficient and fault-tolerant but also relatively simple compared to many vertebrate systems [20]. This successful biological control system enables the locust to produce a wide variety of movements (walking, running, hopping and jumping) and these help it survive in hostile environments [20].

The classical approach for investigating the mechanical, neural and muscular elements of invertebrate reflex limb control systems is to use an ensemble of specific input signals (such as steps or ramps) to analyse the control of a particular movement [46]. These input signals provide a useful tool for probing such systems as they generate responses which are usually easy to interpret and link to limb function. The neural networks that produce and control the reflex movements of invertebrate limbs, whilst relatively simple, still contain many hundreds of neurons, most of which exhibit nonlinear responses. As nonlinear systems do not obey the

principle of superposition [85], complete characterisation of each neuron or network of neurons requires the application of many different input signals which makes this method experimentally time consuming.

The system identification approach, by contrast, fits a mathematical model between an input signal and the measured response of the system. The use of a Gaussian White Noise (GWN) input signal means that the system is simultaneously excited at all frequencies and amplitudes within its operating range [1, 40, 108]. This method, therefore, provides an experimentally convenient and quick way to model the biological system. The goal of this approach is to produce a model which can accurately predict the response of the system to any input, that is mathematically and computationally compact and has parameters that are easy to interpret and link to the function of the system that it represents [87]. Whilst the use of GWN for system identification can be theoretically and experimentally justified [85], the properties of this signal are very different from those normally received by the sensory, inter and motor neurons in the neural networks which monitor the position of the locust's leg under natural operating conditions.

Previous work [54, 98, 117] has successfully applied the system identification approach to model the steady state dynamics (sensitivity to position, velocity or acceleration) and nonlinear responses of invertebrate reflex limb control systems, thereby improving understanding of network function. These studies indicate that neurons typically have a transient response that adapts to a steady state level, but investigation into the transient property has not been reported in previous work [54, 98, 117].

Neuronal adaptation, a decrease in the response of individual or networks of neurons to constant stimulation, is a widespread property of vertebrate and invertebrate nervous systems [102]. Neurons have been found to either change their firing frequency [49] or the amplitude (power) of their synaptic response [44]. It occurs at many stages; in single peripheral sensory neurons [49], in networks of sensory neurons [58] and at central levels, for example, in the human auditory cortex [66]. It has many functions including gain control in sensory cells [16], optimisation of energy consumption [78] and importantly for movement and posture it facilitates stable but reactive limb control [72].

In previous work [54, 98, 117] nonlinear Wiener/Volterra series models were required to achieve accurate predictions of the response of the neural elements in invertebrate reflex limb control systems to GWN stimulation. As these models contain many parameters, and are estimated from signals which contain high levels of noise, they require large amounts of data (typically 20 s) to obtain robust parameter estimates. They cannot, therefore, be applied to model the dynamics and nonlinearity of the transient (adapting) response which occurs during the first few seconds of stimulation and which may be more important for system function than the steady state response.

Given the potential importance and benefits of understanding invertebrate reflex limb control under natural operating conditions and during its adapting response the purpose of this study was threefold. Firstly, to find a model structure which contains few parameters but can still ac-

curately represent the dynamics of the elements of invertebrate reflex limb control systems, and predict their nonlinear behaviour. This will allow the model to be estimated from short lengths of data and the transient response of the system to be investigated. Secondly, to test the ability of this model, with its parameters estimated using GWN stimulation, to predict the response of the system to more natural stimulation. This should allow the conditions under which the models perform well to be determined and their limitations to be explored. Thirdly, to test the ability of the model to determine if invertebrate reflex limb control system dynamics and nonlinear responses are the same during transient and steady state sections. The models developed in this study were estimated and validated using data recorded from the Fast Extensor Tibia (FETi) motor neuron system (Section 1.2).

1.2 FETi System Definition

The position of the tibia relative to the femur in the hind leg of a locust is monitored by a number of internal and external sensors. The focus of the current study is the Femoro-tibial Chordotonal Organ (FeCO) (Figure 1.1A), an internal stretch sensor which monitors the position of the tibia about the femur in the hind leg of a locust [44]. A hardened strand of exoskeleton (apodeme) connects the FeCO to the tibia [44]. To specifically activate the sensory neurons in the FeCO, the current study applies mechanical stimulation produced by an electro mechanical transducer (shaker) to the apodeme of the FeCO, rather than the tibia. This method allows flexion and extension movements of the tibia to be simulated whilst isolating the majority of inputs from other sense organs on the leg (open loop) [44].

Sensory neurons in the FeCO (~90 cells) convert the mechanical stimuli into electrical signals which are integrated by different types of interneurons and transmitted to flexor and extensor motor neurons which activate muscle contraction [20] (Figure 1.1A). Recordings of these electrical signals were made from the Fast Extensor Tibia (FETi) motor neuron as it is large and produces a unique response to extensor muscle stimulation and hence is easy to identify. It should be noted that the ability to identify the FETi motor neuron in different animals is one advantage of using the locust as a model system; similar motor neuron identification would not be possible in human subjects.

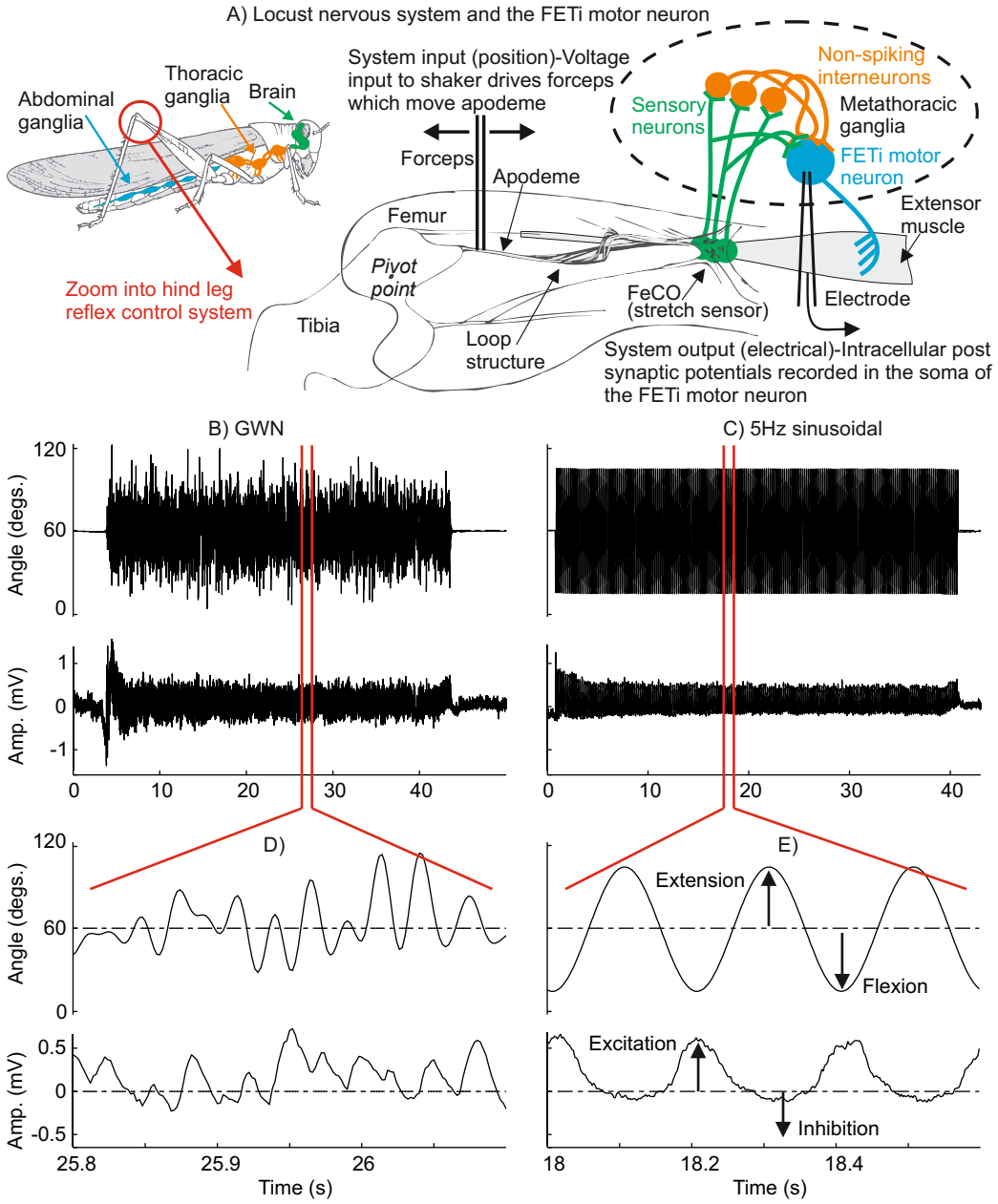

Figure 1.1: The locusts nervous system, the FETi motor neuron and examples of its response to GWN (left column) and 5 Hz sinusoidal (right column) stimulation. (A) The nervous system of the locust and the FETi motor neuron. Also shown are the forceps which attached the apodeme to the electromagnetic shaker used to mechanically excite the system and the glass electrode used to measure the electrical post synaptic potentials in the FETi motor neuron. (B) (upper trace) The GWN input signal and (lower trace) FETi response. (B) (lower trace) The transient response of FETi to GWN stimulation can be seen between ~ 4 and 8 s and its steady state response between ~ 15 and 40 s. (C) (upper trace) The 5 Hz sinusoidal stimulation signal and (lower trace) FETi response. (C) (lower trace) The transient response of FETi to 5 Hz sinusoidal stimulation can be seen between ~ 1 and 6 s and its steady state response between ~ 10 and 37 s. (D) (upper trace) Zoom into the GWN input signal and (lower trace) FETi response which shows the synaptic nature of the signal. (E) (upper trace) Zoom into the sinusoidal stimulation signal and (lower trace) FETi response.

Models were fitted between the voltage input signal used to drive the shaker amplifier and the synaptic potentials recorded in the soma of the FETi motor neuron. Previous work has shown that FETi produces spikes when preparing for a kick (co-contraction phase [19]), during righting [41] and in scratching [100] but not during standing or walking. It should be noted that in the current study which used GWN, sinusoidal and walking stimulation only synaptic inputs were recorded in FETi (Figure 1.1D and E).

In [73, 97, 98] it was concluded that the properties of the shaker amplifier, shaker, forceps mount and forceps could be ignored. Models, therefore, encompass the transformation of mechanical stimulation into dendritic membrane current, transformation into spiking afferent neuron output and further transformation by the network of local spiking and non-spiking interneurons [20]. This system is referred to simply as FETi in this study. Examples of the transient and steady state open loop reflex responses of FETi brought about by GWN and 5 Hz sinusoidal stimulation can be seen in Figure 1.1B and C respectively. The synaptic nature of its responses can be seen in Figure 1.1D and E.

As in previous work [98], FETi was defined as a deterministic system N_{DS} (Figure 1.2A) whose output $y(t)$ depends only on the input signal $u(t)$

$$z(t) = y(t) + v(t) = N_{DS}(u(t)) + v(t) \tag{1.1}$$

where the measured output $z(t)$ depends on the driving input $u(t)$ and measurement noise $v(t)$, which is assumed to be independent of the input. In the current study the term measurement noise is used to describe both the spontaneous background neural activity and electrical measurement noise. The model used to describe FETi is shown in Figure 1.2B. The output of this model, $\hat{y}(t)$, is an estimate of the output of FETi. This is a "deterministic system identification problem" [123] with the aim of using the model as a tool for improving understanding of system function.

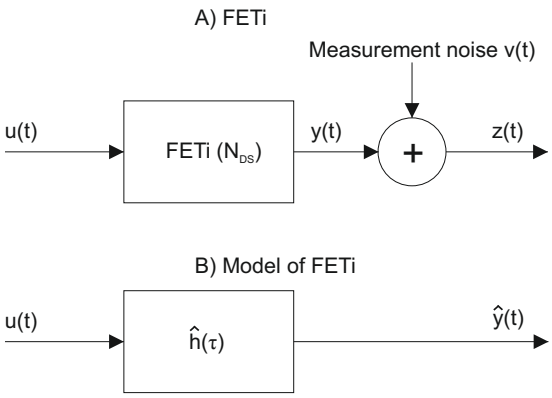

Figure 1.2: (A) FETi with independent measurement noise $v(t)$ and (B) the model used to describe this system.

1.3 Objectives and Scope

The objectives of this study can be summarised as:

1. To refine the experimental methods used to prepare, measure and analyse the reflex response of neuromuscular elements in invertebrate limb control systems.

2. To find a parsimonious nonlinear (Volterra type) model which allows robust parameter estimation from short data lengths and gives accurate predictive performance.

3. To extend previous studies to probe the limitations of the parsimonious model by measuring its accuracy at predicting the response of the system to sinusoidal and more natural walking inputs.

4. To investigate and, if required, improve the robustness of the parameter estimation methods to the properties of the experimental signals.

5. To determine the suitability of the parsimonious model as a tool for modelling the dynamics and nonlinear responses of the neuromuscular elements in invertebrate limb control systems during both transient and steady state response section. This was carried out by applying the model to test the null hypothesis that FETi dynamics and nonlinear responses are the same during transient and steady state sections.

6. To recommend experimental and data analysis methods for further model based studies of invertebrate neurophysiology.

The approach taken in the current study is to extend and develop the Volterra/Wiener methods used in previous studies which required relatively long duration steady state responses (20-30 s) so that robust parameter estimates can be obtained from shorter data lengths. This will allow them to be applied as quasi or piecewise stationary models and hence used to investigate the relatively short duration ($\sim$ 3 s) transient dynamics and nonlinear changes. Quasi stationary methods are a commonly used and established [56, 87] modelling approach which estimate models from a short window of input/output data as the window of data slides through time. It is assumed that any time variation in each window is negligible. The current study is restricted to considering nonlinear Volterra/Wiener series type models. It will consider cascade models, a subset of the Volterra series, consisting of linear Finite Impulse Response (FIR) elements and nonlinear elements which will be represented by polynomial functions.

1.4 Thesis Structure

This thesis contains eight chapters. **Chapter 1** introduces the motivation for this study, provides a definition of the FETi system and outlines the objectives and scope of the study. It also describes the structure of the thesis and the original contributions made by the author.

In **Chapter 2** the modelling methods which have been used by previous studies of biological

limb control systems are reviewed. The focus of this review is on methods which have been applied to invertebrate systems.

In **Chapter 3** the experimental methods which have been used by previous studies of invertebrate chordotonal and mechanical sense organs are reviewed. The focus of the current study, and hence for this review was the FeCO and FETi.

A description of the methods used to prepare, stimulate, measure and record the reflex response of FETi to GWN, sinusoidal and walking input signals is given in **Chapter 4**. It also describes the methods used to obtain the walking stimulus signals and investigates the properties of the shaker amplifier, shaker and forceps mount and the effect they have on the models of FETi. This chapter concludes by considering the consistency of the response of FETi to sinusoidal and walking stimulation.

The aim of the signal processing experiments described in **Chapter 5** was to find a parsimonious Volterra type model structure that would allow the transient and steady state dynamics and nonlinear responses of FETi to be represented. Previous work [73, 97, 98, 117] has been extended by the use of more natural sinusoidal and walking stimulation signals for model validation with the aim of determining the limitations of the models.

The aim of the work described in **Chapter 6** was to investigate how the properties of the experimental input/output signals (low pass filtered GWN input and output signal with high levels of measurement noise) affects the accuracy of a number of model parameter estimation methods.

Given the results of **Chapter 5** and **Chapter 6** the chosen model structure was used to investigate adaptation of FETi dynamics and nonlinear responses and this work is described in **Chapter 7**.

Chapter 8 summarises and discusses the work carried out by this study and also provides suggestions for future work.

Appendix A provides the results of a computer simulation to investigate two parameter estimation error reduction methods.

Appendix B provides a derivation of the normal equations (the equations used to find the solution to the linear Least Squares problem).

1.5 Original Contributions

The original contributions made by the author to this study and presented in this thesis have been grouped into three categories: i) experimental methods, ii) system identification and iii) model based analysis of neural adaption dynamics and nonlinear responses in invertebrate limb control. This work has focused on modelling the open loop reflex inputs to the FETi motor neuron in the locust's neural limb control circuit to mechanical stimulation of the FeCO stretch

receptor. The methods developed by this study, however, can potentially be applied to other invertebrate and vertebrate systems.

Experimental Methods

This work has improved the equipment and methods used by previous studies to investigate invertebrate neuromuscular limb control systems. It has specifically addressed:

1. Limitations in the mechanical excitation system used by previous studies through design and manufacture of a new forceps mount and characterisation of its frequency response

and developed and applied methods to:

1. Determine if the rate of power adaptation in reflex responses are dependent on stimulus signal type.
2. Measure the response consistency when sinusoidal and walking stimulation is applied in addition to more conventional GWN stimulation.

System Identification

The system identification methods used by previous studies have been extended and developed. In particular, this work has:

1. Determined, from the Volterra type model structures considered in this study, that the LNL cascade model provides the structure most suitable for representing FETi in its transient and steady state response sections.
2. Validated the LNL model obtained using GWN stimulation with the use of more biologically realistic sinusoidal and walking stimulation signals to determine where it performs well and to identify its limitations.
3. Developed three new LNL parameter estimation methods. The Smoothed Korenberg Hunter (SKH) method and the Down-sampled Korenberg Hunter (DKH) method are modified versions of the standard Korenberg Hunter (KH) method. Results show that they effectively reduce estimation error in the parameters of the LNL model. The third method, the Down-sampled Differential Evolution (DDE) method, removes the requirement of the KH based methods for careful parameter initialisation.

Model Based Analysis of Neural Adaptation Dynamics and Nonlinear Responses

1. The use of the parsimonious LNL cascade model structure applied in a quasi stationary fashion coupled with Monte Carlo (MC) simulations has been shown to provide a useful tool for the characterisation of the dynamics and nonlinear responses of the neuromuscu-

lar elements in an invertebrate limb control system during both transient and steady state response sections.

2. Key FETi dynamics were found to remain relatively unchanged during repetitive stimulation while output amplitude adaptation was occurring. Whilst some evidence of a significant change was found in parts of the system's nonlinear response, the effect was small and probably of little physiological relevance. Analysis using biologically more realistic stimulation reinforced this conclusion.

Chapter 2

A Review of System Identification Methods for Modelling Invertebrate Reflex Limb Control Systems

2.1 Introduction

This chapter provides a review of the more commonly used system identification methods for modelling biological limb control systems. It is biased towards methods which have been applied to invertebrate systems as these are the focus of the current study. The aim is to provide an explanation of the methods at a level which is suitable for both engineers and neuroscientists with a background in biology. There are two modelling approaches that can be applied to biological limb control systems: analytic modelling (biophysical modelling) or system identification (black or grey box modelling). An analytic model is built using knowledge of the underlying physical principles of the system. For example, an individual neuron could be represented by a collection of electrical components (Hodgkin-Huxley model [59]). Knowledge about the different components of the locusts hind leg control system and the Femoral Chordotonal Organ (FeCO) and in particular FETi is limited. It would, therefore, be difficult to construct a physiological model of it from first principles.

Previous work [54, 98, 117] has used the system identification approach with a black box model structure to represent elements of biological limb control systems. The parameters of the black box model were estimated using input/output measurements from the system. The black box makes no assumptions about the underlying physical detail of the system. The system is viewed as an object which can be represented by its input and output signals and its transfer characteristics. These models will be referred to as "parametric" models as they contain a relatively small number of parameters [95]. This review is restricted to time domain linear and nonlinear Volterra type models because previous work has demonstrated that these structures can accurately represent these types of systems [87, 93, 123]. It uses the theoretical framework and notation developed by Westwick and Kearny in [121, 123]. Further details can

be found in the reviews [87, 123].

This section begins by introducing linear system identification methods because the nonlinear methods used in this study are simply an extension of the linear models. The robustness of both the linear and nonlinear modelling methods to cope with the properties of the data used in this study (a non-white input signal and an output signal with poor Signal to Noise ratios (SNR)) is illustrated using linear modelling theory as this is easier to understand than with nonlinear models.

2.2 Linear System Identification

This section focuses on causal linear models which have a Finite Impulse Response (FIR) structure. It describes two methods which can be used to estimate the parameters of the model from input/output data; the Minimum Mean Square Error (MMSE) and cross correlation methods. For more details about linear system identification the reader is directed to [81]. Only systems that remain constant with time (time invariant) will be considered in this study.

2.2.1 The Impulse Response Function

A Linear Time Invariant (LTI) system can be parametrically modelled by its Impulse Response Function (IRF), represented by $h(\tau)$. As sampled digital signals are used in this study, the output of this model is calculated using the discrete form of the convolution integral.

$$y(t) = \sum_{\tau=0}^{T-1} h(\tau)u(t-\tau) \tag{2.1}$$

This states that the output of the model, $y(t)$, is the weighted sum of the current and past input samples, $u(t)$. The number of parameters in the model is represented by T. This model structure is often referred to as a Finite Impulse Response (FIR) model or filter.

2.2.2 Minimum Mean Square Error Parameter Estimation

Given the FIR model and the measured input $u(t)$ and output $z(t)$ signals the aim is to find the parameters which can generate the "best" estimate of the measured output. The widely used MMSE approach defines the "best" parameters as those which minimise the difference between the measured output $z(t)$ and the estimated model output $\hat{y}(t)$, in the mean square sense. The MMSE cost function [81] can be written as:

$$\text{MMSE}(\theta) = E\left[(z(t) - \hat{y}(\theta, t))^2\right] \tag{2.2}$$

Where $E[\cdot]$ is the expected (average) value and θ are the parameters of the model. For the measured response of the system Equation 2.2 can be written as:

$$\mathrm{J} = \frac{1}{N}\sum_{t=1}^{N}(z(t) - \hat{y}(t))^2 \tag{2.3}$$

where N is the number of samples of data in the recording. As the output, $\hat{y}(t)$, is a linear function of the model parameters Equation 2.1 may be reformulated as a matrix/vector equation.

$$\hat{\mathbf{y}} = \mathbf{U}\hat{\mathbf{h}} \tag{2.4}$$

where

$$\mathbf{U} = \begin{bmatrix} u(1) & 0 & 0 & \cdots & 0 \\ u(2) & u(1) & 0 & \cdots & 0 \\ u(3) & u(2) & u(1) & \cdots & 0 \\ u(4) & u(3) & u(2) & \cdots & 0 \\ \vdots & \vdots & \vdots & \ddots & \vdots \\ u(N) & u(N-1) & u(N-2) & \cdots & u(N-T+1) \end{bmatrix} \tag{2.5}$$

is a matrix of time delayed input signals. This formulation of $\mathbf{U}$ is called the "pre windowed" method [57]. It makes the assumption that the input data before $u(1)$ are zero which results in the zeros in the top right corner of $\mathbf{U}$. It makes no assumptions about the data after $t = N$. Vectors $\hat{\mathbf{h}}$ and $\hat{\mathbf{y}}$ contain the model parameters $\hat{h}(\tau)$ and the output samples $\hat{y}(t)$, respectively.

$$\hat{\mathbf{h}} = \left[\hat{h}(0)\ \hat{h}(1)\ \hat{h}(2)\ \ldots\ \hat{h}(T-1)\right]^T \tag{2.6}$$

$$\hat{\mathbf{y}} = \left[\hat{y}(1)\ \hat{y}(2)\ \hat{y}(3)\ \ldots\ \hat{y}(N)\right]^T \tag{2.7}$$

Equation 2.3 can be re-written as:

$$\mathrm{J} = \frac{1}{N}\left(\mathbf{z} - \mathbf{U}\hat{\mathbf{h}}\right)^T\left(\mathbf{z} - \mathbf{U}\hat{\mathbf{h}}\right) \tag{2.8}$$

The minimum of J is found by differentiating Equation 2.8 and setting its gradient to zero. The derivation used to obtain this result can be found in Appendix B

$$\frac{\partial \mathrm{J}}{\partial \hat{\mathbf{h}}} = -2\mathbf{U}^T\mathbf{z} + 2\mathbf{U}^T\mathbf{U}\hat{\mathbf{h}} = 0 \tag{2.9}$$

Rearranging Equation 2.9 produces the normal equations

$$\left(\mathbf{U}^T\mathbf{U}\right)\hat{\mathbf{h}} = \mathbf{U}^T\mathbf{z} \tag{2.10}$$

The linear Least Squares estimate of the IRF is given by solving:

$$\hat{\mathbf{h}} = \left(\mathbf{U}^T\mathbf{U}\right)^{-1}\mathbf{U}^T\mathbf{z} \tag{2.11}$$

It should be noted that the matrix inversion is not usually carried out in the form of Equation 2.11 but instead by using the more robust Singular Value Decomposition (SVD) to compute a generalised inverse (Moore-Penrose pseudoinverse) [6]. This method is robust to numerical errors which can occur when working in finite precision arithmetic.

The Least Squares method provides an unbiased estimate $\hat{\mathbf{h}}$ assuming that [81]:

- the measurement noise, $v(t)$, is additive, zero-mean, white and independent of the input $u(t)$ and
- the system can be represented by a linear model.

The difference between the true model parameters $\mathbf{h}$ and the estimated parameters $\hat{\mathbf{h}}$ can be calculated using the standard result for the parameter covariance matrix [6]:

$$E\left[(\hat{\mathbf{h}} - \mathbf{h})(\hat{\mathbf{h}} - \mathbf{h})^T\right] = \sigma_v^2\left[\mathbf{U}^T\mathbf{U}\right]^{-1} \tag{2.12}$$

where σ_v^2 is the variance of the measurement noise. In the current work the errors in the parameter estimates are likely to be large because the levels of noise $v(t)$ in the recordings made from the FETi system are high. It can be seen from Equation 2.12 that the errors in the estimated parameters therefore depend on the inverse of $\mathbf{U}^T\mathbf{U}$.

The SVD not only provides a method of solving Least Squares problems, but also a method of analysing them. Starting with the formula for the Least Squares solution (Equation 2.11) and factoring the matrix $\mathbf{U}^T\mathbf{U}$ using the SVD:

$$\hat{\mathbf{h}} = \left(\mathbf{V}\mathbf{S}\mathbf{V}^T\right)^{-1}\mathbf{U}^T\mathbf{z} \tag{2.13}$$

where $\mathbf{V} = [\mathbf{v}_1\ \mathbf{v}_2 \ldots \mathbf{v}_p]$ is an orthogonal matrix ($\mathbf{V}^T\mathbf{V} = \mathbf{I}$) and $\mathbf{S}$ is a diagonal matrix. The non-negative diagonal elements of $\mathbf{S}$ are called singular values and are arranged in descending order of magnitude.

$$\mathbf{s} = diag\,(\mathbf{S}) = \left[s_1, s_2 \cdots s_p\right] \tag{2.14}$$

where $s_1 \geq s_2 \geq \cdots \geq s_p \geq 0$. $\mathbf{V}\mathbf{S}\mathbf{V}^T$ can be written as:

$$\mathbf{V}\mathbf{S}\mathbf{V}^T = \sum_{i=1}^{p} \mathbf{s}_i\mathbf{v}_i\mathbf{v}_i^T \tag{2.15}$$

The Least Squares solution, can now be written as:

$$\hat{\mathbf{h}} = \sum_{i=1}^{p} \frac{\mathbf{v}_i\mathbf{v}_i^T\mathbf{n}}{\mathbf{s}_i} \tag{2.16}$$

where $\mathbf{n} = \mathbf{U}^T\mathbf{z}$.

The presence of very small singular values ($\mathbf{s_i}$) in the denominator of Equation 2.16 will amplify their corresponding measurement noise terms. Small singular values may occur when the input signal has a coloured spectrum. This introduces estimation error into the parameter estimate and obscures its underlying shape. The smaller the singular value, the greater the noise amplification. The condition number (the ratio of the largest and the smallest singular value) provides a measure of this instability [6]. There are a number of approaches for reducing Least Squares parameter estimation error. Perhaps the simplest solution, which will work with any low pass filtered input signal, is to remove the high frequency IRF estimation error by low pass filtering the parameters. Another approach to reduce the sensitivity of the solution to measurement noise is to truncate the singular values $\mathbf{s_i}$ in Equation 2.16. The difficulty, however, lies in determining where to truncate as if too many terms are removed, the accuracy and resolution of the model will be reduced. The pseudo-inverse based algorithm [123] and regularisation methods, such as Tikhonov regularisation [6] have been developed to address this issue. It should be noted that the price paid for making the parameter estimates less sensitive to measurement noise is reduced model accuracy and biased parameter estimates [6].

Solving Equation 2.11 becomes computationally demanding as the data length N and model order T increases in terms of calculation time and the memory required to store $\mathbf{U}$ [55]. If the input to the system is a white noise signal then the parameters of the model can be estimated more efficiently using the cross correlation method. This method, which is explained in the next section, was used in the previous studies by Kondoh et al. [73, 97, 98].

2.2.3 Cross Correlation Parameter Estimation

A linear system driven by a white noise input, and without measurement noise, has a cross correlation function given by:

$$\phi_{uy}(\tau) = E\left[u(t-\tau)y(t)\right] \tag{2.17}$$

The cross correlation of two signals equals their expected cross product as a function of the time shift between them. Replacing the system's output $y(t)$ in Equation 2.17 with the discrete convolution integral (Equation 2.1) gives:

$$\phi_{uy}(\tau) = E\left[u(t-\tau)\sum_{k=0}^{T-1} h(k)u(t-k)\right] \tag{2.18}$$

$$\phi_{uy}(\tau) = \sum_{k=0}^{T-1} \Phi_{uu}(\tau-k)h(k) \tag{2.19}$$

The system's input/output cross correlation function equals the convolution of the input autocorrelation function with the system's parameters. Assuming zero mean, unit variance white

noise input then $\Phi_{uu}(\tau) = \delta(\tau)$ and

$$\phi_{uy}(\tau) = \sum_{k=0}^{T-1} \delta(\tau - k)h(k) = h(\tau) \tag{2.20}$$

When the input signal is white, the IRF can be estimated simply and computationally efficiently by calculating the system's cross correlation function. The cross correlation function (Equation 2.17) is calculated in this study by using the commonly used biased estimator:

$$\hat{\phi}_{uy}(\tau) = \frac{1}{N} \sum_{i=\tau}^{N} u(i - \tau)y(i) \tag{2.21}$$

It is interesting to note that the cross correlation approach can be used to estimate the IRF with non-white inputs as the Least Squares solution can be formulated in terms of correlation functions [95].

$$\hat{\mathbf{h}} = \mathbf{\Phi}_{uu}^{-1}\phi_{uz} \tag{2.22}$$

Solving Equation 2.22 is equivalent to solving the linear Least Squares estimate (Equation 2.11). Before reviewing nonlinear system identification methods (Section 2.4), the methods used to measure the performance of black box models of biological systems are investigated.

2.3 Model Validation

The object of model validation is to measure how well the model fits the dynamics of the system rather than the dynamics of the system and the noise which will be present in the data. Model validation can be carried out in a number of ways [95] but the most commonly used with nonlinear models of biological systems [87, 123] splits the data into two sections and uses one section to estimate the model (estimation data) and the other to validate the model (validation data). This method assumes that the noise is different between the two sections and so should give a realistic measure of the ability of the model to predict new data.

Model performance is often measured [73, 97, 98] by calculating the percentage Mean Square Error (%MSE) difference between the recorded neural output signal, $z(t)$, and the predicted model output signal, $\hat{y}(t)$, using validation data (Figure 1.2).

$$\%MSE = 100 \times \frac{Var(z - \hat{y})}{Var(z)} \tag{2.23}$$

$Var(x)$ is calculated using

$$Var(x) = \frac{1}{N} \sum_{t=1}^{T} x^2(t) - \left(\frac{1}{N} \sum_{t=1}^{T} x(t) \right)^2 \tag{2.24}$$

where N is the number of samples in the signal x. Model performance improves as the %MSE performance measure decreases.

2.4 Nonlinear System Identification

This section provides an introduction to the Volterra and Wiener series models and the Least Squares, cross correlation and the Wiener Laguerre methods which can be used to estimate their parameters. Cascade models, a restricted subset of the Volterra series, are also considered because they have successfully been applied to many nonlinear biological systems [51, 52, 65]. They are useful because they can represent some nonlinear systems much more efficiently than the Volterra or Wiener series and their parameters may be easier to interpret and link to the function of the system.

2.4.1 The Volterra Series

The Volterra series can be used to model a nonlinear, time invariant, system. As sampled signals are analysed in this study, it is necessary to use the discrete form of the Volterra series. This series is a generalisation of the discrete convolution integral (Equation 2.1) for a linear system involving an infinite sum of terms. For a causal, finite memory, time-invariant system the relationship between the input and output signals can be represented by

$$y(t) = \sum_{n=0}^{N_h} \sum_{\tau_1=0}^{T-1} \cdots \sum_{\tau_n=0}^{T-1} h_n(\tau_1, \ldots, \tau_n) u(t-\tau_1) \ldots u(t-\tau_n) \tag{2.25}$$

where N_h is the number of kernels (h_n) in the series. For example, the 2^{nd} order Volterra model is given by

$$y(t) = h_0 + \sum_{\tau_1=0}^{T-1} h_1(\tau_1) u(t-\tau_1) + \sum_{\tau_1=0}^{T-1} \sum_{\tau_2=0}^{T-1} h_2(\tau_1, \tau_2) u(t-\tau_1) u(t-\tau_2) \tag{2.26}$$

The zero order kernel, h_0, is an offset term which is present in the output regardless of the input; this is zero for a linear system. The first order kernel, h_1, has the same form as the discrete convolution integral (Equation 2.1). It does not, however, represent the system's impulse response, as this will contain components from all the kernels ($h_0 + h_1 + h_2 + \ldots$). The second order kernel, h_2, is a generalisation of the first order kernel and it defines how two copies of the input signal interact for different delays τ_1 and τ_2. The kernel is set to be symmetric about its diagonal so that

$$h_2(\tau_1, \tau_2) = h_2(\tau_2, \tau_1) \tag{2.27}$$

It should be noted that if the Volterra series is truncated it will result in a reduction in its ability to represent certain systems. The truncated Volterra series will not be able to represent systems which have higher than a second order nonlinearity and, for example, those which exhibit a hard nonlinear behaviour, such as saturation or rectification.

2.4.2 Volterra Series Parameter Estimation

Given the Volterra series model and input/output measurements the aim is to find the parameters of the kernels which minimise the mean square error between the model output and the measured output. Because the kernels of the Volterra series are correlated with each other they must be estimated simultaneously; this can be achieved using the Least Squares optimisation method. This method can be applied because even though the Volterra model is nonlinear in its structure it is still linear in its parameters.

Equation 2.26 is reformulated as the matrix/vector equation:

$$\mathbf{y} = \mathbf{U}\mathbf{h} \tag{2.28}$$

where:

$$\mathbf{U} = [\mathbf{U_0}\ \mathbf{U_1}\ \mathbf{U_2}] \tag{2.29}$$

For example, $\mathbf{U_1}$ is the matrix of time delayed signals corresponding to the Volterra kernel parameters $\mathbf{h_1}$ where:

$$\mathbf{U_1} = \begin{bmatrix} u(1) & 0 & 0 & \cdots & 0 \\ u(2) & u(1) & 0 & \cdots & 0 \\ u(3) & u(2) & u(1) & \cdots & 0 \\ u(4) & u(3) & u(2) & \cdots & 0 \\ \vdots & \vdots & \vdots & \ddots & \vdots \\ u(N) & u(N-1) & u(N-2) & \cdots & u(N-T+1) \end{bmatrix} \tag{2.30}$$

As the parameters h are a linear function of the output the Least Squares estimate of the Volterra parameters is given by solving:

$$\mathbf{h} = \left(\mathbf{U}^T\mathbf{U}\right)^{-1}\mathbf{U}^T\mathbf{z} \tag{2.31}$$

As with the linear case (Section 2.2.2), the matrix inversion is not usually carried out in the form of Equation 2.31 but using the SVD to compute a generalised inverse [6].

The Least Squares method, however, becomes computationally expensive even for relatively low order models with short memory lengths. For example, the calculation of the first three Volterra kernels with a kernel memory length (T) of 40 samples requires the inversion of a matrix containing $861 \times 861 = 741321$ elements $(1 + T + (1 + T)(T/2)) = 861$. Barrett [9], Zadeh [128] and Wiener [125] realised that re-arranging the Volterra series into an orthogonal form would allow each kernel to be estimated independently, significantly reducing their computational cost. The Wiener method [125] is explained in the next section.

2.4.3 The Wiener Series and the Cross Correlation Parameter Estimation Method

Wiener rearranged the Volterra series so that each kernel is orthogonal to each other when the input $u(t)$ is a Gaussian white noise signal. Lee and Schetzen [80] modified Wiener's continuous time series for the discrete time case.

$$y(t) = \sum_{n=0}^{\infty} G_n \left[\mathbf{k_n}(\tau_1, \ldots, \tau_n); u(t')\ t' \leq t\right] \tag{2.32}$$

As pointed out by Westwick and Kearney [123], the discrete Wiener series is a sum of operators (an operator maps a function on to a function). Traditionally the terms of the Wiener series have been referred to as functionals. The first three Wiener operators are:

$$G_0[\mathbf{k_0}; u(t)] = \mathbf{k_0} \tag{2.33}$$

$$G_1[\mathbf{k_1}(\tau_1); u(t)] = \sum_{\tau_1=0}^{T-1} \mathbf{k_1}(\tau_1) u(t - \tau_1) \tag{2.34}$$

$$G_2[\mathbf{k_2}(\tau_1, \tau_2); u(t)] = \sum_{\tau_1=0}^{T-1} \sum_{\tau_2=0}^{T-1} \mathbf{k_2}(\tau_1, \tau_2) u(t - \tau_1) u(t - \tau_2) - \sigma_u^2 \sum_{\tau_1=0}^{T-1} \mathbf{k_2}(\tau_1, \tau_2) \tag{2.35}$$

This re-arrangement allows a cross correlation approach, similar to that used for a linear system (Section 2.2.3), to be used to estimate the parameters of the Wiener kernels. The Lee and Schetzen [80] cross correlation method obtains a computationally efficient Least Squares estimate of the kernel parameters if the input signal is a GWN. Their algorithm proceeds as follows:

The zero order kernel $\hat{\mathbf{k}}_\mathbf{0}$ is independent of the input signal and is estimated by taking the mean value of the output signal

$$\hat{\mathbf{k}}_\mathbf{0} = \frac{1}{N} \sum_{t=1}^{N} y(t) \tag{2.36}$$

This zero order kernel is subtracted from $y(t)$ to produce the zero order residual

$$v_0 = y(t) - \hat{\mathbf{k}}_\mathbf{0} \tag{2.37}$$

The first order kernel estimate is the cross correlation between the input $u(t)$ and the zero order residual v_0, normalised with respect to the input power σ_u^2

$$\hat{\mathbf{k}}_\mathbf{1}(\tau) = \frac{1}{N\sigma_u^2} \sum_{t=1}^{N} u(t - \tau_1) v_0(t) \tag{2.38}$$

The output from the first order kernel is calculated by convolution

$$\hat{y_1}(t) = \sum_{\tau_1=0}^{T-1} \hat{\mathbf{k}}_\mathbf{1}(\tau_1) u(t - \tau_1) \tag{2.39}$$

and this is subtracted from the zero order residue v_0 to produce the first order residue

$$v_1(t) = v_0(t) - \hat{y_1}(t) \tag{2.40}$$

The second order kernel is estimated using the normalised second order cross correlation

$$\hat{\mathbf{k}}_{\mathbf{2}}(\tau_1, \tau_2) = \frac{1}{2N\sigma_u^4} \sum_{t=1}^{N} u(t-\tau_1)u(t-\tau_2)v_1(t) \tag{2.41}$$

The higher order kernels can be estimated in the same fashion.

One disadvantage of using the Wiener series, rather than the Volterra series, is that the model is dependent on the input signal (σ_u^2 term in Equation 2.35). This characteristic does not fit the aim of creating a model which can represent the response of the system to arbitrary inputs. This problem, however, can be overcome by converting the Wiener kernels into their Volterra form [85, 104].

Another disadvantage of this approach is that as the input signal obtained from experiments will often be coloured rather than white, the terms of the Wiener series will not be orthogonal. The Lee and Schetzen algorithm will therefore give biased kernel estimates and this will reduce the performance of the model. A theoretical treatment of how different Volterra/Wiener parameter estimation methods affect the accuracy of the model is provided by Marmarelis [87].

Time [75, 105] and frequency domain [48] correlation based parameter estimation methods have been developed to work with coloured Gaussian input signals. These methods, however, have their limitations as they can only cope with slightly coloured input signals [120] and the estimation of cross correlations requires relatively large sample sizes [47]. An alternative, which was probably used by [73, 97, 98], is the method detailed in [105] which pre-whitens the coloured input signal using a linear filter.

The Least Squares parameter estimation method (Section 2.4.2) does not assume a white input signal and so should provide more accurate parameter estimates [123]. The application of the Least Squares method to many systems, however, is impractical because as model order increases it quickly becomes computationally too expensive to store and time consuming to invert $\mathbf{U}^T\mathbf{U}$ (Equation 2.31) for standard computer systems. The Wiener Laguerre method [86], which is described in Section 2.4.4, is one of a number of methods which have been developed to reduce the computational load of the Least Squares approach

2.4.4 The Wiener Laguerre Method

The Wiener Laguerre method reduces the computational load of the Least Squares approach by using a basis function (the Laguerre expansion basis) to reduce the number of polynomial coefficients in the regression [123]. As the Laguerre filters (Equation 2.45) are orthogonal this should lead to a well-conditioned problem. Furthermore, by recursively applying the same filter (Equation 2.46), the output of the Laguerre filters can be computed efficiently.

The following algorithm shows how the Wiener Laguerre method can be used to estimate the kernels of a 2^{nd} order Volterra series. The 2^{nd} order Volterra series can be expanded on a Discrete Laguerre Filter (DLF) basis

$$y(t) = c_0 + \sum_{j_1=0}^{J_{WL}-1} c_1(j_1)\vartheta_{j_1}(t) + \sum_{j_1=0}^{J_{WL}-1}\sum_{j_2=0}^{J-1} c_2(j_1, j_2)\vartheta_{j_1}(t)\vartheta_{j_2}(t) \tag{2.42}$$

where J_{WL} is the number of functions in the decomposition and c represents the coefficients of the Volterra kernels. The transformed input data $\vartheta_j(t)$ are obtained using

$$\vartheta_j(t) = \sum_{m=0}^{L-1} L_j(m)u(t-m) \tag{2.43}$$

where L_j, the j^{th} order Laguerre function, is calculated using

$$L_j(\tau) = \alpha^{\frac{(\tau-j)}{2}}(1-\alpha)^{\frac{1}{2}} \sum_{k=0}^{j}(-1)^k\binom{\tau}{k}\binom{j}{k}\alpha^{j-k}(1-\alpha)^k \tag{2.44}$$

where α, the decay parameter, controls the damping of the Laguerre function ($0 < \alpha < 0$) and $\tau \geq 0$. The output of the Laguerre filter $\vartheta_0(t)$ is calculated using

$$\vartheta_j(t) = \sqrt{\alpha}\vartheta_0(t-1) + T_s\sqrt{(1-\alpha)}u(t) \tag{2.45}$$

where T_s is the sampling interval. The output of the remaining filters was calculated recursively using

$$\vartheta_j(t) = \sqrt{\alpha}\vartheta_j(t-1) + \sqrt{\alpha}\vartheta_{j-1}(t) - \vartheta_{j-1}(t-1) \tag{2.46}$$

The coefficients $c(j)$ were obtained using the Least Squares method. The Volterra kernels could then be constructed using

$$h_1(\tau_1) = \sum_{j=0}^{J_{WL}-1} c_1(j_1)L_{j_1}(\tau_1) \tag{2.47}$$

and

$$h_2(\tau_1, \tau_2) = \sum_{j_1=0}^{J_{WL}-1}\sum_{j_2=0}^{J_{WL}-1} c_2(j_1, j_2)L_{j_1}(\tau_1)L_{j_2}(\tau_2) \tag{2.48}$$

2.4.5 Cascade Models

Cascade models are a subset of the Volterra series which consist of dynamic linear (h, g) and static nonlinear (m) elements (Figure 2.1). The LN (Linear Nonlinear) or Wiener model consists of a dynamic (with memory) linear element (h) followed by a static (without memory) nonlinearity (m) (Figure 2.1A), which is chosen to be a polynomial function given by

$$m(x(t)) = \sum_{q=0}^{Q} c^{(q)}x^q(t) \tag{2.49}$$

where Q is the polynomial order, c its coefficients and x the input signal to the nonlinearity. The output of the LN model is thus calculated using

$$y(t) = \sum_{q=0}^{Q} c^{(q)} \left(\sum_{\tau=0}^{T-1} h(\tau) u(t-\tau) \right)^q \tag{2.50}$$

The NL (Nonlinear Linear) or Hammerstein model consists of a static nonlinearity followed by a dynamic linear element (Figure 2.1B). Its output can be calculated using

$$y(t) = \sum_{\tau=0}^{T-1} h(\tau) \left(\sum_{q=0}^{Q} c^{(q)} u^q(t-\tau) \right) \tag{2.51}$$

The LNL (Linear Nonlinear Linear) or Wiener Hammerstein model consists of two dynamic linear elements, $h(\tau)$ and $g(\sigma)$, separated by a static nonlinear element (Figure 2.1C). The output of this model is given by

$$y(t) = \sum_{\sigma=0}^{T-1} g(\sigma) \sum_{q=0}^{Q} c^{(q)} \left(\sum_{\tau=0}^{T-1} h(\tau) u(t-\sigma-\tau) \right)^q \tag{2.52}$$

As the cascade models are a subset of the Volterra series, their parameters can be transformed directly into Volterra form. The n^{th} order Volterra kernel of the LN cascade can be calculated from the parameters of this cascade using

$$\mathbf{h}_n(\tau_1, \ldots, \tau_n) = c^n h(\tau_1) h(\tau_2) \ldots h(\tau_n) \tag{2.53}$$

The Volterra kernels of the NL cascade are given by

$$\mathbf{h}_n(\tau_1, \ldots, \tau_n) = c^n h(\tau_1) \delta(\tau_1, \tau_2) \delta(\tau_1, \tau_3) \ldots \delta(\tau_1, \tau_n) \tag{2.54}$$

where $\delta(\tau_1, \tau_2)$ is the Kronecker delta.

The Volterra kernels of the LNL cascade are

$$\mathbf{h}_n(\tau_1, \ldots, \tau_n) = c^n \sum_{\sigma=0}^{T-1} g(\sigma) h(\tau_1 - \sigma) h(\tau_2 - \sigma) \tag{2.55}$$

2.4.6 Cascade Model Parameter Estimation

As the cascade models are nonlinear in their parameters and have a differentiable cost function their parameters can be estimated using a nonlinear local optimisation method. One of the most widely used local optimisation methods for estimating the parameters of these models for biological applications was developed by Korenberg and Hunter [65, 74]. This method will be referred to as the KH method. The iterative methods to estimate the parameters of the LN, NL and LNL models are summarised by Algorithms 1, 2 and 3. In the current study the linear

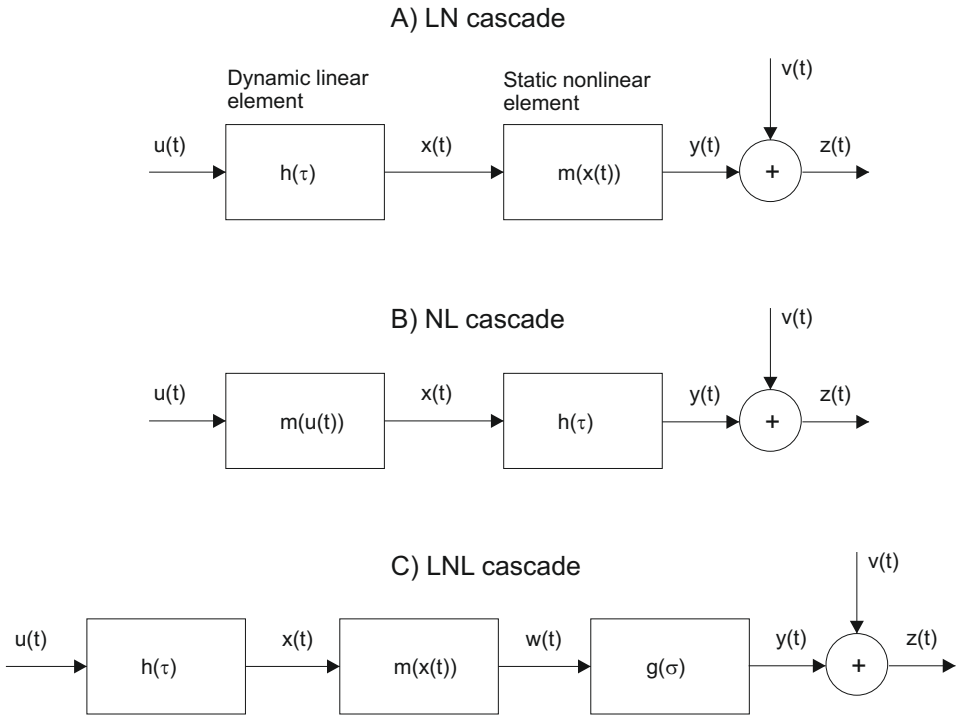

Figure 2.1: Block diagrams of the (A) LN, (B) NL and (C) LNL cascade models.

elements of the cascade models will be estimated using the Least Squares method, rather than the cross correlation approach used by Korenberg and Hunter [65, 74] as this approach is less sensitive to the properties of the input signal.

Algorithm 1 LN cascade parameter estimation

1: Estimate the Impulse Response Function (IRF) $\hat{h}(\tau)$ between the input $u(t)$ and output $z(t)$ signals (Least Squares method) (Figure 2.1A)
2: Estimate the intermediate signal $\hat{x}(t)$ by filtering $u(t)$ with $\hat{h}(\tau)$
3: Fit a polynomial between $\hat{x}(t)$ and the measured output z(t)
4: Calculate the %MSE (Equation 2.23) between the estimated model output $\hat{y}(t)$ and z(t)
5: If the %MSE reduces from the last iteration then go to step 6, else exit with the current parameter estimates
6: Estimate the inverse of the nonlinearity by fitting a polynomial between $\hat{y}(t)$ and $\hat{x}(t)$ (Least Squares estimate)
7: Compute a new estimate of $\hat{h}(\tau)$ using $u(t)$ and $\hat{x}(t)$
8: Return to step 2

Korenberg and Hunter [65, 74] chose to use the Levenberg Marquardt gradient descent method to minimise J in the LNL parameter estimation algorithm (Algorithm 3, step 4). This iterative method is a standard tool for solving nonlinear Least Squares problems [6, 123]; it combines the robust convergence properties of the steepest descent method with the faster convergence of the Gauss Newton method [6, 123]. As there are already many explanations of these methods [6, 123] only a quick overview, following the derivation given by [123], will be provided.

The objective of gradient descent methods is to find the parameters $\boldsymbol{\theta}$ which give the minimum MSE difference between the measured output $z(t)$ and the model output $\hat{y}(t)$. The cost function

Algorithm 2 NL parameter estimation

1: Fit a linear system between $z(t)$ and $u(t)$ to obtain an initial estimate of the inverse of $\hat{h}(\tau)$, $\hat{h}(\tau)^{-1}$ (Figure 2.1B)
2: Filter $z(t)$ by $\hat{h}(\tau)^{-1}$ to obtain $\hat{x}(t)$
3: Fit a polynomial $\hat{m}(u(t))$ between $\hat{x}(t)$ and $u(t)$
4: Obtain a new estimate of $\hat{x}(t)$ given $\hat{m}(u(t))$
5: Re-estimate $\hat{h}(\tau)$ given $\hat{x}(t)$ and $z(t)$
6: Calculate the %MSE difference between model output $\hat{y}(t)$ and measured output $z(t)$
7: If the %MSE reduction is small compared to last iteration, exit with current parameters
8: Else, compute a new estimate of $\hat{h}(\tau)^{-1}$ using the current $\hat{x}(t)$ and $z(t)$. Return to step 2

Algorithm 3 LNL parameter estimation

Require: Initial estimate of $\hat{h}(\tau) = (\frac{1}{fs}, 0, 0, \ldots, 0)$

1: Filter $u(t)$ by $\hat{h}(\tau)$ to obtain $\hat{x}(t)$ (Figure 2.1C)
2: Fit the NL system between $\hat{x}(t)$ and $z(t)$ using Algorithm 2
3: If first iteration or significant improvement in model accuracy then continue, else exit with current parameters
4: Obtain a new estimate of $\hat{h}(\tau)$ using the Levenberg-Marquardt (LM) [88] gradient based method to minimise the difference between the predicted and measured output signal, given the current estimate of the NL system. Return to step 2

is written as

$$\mathrm{J}(\boldsymbol{\theta}) = \frac{1}{2N}\sum_{t=0}^{N-1}(z(t) - \hat{y}(t,\boldsymbol{\theta}))^2 \tag{2.56}$$

The factor $1/2$ is included for convenience. Gradient descent optimisation methods start with an initial guess for the parameters $\boldsymbol{\theta_k}$. With each iteration the parameters are modified by a factor in the vector $\boldsymbol{d_k}$.

$$\boldsymbol{\theta_{k+1}} = \boldsymbol{\theta_k} + \boldsymbol{d_k} \tag{2.57}$$

The steepest descent method simply follows the steepest gradient on the error surface

$$\boldsymbol{\theta_{k+1}} = \boldsymbol{\theta_k} + \mu_k \frac{\partial \mathrm{J}(\boldsymbol{\theta_k})}{\partial \boldsymbol{\theta_k}} \tag{2.58}$$

where μ_k is the step size. The gradient is calculated from Equation 2.56 using the chain rule

$$\frac{\partial \mathrm{J}(\boldsymbol{\theta_k})}{\partial \boldsymbol{\theta_k}} = -\frac{1}{N}\sum_{t=0}^{N-1}(z(t) - \hat{y}(t,\boldsymbol{\theta_k}))\,\frac{\partial \hat{y}(t,\boldsymbol{\theta_k})}{\partial \boldsymbol{\theta_k}} \tag{2.59}$$

Defining the Jacobian $\boldsymbol{J_{ac}}$ as

$$\boldsymbol{J_{ac}}(t,i) = \frac{\partial \hat{y}(t,\boldsymbol{\theta_k})}{\partial \boldsymbol{\theta_k}(i)} \tag{2.60}$$

allows the gradient to be written as

$$\frac{\partial \mathrm{J}(\boldsymbol{\theta_k})}{\partial \boldsymbol{\theta_k}} = -\frac{1}{N}\boldsymbol{J_{ac}}^T\boldsymbol{\epsilon} \tag{2.61}$$

where $\boldsymbol{\epsilon}$ is a vector containing the error signal $\epsilon(t,\theta) = z(t) - \hat{y}(t,\theta)$. The steepest descent method

is simple and easy to implement but it can be slow to converge. Second order techniques attempt to decrease convergence time by using information about the curvature of the error surface as well as its gradient. Calculating second order derivatives of the model, however, is computationally very expensive so second order methods often estimate curvature information. One such method, called the Gauss Newton method [6, 123], updates the parameters $\boldsymbol{\theta}$ using

$$\boldsymbol{d_k} = \mu_k(\boldsymbol{J_{ac}}^T\boldsymbol{J_{ac}})^{-1}\boldsymbol{J_{ac}}^T\boldsymbol{\epsilon} \tag{2.62}$$

The Levenberg Marquardt method adds what can be thought of as a damping term, $\mu_k\mathbf{I_M}$, to the parameter update

$$\boldsymbol{d_k} = \left(\frac{1}{N}\boldsymbol{J_{ac}}^T\boldsymbol{J_{ac}} + \mu_k\mathbf{I_M}\right)^{-1}\boldsymbol{J_{ac}}^T\boldsymbol{\epsilon} \tag{2.63}$$

where $\mathbf{I_M}$ is an identity matrix. This damping term improves the condition of $(\boldsymbol{J_{ac}}^T\boldsymbol{J_{ac}})^{-1}$, which reduces estimation error in the parameters of the first linear element of the LNL model. This is a similar approach to that used by Tikhonov regularisation [6].

2.5 Conclusions

This chapter has provided a description of a number of linear and nonlinear system identification methods suitable for modelling biological limb control systems. This literature review has highlighted the problems of the Wiener series model and the cross correlation parameter estimation method. To summarise, this method produces a model which is dependent on the input signal and this characteristic does not fit with the aim to produce a model which can represent the response of the system to arbitrary inputs. Furthermore as the input signals obtained from experiments will often be coloured rather then white, the Wiener series terms will not be orthogonal. This will result in biased kernel estimates and a reduction in the performance of the model. Despite the disadvantages of the Wiener series model and the cross correlation parameter estimation method it has become one of the most commonly applied tools for modelling invertebrate stretch receptors [48, 73, 97, 98, 110, 117].

This review has also identified that the Volterra series model coupled with the Least Squares parameter estimation method overcomes the problems of the Wiener series model and the cross correlation approach. The Least Squares parameter estimation method does not assume a white input signal and so should provide more accurate parameter estimates. The computational and data length requirements of using the Volterra series model with the Least Squares approach would, however, make calculation of higher than second order kernels impractical. As explained in this review, the Wiener Laguerre method and the cascade models provide a parsimonious alternative which can allow higher order nonlinear responses to be represented.

Chapter 3

A Review of the Methods used to Investigate Invertebrate Reflex Limb Control Systems

3.1 Introduction

The objective of this review is to describe and evaluate the experimental methods which have been used in previous studies of invertebrate reflex limb control systems. It also investigates how system identification methods have been applied and how the resulting models are used and interpreted. Following examination of the literature, two methods for studying the function of such systems are considered in detail. Before proceeding to describe and evaluate these two methods, an explanation of the locust's central nervous system, its hind leg control system and the Femoral Chordotonal Organ (FeCO) will be given.

3.2 The Local Hind Leg Resistance Reflex of the Locust

The central nervous system of a locust consists of a brain and a chain of segmental ganglia (collections of neurons) joined by nerve connectives (Figure 3.1A). The insect's brain determines its overall behaviour and is responsible for setting the direction and speed of its movements [20]. Three ganglia in the thorax contain the neurons that control movement of the legs; they receive inputs from the brain and sensory receptors in and on the legs [20].

The sensory receptors associated with the locust leg can be divided into two groups, exteroceptors and proprioceptors. Exteroceptors provide animals with information about the external environment [20]. In the case of the locust, these exteroceptors are hairs which sparsely cover its legs and respond to touch and certain chemicals. They provide the locust with a collision avoidance system which allows it to monitor contact with its six legs without having to use its eyes. Proprioceptors monitor the position and movement of joints and the forces generated

by the muscles. The position and movement of locust leg joints are monitored by seven chordotonal organs, strand receptors, hair plates and a small number of multipolar joint receptors [20].

The proprioceptor which monitors the position of the tibia relative to the femur in the hind leg of the locust is the FeCO (Figure 3.1). It is an elastic strand which crosses the joint and contains approximately 90 sensory neurons [20] (Figure 3.1C). Imposed movement of the tibia causes the FeCO to stretch and this mechanical stimulus is converted into electrical signals by the sensory neurons. These signals are transmitted to motor neurons, either directly or through interneurons, which activate muscle contraction to oppose the movement [20]. Reflexes which resist such passive limb movements are known to occur in the legs of a number of arthropods [30].

Negative, or resistance, feedback such as this helps to maintain postural stability in both invertebrates and vertebrates [28]. These resistance reflexes have been shown to be consistent [44, 132] but depending on the behaviour of the animal they can be turned off or modified in both gain and phase [20, 133]. It should be noted that in vertebrates, the proprioceptors which monitor joint position and are involved with resistance (stretch) reflexes are the muscle spindles and that these, unlike the chordotonal organs in invertebrates, lie within the skeletal muscles [28].

Figure 3.1B and C are drawings of the locust FeCO shown to aid understanding of its structure. The group of neurons which make up the FeCO are attached to the wall of the femur, the tibia and the flexor tibiae muscle by connective ligaments (Figure 3.1B). Some of the stretch sensitive dendrites of these sensory cells project into the apodeme (Figure 3.1C) which connects the FeCO to a protrusion on the tibia near the point where the tibia and femur rotate (main ligament in Figure 3.1B). The neurons in the FeCO are mechanoceptors which convert mechanical stimuli into electrical activity.

As investigations into the properties of the sensory neurons in the locust FeCO stimulate the apodeme and not the sensory neuron directly, the response of these neurons will therefore be affected by the properties of the apodeme. In 1991 Shelton et al. [109] showed that the mechanical FeCO structure was far more complex than had previously been thought. By using scanning electron microscopy their biomechanical study discovered a loop structure in the apodeme connecting the FeCO to the femoro tibial joint (Figure 3.1C).

Shelton et al. [109] and Burrows [20] believed that this mechanical structure would have considerable effect on the response of the sensory neurons in the FeCO. Field et al. [46] proposed that this loop structure forms the basis for mechanical range fractionation. The loop structure in the apodeme consists of strands of different lengths. As the tibia moves, these strands are sequentially tightened and cause different neurons to respond - a mechanical range fractionation mechanism. It has been hypothesised [20] that this mechanism may be used to increase the resolution and hence the sensitivity of the FeCO without reducing its range.

Shelton et al. [109] pointed out that the mechanical properties of the FeCO system need to be

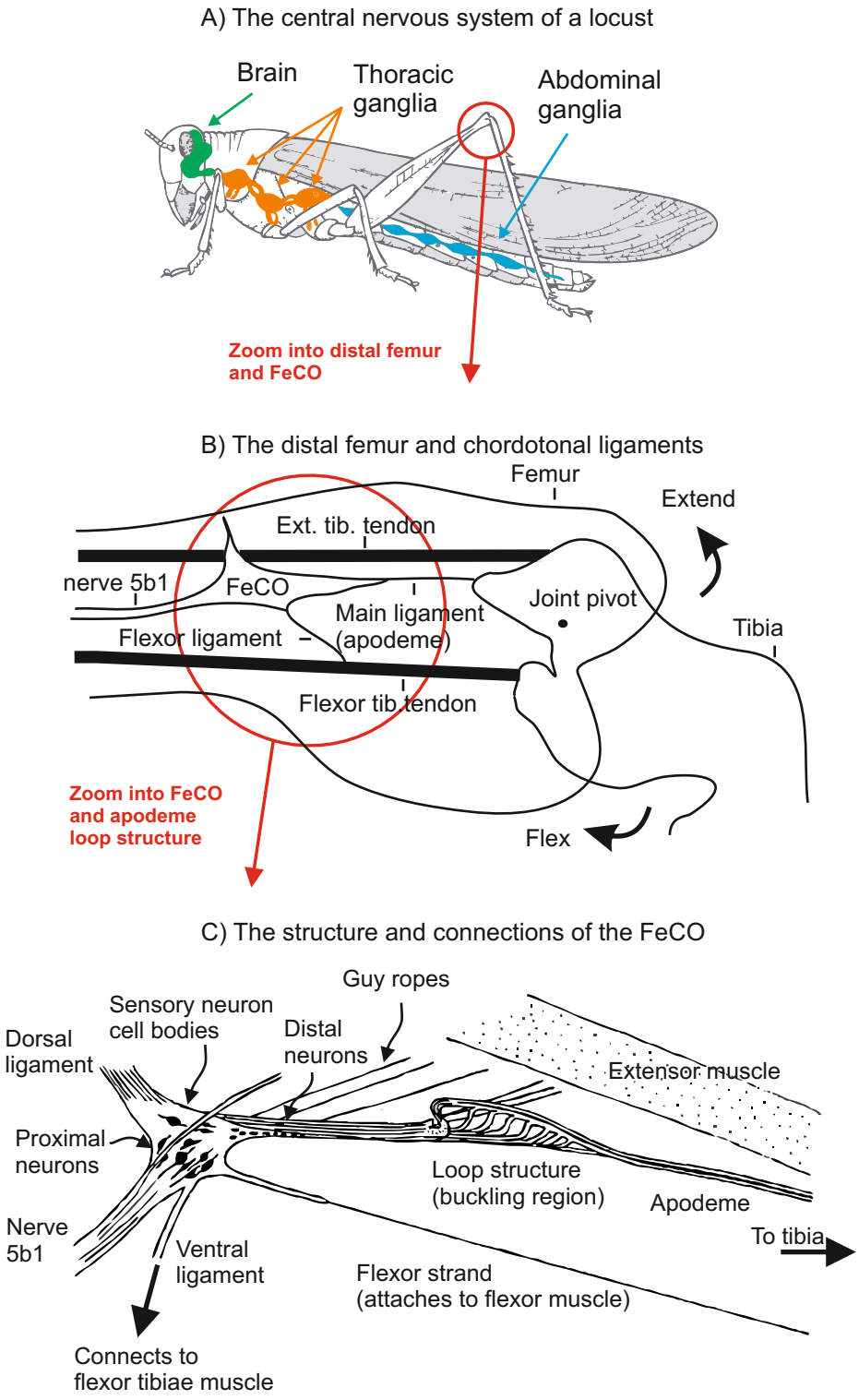

Figure 3.1: Diagrams of the FeCO in the hind leg of a locust. (A) The locust and its central nervous system. (B) The distal femur and the chordotonal ligaments (From [132], Journal of Experimental Biology 116(1):435-461, with permission). (C) The structure and connections of the FeCO based on dissections (Section 4.3.3).

understood before a description of the properties of the sensory neurons would be complete. Investigation of the mechanical components of the FeCO and its attachment ligaments [89] and their contribution to sensory response through direct manipulation and measurement was outside the scope of the current study.

Many of the studies which have investigated the FeCO system through mechanical stimulation [73, 97, 98] do not state which side of the loop structure was grasped and moved. This could result in the generation of inconsistent results between experiments. The loop structure could also easily be damaged and Shelton et al. [109] believed that a damaged loop structure would cause spurious results.

There are four types of neurons which receive direct input from locust FeCO sensory neurons: spiking local interneurons, non-spiking interneurons, motor neurons, and spiking intersegmental interneurons [46]. In the locust, some of the FeCO sensory neurons can make direct connections with several of the nine flexor tibiae motor neurons and other sensory neurons make direct connections with the two extensor tibiae motor neurons, but none connect to both [20]. The synaptic inputs to motor neurons, and their spiking output response, in locust proprioceptive systems and in other invertebrate limb control systems have received much less attention than the sensory neurons. This may be because the response of the motor neurons can be affected by signals from other parts of the locust's nervous system, over which the experimenter has little control.

Due to the relatively large size and small number of motor neurons that activate the tibial flexor and extensor muscles, and unlike the FeCO sensory neurons which are much smaller and more abundant, it is possible to identify the different motor neurons as unique individuals. This allows the models estimated using data from different locusts to be compared, providing valuable insight into the ability of the model to generalise between animals and provides motivation to investigate the response of the motor neurons.

The extensor tibia muscle is controlled by just two excitatory motor neurons, the Fast Extensor Tibia (FETi) and the Slow Extensor Tibia (SETi). It also receives inputs from a common inhibitor [20, 61].

The terms slow and fast do not refer to the speed of the neurons transient response but to the type of muscle fibre which the motor neuron innervates. Slow motor neurons usually fire steadily over long periods and therefore tend to innervate postural muscle fibres which are relatively fatigue resistant. Fast motor neurons may have a more bursty firing pattern and innervate fast twitch muscle fibres [32]. The FETi is a fast motor neuron; its function is to generate rapid jumping movements [20]. This motor neuron produces action potentials during the preparation for jumping and kicking movements (co-contraction phase [18, 19]) and during righting [41]. Recently it has also been shown to be active at lower limb velocities for grooming and scratching movements [100].

The following two sections review the methods which have been used to investigate the sensory neurons in the FeCO and the local interneurons and motor neurons with which they connect (the

femur/tibia control loop). They will explain how these methods have improved understanding of the responses of the sensory and motor neurons to imposed movements of the apodeme of the FeCO.

3.3 Physiological Input Methods for Studying FeCO Function

Early investigations into the function of the sensory, inter and motor neurons in the femur/tibia control loop used simple step, ramp and sinusoidal input signals to move the tibia [116]. These input signals were chosen as they are easy to generate and provide responses which are easy to interpret. They are referred to as physiological input signals in the literature - but do not necessarily provide a good match to the stimuli encountered in the locust's natural environment.

A review of the literature has revealed that there are two methods which have been used to measure the electrical signals produced by the neurons in the FeCO system. The extracellular approach (which uses electrodes placed outside the neurons) has been used to measure the potential difference between two points along the length of a nerve. Recordings using this technique often contain the spiking responses of a number of different neurons, which it is sometimes possible to separate. By using the intracellular approach (placing electrodes within the neuron) it is possible to record both the synaptic and spiking response of individual neurons [132].

3.3.1 Extracellular Studies

The ability of the sensory neurons in the chordotonal organ to transform the mechanical information relating to the joint's position, velocity and acceleration into electrical signals for the nervous system was first investigated using whole nerve recordings [116]. They investigated the static discharge or tonic properties of the sensory neurons when the tibia was set at a number of different positions. Its phasic properties were investigated using sinusoidal and ramp inputs. The terms tonic and phasic are used to characterise neurons by their rate of adaptation. Tonic neurons either adapt slowly or not at all. In contrast, phasic neurons adapt rapidly. Using whole nerve recordings Usherwood et al. [116] were able to establish that the FeCO provides information about joint position (tonic), movement (phasic) and the direction of the movement.

Usherwood et al. [116] were not able to record from individual sensory neurons using the extracellular method so they could only speculate whether the increase in spike frequency with joint angle was due to an increase in firing of the same tonic neuron or different combinations of neurons (range fractionation).

Using intracellular recording techniques (Section 3.3.2), however, Matheson [91] was able to record the signal from individual neurons which showed that some neurons are only responsive to parts of the range of joint angle (range fractionation).

Whole nerve recordings from FeCO sensory neurons made by Usherwood et al. [116] allowed

them to observe that the phasic response of FeCO neurons increases in frequency and reduces in duration as the frequency of the sinusoidal movement increases. They also noted that the response was smaller and briefer with flexion of the tibia. They proposed that the variation in spiking frequency for extension and flexion could be produced because different sensory units responded to different directions of movement. This response type could also be produced by a single neuron; the change in spiking frequency could be due to the elastic properties (elastic hysteresis) of the FeCO or signal transformation by the neurons [20]. Intracellular studies, the results of which are presented in the next section, have shown that single neurons show hysteresis in their spiking frequency response.

3.3.2 Intracellular Studies

Whole nerve recordings can only give limited insight into the function of the sensory neurons in the FeCO and cannot provide details about the individual neurons. The responses of the individual sensory neurons in the chordotonal organ of a locust were first investigated by Zill [132] in 1985. These investigations used intracellular techniques to measure and record the electrical responses produced when the tibia was moved with physiological input signals. It should be noted that only the responses of the proximal group of FeCO sensory neurons (Figure 3.1C) have ever been investigated. The proximal group contains thirty to fifty sensory neurons [89]. The work by Zill was extended by Matheson in 1990 [90] and he classified the sensory neurons in the FeCO into different categories of mechano-sensitivity and mapped out their locations. In broad terms, Matheson found sensory neurons which respond to tibial position only; velocity only; position and velocity; and more complex stimuli such as velocity and acceleration and position. Matheson also found that the neurons were usually directionally sensitive, responding to either flexion or extension of the tibia but not usually to both. Some of the neurons responded over the full range of joint angles, while others responded only to parts of the range, providing evidence of range fractionation.

The sensory neurons in the FeCO of the stick insect were shown by Hofmann [60] and Buschges [25] to have similar response types to those found in the locust. Recordings from sensory neurons in the stick insect mesothoracic FeCO are used to illustrate the different response types (Figure 3.2A - D). A position sensitive neuron fires with increasing spike frequency as the leg is flexed (Figure 3.2A). As the leg is flexed back to its starting position the difference in its response compared with extension can be seen (Figure 3.2A); it should be noted that this response is nonlinear. The position and velocity sensitive neurons in the stick insect and locust can show hysteresis of up to 20% in their spiking frequency response depending from which direction the leg approaches a particular position [20]. This led Burrows to suggest that this direction dependent response is caused by the viscoelastic ligament which attaches the tibia to the FeCO, as a viscoelastic material exhibits hysteresis. The responses of velocity, acceleration and deceleration sensitive neurons are shown in Figure 3.2B, C and D respectively. Accelerations only occur at the beginning and end of ramp and hold signals. The response of the velocity sensitive neuron in Figure 3.2B is nonlinear as it responds more to the positive

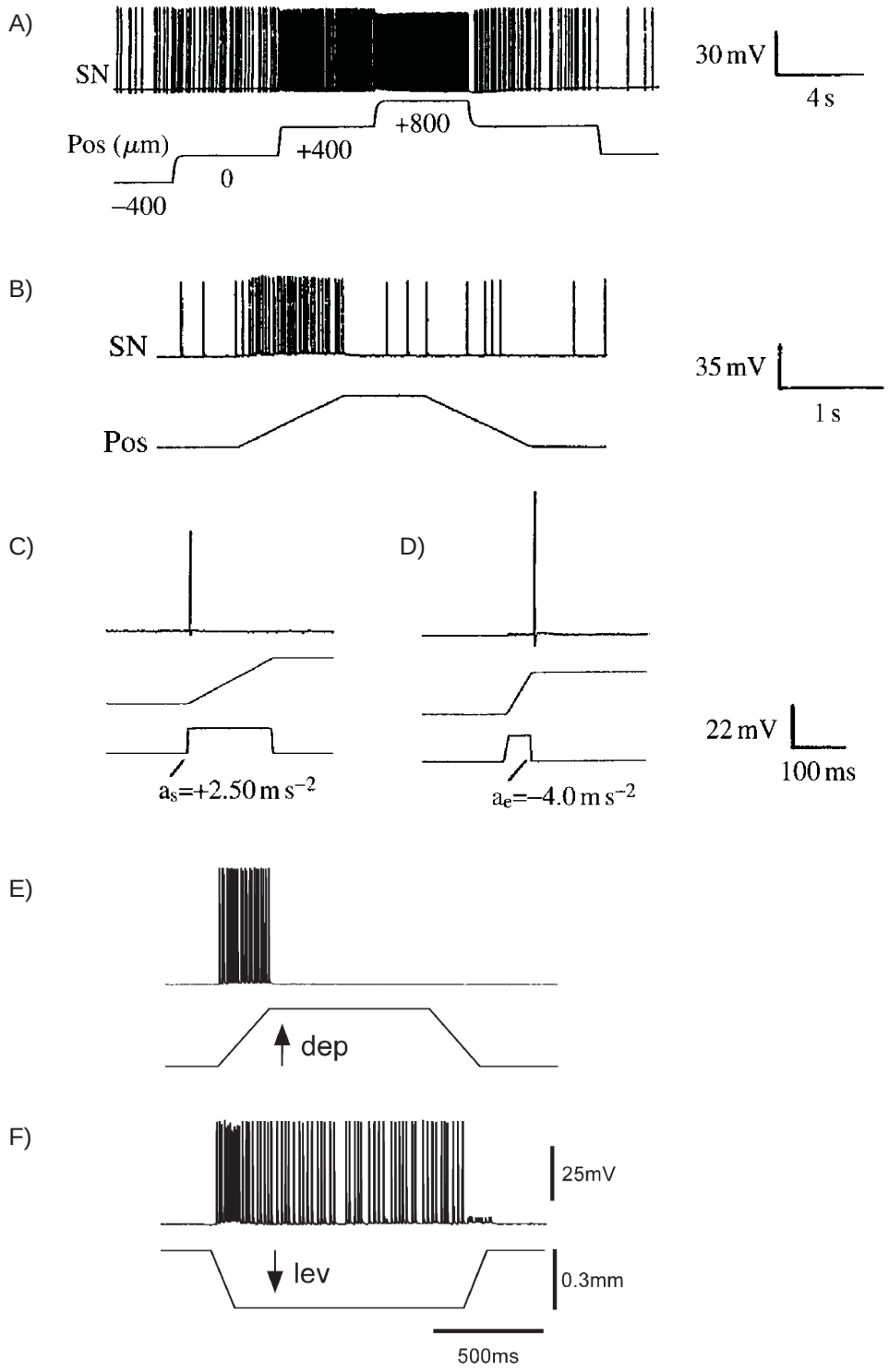

Figure 3.2: Selection of sensory neuron response types from the stick insect and crab joint chordotonal organs. (A) Position, (B) velocity, (C) acceleration and (D) deceleration response types from the stick insect (From [25], Journal of Experimental Biology 189(1):285-292, with permission). (E) Velocity and (F) velocity-position responses from the crab (From [54], Journal of Neurophysiology 89(4):1815-1825, with permission). Depression represented by dep and levation by lev.

gradient than to the negative gradient.

Many of the response types found in the sensory neurons of the stick insect and locust chordotonal organ have also been found in the chordotonal organ which monitors a crab's coxo-basal leg joint [54]. Figures 3.2E and F show the velocity and velocity-position response types from the crab.

The reflex effects that imposed movements have on the motor neurons in the femur/tibia control loop have also been investigated using using intracellular methods [44, 45].

3.3.3 Limitations of Studies using Physiological Input Signals

Physiological input signals are a useful tool for investigating the neurons in the femur/tibia control loop and they generate responses which are relatively easy to interpret and link to locust limb function. Since many different physiological signals need to be applied to ensure complete characterisation of the system, this method can be experimentally time consuming. This can potentially be a problem when trying to record from the smaller sensory- and inter- neurons in this system as they have a relatively short experimental life (minutes). Also, if the ensemble of input signals does not sufficiently cover the operating range of the system, important response types may not be observed. Physiological input signals, however, cannot fully represent the dynamics of the response of the system because under 'real' operating conditions the input will contain changing positions, velocities and accelerations. An alternative approach which has been used to analyse the response of neurons in femur/tibia control loops uses the system identification approach with a white noise input signal (Section 3.4).

3.4 White Noise System Identification Methods for Studying System Function

A white noise signal can be used to drive a system at all frequencies within its operating range and hence it is useful for analysing the response of sensory neurons in the chordotonal organ. This approach ensures that the system is excited at all frequencies in its operating range, is experimentally quick and provides a model of the system which characterises its properties.

Physiological systems are often represented by nonlinear Volterra/Wiener models [87]. Nonlinear models are required as neurons often exhibit nonlinear behaviour, such as saturation and single direction responses. For example, the response of the velocity sensitive neurons shown in Figure 3.2B and E is nonlinear as the neuron only responds to depression of the leg. If the system was linear, then the sensory neuron would have also responded to the section of the ramp signal with a negative gradient. With white noise stimulation, and unlike the case when physiological input signals are used, it is not immediately clear to what part of the white noise signal the neurons in the chordotonal organ respond. It is the shape of the Volterra/Wiener model kernels which provides information about the way in which the neuron responds.

3.4.1 Modelling the System using the White Noise Approach

Kondoh et al. [73, 97, 98] applied the white noise modelling approach to the sensory and motor neurons in the femur/tibia control loop. They used adult male and female locusts, *Schistocerca gregaria*, in their experiments. The animals were fixed in modelling clay and the apodeme of the FeCO was exposed and grasped by forceps. To ensure that movement of the apodeme did not cause movement of the tibia, it was cut close to its connection with the tibia. The FeCO is mechanically linked to some of the muscles which cause joint movement so contraction of these flexor and extensor muscles will change the response properties of the sensory neurons in the FeCO. The amount that these muscles could contract was limited by fixing the position of the leg. The forceps were attached to a shaker (Ling Altec 101, LDS Test and Measurement) which was driven by a filtered Gaussian White Noise (GWN) signal. The GWN signal was generated using a random binary generator (CG-742, NF Circuit Design Block) which was bandlimited in frequency to between 0 and 200 Hz. This signal was further filtered by a low pass filter with either a 27, 58 or 117 Hz cut off frequency before it was applied to an amplifier, the output of which drove the shaker. The spiking output of the sensory neurons of the FeCO was measured using electrodes inserted into their axons [23]. Electrodes were also used to measure the synaptic inputs (graded potentials) to the flexor and extensor tibia motor neurons (electrodes were inserted into the cell bodies).

The chosen model structure was made up of the first and second order kernels of the Wiener series (Section 2.4.2); the first order kernel provides a model of the linear response of the system, the second order kernel models the nonlinear response. A Schmitt trigger circuit was used to convert the spikes in the spike train signals into unitary pulses of 2 ms duration. The parameters of the first and second order kernels were estimated using Lee and Schetzen's [80] method which cross correlates the output signal with the bandlimited (0-200 Hz) GWN input signal (Figure 3.3). It should be noted that this input signal was low pass filtered before being applied to the amplifier which drives the shaker. This approach was taken because Kondoh et al. [73] found that using the band limited GWN (0-200 Hz) input signal rather than the low pass filtered input signal (cut off frequency of either 27, 58 or 117 Hz) applied to drive the shaker amplifier improved the performance of their models (Figure 3.3). The properties of the low pass filter, the shaker amplifier and the shaker itself are therefore included in the model.

3.4.2 Model Interpretation

The first order kernel represents the response of a linear system to an impulse. Kondoh et al. [73] write "The first-order kernel of an FeCO afferent represents its response to an "impulse like" change of the femorotibial joint angle (flexion of the tibia followed by an extension back to the starting angle)". Figure 3.4 shows the first order kernels of sensory neurons which are sensitive to just the position of the tibia and to both the position and the velocity of the tibia. The units of the first order kernel are spike density, $spikes \cdot deg^{-1} \cdot s^{-1}$. In [73], Kondoh et al. interpret the initial positive increase in the kernel as indicating an increase in spike frequency

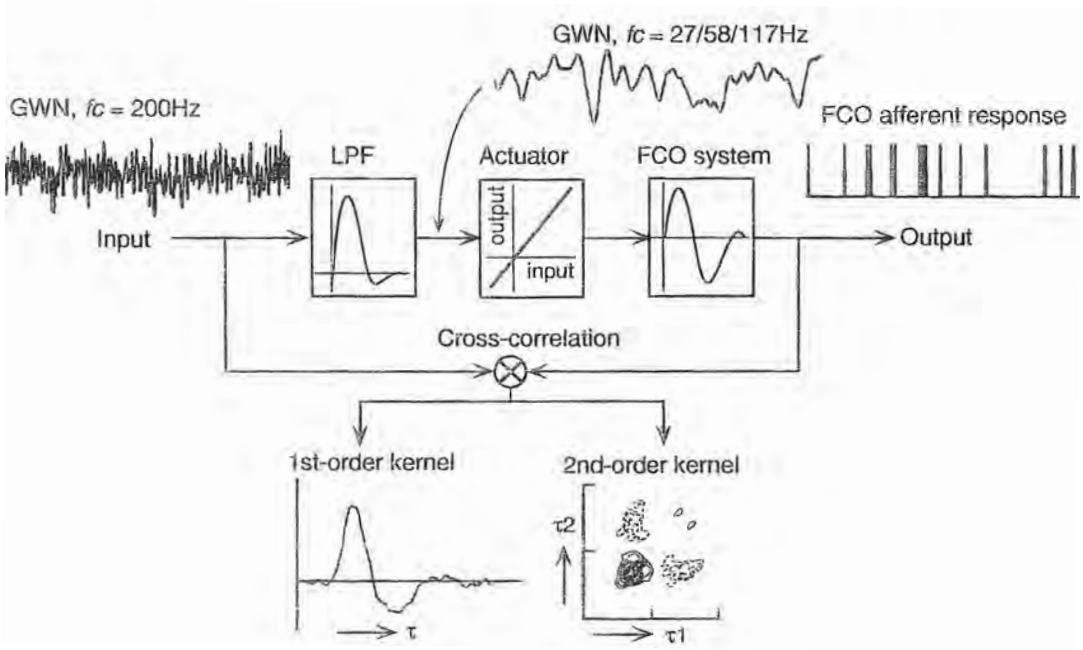

Figure 3.3: Gaussian White Noise system identification set-up used by Kondoh et al. [73] and the 1^{st} and 2^{nd} order Wiener kernels of a FeCO sensory neuron (From [73], Journal of Experimental Neurophysiology 73(5):1829-1842, with permission).

and therefore propose that the neuron is flexion sensitive (Figure 3.4). A decrease in spike frequency is indicated by a negative kernel value, so a kernel with a peak which initially goes negative indicates an extension sensitive neuron. An interpretation based purely on the first order kernel is incomplete as it is necessary to take into account both the shape of the 1^{st} and 2^{nd} order Wiener kernels to ascertain whether a neuron is flexion or extension sensitive, as was carried out in [117]. This is because the 1^{st} order kernel, which represents the linear response of the system, will be sensitive to both flexion and extension.

Analysis of the shape of the first order kernel in the time and frequency domain is used to characterise the response property of each neuron. Kondoh et al. [73], using the white noise method, found all of the response types described in the study of locust chordotonal organ by Matheson [90], who used physiological input signals. Kondoh et al. [73], however, concluded that the use of the narrow, artificial classes by Matheson [90], Hofmann [60] and Buschges [25] can be misleading. They argued that very few neurons are sensitive to only one movement type and the majority of sensory neurons display different response types depending on the frequency of stimulation.

The second order, nonlinear, kernels are more difficult to interpret. Kondoh et al. [73] only used the diagonal part of the second order (two dimensional) kernel in their analysis. As with other investigations [54], the off diagonal elements were ignored. The conclusion drawn about the second order kernel was that it represents a compression nonlinearity or half-wave rectification and allows the model to represent the direction coding property of the sensory neurons.

It is important to emphasise that the models presented by Kondoh et al. [73] are more than just models of the sensory neurons in the femur/tibia control loop . These models are estimated

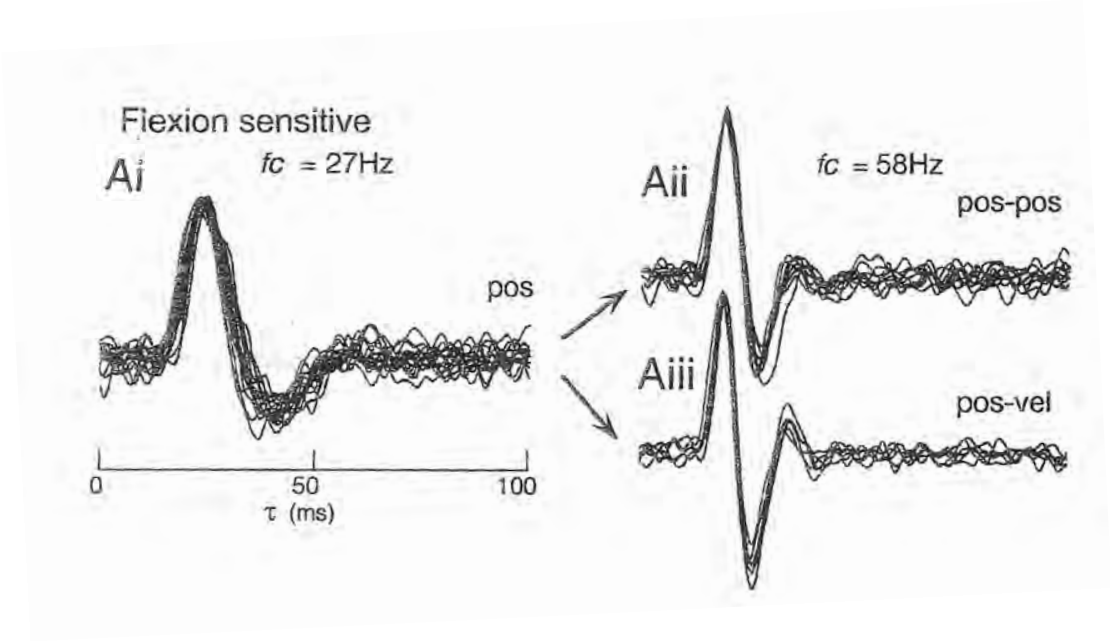

Figure 3.4: Models of flexion sensitive sensory neurons from the locust FeCO (From [73], Journal of Experimental Neurophysiology 73(5):1829-1842, with permission). The shape of the first order kernel is used to classify the neurons into different response types. (Ai) The kernel of a position sensitive neuron. (Aii) The response of some of the neurons remains the same with increased stimulus frequency, (Aiii) but some of the neurons exhibit a position-velocity response.

from input and output signals measured and recorded from experiments on locusts. The input signal, used to estimate the parameters of the model, is not the position of the FeCO apodeme but is the bandlimited (0-200 Hz) GWN signal which is low pass filtered before being applied to the amplifier which drives the shaker. The output signal is the electrical output signal produced by either sensory or motor neurons. So, for example (see Figure 3.3), a model of a sensory neuron actually includes the properties of: the shaker amplifier; a low pass filter (with a cut off frequency of either 27, 58 or 117 Hz) applied to the white noise signal before the signal is fed into the shaker; the shaker; the mechanical properties of the apodeme and the transformation of the mechanical stimulus to dendritic membrane current followed by its transformation into spiking neuron output.

Newland and Kondoh also fitted the Wiener kernels between the GWN signal used to move the apodeme of the FeCO and the synaptic inputs measured in the soma of the flexor [97] and extensor [98] tibiae motor neurons. Their results will be discussed in Section 5.3.3 to aid comparison with the results obtained in the current study. The application of the white noise approach to other animals will be considered in the next section.

3.4.3 Application of White Noise Analysis to Other Animals

The study by Gamble and DiCaprio [54] uses the white noise system identification technique with a Wiener model structure to investigate the properties of the sensory neurons in the chor-

dotonal organ monitoring joint position in the leg of a crab. This study noted that the mean rate of firing of the sensory neurons during the first few seconds of white noise stimulus was higher than that in their steady state (~35 s) response.

Mitsis et al. [93] have recently used white noise system identification to model the sensory neurons in a spider's lyriform organ, a strain sensor embedded in its exoskeleton. These investigations show that the sensory neurons are able to encode more than one aspect of movement (position, velocity and acceleration) depending on the frequency of excitation and reinforce the results published by Kondoh et al. [73]. It is interesting to note that Gamble and DiCaprio [54] and Mitsis et al. [93] actually measure the position of the sense organ they are stimulating and use this as the input signal for model estimation. The methods which have been previously used to mechanically excite mechanical sense organs and measure their displacement will now be considered.

3.4.4 Mechanical Excitation Method and Position Measurement

Most investigations into the properties of the sensory neurons in the FeCO have excited the FeCO apodeme rather than moving the tibia (Kondoh et al. [73, 97, 98]). It is desirable to use this method because if the whole tibia is moved the FeCO sensory neurons and the inter and motor neurons to which they connect may receive inputs from other sense organs in the leg (for example other chordotonal organs and strand receptors).

Kondoh et al. [73] used a shaker to excite the apodeme of the FeCO. The GWN input signal used to drive the shaker was assumed to equal the GWN modulated position of the apodeme [97]. This assumption was tested by using a strain gauge attached to a piece of plastic as a displacement sensor. This sensor was fixed at 90° to the forceps and the output of the strain gauge was recorded. The strain gauge output signal and the input signal were compared and found to be similar.

A more rigorous approach was taken by Gamble and DiCaprio [54] and Mitsis et al. [93]. These investigators measured the position of the connection to the mechanical sense organ being stimulated and used this signal as the input signal for estimating the models parameters. Mitsis et al. [93] used a piezoelectric stimulator (LVPZ translator and PZZ controller from Polytec Physik-Instruments) with position control feedback to move the spider's lyriform organ. The position of this mechanoreceptor was measured using a position transducer which is part of the piezoelectric stimulator. Gamble and DiCaprio [54] used an electromechanical puller to move the crab's coxo-basal chordotonal organ. Their puller was constructed from a five inch diameter loud speaker cone. The position of the chordotonal organ was monitored by an optical position sensor which consisted of a light source, photodiode and optical wedge scale. This system is based on the system described by Hofmann and Koch [60].

3.5 Conclusions

Initial investigations into the function of the FeCO used physiological input signals (steps, ramps and sinusoids) to move either the tibia or the apodeme which connects the FeCO to the tibia. These input signals are amenable to interpretation and have provided a valuable insight into the function of the sensory neurons in the locust FeCO and many other animal mechanoreceptors. The disadvantage of this approach is that it is time consuming as many different stimuli need to be applied to characterise the response of the components of the FeCO system. Also, even though steps, ramps and sinusoids have been named "physiological" signals they may not be particularly well matched to the movements of the tibia which occur when the locust is in its natural environment.

A GWN input signal has been used in more recent investigations into locust and crab joint chordotonal organs and other mechanosensory systems. A white noise signal contains equal power at all frequencies and so excites the system at all frequencies within its operating range. The advantage of this approach is that it is quick, requiring less than 30 seconds of input/output response for system characterisation over a wide frequency and amplitude range. A GWN input has desirable properties for system identification but is very different from the stimuli the chordotonal organ receives under natural operating conditions. It is likely that sensory systems have evolved to be optimised for processing natural stimuli (Felson and Dan [43]) so the use of GWN probing signals may not reveal important natural responses. Compared with physiological and white input signals, natural stimuli are functionally more relevant and have been shown to be more effective for driving sensory neurons [115].

The majority of studies of insect mechanoreceptor systems have used either physiological input signals or GWN system identification techniques with Volterra or Wiener model structures. The Volterra/Wiener models generated using the white noise technique are most often validated by testing the ability of the model to predict the response of the mechanoreceptor to a white noise stimulus signal different from that used to estimate the model. French et al. [53], in what would appear to be the only previous test of the ability of a model generated using the white noise system identification technique to predict the response of a mechanoreceptor to a physiological input signal, found that even a third order nonlinear Volterra model could not adequately predict the responses of the mechanoreceptor to a step signal. This suggests that care should be taken when interpreting and linking the responses of the model to the natural function of the mechanoreceptor and the limb which it controls. It also provides motivation for the current study to test if models fitted between the GWN input signal and the response of the system, measured in the FETi motor neuron, can predict the system's response to physiological and, ideally, natural stimuli such as walking.

Spiking and non spiking neurons in the local networks that control limb movements in both the locust and crab are known to adapt their output amplitude or spike firing rate to repetitive stimulation [44, 54, 98, 116]. However, little work has been carried out to investigate the property of these systems during their transient response. Furthermore, as the nonlinear Wiener/Volterra series models used in previous studies [54, 98, 117] contain many parameters they require large

amounts of data (typically 20 s) to obtain robust parameter estimates. Methodological issues, therefore, restrict modelling analysis to the systems steady state response. However, the dynamics and nonlinearity of the transient (adapting) response which occurs during the first few seconds of stimulation may be more important to system function. It would appear that no previous studies have applied the GWN system identification technique to investigate adaptation in invertebrate local reflex control systems.

Chapter 4

FETi Responses to GWN, Sinusoidal and Walking Stimulation

4.1 Introduction

The aim of the work presented in this chapter was twofold. First to verify, and if necessary modify and improve, the experimental methods used in previous studies [73, 97, 98, 117] of locust neuromuscular reflex limb control to GWN stimulation. Second to extend those studies to consider how the Fast Extensor Tibia (FETi) motor neuron in the locusts femur/tibia reflex limb control loop (Section 1.2) responded to potentially more relevant sinusoidal and walking based stimulation signals. These responses are also used in Chapters 5 and 7 for model validation.

This chapter commences by describing the animal preparation and recording methods. Next, the methods used to acquire the walking stimulus signals and transform the femoral tibial joint angle into apodeme position are described. As the model of FETi included the shaker amplifier, shaker and forceps mount, the properties of this part of the system and their effects on the model were also investigated. Analysis of the rate of adaptation (power) of FETi to GWN, sinusoidal and walking stimulation was used to aid definition of the transient and steady state FETi response sections. This chapter concludes by investigating if the response of FETi to sinusoidal and walking stimulation is consistent along the length of individual recordings and across animals.

4.2 Methods

4.2.1 Animal Preparation and Recording Method

Preparation of the adult male and female locusts, *Schistocerca gregaria*, was carried out by Professor Philip Newland following the method described in [98]. The locusts were fixed, ventral side uppermost, in modelling clay (Figure 4.1). A hind leg was rotated through 90° and fixed anterior face uppermost. The angle between the femur and the abdomen was set at 60°; the angle between the tibia and the femur was also set at 60° (Figure 4.1). A section of

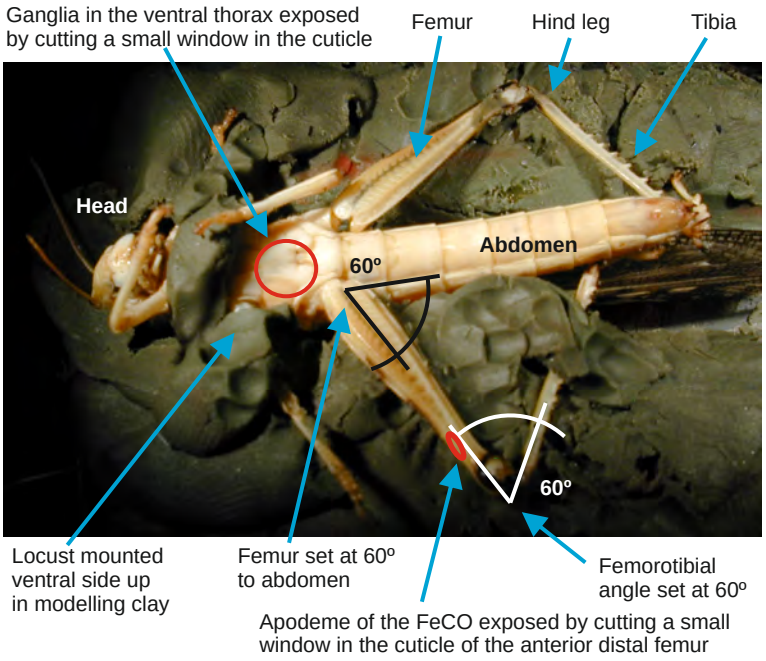

Figure 4.1: Locust mounted in modelling clay.

exoskeleton (cuticle) in the ventral thorax was removed to expose the meta and mesothoracic ganglia (Figure 1.1 and 4.2B). The ganglia were supported by fixing them to a wax coated silver platform using fine pins (Figure 4.2B). This platform also served as the reference electrode and was connected to the ground input of an amplifier (Axoclamp 2A amplifier, Axon Instruments, US). The thorax was continuously bathed in locust saline [63], supplied at room temperature (22-24°C) from a feed attached to the back of the platform. The enzyme protease (Sigma type XIV) was applied to soften the sheath surrounding the metathoracic ganglia to allow it to be penetrated by an electrode. After 1 minute, the protease was washed off with locust saline solution, applied using a pipette. A glass micro-electrode, filled with a conducting electrolyte (2M potassium acetate), was driven though the sheath and into the soma of the FETi motor neuron. The DC resistance of the electrode was estimated to be between 50-80MΩ. A chlorided silver coated wire, inserted into the glass electrode, was used to connect the electrolyte to the Axoclamp amplifier. The excitatory post-synaptic potentials measured in the soma of the FETi motor neuron were amplified before being converted from analogue to digital form using an Analogue to Digital (AD) input on a USB 2527 data acquisition board (Measurement Com-

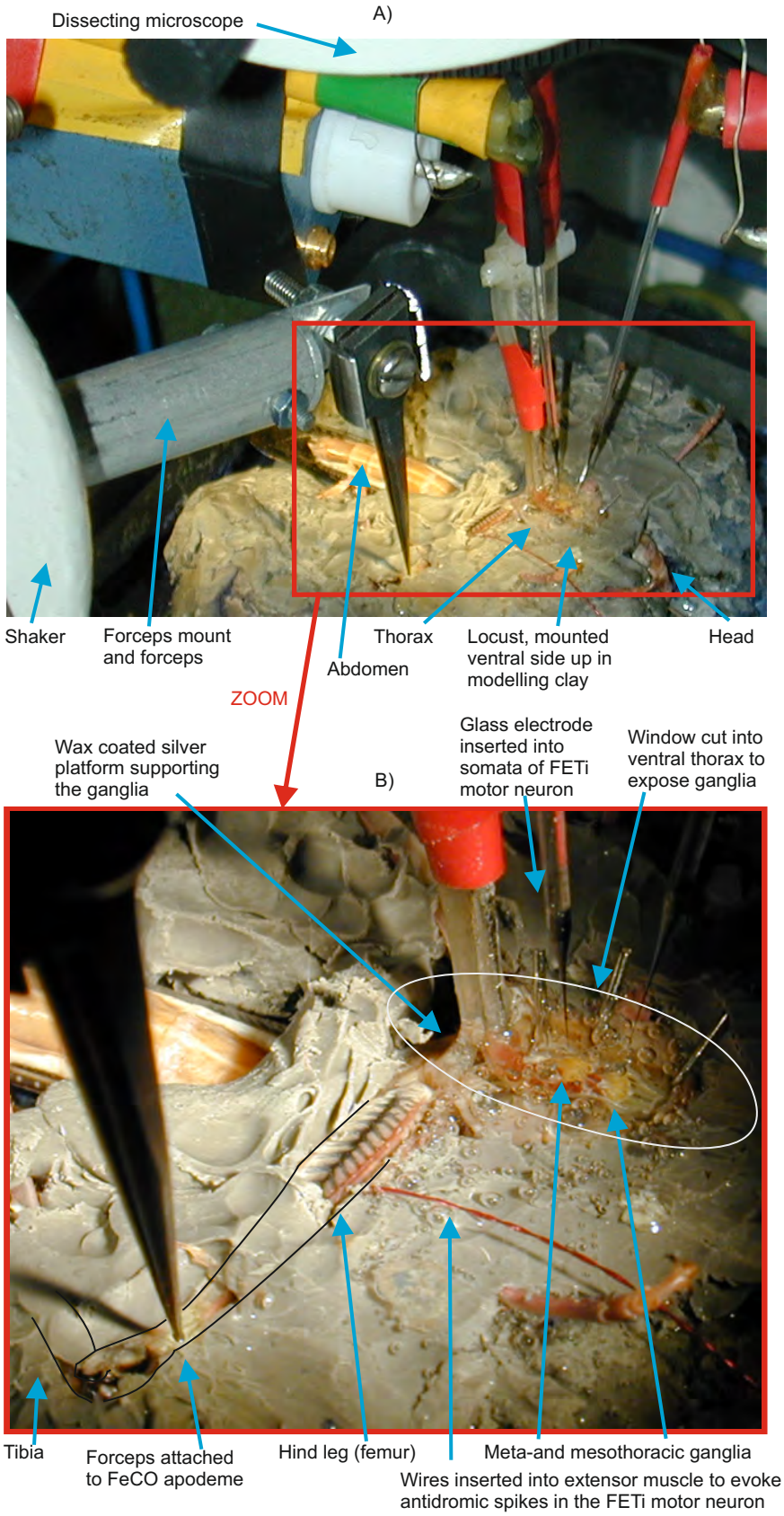

Figure 4.2: Locust preparation. (A) Overview of locust preparation and (B) magnified view of preparation. Note the outline of the hind leg has been traced to aid understanding.

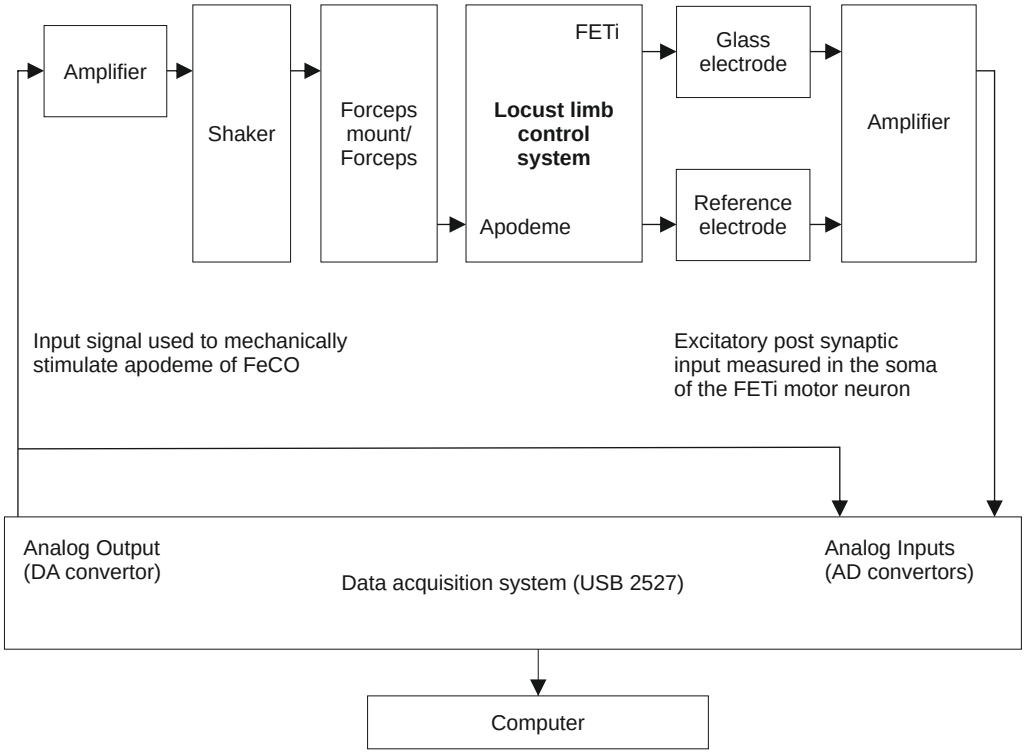

Figure 4.3: Block diagram of system set-up.

puting, Norton, MA, USA)(Figure 4.3). The digital signals were stored for further analysis on a computer hard-drive.

Identification of the FETi motor neuron was made based on a description of the location of its relatively large soma (40μm) [22] and by the fact that it produces unique antidromic (spike conduction opposite to its normal direction of travel) spikes when the extensor muscle is made to twitch [62]. Contractions were produced by applying a voltage to a pair of 50μm diameter copper wires, insulated except at the tips, inserted into the muscle (Figure 4.2B). Next, the apodeme of the FeCO was exposed (by cutting a small window in the cuticle of the anterior distal femur) and attached to the forceps (Figure 4.2B). The position of this window was determined from results of dissections to identify the position of the FeCO apodeme loop structure and supporting guy ropes (Section 4.3.3, Figure 4.9) and also from information reported by Shelton et al. [109]. The window was kept as small as possible to ensure that the loop structure and supporting guy ropes were not damaged but large enough to allow free movement of the end of the forceps. Keeping the window small also helped to minimise the risk of the leg becoming damaged if the locust tried to kick. Forceps were attached to the apodeme close to its insertion point into the tibia. To ensure that movement of the apodeme did not cause movement of the tibia, it was cut close to its connection with the tibia. The FeCO is mechanically linked to some of the muscles which cause joint movement so contraction of these flexor and extensor muscles would change the response properties of the sensory neurons in the FeCO and potentially the response of the FETi motor neuron. The amount that these muscles could contract was limited by fixing the position of the leg; the femoral tibial angle was set at 60°.

The forceps were attached to a shaker (Ling Altec 101, LDS Test and Measurement, Denmark) and were moved by different stimulus signals (Section 4.2.2). Digital stimulus signals were generated in MATLAB and converted into analogue form using one of the Digital to Analogue (DA) converters on the USB 2527 data acquisition board and amplified before driving the shaker (Figure 4.3). The amplifier was built by the author for the current project based on a design used by Newland [73]. The Graphical User Interface and software to drive the USB 2527 data acquisition board was also developed by the author using MATLAB and the data acquisition toolbox.

The results in Section 4.3 are based on six successful recordings from the FETi motor neuron in different animals made by Professor Philip Newland.

4.2.2 Method of Stimulus Signal Generation and Conversion of Apodeme Position into Femoral Tibial Angle

A description of the methods used to generate a bandlimited GWN signal, three walking signals and a range of sinusoidal stimulus signals, which were applied to the shaker to move the apodeme of the FeCO, is provided in the next two sections.

The stimulus signals, applied to the shaker, caused the apodeme of the FeCO rather than the angle of the tibia relative to the femur to be changed. It was therefore necessary to find a method to convert apodeme position into femoral tibial angle to allow stimulus signal calibration to be carried out. This method was also required to allow joint angle signals, generated from videos of the locust walking, to be converted into apodeme position signals which could be applied to the shaker.

Rather than rely on previous results [44] which used callipers to measure apodeme position, experiments were conducted in the current study using image processing methods. The apodeme of the FeCO was exposed by dissection and photographed with femoral tibial joint angles ranging from 10° (flexed) to 190° (extended) at 10° intervals (Figure 4.4). A software program was written in MATLAB by the author to allow the position of the FeCO apodeme to be marked on the images. The marker was placed on a distinct colour change which occurred at approximately 0.5mm from the insertion of the apodeme into the tibia (Figure 4.4). A linear function was fitted to the mean value obtained from three successful experiments in different animals. This function allowed apodeme position to be converted into femoral tibial angle.

GWN and Sinusoidal Stimulus Signals

A GWN signal was generated in MATLAB using its random number generator ('randn'). This independent random number generator draws its values from a Gaussian distribution with a mean of zero and a standard deviation (σ) of one. This signal was bandlimited between 0 and 50 Hz using a 5^{th} order Butterworth low pass filter with a cut off frequency of 50 Hz. It was then scaled so that approximately 99.7% (-3σ to 3σ) of its values fell between 5° and 115°

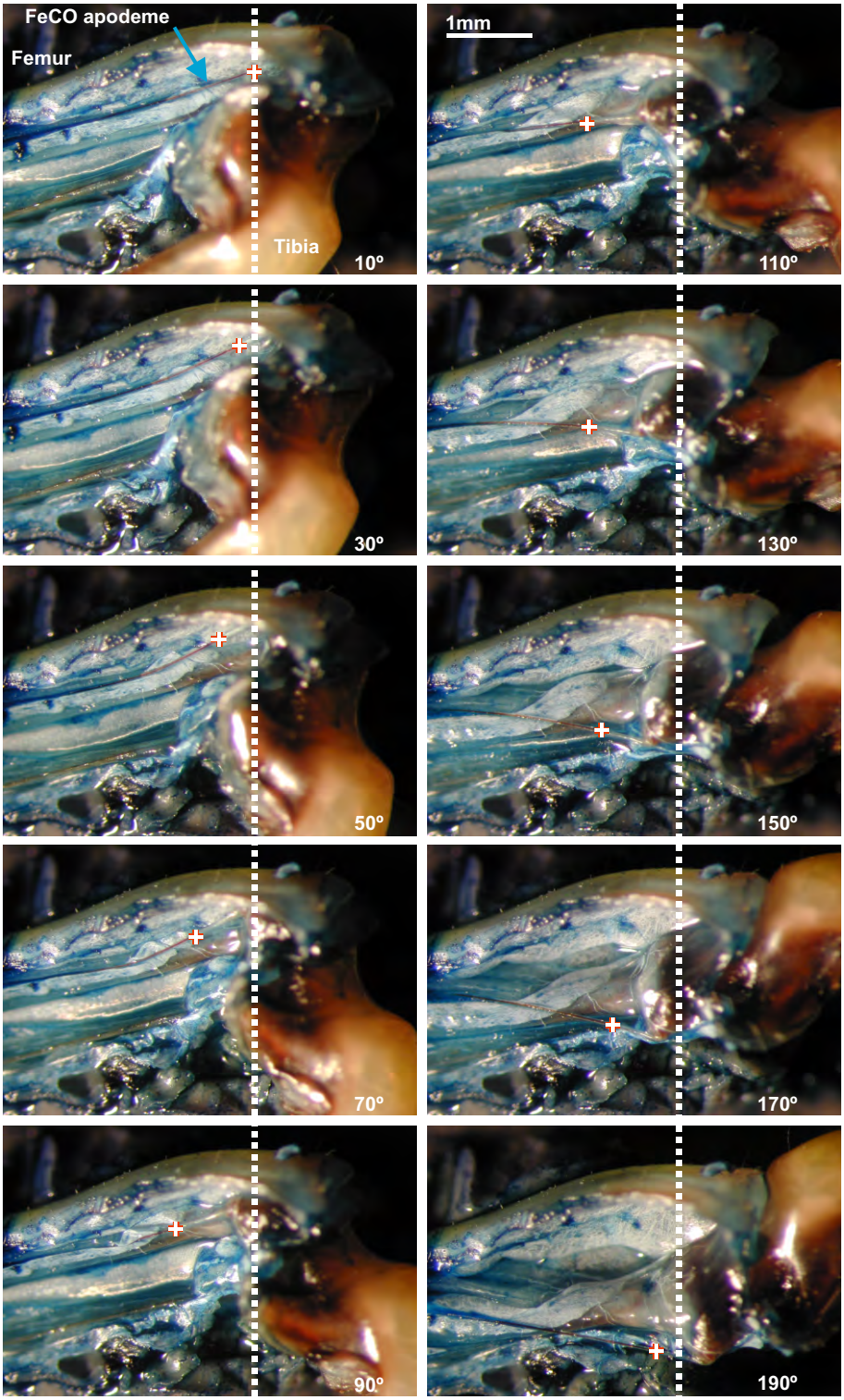

Figure 4.4: Photographs showing displacement of the FeCO apodeme with femoral-tibial joint angle. The dotted vertical line is used to show the position of the apodeme when the tibia is set at 10°. Note it was possible to mark the apodeme because of a distinct colour change.

[98]. This matches the range of apodeme displacement covered by the GWN stimulus signal used in the study by Newland and Kondoh [98].

The scaling factor was determined experimentally using the following method. The bandlimited GWN signal was generated in MATLAB and applied to the shaker amplifier using the USB 2527 data acquisition board. The shaker was disconnected from the locust's apodeme. A Keyence Laser displacement sensor (LK-G3001V controller, LK-G32 Head, Keyence, Milton Keynes, UK) was used to measure the displacement of the forceps attached to the shaker for a given GWN input signal. Apodeme displacement was converted into joint angle and its amplitude distribution was calculated. This experiment was repeated a number of times, adjusting the gain factor applied to the GWN input signal in each run, until approximately 99.7% of the values of the joint angle distribution fell into the desired range. In addition sinusoidal stimulus signals, with amplitude values which corresponded to a joint range between 16° and 102°, were generated with frequencies of 1, 2, 5 and 10 Hz. The focus of this study is on the response of FETi to the 5 Hz sinusoidal stimulation signal in an attempt to make this signal functionally relevant to match the stepping frequency of 5.1 Hz 0.56 Hz (n=10) observed by Blackburn et al. [13].

Walking Stimulus Signals

Natural stimulus signals were estimated from video recordings of the locusts walking, obtained from a high speed camera (Redlake Imaging, Tring, UK) with a frame rate of 250 frames per second. Filming was carried out in a temperature controlled room at 20°C. Walking was initiated by prodding the locust's abdomen. Video sequences were saved in Audio Video Interleaved (.avi) format and then loaded into a program written in MATLAB by the author, a screen shot of which is shown in Figure 4.5. Only video sequences in which the locust moved perpendicular to the camera were retained for analysis.

The Audio Video Interlaced file was de-interlaced by replacing the data in odd rows of each frame with that in its even rows (line doubling). Markers were then manually placed down the centre of the tibia and the femur of the hind leg in each frame (Figure 4.5). The angle between the markers was calculated in each frame of video. Two walking signals, containing the variation in joint angle with time, were extracted from the captured video footage.

The length of these signals was extended, by repeating them, to create walking input sequences between approximately 15 and 25 seconds long (Figures 4.12 and 4.13). These input signals will be referred to as walk 1 and walk 2. To reduce the possibility of high frequency components being introduced into these extended signals, the transitions between each section were smoothed using a 4^{th} order low pass Butterworth filter with a cut off frequency of 50 Hz. The filter was applied in the forward and reverse direction to avoid introducing any phase delay (zero phase). Joint angle was converted into apodeme displacement using a linear function (Section 4.3.1).

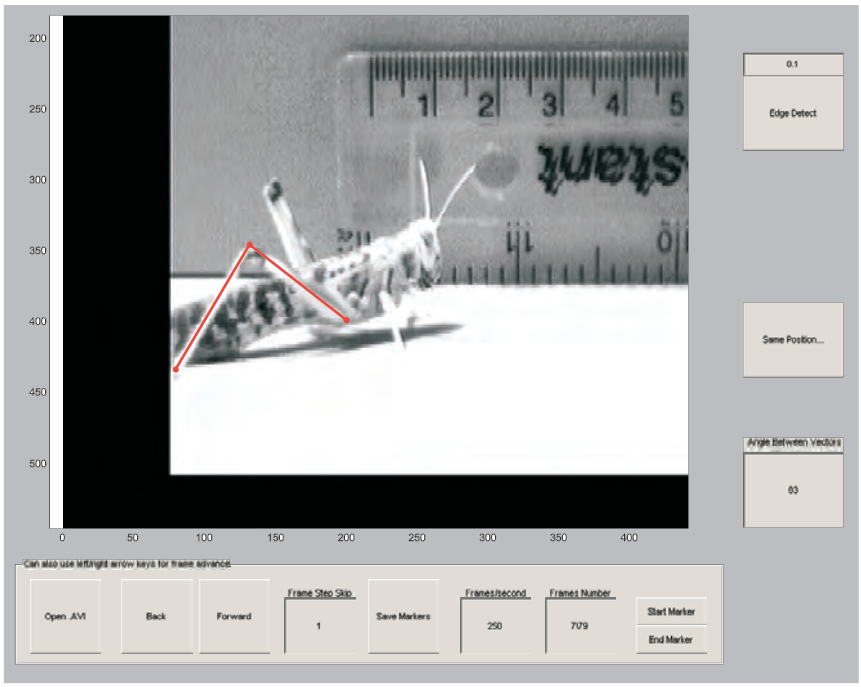

Figure 4.5: Locust hind leg tracking software. This software allowed the angle between the tibia and the femur to be marked in each frame of the locust walking videos. The variation of joint angle with time was used to create the walking stimulation signals.

4.2.3 Shaker Amplifier, Shaker and Forceps Model

The mechanical and electrical properties of the shaker amplifier, shaker, forceps mount and forceps (Figure 4.6) were included in the previous models of the sensory neurons and motor neurons published in [73, 97, 98]. These studies assume that these components have a flat frequency response with no delay. Measurements conducted by the current study revealed a resonant behaviour when the old forceps mount was used so a new forceps mount was constructed (Figure 4.6).

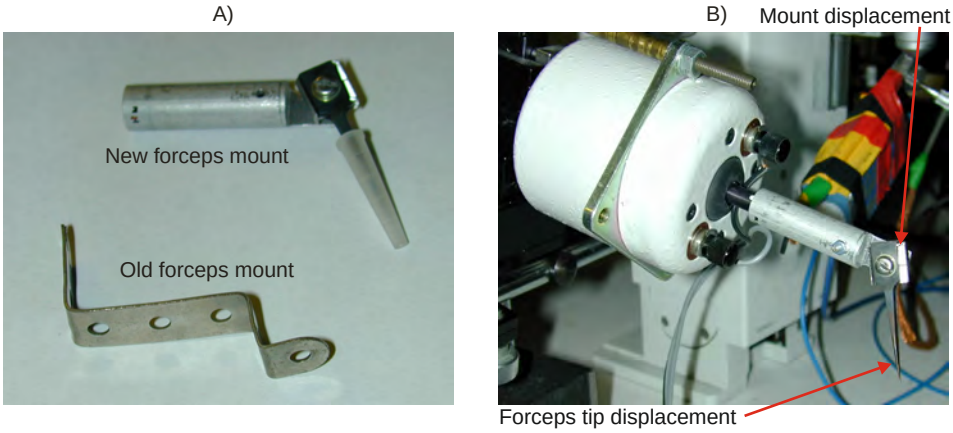

Figure 4.6: (A) New and old forceps mount and (B) the new forceps mount attached to the shaker. (B) The location where mount displacement and forceps tip displacement were measured.

Ideally the displacement of the locust's apodeme should be measured directly, enabling the response of the amplifier, shaker and forceps mount to be removed from the model of FETi. It was hoped that this could be achieved in the current study, using the available Keyence laser displacement measuring system with the signal produced being used for system identification. The complex locust preparation and equipment set up (Figure 4.2), coupled with the size and range of the Keyence laser displacement sensor, prevented the use of this system. Instead, for the current study, as in the work by Newland and Kondoh [98], the voltage input to the shaker amplifier was used as the input for system identification.

As the amplifier, shaker, forceps mount and forceps could potentially mask or alter the models of FETi it was important to gain an understanding of their mechanical and electrical properties. This was achieved using a system identification approach similar to that used for constructing nonlinear models of FETi but using a linear FIR model.

$$y(t) = \sum_{\tau=0}^{T-1} h(\tau)u(t-\tau) \tag{4.1}$$

This states that the output of the model, $y(t)$, is the weighted sum, $h(\tau)$, of the current and past input samples, $u(t)$. The Impulse Response Function (IRF) is represented by $h(\tau)$. Linear FIR models were fitted (Least Squares method, Section 2.2.2) between the band limited (0-200 Hz) GWN input voltage to the shaker and the displacement of (i) the forceps mount (ii) a point near the end of the forceps and (iii) a point near the end of the forceps when they were attached to the apodeme. The frequency dependent amplitude and phase characteristics of these components could then be observed by calculating the frequency response of the FIR model. Displacement was measured using the Keyence laser displacement sensor. The data sheet for this sensor states that it can measure displacement with an accuracy of 10's of μm which is small compared to the 1200 μm total movement range of the apodeme (Figure 4.7).

4.2.4 Adaptation of Response Power

The power in the response of FETi to GWN, sinusoidal and walking stimulation was calculated from five animals using 1 s long non overlapping windows. It should be noted that data from Animal 3 were excluded because the recording was short. The responses to the different stimulation signals allowed the transient and steady state response sections to be defined. They also allowed the effect of the different stimulation signals on the rate of power adaptation to be investigated.

The change in signal power over time was modelled using the exponential equation $y(t) = A + Be^{(\frac{-t}{\tau})}$ where t represents time and $y(t)$ represents base line normalised power. The base line power (BLP) value was calculated from a 1 s window taken from each recording before stimulation was applied. The final steady state power was represented by A, and $A + B$ represents the peak power amplitude. Adaptation rate was quantified by the time constant τ which represents the time taken for the BLP normalised neural power to fall to 63.2% of its final steady state value. The Nelder Mead (simplex) [94] iterative search method was used to esti-

mate the time constant τ and A and B.

4.2.5 Response Consistency

The consistency of the response of FETi to sinusoidal and walking input signals was investigated using a coherent averaging approach. The coherent averaging method is commonly used as a method of background noise reduction [131]. Noise reduction is achieved by averaging the response of a system to a repeated stimulus. Assuming that the system's response does not vary with time, the level of random background noise should be reduced by this process. The response of FETi to sinusoidal stimulation was segmented by detecting the position of the positive peak values in the sinusoidal input signal. Averaging was carried out over two period cycles. The response of the system to walking stimulation was segmented by detecting the position of the positive peak values in the walking input signals.

The consistency of the system's response was quantified by comparing the standard deviation of the measurement noise before (baseline measurement noise) and after (steady state measurement noise) stimulation was applied. Note that it was assumed that the measurement noise consisted of additive spontaneous background neural activity and electrical measurement noise (Section 1.2). The baseline measurement noise was measured by calculating the standard deviation of a 1 s (500 sample) section of the response of FETi before the stimulation signal was applied (the standard deviation was calculated along the length of the signal). An estimate of the measurement noise present in the steady state response of the motor neuron (steady state measurement noise) was obtained by subtracting the coherent average values from the values of the first cycle in the steady state response. The steady state measurement noise was quantified by calculating the standard deviation of this signal (the standard deviation was calculated along the length of the signal). If the baseline and steady state measurement noise values are similar then this would suggest that stimulation of the FeCO did not change background neural activity.

4.3 Results and Discussion

4.3.1 Joint Rotation to Apodeme Displacement

As described in Section 4.2.2 it was necessary to find a method to convert femoral tibial joint angle into apodeme displacement. The drawing shown in Figure 4.7A was created to show how the eccentric insertion of the FeCO apodeme into the tibia converts the rotation of the tibia into approximately linear movement at the FeCO. It was made by tracing the position of the FeCO apodeme over a range of different joint angles. Joint angles were measured between the centre of the femur and the centre of the tibia.

The displacement of the apodeme of the FeCO with different joint angles was successfully measured in three locusts and is plotted in Figure 4.7B. The results obtained by Field and

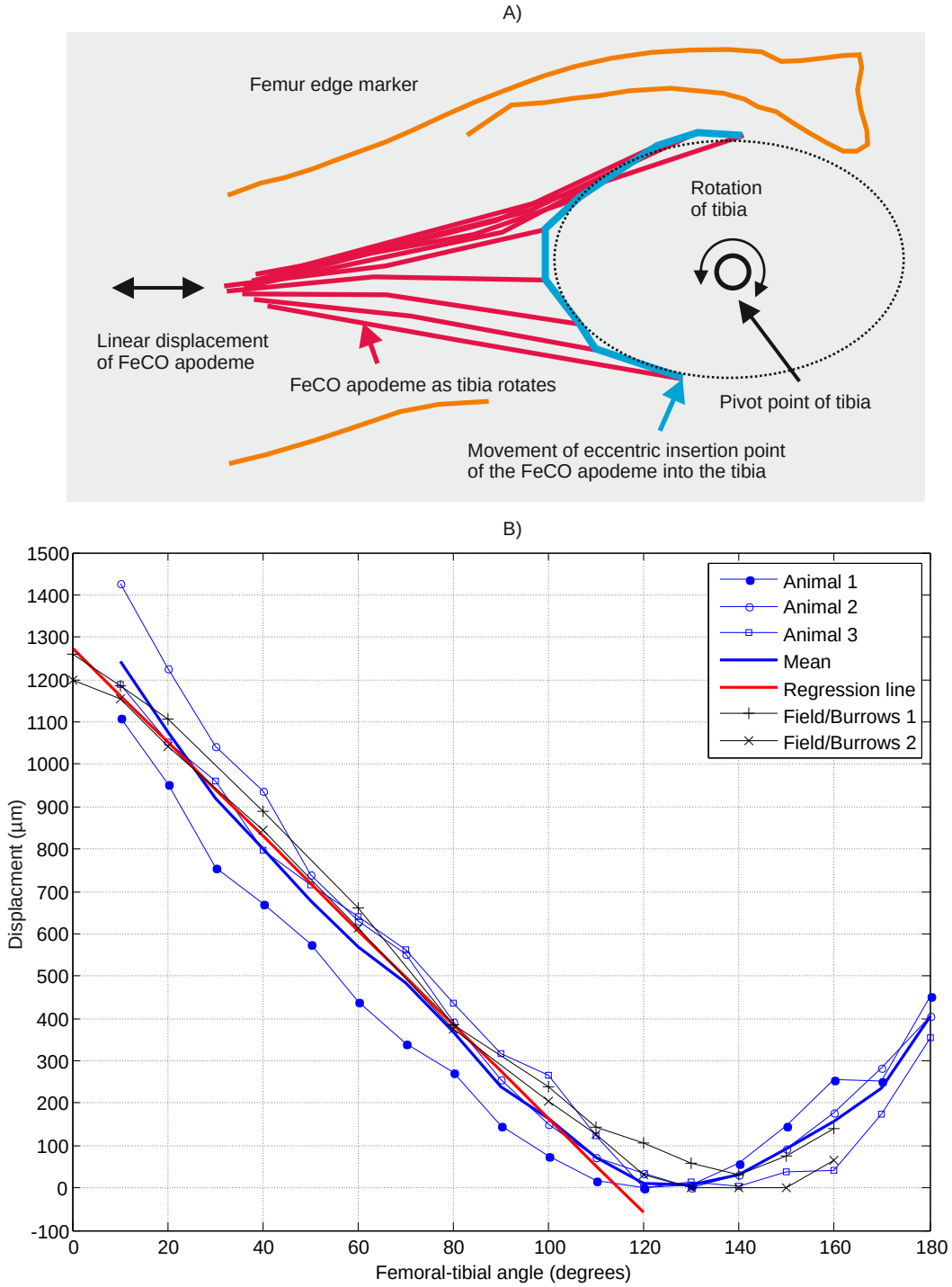

Figure 4.7: (A) Illustrative sketch showing the displacement of the apodeme with femoral tibial joint rotation. (B) Plot showing how the displacement of the FeCO apodeme varies with femoro-tibial angle for three animals (A1-A3), the mean (n=3) and the regression line (from experiments carried out in this study). This relationship is predominantly linear over the range of angles used in this study (0 to 120°). Ambiguity in this relationship exists between displacements of approximately 0 and 500μm. However, the tibia only extends past 140° during kicking movements which occur at frequencies greater than 100 Hz [21]. As the highest frequency of stimulation applied in the current study is 50 Hz, this ambiguity can be ignored. The results presented by Field and Burrows [44] have been plotted on the graph for comparison.

Burrows [44] were copied from a graph presented in their paper and they have been plotted for comparison alongside the results obtained in the current study (Figure 4.7), revealing a close match.

The current study will only consider the responses of FETi to femoral tibial joint angles between 0 and 120° to allow comparison with the results obtained by Newland and Kondoh [98]. The relationship between joint angle and apodeme position in this range can be represented with sufficient accuracy using a linear function (Figure 4.7). Linear regression was used to fit the linear function to the mean of these data to allow joint angle to be converted into apodeme position.

It should be noted that there is ambiguity in the relationship between displacements and angles over the range of 0 and 500μm. The tibia, however, only extends past 140° during kicking movements which occur at frequencies greater than 100 Hz [21]. The focus of the current study was on slower movements excluding kicks with stimulation signal frequency limited to 50 Hz [21].

It should also be noted that as in a previous study [44], given that the apodeme to tibial insertion is composed of hard rather than soft tissue, it was assumed that the steady state displacement angle relationship (Figure 4.7) holds for dynamic excitation signals.

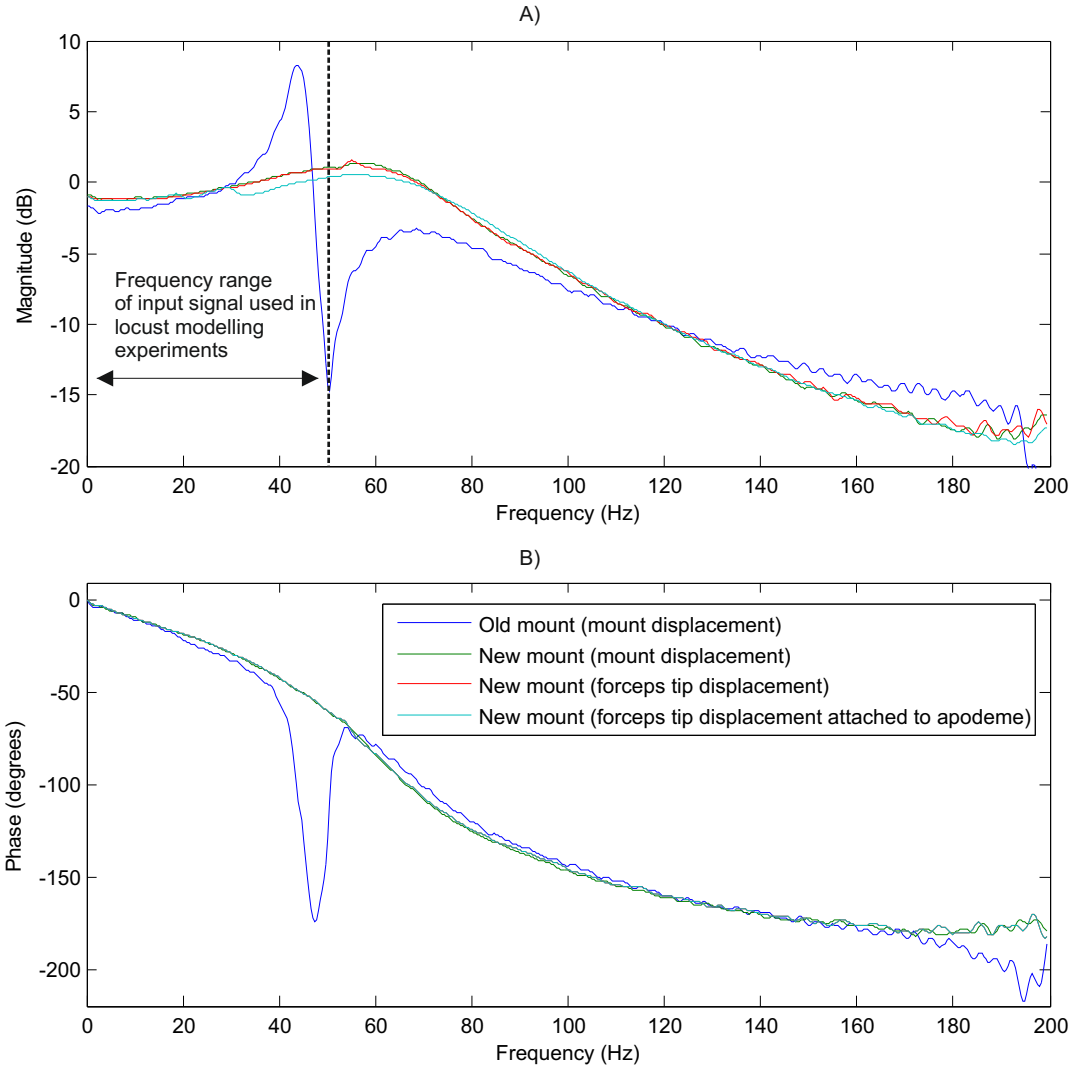

Figure 4.8: (A) Magnitude and (B) phase response of linear FIR models of the shaker amplifier, shaker, forceps mount (old and new) and forceps. The frequency response of the model of the old mount shows a sharp resonance between 43 and 50 Hz which could significantly modify the characteristics of the model of FETi. The frequency response of the new forceps mount, designed by the author, moves any resonance to a higher frequency, out of the range of interest.

4.3.2 Shaker and Forceps Model

The frequency response of linear FIR models of the shaker amplifier, shaker and the old and new forceps mounts are plotted in Figure 4.8. The first model was fitted between the bandlimited (0-200 Hz) GWN input signal applied to the shaker amplifier and the output signal, given by the displacement of the 'old' forceps mount as used by Newland and Kondoh [98]. The displacement of the mount was measured on the forward facing surface of the forceps where they are attached to the mount (Figure 4.6 B, mount displacement). The frequency response of the linear model shows a sharp resonance between 43 and 50 Hz (Figure 4.8A, old mount) which could significantly modify the characteristics of the model of FETi.

The resonance probably occurred because the old forceps mount was made from a bent piece

of Meccano strip which was quite flexible (Figure 4.6A). A new forceps mount was designed by the author, made from thin-walled aluminium tube that was both light and rigid, moving any resonance to a higher frequency, out of the range of interest. With the new forceps mount the resonance disappeared (Figure 4.8).

Recordings of the displacement at a point near the tip of the forceps were made when the forceps were attached and also when they were not attached to the apodeme. The frequency response of the model obtained when displacement was measured near the tip of the forceps was very similar to that obtained when measurements were taken at the forceps attachment point on the mount (mount displacement, Figure 4.8). When the forceps were attached to the apodeme the frequency response showed slight damping between 30 and 65 Hz (Figure 4.8A).

The magnitude response of the linear FIR model of the shaker amplifier, shaker, new forceps mount and forceps when attached to the apodeme is flat within 2dB between 0 and 50 Hz. The %MSE performance of the model (Section 2.3) was <1% and its impulse response clearly decayed to zero before the end of the filter.

In the current study, therefore, it was considered that the amplitude response of the electromechanical arrangement at the input could be neglected. The phase response of the model is approximately linear between 0 and 50 Hz. Assuming a linear phase change ϕ of 1°/Hz the group delay of the FIR filter, the derivative of the filter's phase with respect to frequency, can be calculated using

$$G = \frac{\Delta\phi_{degrees/Hz}}{360} \tag{4.2}$$

resulting in a group delay of approximately 2.8 ms. As the majority of this delay (∼)2 ms was caused by the Keyence laser displacement sensor's signal processing module (based on calculations from the data sheet) rather than the amplifier, shaker, forceps mount and forceps, it was also neglected in further work.

4.3.3 Loop Structure

A drawing of the loop structure of the apodeme (Figure 4.9A) was made from three successful dissections of the locust's hind leg, an example of which can be seen in Figure 4.9B and also from information provided by Shelton et al. [109].

Reference to this drawing has enabled the location of the loop structure relative to the markers on the exterior of the leg to be determined. This information has allowed the dissections carried out in the current study to be more accurately positioned, enabling the apodeme to be grasped between the loop structure and its connection into the tibia thereby minimising the risk of causing damage to this structure. It should be noted that the properties of the loop structure are included in the models of FETi. It is likely that this structure has a strong nonlinear response. These dissections have also revealed a previously not reported bifurcation of the flexor strand (Figure 4.9B).

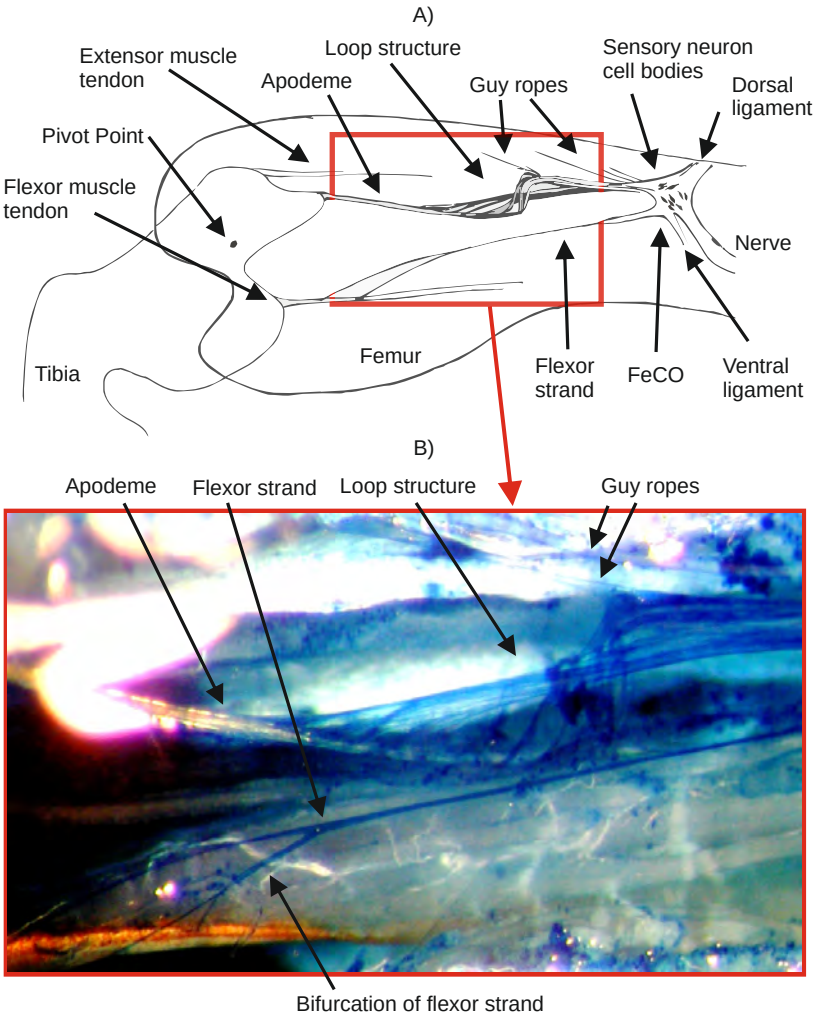

Figure 4.9: (A) Drawing of loop structure and (B) a photograph of one of the dissections showing loop structure.

4.3.4 Typical Responses of FETi to GWN, Sinusoidal and Walking Stimulation

The band limited (0-50 Hz) GWN, 5 Hz sinusoidal and the two walking stimulus signals are plotted in the time and frequency domain in Figures 4.10 to 4.13 respectively, along with an example of typical post synaptic responses recorded in the soma of the FETi motor neuron. As was found in other investigations which used similar input signals [44, 98] to stimulate the FeCO only synaptic inputs were recorded in FETi. Measurement noise was taken as the response of FETi prior to stimulation. It should be noted that baseline drift was removed using a high pass filter with a cut off frequency of 0.2 Hz (Section 5.2.1).

Transient and steady state sections of FETi responses were defined using visual analysis of the signals (Figures 4.10 to 4.13 respectively) and the mean power level (Section 4.3.5, Figure 4.14). The steady state section of FETi response was defined as the response which occurred after 10 s of stimulus onset, for example between 13 and 40 s in Figure 4.10A. The transient section was defined as the response which occurred within the first 3 s after stimulus onset, for

example between 3 and 6 s in Figure 4.10A. A transition period occurs between the transient and steady state sections (Figure 4.10A).

An example of the response of FETi to GWN stimulation of the FeCO is shown in Figure 4.10A. The high level of measurement noise can be seen when the input signal is constant (0-3 s). Zooming into a section of steady state response allows its synaptic nature (continually varying with time) to be seen (Figure 4.10B). The band limited (0-50 Hz) characteristic of the GWN input signal is shown in its power spectrum (Figure 4.10C). The majority of power in the response of FETi to this input signal and in the measurement noise is also found in the frequency range between 0 and 50 Hz (Figure 4.10C). The amplitude distribution of the band limited GWN input signal is shown in Figure 4.10D.

The response of FETi to 5 Hz sinusoidal stimulation is shown in Figure 4.11A. As with the GWN stimulus signal, transient (2-5 s) and steady state (15-38 s) responses are present. Zooming into a 0.6 second period of the steady state response (Figure 4.11B) allows the consistency of the response of the system to be seen. The consistency of the response of the system to sinusoidal inputs is explored further in Section 4.3.6 using a coherent averaging approach. Field and Burrows [44] observed response adaptation and consistency in FETi when the FeCO was stimulated using a repetitive 2 Hz triangular signal.

The nonlinear half wave rectifying nature of FETi to sinusoidal stimulation can clearly be seen by plotting its output signal in the time and frequency domain (Figure 4.11B and C). FETi receives excitatory inputs when the leg is flexed (Figure 4.11B), and no inputs when the leg is extended, behaviour consistent with a reflex response. Analysis of the response of the system to 5 Hz sinusoidal stimulation in the frequency domain reveals that most of the power in the output of FETi is contained within the 5 Hz fundamental and the 10 Hz first harmonic; there is less power in the second to fifth harmonics (Figure 4.11C). The difference between the amplitude distribution of this sinusoidal input signal and the GWN signal should be noted (Figures 4.10D and 4.11D respectively). The sinusoidal input spends most of its time at the extremes of its range of movement while the GWN signal spends most of its time about the neutral position (60°).

The response of FETi to walking inputs are shown in Figures 4.12 and 4.13. As walk 1 (Figure 4.12A and B) spends most of its time in a range of extended positions, between 60 and 80°, there is less response from FETi than for walk 2 (Figure 4.13A and B). A larger response is measured from FETi when it is stimulated with the walk 2 input signal (Figure 4.13A and B) because this stimulus spends most of its time in a range of flexed positions (20 to 60°), where the reflex response of the system occurs. The large peaks in the amplitude distribution plots (Figures 4.12D and 4.13D) at 60° represent where the repeated sections of signal have been joined. In walk 2, the locust rests with its joint angle at 45° (Figure 4.13B at 16 s) and this causes the large peak in the amplitude distribution plot (Figure 4.13D) at 45°. The fastest step cycle found in the two walking signals was approximately 4 cycles per second, the slowest approximately 1 cycle per second. These values fall within the range found by Burns [17] in his more detailed investigation into locust walking patterns. They are also similar to those

found by Blackburn et al. [13].

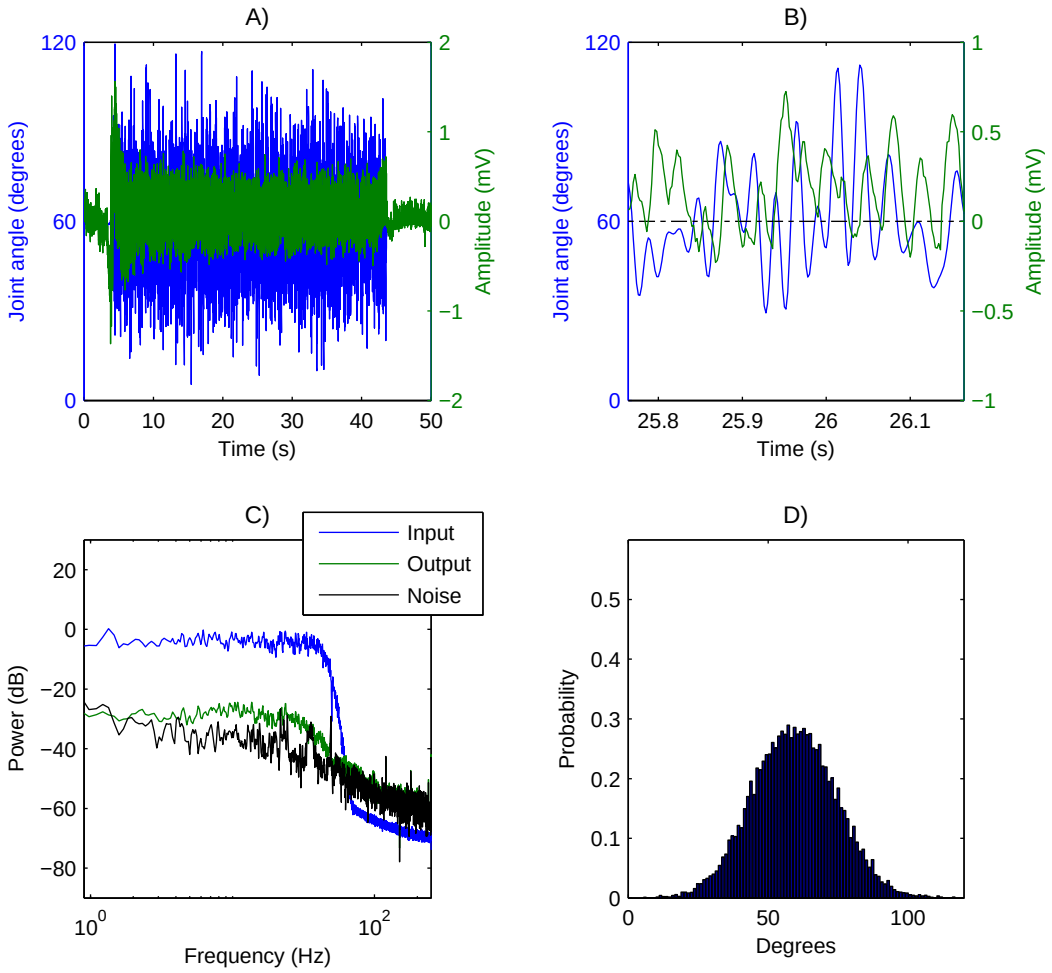

Figure 4.10: (A) Typical response of FETi to GWN stimulation. (B) A zoom into the steady state section shows the synaptic nature of the motor neuron's response. Leg flexion occurs between 0 and 60° and extension between 60 and 120°. Excitatory and inhibitory inputs are represented by positive and negative voltages respectively. (C) An estimate of the power spectrum of the input signal, the response of FETi (Output) and the measurement noise (Noise). Measurement noise was taken as the response of FETi prior to stimulation. (D) The amplitude distribution of the input signal. Note that baseline drift was removed using a high pass filter with a cut off frequency of 0.2 Hz (Section 5.2.1).

4.3.5 Power Adaptation and the Definition of Transient and Steady State Sections

The mean power (n=5) and ± 2 standard deviations of the response of FETi to GWN and sinusoidal stimulation are plotted in Figure 4.14A, where S1, S2, S5 and S10 represent the 1, 2, 5 and 10 Hz sinusoidal stimulation frequencies. The mean power (n=5) and ± 2 standard deviations of the response of FETi to GWN and walking stimulation are plotted in Figure 4.14B, where W1 and W2 represent the two walking stimulation signals walk 1 and walk 2. The mean power was calculated using 1 s long non overlapping windows.

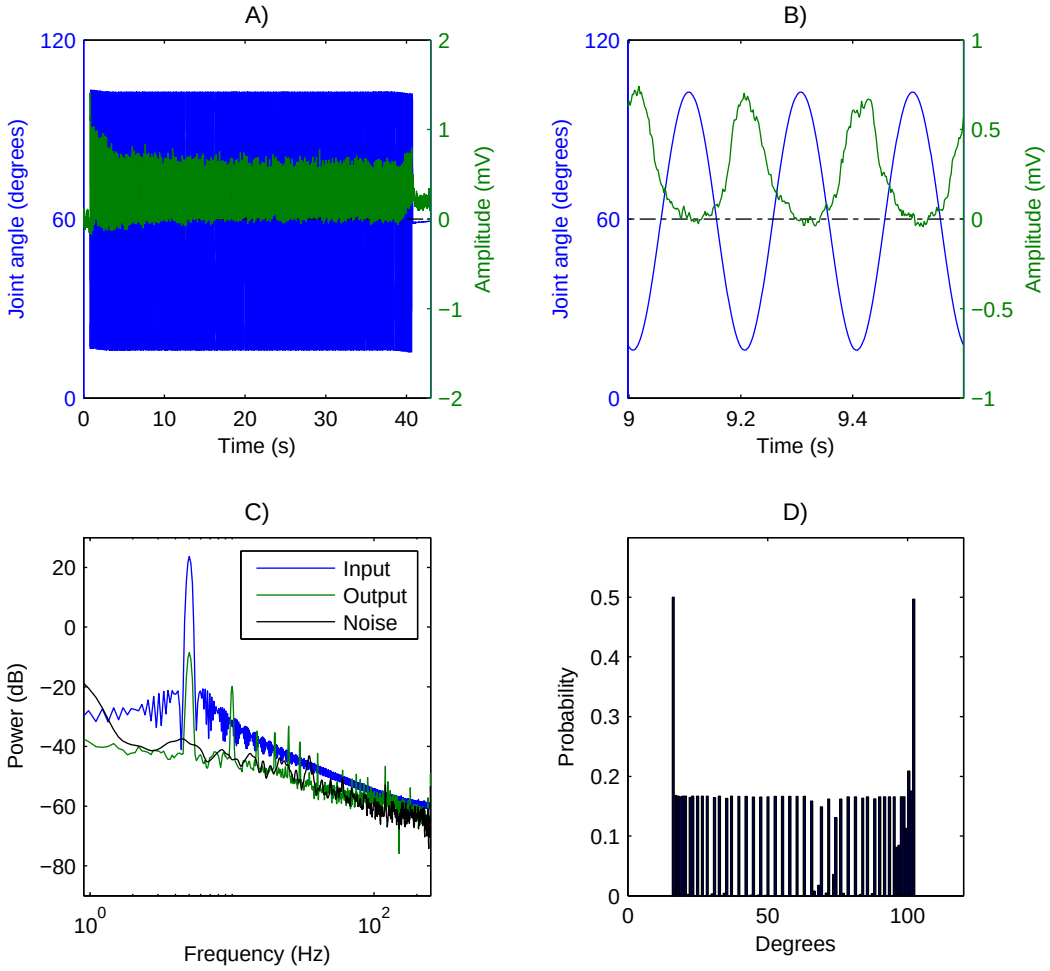

Figure 4.11: (A) Typical response of FETi to 5 Hz sinusoidal stimulation. (B) A zoom into the steady state section shows the synaptic nature of the motor neuron's response. Leg flexion occurs between 0 and 60° and extension between 60 and 120°. Excitatory and inhibitory inputs are represented by positive and negative voltages respectively. (C) An estimate of the power spectrum of the input signal, the response of FETi (Output) and the measurement noise (Noise). Measurement noise was taken as the response of FETi prior to stimulation. (D) The amplitude distribution of the input signal. Note that baseline drift was removed using a high pass filter with a cut off frequency of 0.2 Hz (Section 5.2.1).

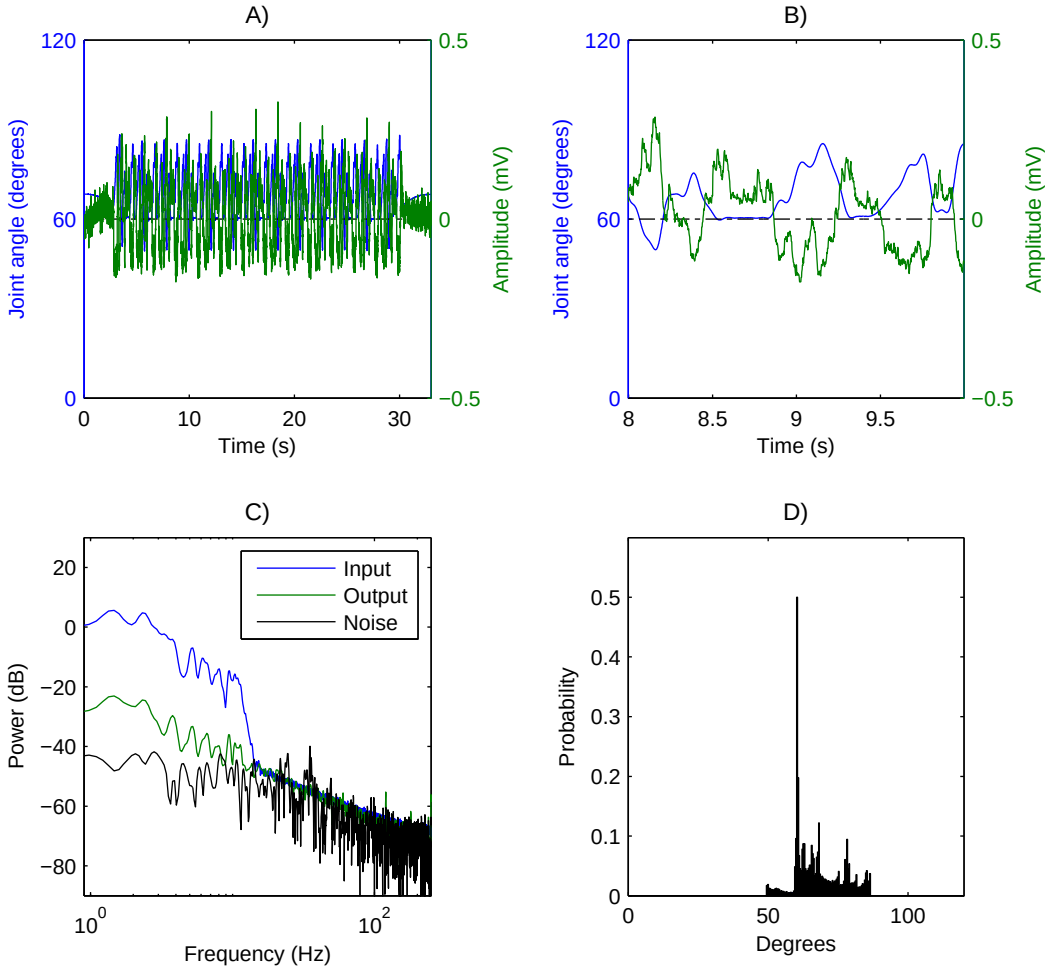

Figure 4.12: (A) Typical response of FETi to a walking input signal (walk 1). (B) A zoom into the steady state section shows the synaptic nature of the motor neuron's response. Leg flexion occurs between 0 and 60° and extension between 60 and 120°. Excitatory and inhibitory inputs are represented by positive and negative voltages respectively. (C) An estimate of the power spectrum of the input signal, the response of FETi (Output) and the measurement noise (Noise). Measurement noise was taken as the response of FETi prior to stimulation. (D) The amplitude distribution of the input signal. Note that baseline drift was removed using a high pass filter with a cut off frequency of 0.2 Hz (Section 5.2.1).

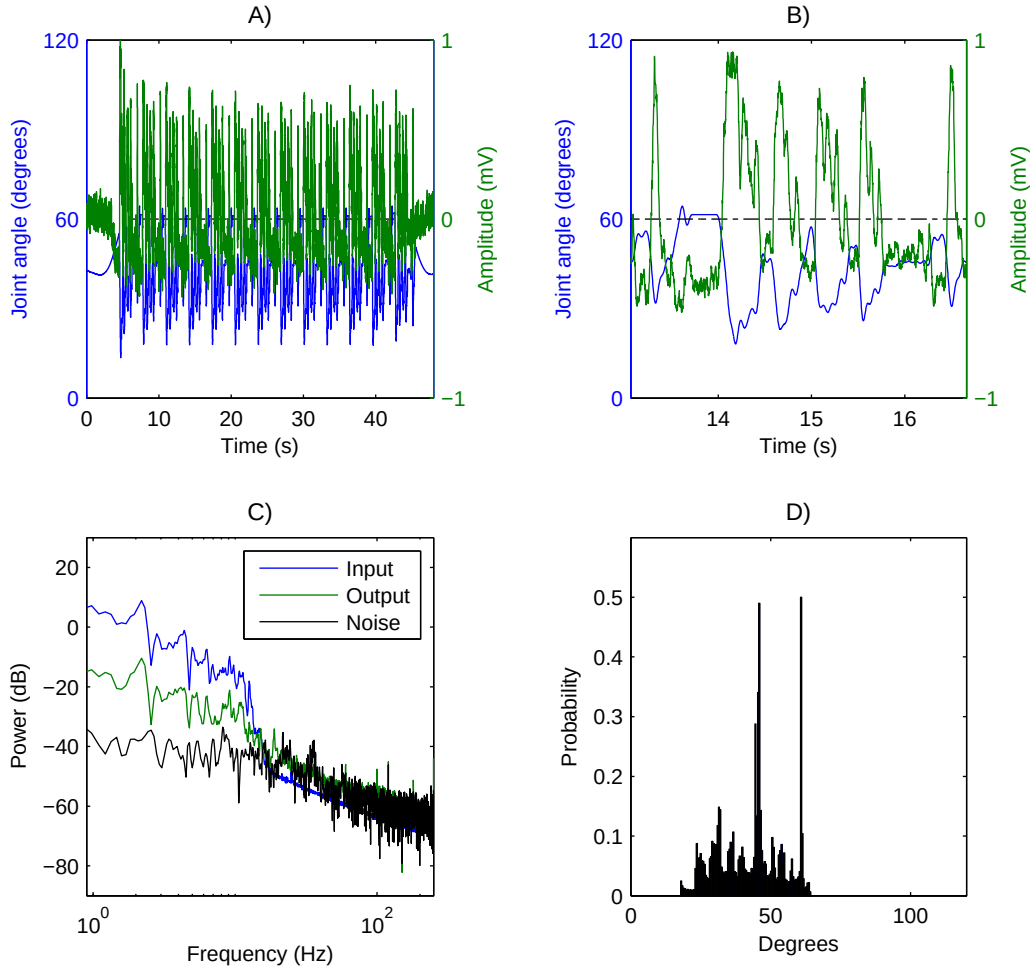

Figure 4.13: (A) Typical response of FETi to a walking input signal (walk 2). (B) A zoom into the steady state section shows the synaptic nature of the motor neuron's response. Leg flexion occurs between 0 and 60° and extension between 60 and 120°. Excitatory and inhibitory inputs are represented by positive and negative voltages respectively. (C) An estimate of the power spectrum of the input signal, the response of FETi (Output) and the measurement noise (Noise). Measurement noise was taken as the response of FETi prior to stimulation. (D) The amplitude distribution of the input signal. Note that baseline drift was removed using a high pass filter with a cut off frequency of 0.2 Hz (Section 5.2.1).

The large fluctuations in the rate of power adaptation when walking stimulation signals were applied makes it difficult to draw any conclusions (Figure 4.14B) and so further analysis was not carried out. It should also be noted that data from Animal 3 were excluded because the recording was short. To aid comparison, power values were normalised by their maximum values.

Visual analysis of the rate of power adaptation when GWN and sinusoidal stimulation signals are applied suggests that they are similar (Figure 4.14A). Further analysis was carried out by modelling the change in signal power over time using an exponential function. The time constants calculated from the response to bandlimited 50 Hz GWN and sinusoidal stimulation (1, 2, 5 and 10 Hz) are shown in Figure 4.15. No significant difference between the time constant values from GWN and sinusoidal data (Kruskal Wallis, $p > 0.05$) was found.

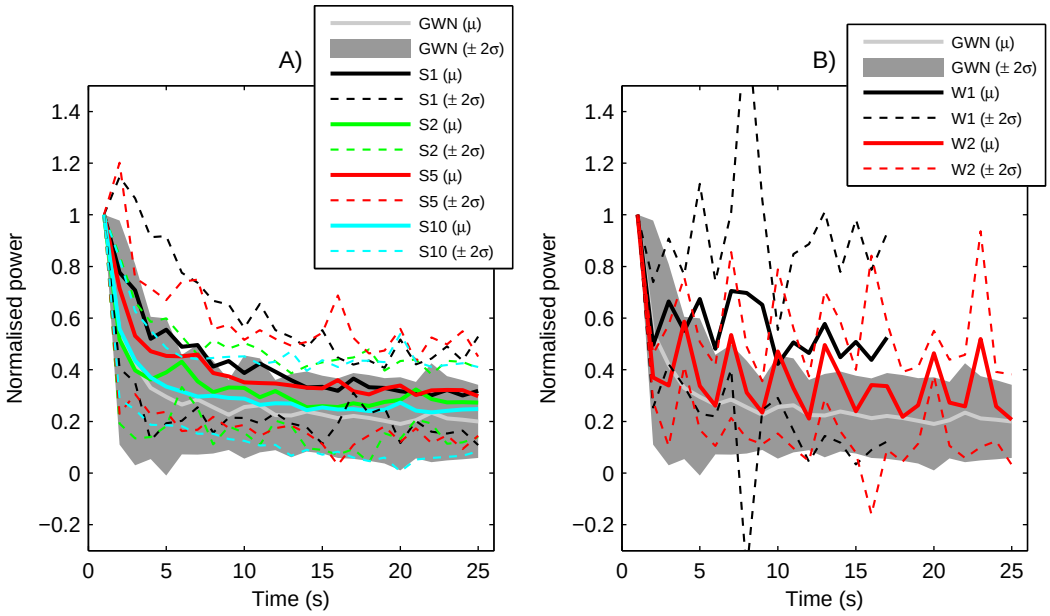

Figure 4.14: FETi output power adaptation. (A) The mean (n=5) and ± 2 standard deviation (σ) of power in the response of FETi to GWN and sinusoidal stimulation (1 Hz, 2 Hz, 5 Hz and 10 Hz represented by S1, S2, S5 and S10 respectively). (B) The power in its response to GWN and walking stimulation (walks 1 and 2 represented by W1 and W2). Power was calculated from 1 s long non overlapping windows. Maximum power values are normalised to aid comparison. The power in the response to both stimulation signals decreases quickly over the first few seconds. At 10 s response power has decreased to a relatively constant level at which it remains. The transient (TR) section of the response is defined as the first 3 s after stimulation onset. The steady state (SS) section of the response is defined as the response occurring after 10 s of stimulation onset. Stimulation started at 0 s.

Transient and steady state sections of FETi responses were defined using visual analysis of the mean power level (Figure 4.14) and of the signals. The transient section was defined as the response which occurred within the first 3 s after stimulus onset (Figure 4.14A and B). The steady state section of FETi response was defined as the response which occurred after 10 s of stimulus onset (Figure 4.14A and B). A transition period occurred between 3 and 10 s (Figure 4.14A and B).

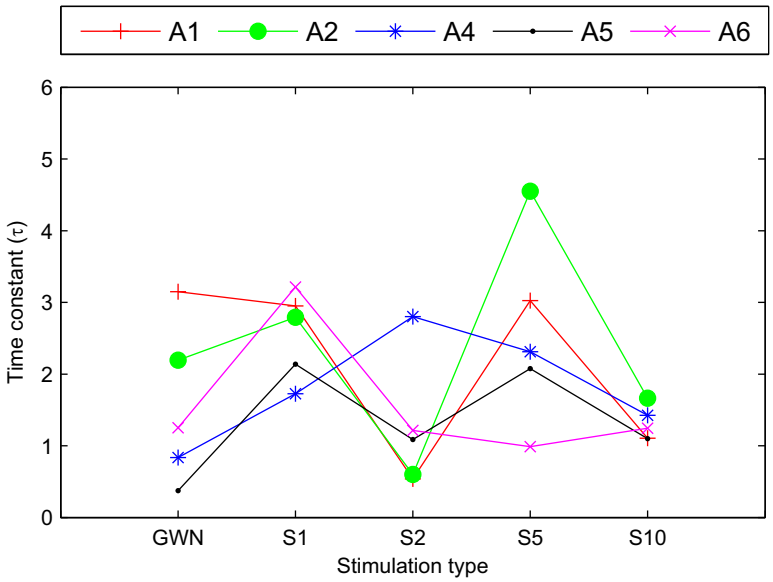

Figure 4.15: The variation in the time constant values of the exponential models of output power adaptation of FETi to GWN and sinusoidal stimulation (1 Hz, 2 Hz, 5 Hz and 10 Hz represented by S1, S2, S5 and S10 respectively). It should be noted that data from Animal 3 were excluded because the recording was short.

4.3.6 Response Consistency

The coherent averaging approach was used to allow the consistency of the steady state response of FETi to 5 Hz sinusoidal stimulation and walking stimulation signals (walk 1 and 2) to be visualised (Figures 4.16, 4.17 and 4.18A to F). It also allows response consistency across the six animals to be visualised (Figures 4.16, 4.17 and 4.18G).

The consistency of the response of FETi was probed further by comparing the standard deviation of the measurement noise before (baseline measurement noise, BMN) and after (steady state measurement noise, SSMN) stimulation was applied. The BMN was measured by calculating the standard deviation of a 1 s (500 sample) section of the response of FETi before the stimulation signal was applied (the standard deviation was calculated along the length of the signal). An estimate of the measurement noise present in the steady state response of the motor neuron (the SSMN) was obtained by subtracting the coherent average from the values of the first cycle (1 s long block of data) in the steady state response. The SSMN was then measured by calculating the standard deviation of this signal (the standard deviation was calculated along the length of the signal) (Figure 4.19). It should be noted that measurement noise was taken as the response of FETi prior to stimulation and that baseline drift was removed using a high pass filter with a cut off frequency of 0.2 Hz (Section 5.2.1).

The null hypothesis that the BMN and the SSMN are the same could not be rejected (Kruskal Wallis, $p > 0.05$) (for the steady state response to 5 Hz sinusoidal and walking stimulation signals walk 1 and walk 2). Stimulation of the FeCO does not significantly change the level of background neural activity. It is possible that changes along the length of the steady state response (Figures 4.16, 4.17 and 4.18) are caused by measurement noise present in the recordings

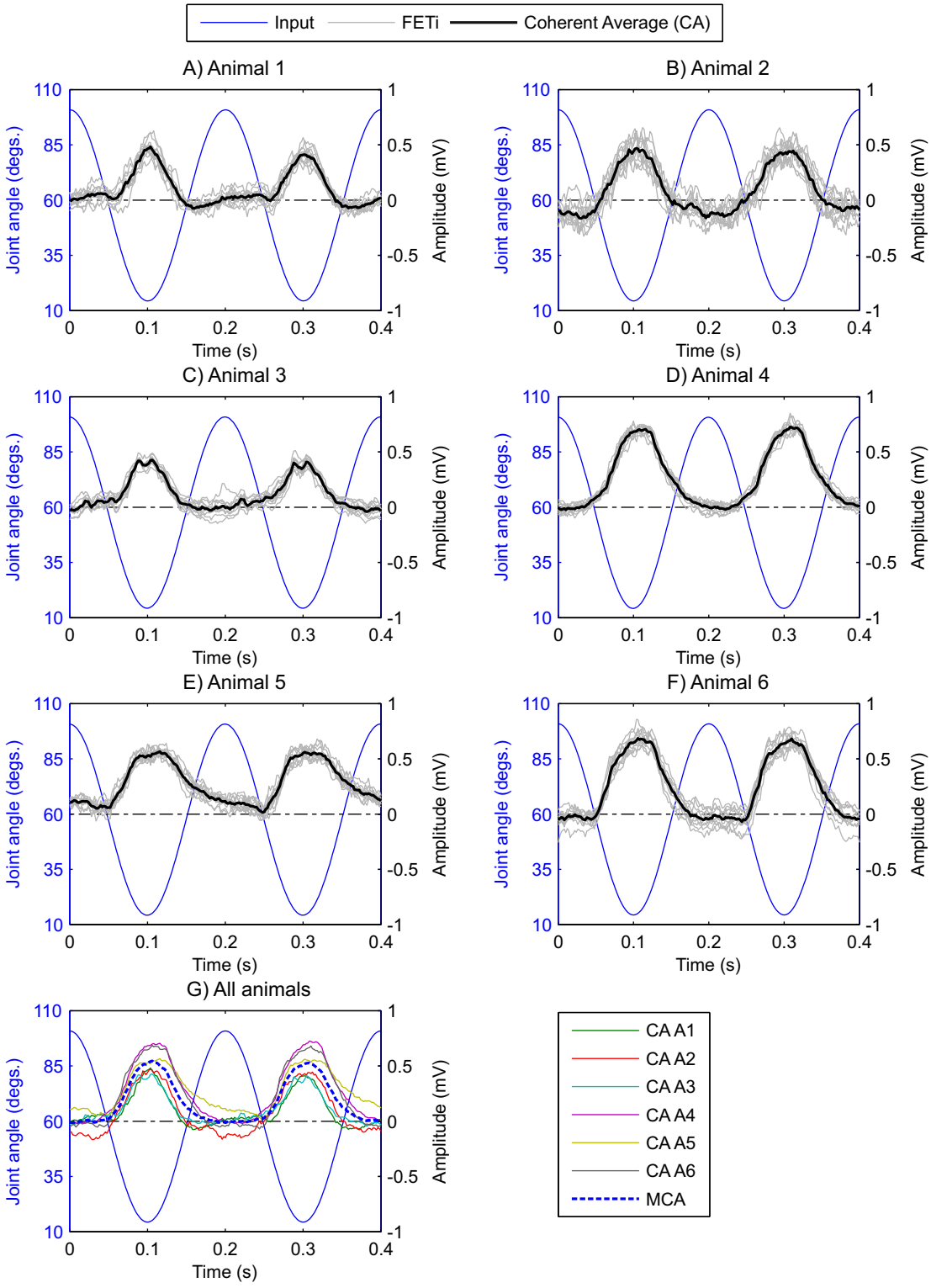

Figure 4.16: (A) - (F) A coherent averaging approach shows the consistency of the response of FETi to 5 Hz sinusoidal stimulation along the length of the steady state section in each animal. (G) The mean coherent average (MCA) across all animals. Leg flexion occurs between 0 and 60° and extension between 60 and 120°. Excitatory and inhibitory inputs to FETi are represented by positive and negative values respectively. Note that baseline drift was removed using a high pass filter with a cut off frequency of 0.2 Hz.

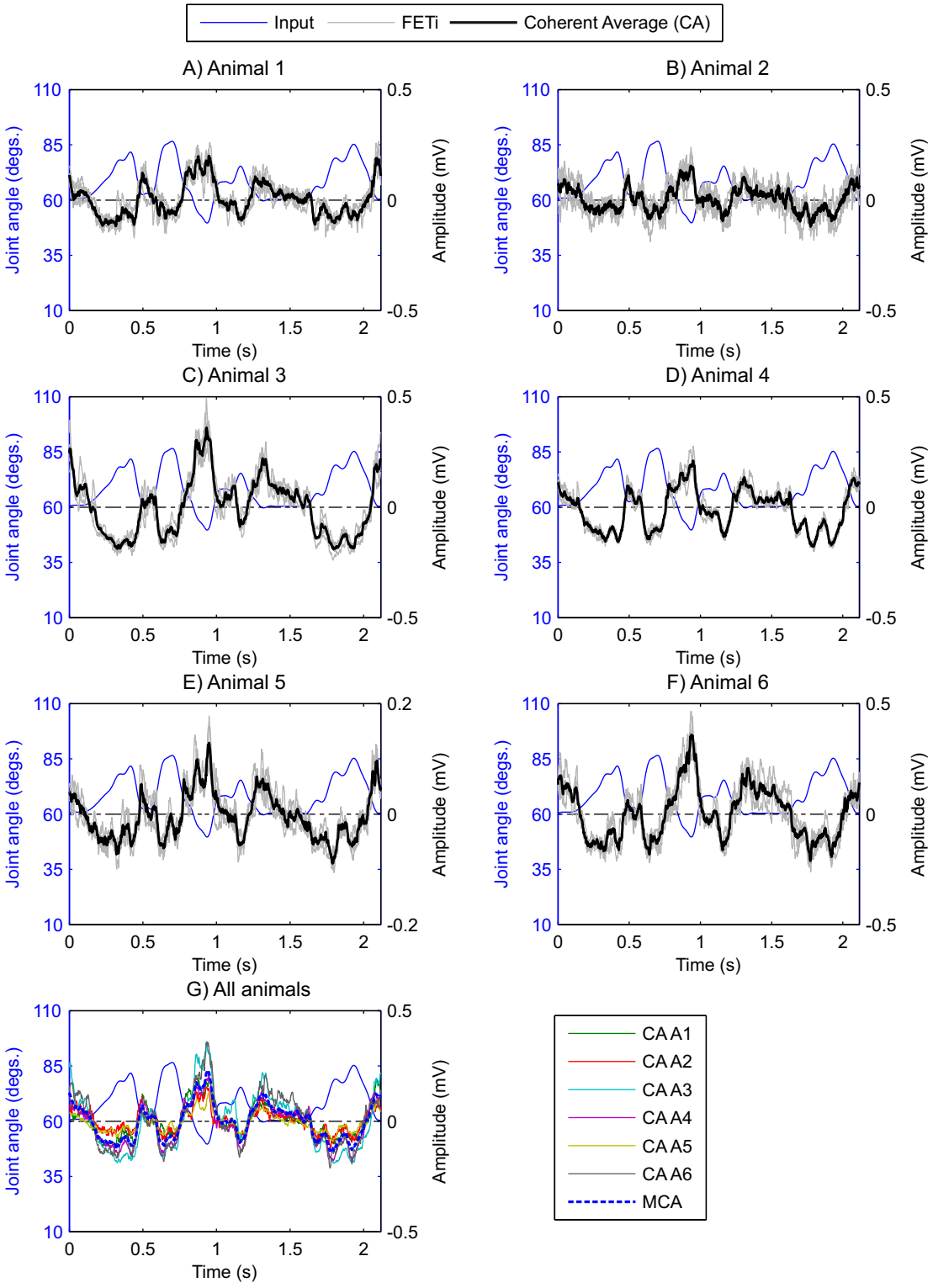

Figure 4.17: (A) - (F) A coherent averaging approach shows the consistency of the response of FETi to walking stimulation walk 1 along the length of the steady state section in each animal. (G) The mean coherent average (MCA) across all animals. Leg flexion occurs between 0 and 60° and extension between 60 and 120°. Excitatory and inhibitory inputs to FETi are represented by positive and negative values respectively. Note that baseline drift was removed using a high pass filter with a cut off frequency of 0.2 Hz.

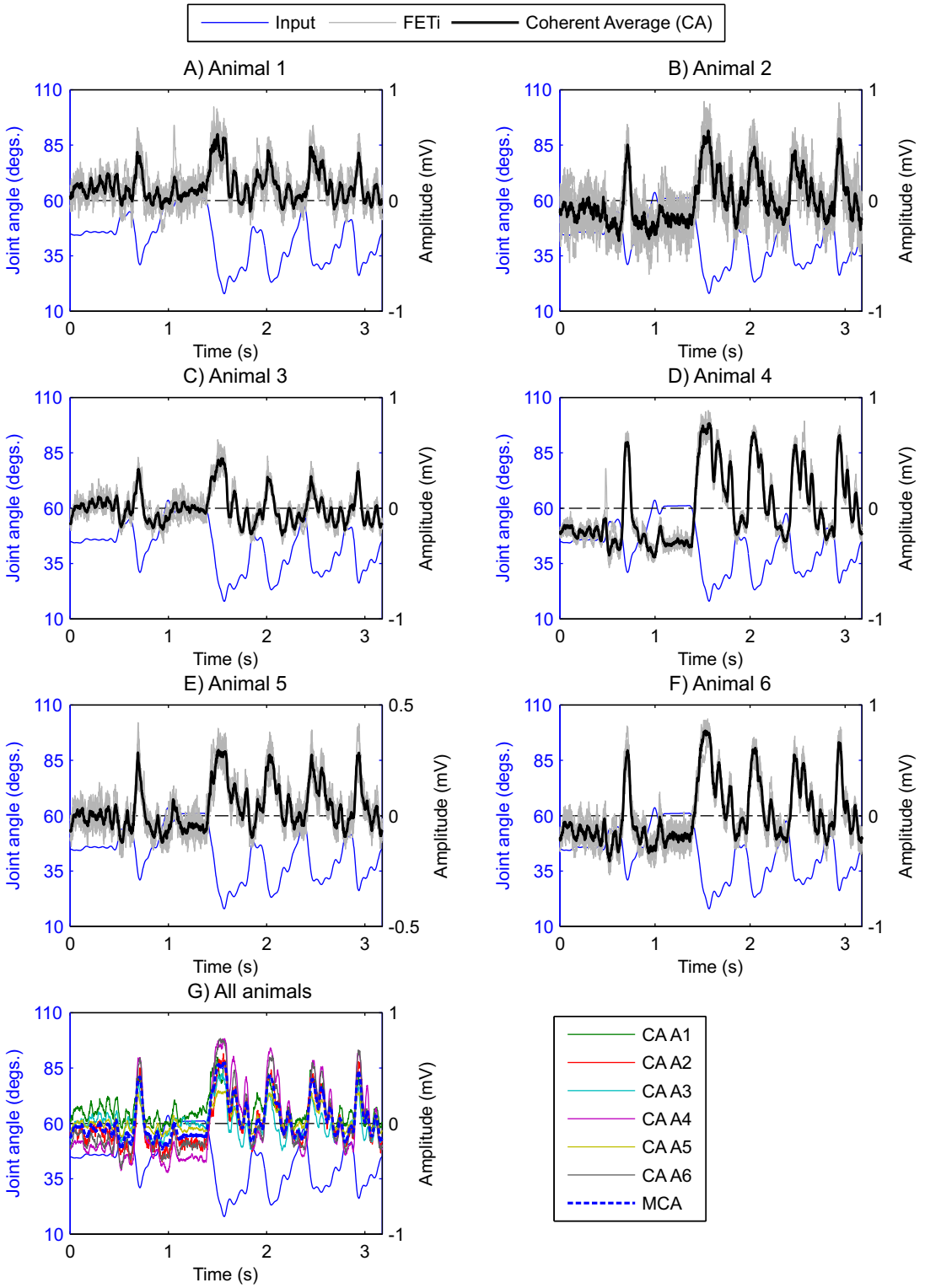

Figure 4.18: (A) - (F) A coherent averaging approach shows the consistency of the response of FETi to walking stimulation walk 2 along the length of the steady state section in each animal. (G) The mean coherent average (MCA) across all animals. Leg flexion occurs between 0 and 60° and extension between 60 and 120°. Excitatory and inhibitory inputs to FETi are represented by positive and negative values respectively. Note that baseline drift was removed using a high pass filter with a cut off frequency of 0.2 Hz.

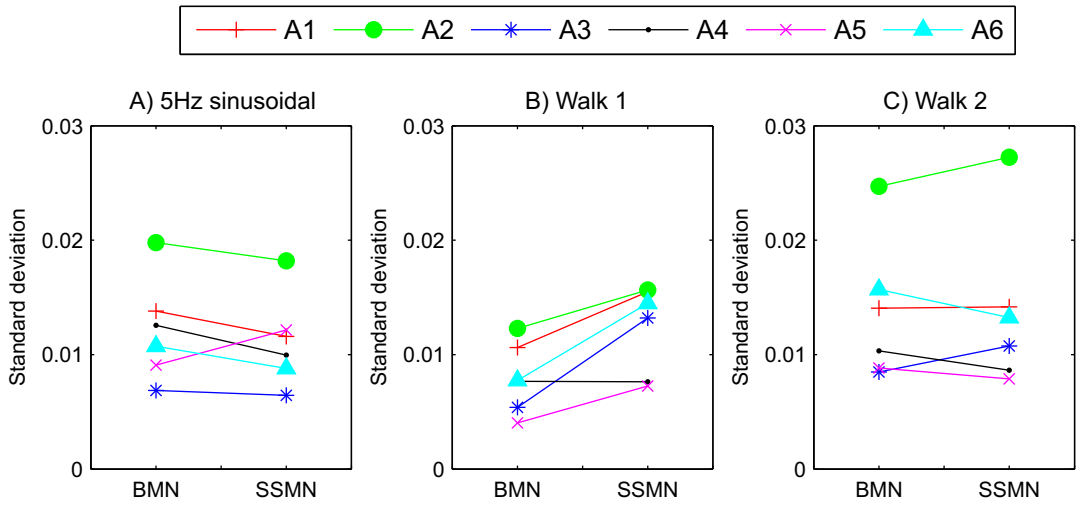

Figure 4.19: (A) The standard deviation of the baseline measurement noise (BMN) and the steady state measurement noise (SSMN) in the response of FETi to 5 Hz sinusoidal stimulation from animals 1 to 6 (A1 to A6). (B) and (C) show the results for walking stimulation (walk 1 and 2 respectively). The BMN was measured by calculating the standard deviation of a 1 s (500 sample) section of the response of FETi before the stimulation signal was applied. An estimate of the measurement noise present in the steady state response of the motor neuron was obtained by subtracting the coherent average from the values of the first cycle (1 s long block of data) in the steady state response. The SSMN was measured by calculating the standard deviation of this signal. The null hypothesis that the BMN and the SSMN are the same could not be rejected (Kruskal Wallis, $p > 0.05$, for all three stimulation signals). Stimulation of the FeCO does not significantly change the level of background neural activity.

rather than time varying changes in the system's response.

The results shown in Figures 4.16, 4.17 and 4.18 match the results obtained in [45] and [20] in that the level of FETi excitation depends on the position of the femoral tibial joint, with the excitation being greatest at small angles (flexion), behaviour consistent with a reflex response.

The response of the system into and out of flexion when 5 Hz sinusoidal stimulation (Figure 4.16) was applied is in general symmetrical. The response of the system to walking stimulation shows how small variations in angle within the gait cycle can modulate the response strongly (Figures 4.17 and 4.18). It is interesting to note that the peak response of the system to walk 2 (Figure 4.18G) appears to precede the peak angle of the input signal, suggesting a sensitivity to velocity.

4.4 Summary

This chapter has described the experimental methods used by the current study to record the reflex response of FETi to GWN, sinusoidal and walking stimulation. Previously used methods have been improved; a new forceps mount has been designed, built and tested and dissections have been carried out to identify the location of the loop structure. These dissections have revealed a not previously described bifurcation of the flexor strand.

Previous work [73, 97, 98, 117] has also been extended by carrying out a detailed model based investigation into the properties of the shaker amplifier, shaker, new forceps mount and forceps. It is important to quantify the properties of this system as it is included in previous system identification models of FETi [98] and in those described in Chapters 5 and 7. Frequency domain analysis of the linear FIR model of this system has shown that its response is flat to within 2dB and that it has an approximately linear phase response over the frequency range of interest (0-50 Hz). The properties of the electromechanical arrangement will therefore have little impact on models of FETi, and for the purpose of the current study they were neglected.

Furthermore, previous studies [73, 97, 98, 117] have been extended to consider output power adaptation of FETi in the femur/tibia control loop. The majority of output power adaptation was found to occur within the first 3 s of stimulus onset. Steady state response occurred after 10 s and power remained at a relatively constant level for the next 20 to 30 s (the duration of the experiments). Similar results were found in a study which used 2 Hz sinusoidal stimulation [44]. Modelling and statistical analysis has shown that the adaptation rate (power) of FETi to GWN and sinusoidal stimulation is generally similar. Analysis of adaptation rate has also aided the definition of the transient and steady state response of FETi. The transient section was defined as the response which occurred within the first 3 s after stimulus onset. The steady state section of FETi response was defined as the response which occurred after 10 s of stimulus onset. It should be noted that, as was found in other investigations which used a similar experimental set-up and input signals [44, 98] to stimulate the FeCO as the current study, only synaptic inputs were recorded in FETi (Figure 1.1D and E).

The consistency of the response of FETi to GWN stimulation across animals has previously been shown [98] through analysis of the parameters of models fitted to these data. Such analysis provides a useful tool to validate model quality if the Signal to Noise ratio (SNR) is poor, as was often the case in [73, 97, 98, 117]. In such cases the %MSE value (Section 2.3) will be poor simply because the measured output signal will contain high levels of noise which the estimated model cannot predict [87].

Results presented in this chapter extend the modelling work in [98] by showing (using a non modelling approach) that the reflex response of FETi to sinusoidal and importantly, natural walking stimulation, is consistent along the length of the steady state response of each animal and across animals. This consistency suggests that the response of FETi to these signals is stationary. Statistical analysis shows that stimulation of the FeCO does not significantly change the level of background neural activity. The consistency of the response of FETi to sinusoidal and walking stimulation found in each animal and across animals strongly suggests that the experimental protocol produces robust and repeatable results. One advantage of the "non modelling" approach is that it is simpler to understand than the modelling approach used in [73, 97, 98, 117].

Chapter 5

FETi System Identification: Model Structure Selection, Parameter Number Optimisation and Natural Validation

5.1 Introduction

The aim of the work described in this chapter was threefold. Firstly to find a parsimonious model structure which would allow the dynamics and nonlinear response of FETi to be investigated and compared to its steady state responses (Chapter 7). Secondly to find a method to determine the optimum number of parameters contained in a given model type. Thirdly to extend previous work [73, 97, 98, 117] to validate the models estimated from the GWN input/output data recorded from FETi by measuring their ability to predict the response of FETi to the more natural input of sinusoidal and walking signals. The aim of these experiments was to determine the conditions under which the models perform well and to explore their limitations.

The system identification approach, coupled with GWN stimulation, provides an experimentally convenient and quick way to describe the steady state responses of the sensory neurons in the FeCO and the local interneurons and motor neurons with which they connect. Previous work [98] used a 2^{nd} order Wiener model to represent the reflex response of FETi to GWN stimulation. Such a model, however, was not suitable for application in the current study because it contains many parameters and therefore requires large amounts of data (typically 20 s) to obtain robust parameter estimates. This restriction was overcome in the current study by using the Volterra series with the smooth Laguerre basis function to significantly reduce the number of free parameters in the model [86]. Cascade models, a subset of the Volterra series, were also considered because they provide a parsimonious means of increasing the order of

the nonlinearity, which is especially important for application to short data segments. Previous work [51, 52, 65] has shown them to be effective for representing nonlinear biological systems. Furthermore, cascade models simplify the analysis of the nonlinear response of the system as, unlike the nonlinear elements of the Volterra model, their nonlinear polynomial element remains in two dimensional space regardless of their order and as they are a subset of the Volterra series, it is possible to transform their parameters into Volterra form. This means that the cascade models can be used with the classification approach used by previous studies [73, 97, 98, 117].

The number of parameters a model contains can have a considerable effect on its quality and the computational cost to calculate its parameters [81, 130]. Often, however, studies which apply system identification methods to physiological systems do not state how the number of parameters in the model are chosen or if it is considered important [54, 73, 93, 97, 98]. In the current study the optimum number of parameters for each model type was determined before their performance was compared.

5.2 Methods

This section commences with a description of the signal preprocessing methods (Section 5.2.1). Next, a brief description of the different model structures compared in the current study is given (Section 5.2.2). The section concludes with an explanation of the method used to measure model predictive performance and optimise the number of parameters it contains and measure its ability to generalise to predict the response of FETi to sinusoidal and natural stimulation.

5.2.1 Signal Preprocessing

The signal preprocessing methods used by Kondoh et al. [73, 97, 98] were modified for the purpose of this investigation. They re-sampled their signals at 2 KHz and then used a band pass filter with a 0.5 to 200 Hz passband to remove the low frequency noise and higher frequency components above 200 Hz which did not contain useful information. In the current investigation the signals were re-sampled at 500 Hz, the 250 Hz anti aliasing filter removing unwanted high frequency components. By down-sampling the data further its storage requirements and processing time were reduced.

The signals recorded from FETi tended to be corrupted by low frequency noise which typically consisted of a slow time varying drift (baseline drift) (Figure 5.1B). The baseline drift was evident in all the intracellular neuron recordings and may have been caused by the movement of ions between the electrode and the neuron [87]. This drift was removed using a high pass filter with a cut off frequency of 0.2 Hz (Figure 5.1C). A 3^{rd} order high pass Butterworth filter was chosen, and applied in the forward and reverse direction to avoid introducing any phase delay (zero phase).

The signals were plotted in the time domain for initial visual analysis (Figure 5.1) to allow poor quality recordings to be identified and rejected. The high level of background measurement noise present in the recording before the input signal was applied (Figure 5.1C, section s1) should be noted. This measurement noise consists of electrical measurement noise and background neural activity (Section 1.2). Electrical measurement noise is added to the signal by the amplifier and the data acquisition system. The spectrum of the noise, input and output signals is plotted in Figure 5.1D. It should be noted that the high level of background noise effectively masks system output at frequencies greater than 50 Hz (Figure 5.1D).

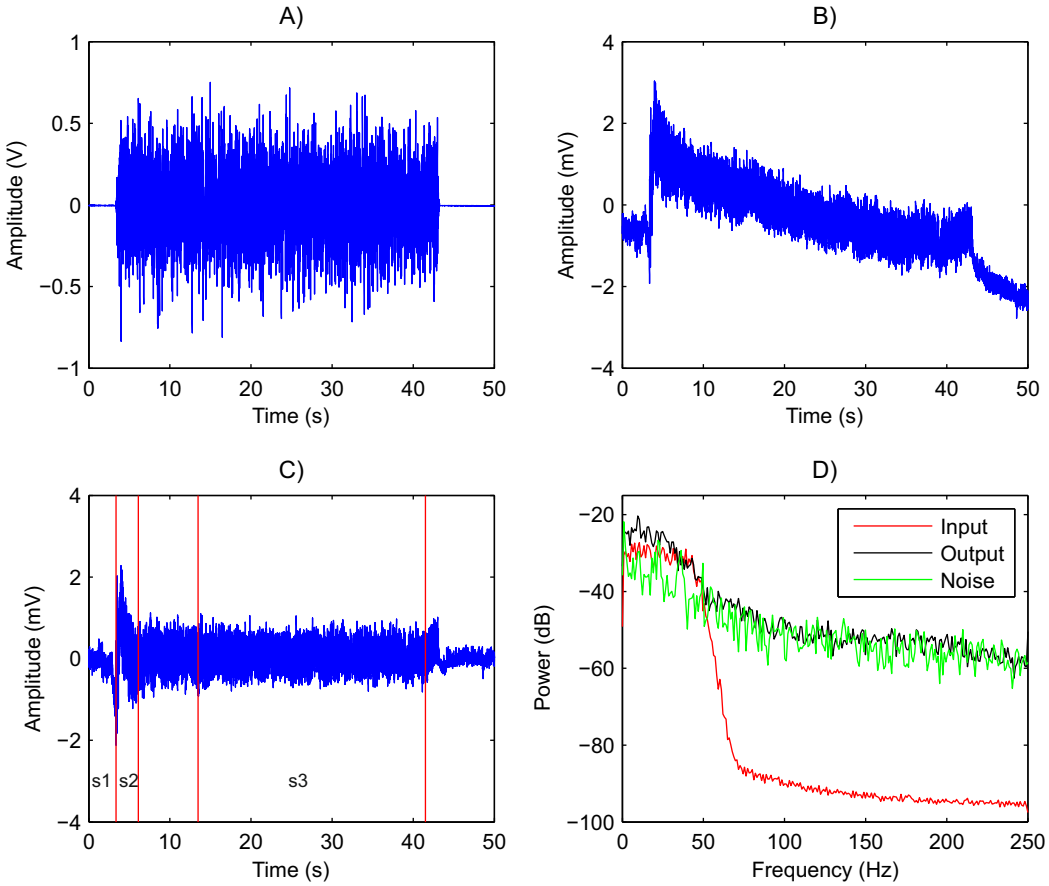

Figure 5.1: Signal preprocessing. (A) The bandlimited (0-50 Hz) GWN signal used to move the apodeme of the FeCO. (B) A typical output signal recorded from FETi, note the baseline drift. (C) The preprocessed output signal, sections s1, s2 and s3 mark the noise, the transient response of FETi and its steady state response respectively. (D) The spectrum of the input signal, the steady state FETi response (s3) and the measurement noise signal (s1).

5.2.2 System Identification

The 2^{nd} and 3^{rd} order Volterra, and the Linear Nonlinear (LN), Nonlinear Linear (NL) and Linear Nonlinear Linear (LNL) cascade models were used in the current study. Linear models are not applied to FETi as previous work has shown that nonlinear models provide more accurate predictive performance [98] and its response is clearly nonlinear (Figure 1.1E). A brief description of the nonlinear models structures follows, full details can be found in Chapter 2.

The output of the 2^{nd} order Volterra model is given by

$$y(t) = h_0 + \sum_{\tau_1=0}^{T-1} h_1(\tau_1)u(t-\tau_1) + \sum_{\tau_1=0}^{T-1}\sum_{\tau_2=0}^{T-1} h_2(\tau_1,\tau_2)u(t-\tau_1)u(t-\tau_2) \tag{5.1}$$

The output of the 3^{rd} order Volterra model is given by

$$y(t) = h_0 + \sum_{\tau_1=0}^{T-1} h_1(\tau_1)u(t-\tau_1) + \sum_{\tau_1=0}^{T-1}\sum_{\tau_2=0}^{T-1} h_2(\tau_1,\tau_2)u(t-\tau_1)u(t-\tau_2) + \sum_{\tau_1=0}^{T-1}\sum_{\tau_2=0}^{T-1}\sum_{\tau_3=0}^{T-1} h_3(\tau_1,\tau_2,\tau_3)u(t-\tau_1)u(t-\tau_2)u(t-\tau_3) \tag{5.2}$$

The Volterra kernels were estimated using the Wiener Laguerre method (Section 2.4.4). The decay parameter α (Equation 2.44) which controls the damping of the Laguerre function was chosen following the guidelines given in [87, 123]. A value of $\alpha = 0.2$ and $J = 6$ was chosen based on preliminary experiments.

The output of the LN model is calculated using

$$y(t) = \sum_{q=0}^{Q} c^{(q)} \left(\sum_{\tau=0}^{T-1} h(\tau)u(t-\tau) \right)^q \tag{5.3}$$

The output of the NL model is calculated using

$$y(t) = \sum_{\tau=0}^{T-1} h(\tau) \left(\sum_{q=0}^{Q} c^{(q)} u^q(t-\tau) \right) \tag{5.4}$$

The output of the LNL model is calculated using

$$y(t) = \sum_{\sigma=0}^{T-1} g(\sigma) \sum_{q=0}^{Q} c^{(q)} \left(\sum_{\tau=0}^{T-1} h(\tau)u(t-\sigma-\tau) \right)^q \tag{5.5}$$

The parameters of the cascade models were estimated using an iterative local optimisation method [65, 74]. A summary of the algorithms can be found in Section 2.4.6. The Smoothed Korenberg Hunter (SKH) method, a variant of the KH method, has been developed by the current study to reduce estimation error in the linear elements of the LN and NL models and in the second linear element of the LNL model ($g(\tau)$).

For the LN model, the SKH method applies a low pass filter to the estimate of the IRF $\hat{h}(\tau)$, Step 1, Algorithm 1. This filter is also applied to $\hat{h}(\tau)$ at Step 7, Algorithm 1. The parameters of $\hat{h}(\tau)$ are zero padded before the smoothing filter is applied, a 4^{th} order low pass Butterworth filter with a cut off frequency of 50 Hz. The filter is applied in the forward and reverse direction to avoid introducing any phase delay (zero phase). As the estimation errors occur at frequencies above 50 Hz (the highest frequency component in the bandlimited GWN input signal) they can be removed from $\hat{h}(\tau)$ using this low pass filter.

For the NL model, the SKH method applies the smoothing filter to the estimate of the inverse of $\hat{h}(\tau)$ ($\hat{h}(\tau)^{-1}$, Step 1, Algorithm 2). It also applies the filter to the estimate of $\hat{h}(\tau)$ at Step 5 and to ($\hat{h}(\tau)^{-1}$, Step 8 (Algorithm 2).

For the LNL model the SKH method only applies the smoothing low pass filter to the second linear element in the model $\hat{g}(\tau)$. As $\hat{g}(\tau)$ is the linear element in the Hammerstein (NL) model it is represented by $\hat{h}(\tau)$ in Algorithm 2. The low pass filter is, therefore, applied to the estimate of the inverse of $\hat{h}(\tau)$ ($\hat{h}(\tau)^{-1}$, Step 1 and 8, and to the estimate of $\hat{h}(\tau)$ at Step 5, Algorithm 2). It is unnecessary to apply the filter to the first linear element in the LNL model because this is estimated using the Levenberg Marquardt method which effectively reduces high frequency estimation error with a damping term (Equation 2.63, Section 2.4.6).

5.2.3 Measuring Predictive Performance, Optimising the Number of Parameters and Natural Validation

Predictive performance was measured by calculating the percentage Mean Square Error (%MSE) difference between the recorded FETi motor neuron output, $z(t)$, and the predicted model output, $\hat{y}(t)$ [123] (Figure 1.2).

$$\%MSE = 100 \times \frac{Var(z - \hat{y})}{Var(z)} \tag{5.6}$$

$Var(x)$ was calculated using

$$Var(x) = \frac{1}{T}\sum_{t=1}^{T} x^2(t) - \left(\frac{1}{T}\sum_{t=1}^{T} x(t)\right)^2 \tag{5.7}$$

where T is the number of samples in the signal x.

The performance of the different model types was determined by calculating the %MSE difference (Equation 5.6) between the predicted output of the model and the measured output of the neuron, using validation data. Validation was carried out using the last 3 s of the recording.

Before the performance of the different model types was compared, the number of parameters they contained was optimised. As six sets of data were available, for a given model type, six models were estimated. Parameters were estimated from a 3 s block of steady state data. It should be noted that a 3 s block duration limits a models ability to represent signals with frequencies of less than $0.\dot{3}$ Hz. The %MSE performance of each of these models with a varying number of parameters was calculated, using validation data. The optimum number of parameters for a given model type was determined from the minimum %MSE value, achieved in each animal, averaged across all animals.

The ability of the models to generalise was tested by measuring their %MSE performance to predict the response of FETi to 1, 2, 5 and 10 Hz sinusoidal stimulation and walking inputs (walk 1 and walk 2). Models, with their parameters estimated from GWN input/output data, were evaluated by calculating the %MSE difference (3 s sections of data) between the measured output of FETi to the "natural" stimulation signals and the predicted model output of the

corresponding stimulation signal.

5.3 Results

The results described in this section are based on six successful recordings from the FETi motor neuron in different animals made by Professor Philip Newland.

5.3.1 Optimisation of the Number of Model Parameters

The number of parameters each model contained was optimised before the predictive performance of the different model structures was compared. The variation in the %MSE predictive performance of the 2^{nd} and 3^{rd} order Volterra (Wiener Laguerre estimation method) and the LN, NL and LNL cascade models is shown in Figure 5.2. Note that model performance improves as the %MSE value decreases. Model accuracy was calculated using validation data and parameters were estimated from a 3 s block of steady state response.

In general there is a plateau in the %MSE curves (Figure 5.2A, C, D and E) and once this flat area has been reached an increase in the number of parameters has little effect on performance. For the 2^{nd} order Volterra and cascade models the exact choice of the number of model parameters is therefore not critical provided that the plateau is reached. The exception is the %MSE curve for the 3^{rd} order Volterra model (Figure 5.2B). An excessive number of parameters in this model type can have a considerable effect on model performance (Figure 5.2B), indicating over training [95]. Model over training can occur if the model has sufficient free parameters to fit the measurement noise, resulting in an overestimate of model performance, and incorrect model parameters on training data and potentially poor performance when tested on validation data. The minimum %MSE performance of the 2^{nd} order Volterra model of 31.8% (Figure 5.2A) occurs when it contains a total of 36 parameters ($J = 7$). It should be noted that this is the number of the reduced set of parameters used in the regression matrix of the Wiener Laguerre method. The total number of parameters M is given by

$$M = \frac{(J+Q)!}{J!Q!} \tag{5.8}$$

where J is the number of functions in the decomposition ($J = 6$), Equation 2.42, and Q is the order of the Volterra series [87]. The minimum %MSE performance of the 3^{rd} order Volterra model of 36.3% (Figure 5.2B) occurs when it contains 84 parameters ($J = 7$). As the cascade models contain dynamic linear and static nonlinear elements it was necessary to determine the variation in %MSE performance across both of these variables to enable the optimum number of parameters to be found. The mean %MSE performance for the LN, NL and LNL models with the number of linear parameters they contain (L) and polynomial order (P) is plotted in Figure 5.2C, D and E. These results show that the optimum LN cascade model had a mean %MSE performance of 38.9% and contained 34 linear parameters and 5 polynomial coefficients (4^{th} order polynomial) (Figure 5.2C). The optimum NL cascade had a mean %MSE

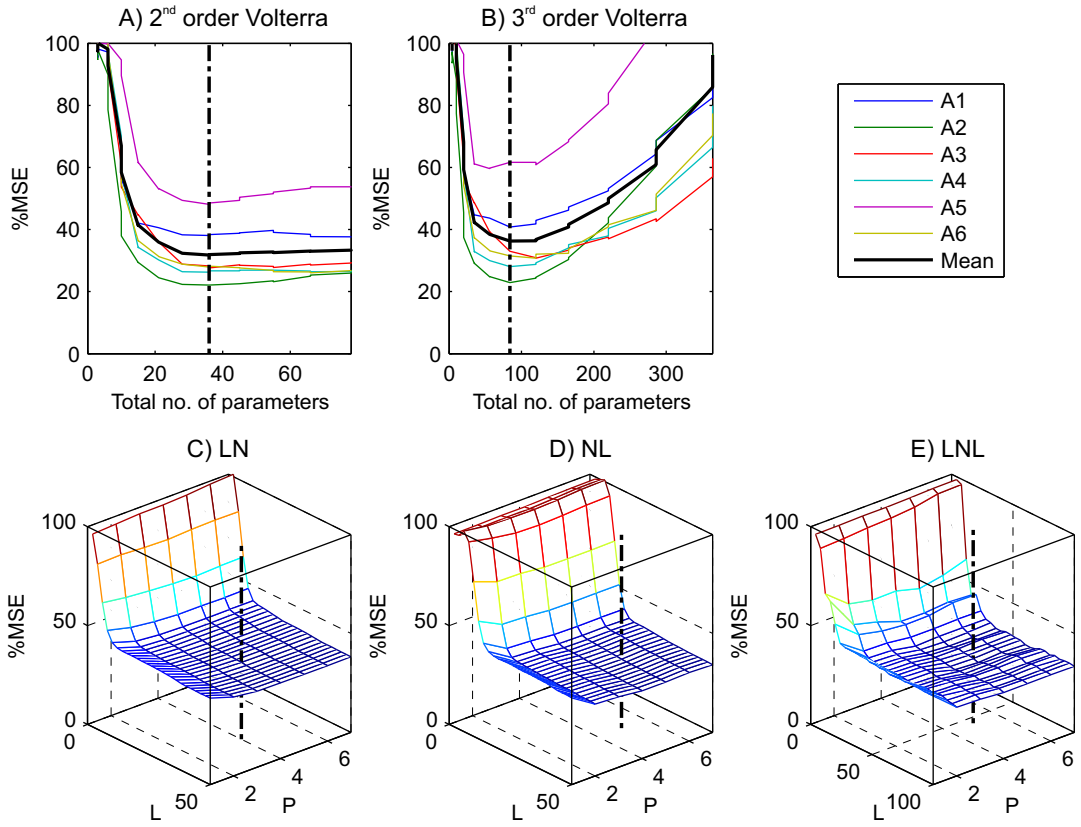

Figure 5.2: Variation of %MSE model predictive performance for the different model structures with the number of parameters they contain. The panel, top right, defines the traces, for example A1 represents the results obtained from Animal 1. (A) and (B) The %MSE variation for the 2^{nd} and 3^{rd} order Volterra models respectively. The mean %MSE value is marked using a thick solid black line. (C) - (E) The mean (n=6) %MSE variation for the LN, NL and LNL cascade models respectively. The variables L and P represent the total number of linear parameters and the polynomial order respectively. The minimum mean %MSE value of the different model types is marked using a vertical dotted thick black line (A to E). Note that model performance improves as the %MSE value decreases and that model accuracy was calculated using validation data. In general (A), (C), (D) and (E) there is a plateau in the %MSE curves and once this area has been reached a change in the number of parameters has little effect on model performance.

performance of 34.9% and contained 32 linear parameters and 6 polynomial coefficients (5^{th} order polynomial) (Figure 5.2D). The optimum LNL model had a mean %MSE performance of 32.8% and contained 28 parameters in each linear element and 6 polynomial coefficients (5^{th} order) (Figure 5.2E).

The predictive performance of the different model types, with their optimum number of parameters, is compared in the next section.

5.3.2 The Predictive Performance of the Different Model Types

Having found the optimum number of parameters for each model structure (Section 5.3.1) it was possible to compare their performance at predicting the responses of FETi to GWN, sinusoidal and walking stimulation. Scatter plots (Figure 5.3) are used to show the predictive accuracy of the different model types calculated using data recorded in six different locusts. The ability of the nonlinear 2^{nd} and 3^{rd} order Volterra and cascade (LN, NL and LNL) models to predict the response of FETi to GWN stimulation is shown in Figure 5.3A. Predictive accuracy was measured using the %MSE metric on validation data (3 s block from the end of the steady state section).

The mean (n=6) performance on validation data for the 2^{nd} and 3^{rd} order Volterra models and the LN, NL and LNL cascade models was 28.7, 27.5, 36.1, 34.5 and 29.9 %MSE respectively (Table 5.1). Statistical analysis of these data using the Kruskal Wallis test [77] found no significant difference ($p > 0.05$) between the predictive performance of the models, but numbers of cases are low (n=6).

The ability of these models to predict the response of FETi to walking and sinusoidal stimulation is also shown in Figure 5.3B to G. The results for 1, 2, 5 and 10 Hz sinusoidal stimulation are shown in Figure 5.3B to E respectively. The results for walk 1 and walk 2 are shown in Figure 5.3F and G. Mean %MSE values for the different model types are given in Table 5.1. The predictive performance of the models is generally less accurate with sinusoidal and walking stimulation signals (Figure 5.3B - G) than with GWN stimulation (Figure 5.3A and see Table 5.1). However, the predictive performance of the LNL model with GWN stimulation (29.9%MSE) and with 5 and 10 Hz sinusoidal stimulation (33.5 and 30.2%MSE respectively) is very similar (Table 5.1). Reasons for the poor predictive performance of the models with the sinusoidal (1 and 2 Hz) and the walking stimulation signals are investigated in Section 5.3.5.

As the 3^{rd} order Volterra model is computationally more complex and has parameters which are more difficult to interpret than the 2^{nd} order Volterra model it will not be considered further.

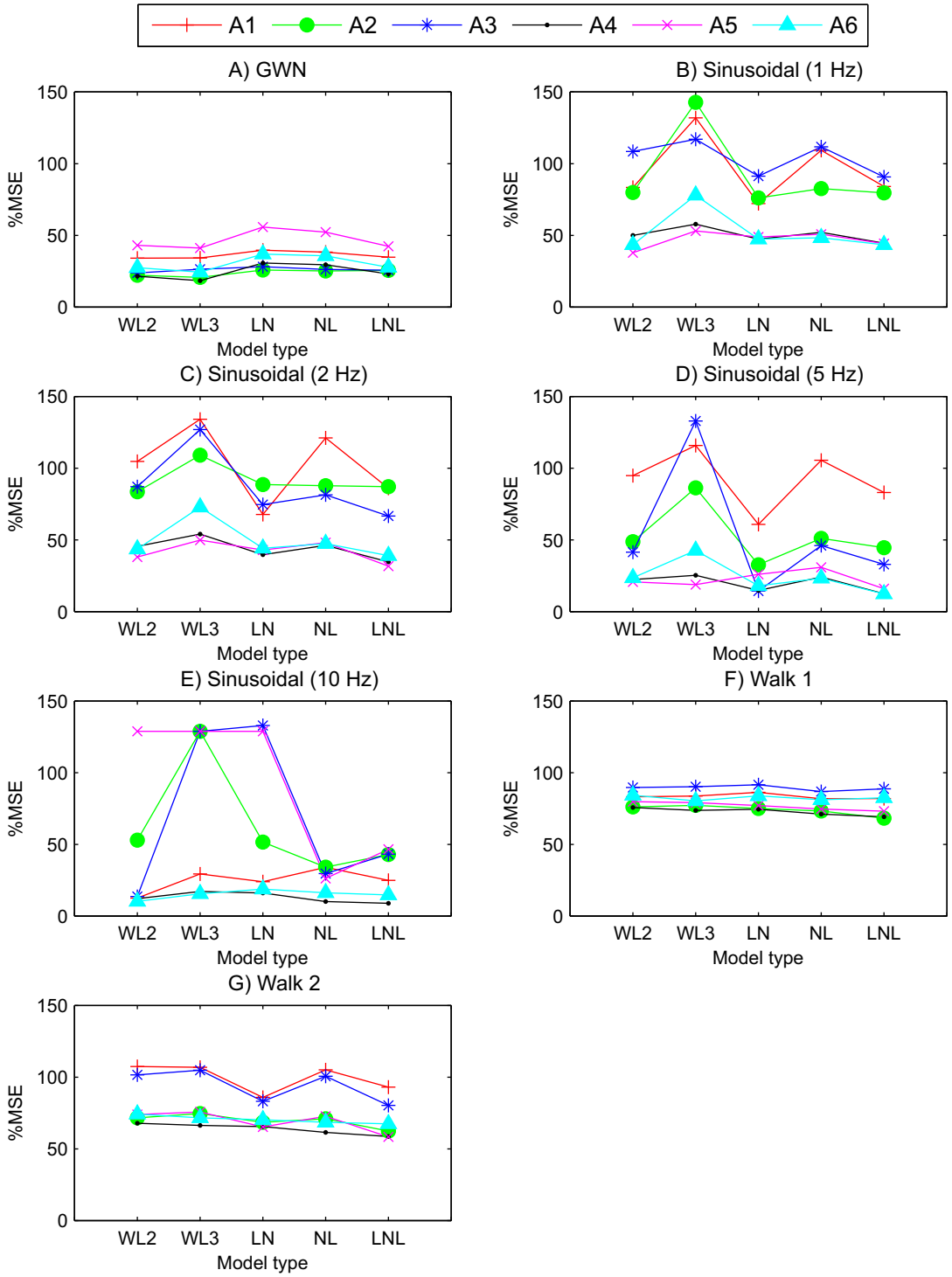

Figure 5.3: Validation of the 2^{nd} and 3^{rd} order Volterra models (WL2 and WL3) and the LN, NL and LNL cascade models using (A) GWN, (B) - (E) 1, 2, 5 and 10 Hz sinusoidal, (F) walk 1 and (G) walk 2 stimulation signals. Model parameters were estimated from a 3 s long block of GWN estimation data. %MSE accuracy was calculated using validation data for GWN stimulation (3 s block). Results are shown for data recorded from animals 1 to 6 (A1 to A6).

Model type	WL2	WL3	LN	NL	LNL
No. of parameters	36	84	39	38	62
GWN	28.7	27.5	36.1	34.5	29.9
S1	67.2	99.8	63.8	75.8	64.4
S2	67.1	93.8	59.6	72.0	57.5
S5	41.9	73.1	27.7	46.8	33.5
S10	41.9	85.3	65.5	25.0	30.2
W1	81.4	80.7	81.3	78.1	77.2
W2	82.8	83.3	73.1	79.9	70.0

Table 5.1: The %MSE predictive performance of the different model types with GWN (validation data), sinusoidal and walking stimulation. %MSE is calculated using 3 s long blocks of data. The 2^{nd} and 3^{rd} order Volterra models and the LN, NL and LNL cascade models are represented by WL2, WL3, LN, NL and LNL respectively.

5.3.3 Model Parameters

The parameters of the 2^{nd} order Volterra and cascade models are analysed in the time and frequency domain in the following sections.

Volterra Model

The mean (n=6) normalised 1^{st} and 2^{nd} order kernels of the Volterra models of FETi, containing their optimum number of parameters, are plotted in Figure 5.4A and B. The parameters of the Volterra models were estimated using the Wiener Laguerre method. The six individual 1^{st} and 2^{nd} order Volterra kernels are shown in Figure 5.4A and Figure 5.4C to H respectively.

The 1^{st} order kernel (Figure 5.4A), which represents the linear response of the system, is very similar to the 1^{st} order Wiener kernel published by Newland and Kondoh [98] (Figure 5.6A). The first order kernel estimated by Newland and Kondoh [98] has a positive peak at τ = 19.9± ms 2.1 (SD) (n=17). In the current study, the first order kernel has a positive peak at τ = 23± ms 5 (SD) (n=6).

The mean frequency and phase response of the averaged 1^{st} order Volterra kernels, estimated in the current study, are plotted in Figure 5.5A and B. The mean frequency and phase response of the 1^{st} order Wiener kernels, copied from Newland and Kondoh [98], are plotted in Figure 5.6C and D. As the 1^{st} order kernel represents the linear response of the system, its frequency response in the range between DC and the upper stimulus frequency of the GWN input signal is of interest. The upper stimulus frequency applied in the current study is 50 Hz; Newland and Kondoh [98] used a GWN input signal with an upper stimulus frequency of 58 Hz. It is worth noting that they estimated the kernels using a 200 Hz GWN input signal; a 58 Hz low

pass filter was applied to this signal before it was used to drive the shaker (Figure 3.3).

Analysis of the mean 1^{st} order Volterra kernel (n=6), estimated in the current study in the frequency domain, shows that gain increases from approximately 12dB at 0.5 Hz to a maximum of 19dB at 17 Hz and then drops to 3.4dB at 50 Hz (Figure 5.5A). Analysis of the mean 1^{st} order Wiener kernel (n=17), estimated by Newland and Kondoh [98], in the frequency domain shows that gain increases from approximately -1dB at 0.5 Hz to a maximum of 6.4dB at 10 Hz and then drops to -4.5dB at 50 Hz (Figure 5.6C). Both kernels have a bandpass response (between 0 and 50 Hz) with an approximately linear phase response (Figure 5.5B). It should be noted that whilst the absolute values between studies are different, it is the underlying response shapes which are important and which are similar.

The mean value of the 2^{nd} order Volterra kernels is also very similar to the 2^{nd} order Wiener kernels estimated by Newland and Kondoh [98]. In the current work the 2^{nd} order Volterra kernel has a positive elongated peak on the diagonal at $\tau_1 = \tau_2 = 16 - 34$ ms followed by two smaller negative off diagonal peaks. Their 2^{nd} order kernel has a positive elongated peak on the diagonal at $\tau_1 = \tau_2 = 15 - 30$ ms and two smaller negative off diagonal peaks. The consistency across animals of the 2^{nd} order Volterra kernels estimated in the current study is shown in Figure 5.4C to H.

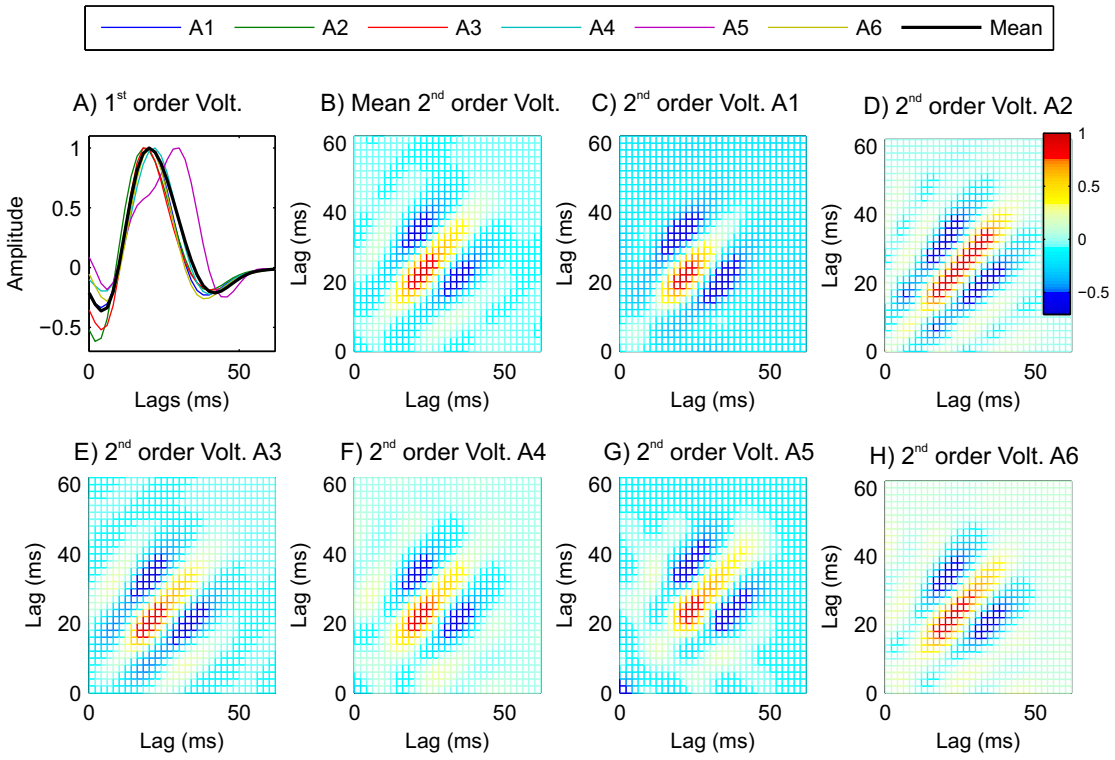

Figure 5.4: The Volterra kernels of FETi. Volterra kernels were estimated using the Wiener Laguerre method. (A) The normalised 1^{st} and (B) the mean of the 2^{nd} order Volterra kernels. (C) - (H) The individual 2^{nd} order Volterra kernels estimated from data recorded from the six animals.

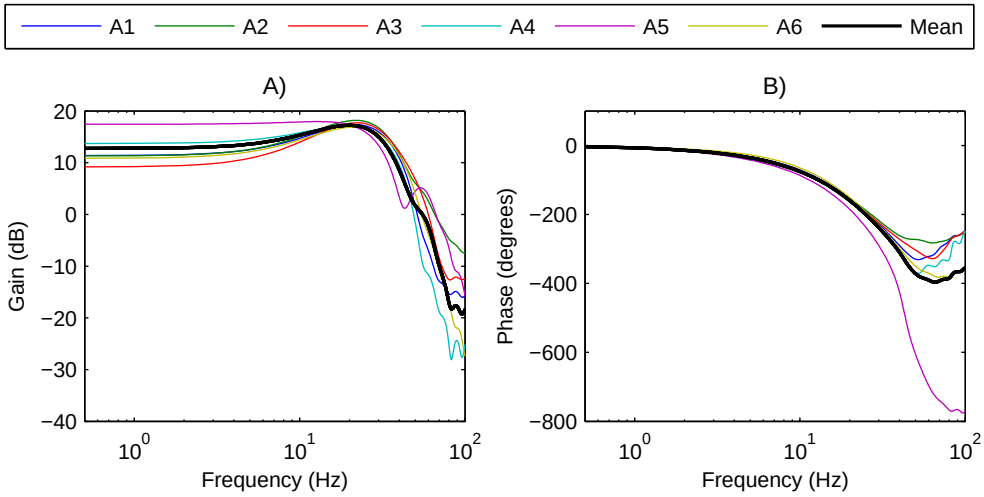

Figure 5.5: (A) The frequency and (B) the phase response of the 1^{st} order Volterra kernels of FETi. Volterra kernels were estimated using the Wiener Laguerre method.

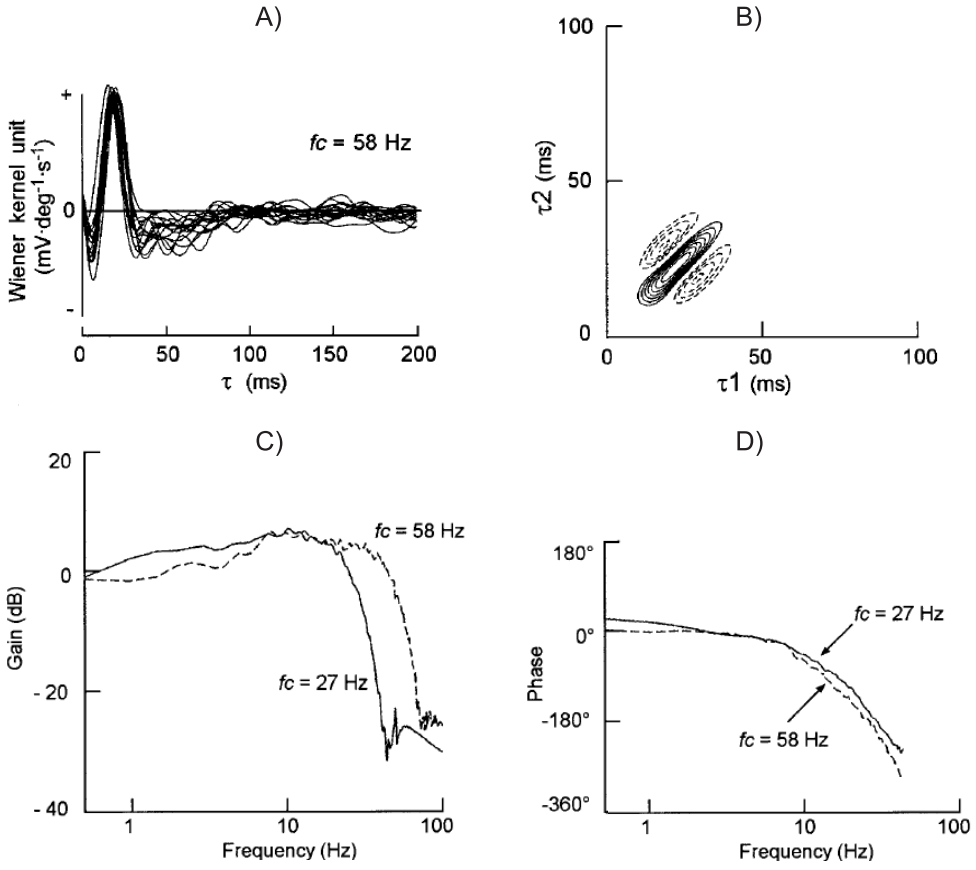

Figure 5.6: The Volterra kernels of FETi obtained by Newland and Kondoh [98] (From [98], Journal of Neurophysiology 77(5):3297-3310, with permission). (A) The 1^{st} and (B) the mean (n=21) 2^{nd} order Volterra kernels. (C) The frequency and (D) the phase response of the 1^{st} order kernel (58 Hz). Note that the frequency response of the 1^{st} order Volterra kernel estimated by Newland and Kondoh [98] using a 27 Hz low pass filtered GWN input signal is also shown in (C) and (D).

Cascade Models

The parameters of the LN, NL and LNL cascade models of FETi, estimated from recordings from six animals, are plotted in Figure 5.7. The linear element of the LN model is shown in Figure 5.7A, the input/output response of its polynomial nonlinearity in Figure 5.7B. The linear element of the NL model is shown in Figure 5.7D, the input/output response of its polynomial nonlinearity in Figure 5.7C. The first and second linear elements of the LNL model are shown in Figure 5.7E and G, the input/output response of its polynomial nonlinearity in Figure 5.7F. Its combined linear element, the convolution of its two linear elements, is shown in Figure 5.7H. It is useful to consider the combined linear element of the LNL model as this allows comparison with the 1^{st} order Volterra kernel used in previous studies [98]. The cascade models have consistent linear and nonlinear parameter estimates across the different animals (Figure 5.7). The linear elements of the LN (Figure 5.7A) and NL (Figure 5.7D) models and the combined linear element $c_{hg}(\tau)$, the convolution of $h(\tau)$ with $g(\tau)$, of the LNL model (Figure 5.7H) are very similar.

Also, the shape of the 4^{th} (LN model, Figure 5.7B) and the 5^{th} order polynomial functions (NL model, Figure 5.7C and LNL model, Figure 5.7F) is very similar and resembles that of a half wave rectifier. Two standard deviations (approximately 95.45%) of the values in the input signal to the polynomial elements are marked by dashed vertical lines. The Gaussian distribution of the input signal causes parameter estimation error to be greatest in the tails of the polynomial elements as fewer data points are available at large amplitude values [50].

5.3.4 The Volterra Kernels of the Cascade Models

The mean value of the six 1^{st} and 2^{nd} order Volterra kernels of FETi are plotted in Figure 5.8A and B. The mean values of the Volterra kernels generated using the parameters of the cascade models are plotted in Figure 5.8A, C, D and E. The parameters of the cascade models were estimated from input/output data recorded from FETi. The parameters of these models were converted into Volterra form using the equations given in Section 2.4.5 to allow comparison with the Volterra kernels.

The 1^{st} and 2^{nd} order Volterra kernels of the average LN model parameters are plotted in Figure 5.8A and C respectively. The parameters of this model were converted into Volterra form using Equation 2.53. The 1^{st} order Volterra kernel is calculated by multiplying the linear element of the LN model by the $c^{(1)}$ polynomial coefficient. The 2^{nd} order Volterra kernel is the outer product of two copies of the parameters of the linear element of the model scaled by the $c^{(2)}$ polynomial coefficient. The LN model fails to produce a 2^{nd} order kernel which can match the diagonal elongated main peak of the 2^{nd} order Volterra kernel estimated directly from experimental data (Figure 5.8 compare C with B)

The 1^{st} and 2^{nd} order Volterra kernels of the average NL model parameters are plotted in Figure 5.8A and D respectively. The NL model was converted into its Volterra form using Equation

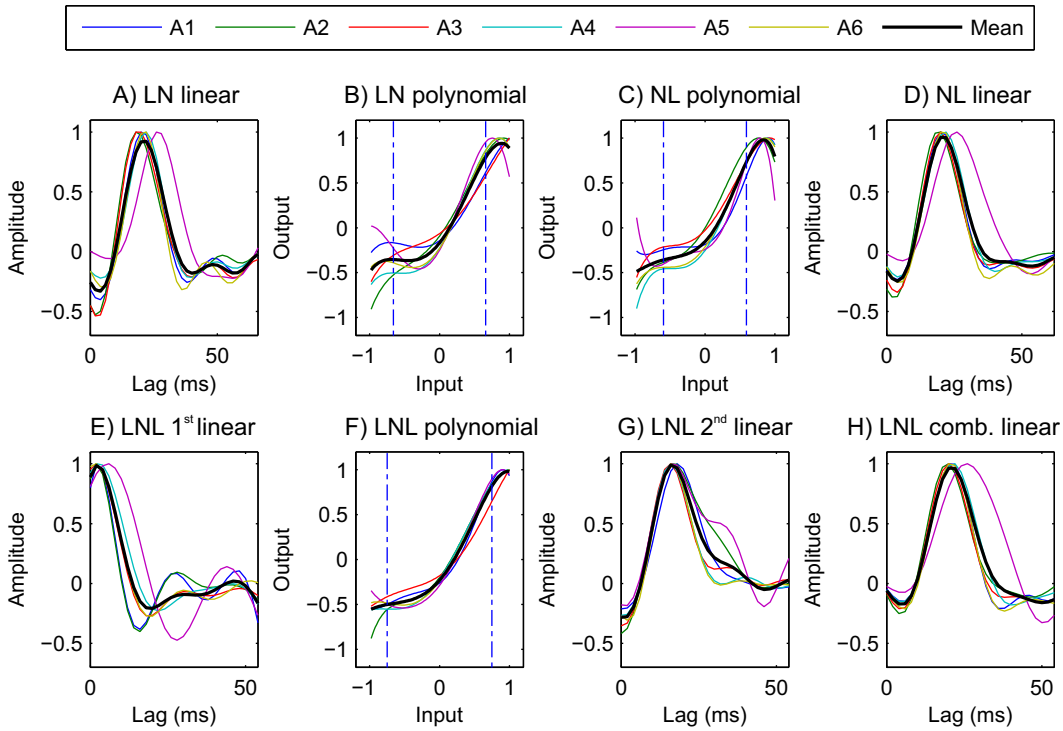

Figure 5.7: (A) - (B) The LN, (C) - (D) NL and (E) - (H) LNL cascade models of FETi. (A) The linear element $h(\tau)$ of the LN model. (B) The input/output response of its polynomial element. Leg flexion occurs when the input signal is between 0 and 1 and extension between 0 and -1. Excitatory inputs to the FETi motor neuron occur when the output signal is between 0 and 1; inhibitory inputs occur when it is between 0 and -1. Two standard deviations of the input signal to the polynomial elements are marked by dashed vertical blue lines. (C) The input/output response of the NL model, (D) shows its linear element. (E) The first linear element $h(\tau)$ of the LNL model, (F) shows the input/output response of its polynomial elements and (G) its second linear $g(\tau)$ element. (H) The combined linear element $c_{hg}(\tau)$ of the LNL model.

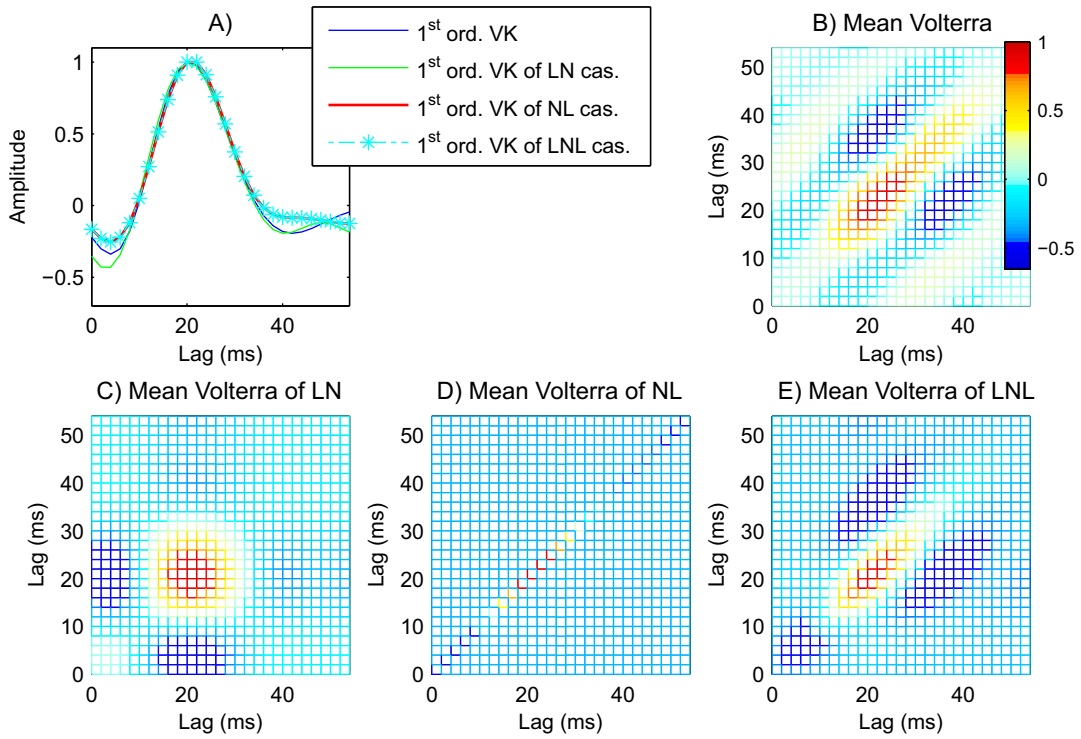

Figure 5.8: The Volterra kernels of the cascade models. The panel shown middle top defines the traces for (A). For example, the 1^{st} order Volterra kernel is abbreviated to 1^{st} ord. VK, and the 1^{st} order Volterra kernel of the LN cascade to 1^{st} ord. VK of LN. (A) The mean (n=6) value of the 1^{st} order Volterra kernels of FETi and the 1^{st} order Volterra kernels of the LN, NL and LNL cascades (mean, n=6). (B) The mean value of the 2^{nd} order Volterra kernels of FETi. (C) - (E) The 2^{nd} order Volterra kernels calculated directly from the mean (n=6) parameters of the LN, NL and LNL cascade models respectively. The similarity of the 2^{nd} order Volterra kernel of the LNL model (E) and the kernel estimated directly from the data (B) should be noted.

2.54. The parameter values of the 2^{nd} order Volterra kernel are only non zero on its diagonal, where $\tau_1 = \tau_2$. These diagonal values are the parameters of the linear element scaled by the value of the $c^{(2)}$ polynomial coefficient. The structure of the NL model allows its 2^{nd} order kernel to better match the diagonal elongated main peak (Figure 5.8 compare D with B) of the Volterra kernel. It cannot, however, capture the negative off diagonal troughs found in the 2^{nd} order Volterra kernel (Figure 5.8B) as this model can only generate values on the diagonal.

The 1^{st} and 2^{nd} order Volterra kernels of the average LNL model parameters are plotted in Figure 5.8A and E. The similarity of the 2^{nd} order Volterra kernel of the LNL model (Figure 5.8E) and the kernel estimated directly from the data (Figure 5.8B) should be noted. The 1^{st} order Volterra kernel is created by convolving the two linear elements of the LNL model and scaling the result by the $c^{(1)}$ polynomial coefficient (Equation 2.55). The 2^{nd} order Volterra kernel is the convolution of the second linear element (g) with two copies of the first linear element (h), for different lags τ_1 and τ_2. The result of this convolution is scaled by the $c^{(2)}$ polynomial coefficient.

Whilst the %MSE predictive performance of the three cascade models is similar, the LNL model with its two linear elements results in a model structure which is better able to generalise and hence to represent the shape of the 2^{nd} order kernel of the Volterra model. For this reason, the LNL cascade will be used in the current study rather than the LN or NL cascade models.

5.3.5 Model Validation with GWN, Sinusoidal and Walking Stimulation

An example of the typical response of FETi to GWN and the 2^{nd} order Volterra and LNL model predictions are shown in the time domain in Figure 5.9A. The responses to walk 1 and walk 2 and model predictions are shown in Figure 5.9B and C. Examples of the typical responses of FETi to sinusoidal stimulation (1, 2, 5 and 10 Hz) and model predictions are shown in Figure 5.10A, B, C and D respectively. All the examples were generated using data from Animal 4.

Analysis of the response of FETi to sinusoidal stimulation shows how the LNL model with its 5^{th} order polynomial element is able to capture the half wave rectifying dynamics of this system (Figure 5.10). It also shows that both model types struggle to capture the amplitude and timing of the response to the low frequency stimulation (1 and 2 Hz) signals (Figure 5.10A and B). This explains the poor %MSE performance with the low frequency sinusoidal (1 and 2 Hz) stimulation signals (Table 5.1) and also with the two walking stimulation signals, which have a similar low frequency content.

5.3.6 Final Model Structure Selection and Interpretation of Model Parameters

Whilst the performance of the different model types was similar, the LNL model structure was chosen for use in the current study because the cascade model structure was more suitable as, unlike the Volterra series models, its nonlinearity remains in two dimensional space, regardless of its order. The LNL cascade model was chosen over the LN and NL structures simply because

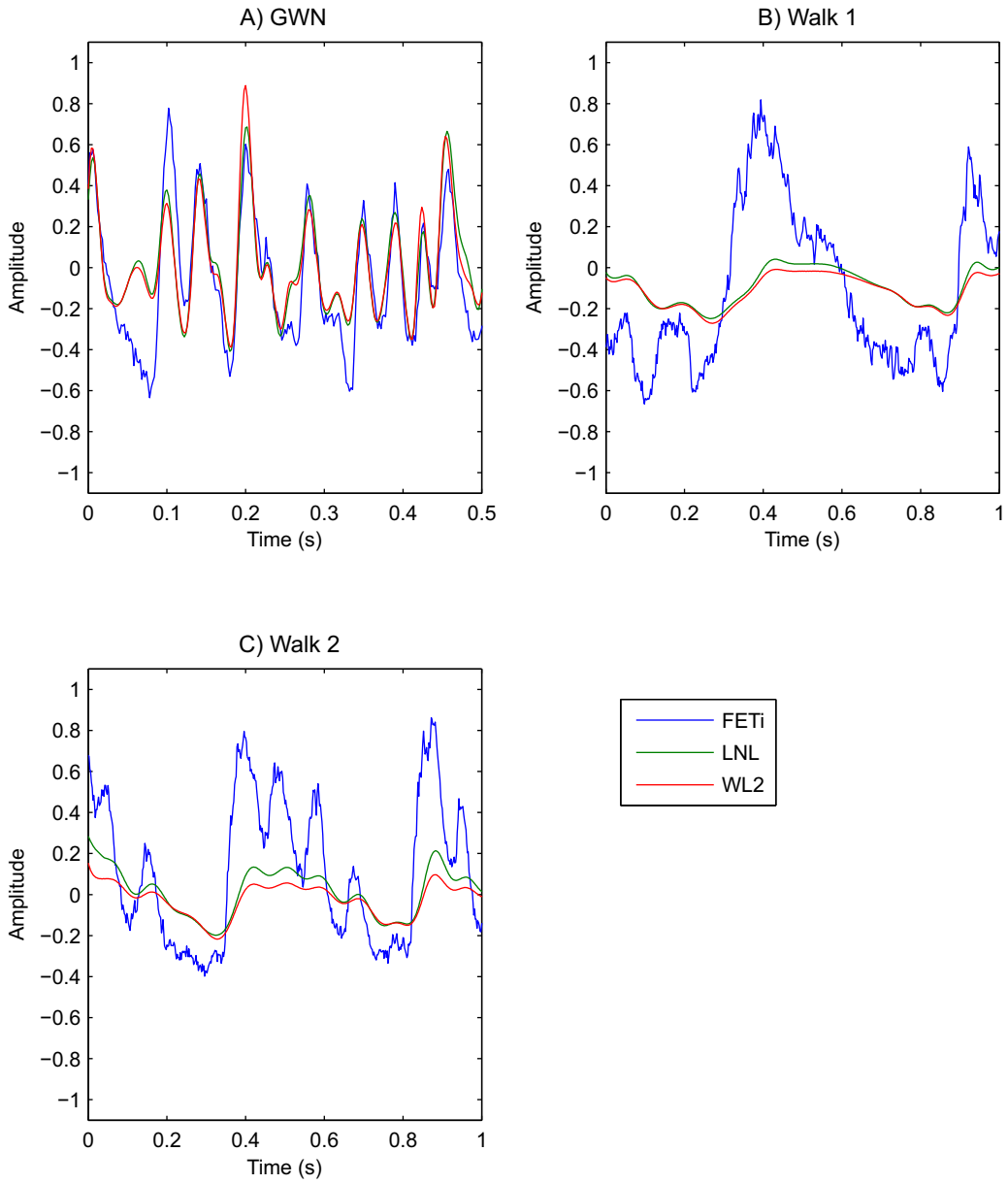

Figure 5.9: LNL and 2^{nd} order Volterra (with parameters estimated using the Wiener Laguerre method, WL2) model validation using (A) GWN, (B) walk 1 and (C) walk 2. Note that model parameters are estimated using GWN estimation data and validation is carried out using GWN validation data and the response of FETi to stimulation of the FeCO with the different walking signals. The examples are generated using data recorded from Animal 4.

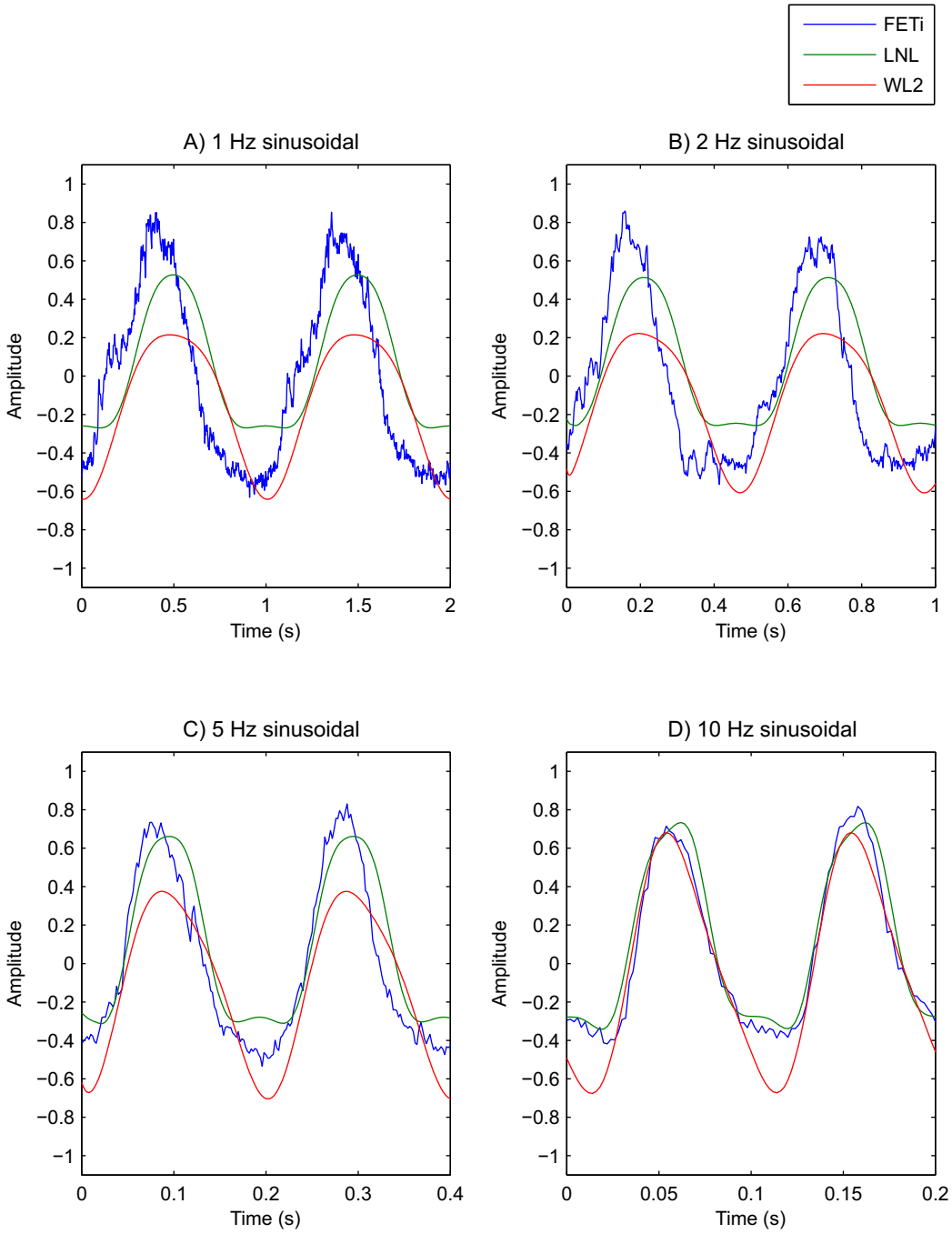

Figure 5.10: (A) - (D) The responses of the LNL and 2^{nd} order Volterra (with parameters estimated using the Wiener Laguerre method, WL2) models to 1, 2, 5 and 10 Hz sinusoidal stimulation. Note that model parameters are estimated using GWN estimation data and validation is carried out using GWN validation data and the response of FETi to stimulation of the FeCO with the different frequency sinusoidal stimulation signals. The examples are generated using data recorded from Animal 4.

it contains more degrees of freedom (Section 5.3.4, Figure 5.8).

The parameters of the LNL models of FETi estimated from data from animals 1 to 6 are plotted in the time domain in Figure 5.11A to D. The impulse response of the first $h(\tau)$ and second $g(\tau)$ linear elements of the model are shown in Figure 5.11A and C respectively. The input/output responses of the polynomial elements are shown in Figure 5.11B and are approximately half wave rectifying in nature. Two standard deviations of the input signal to the polynomial elements are marked by dashed vertical lines. The Gaussian distribution of the input signal causes parameter estimation error to be greatest in the tails of the polynomial elements as fewer data points are available at large amplitude values [50].

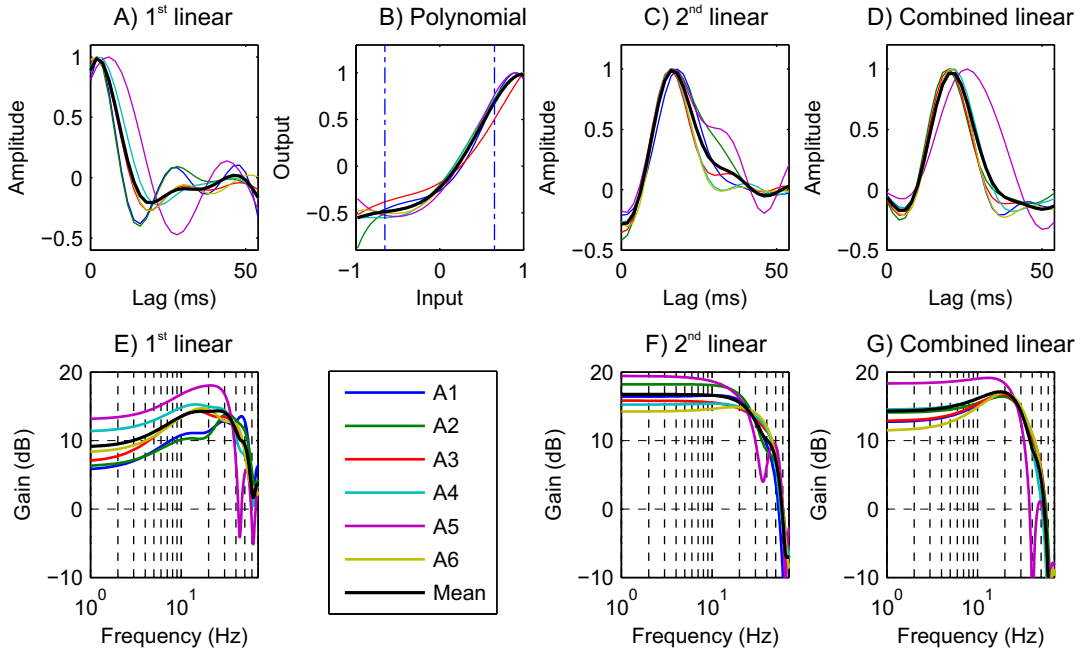

Figure 5.11: The parameters of LNL models of FETi. The panel defines the traces, for example A1 represents the results obtained from Animal 1. (A) The first linear element $h(\tau)$. (B) The input/output response of the polynomial element resembles a half wave rectifier and the directional sensitivity of FETi. Leg flexion occurs when the input signal is between 0 and 1 and extension between 0 and -1. Excitatory inputs to the FETi motor neuron occur when the output signal is between 0 and 1, inhibitory inputs to the FETi motor neuron occur when it is between 0 and -1. Two standard deviations of the input signal to the polynomial elements are marked by dashed blue lines. (C) The second linear element $g(\tau)$. (D) The combined linear element $c_{hg}(\tau)$. (E) The frequency response (magnitude) of $h(\tau)$. (F) The frequency response (magnitude) of $g(\tau)$. (G) The combined linear parameters (the convolution of the parameters of the linear elements) have a bandpass frequency response. FETi was therefore classified as mainly position sensitive but with some velocity sensitivity.

The combined linear element $c_{hg}(\tau)$, the convolution of $h(\tau)$ with $g(\tau)$, is plotted in Figure 5.11D. The frequency responses of the linear elements are plotted in Figure 5.11E, F and G. The range between DC and the upper stimulus frequency of the GWN input signal (50 Hz) is of main interest.

As the gain and delay of the LNL model can be split arbitrarily between its linear elements, its combined linear response is considered. The peak position of the combined linear element of

the LNL model estimated from Animal 5, which occurs at 26 ms, is slightly inconsistent with that of the other animals (Figure 5.11D). Its shape, however, is very similar to that of the other elements (Figure 5.11D) and a similar peak position spread was found by Newland and Kondoh [98] over a larger number of recordings (n=17). The mean (n=6) combined linear parameters of the LNL model have a monophasic kernel (Figure 5.11D) which has a bandpass frequency response (Figure 5.11G). Its mean (n=6) gain increases from approximately 12.4dB at 1 Hz to a maximum of 17.2dB at 15.1 Hz and then drops to 4.4dB at 50 Hz (Figure 5.11G). FETi was therefore classified as mainly position sensitive but with some velocity sensitivity due to the small increase in its frequency response (Figure 5.11G) [35, 54, 98, 117] (Section 7.2.2).

The half wave rectifying function (Figure 5.11B) represents the directional sensitivity of FETi. The inputs to the FETi motor neuron are excitatory (polynomial output values between 0 and 1, Figure 5.11B); the extensor reflex system responds to extension movements. A similar conclusion was reached by Newland and Kondoh [98] but from analysis of the 2^{nd} order Volterra kernel.

5.4 Discussion

This study has extended the system identification methods previously used in studies of invertebrate neuromuscular reflex limb control systems [54, 73, 97, 98, 117] to enable adaptation dynamics and nonlinear responses to be investigated (Chapter 7). Its main contributions have been the application of the cascade models, model parameter number optimisation and the novel use of sinusoidal and walking signals for model validation.

Previous studies [54, 73, 97, 98, 117] used a cross correlation approach to estimate Wiener models [80]. These Wiener models contained hundreds of parameters and therefore required long lengths of data (~20 s) to provide accurate parameter estimates. Such methods, therefore, are unsuitable for investigating the transient response of FETi which only lasts for a few seconds [11]. This study has shown that both the Wiener Laguerre parameter estimation method for the Volterra series [86] and the cascade model structure [74] can greatly reduce the number of model parameters, making them suitable for application to shorter data lengths. No significant difference was found between the %MSE predictive performance of the different models when GWN and more natural sinusoidal and walking stimulation was applied. The LNL cascade model structure, however, was chosen for use in the current study because its polynomial nonlinearity was simpler to analyse, as it remains in two dimensional space regardless of its order unlike the higher order Volterra kernels. Furthermore, the parallel nature of the Volterra model (Equation 2.26) makes it more difficult to interpret as linear and nonlinear responses need to be added and their relative importance (gain) considered. The LNL cascade structure, with its two linear elements, was chosen in preference to the LN and NL structures as it provides greater flexibility, allowing it to more closely match the shape of the 2^{nd} order Volterra kernel estimated in previous work [98].

Before the performance of the different model types was compared the number of parame-

ters they contained (model order) was optimised. Results of experiments which calculate the %MSE performance with increasing model order (Figure 5.2) show that once a plateau in performance is reached change in model order has little effect on its performance. Exact choice of model order, therefore, is not critical provided that this plateau is reached. A LNL model containing 62 parameters, 28 in each linear element and a 5^{th} order polynomial (6 parameters) for the nonlinear element, was shown to give the most accurate mean (n=6) %MSE predictive performance on the steady state response of FETi.

In the current study the %MSE metric was used for determining optimum parameter number rather than the Akaike Information Criterion [2] or the Minimum Description Length [123]. These measures scale fit by the number of parameters in the model, but gave no benefit over the simpler %MSE metric on locust data in previous work [36].

Newland and Kondoh [98] found the predictive performance of a nonlinear 2^{nd} order Wiener model to be 30% (n=17). Very similar results were obtained in the current study; the mean %MSE of the 2^{nd} order Volterra model was 29.9% (n=6). A difference in performance was expected as the current study uses slightly different experimental, signal preprocessing and system identification methods. It should be noted that the cut off frequency of the low pass filter applied to the GWN input signal in the current study was 50 Hz compared to 58 Hz in the study by Newland and Kondoh [98].

Newland and Kondoh [98] categorize responses of the mechanical and neural elements of FETi based on the frequency response of the 1^{st} order Wiener kernel. They suggest that the electrical (synaptic) inputs to the FETi mainly encode position information with only minor velocity dependence. This conclusion was reached because they interpret the frequency response of the 1^{st} order kernel as being constant gain and low passed. The frequency response of the 2^{nd} order Wiener kernel was not analysed by Newland and Kondoh [98], possibly because its interpretation is much less intuitive than the 1^{st} order kernel [85]. Instead, the 2^{nd} order Wiener kernel was analysed in the time domain; its shape led Newland and Kondoh [98] to propose that it represented a compression non-linearity.

Analysis of the parameters of the LNL model of FETi in the current study leads to a similar conclusion with FETi being classified as mainly position sensitive but with some velocity sensitivity due to the small increase in its frequency response (Figure 5.7G) [35, 54, 98, 117] (Section 7.2.2). A similar conclusion was also reached in a study which used narrow band (triangular) stimulus signals at frequencies between 0.1 and 20 Hz [44]. The half wave rectifying function represents the directional sensitivity of FETi; the extensor reflex system responds to control (oppose) flexion movements. A similar conclusion was reached by Newland and Kondoh [98] but from analysis of the 2^{nd} order Volterra kernel.

The rather high %MSE performance of the nonlinear models (around 30%), suggests that they provide quite a poor fit to the system. The recordings prior to the start of stimulation, when the input is constant, show considerable measurement noise (Figure 5.1C, section s1) and one cannot expect the model to be able to predict the random components of this signal. The consistency of the estimated kernels (Figures 5.4 and 5.7) also suggests that the model fit is

good [85] and that predictive performance of the model is poor because of the low Signal to Noise Ratio (SNR). Here the noise (measurement noise) has been defined as consisting of electrical measurement noise and background neural activity (Section 1.2).

The use of a GWN signal for system identification can be theoretically and experimentally justified [87]; however, the properties of this signal are very different from those received by the sensory neurons in the neural networks which monitor the position of invertebrate legs under natural operating conditions [20, 126]. Few studies have tested the ability of models generated using the white noise system identification technique to predict the response of limb control systems to natural stimulation.

In the current study LNL models of FETi have been validated using its response to sinusoidal and walking stimulation which is biologically more relevant than GWN stimulation [13]. As in previous work [53] the LNL model struggled to accurately predict the output of FETi to the 1 and 2 Hz sinusoidal and the walking stimulation. The mean (n=6) %MSE performance of the LNL model with 1 and 2 Hz sinusoidal stimulation and walking stimulation walk 1 and walk 2 was 64.4%, 57.5%, 77.2% and 70.0% respectively. The mean (n=6) %MSE performance with GWN stimulation was 29.9%. Through time domain signal analysis it was determined that the poor performance of the model probably occurred because it failed to capture the amplitude and timing of the responses to low frequency sinusoidal and walking stimulation ($<$ 2 Hz). It is quite possible, that a model optimised over such a wide frequency range is not able to provide accurate prediction of the low frequency response of FETi to sinusoidal and walking stimulation which only cover the 0-10 Hz frequency range [81]. Care, therefore, needs to be taken when interpreting and linking the responses of the model to the natural function of FETi and the limb which it controls when input signal frequencies are below 2 Hz. Unlike previous work [53], however, the LNL model could predict the output of FETi to 5 and 10 Hz sinusoidal stimulation as accurately as it could predict its response to GWN (29.9%MSE). The mean (n=6) %MSE performance of the LNL model with 5 and 10 Hz sinusoidal stimulation was 33.5% and 30.2% respectively. A 5 Hz frequency is functionally relevant as it matches the stepping frequency of 5.1 Hz ± 0.56 Hz observed in other work [13], from ten animals.

Before the LNL model was used to investigate adaptation of the dynamics and nonlinear responses of FETi to GWN stimulation further work was carried out to investigate the convergence properties of its parameter estimation method (Chapter 6).

Chapter 6

Analysis of LNL Parameter Estimation Methods

6.1 Introduction

The aim of the work described in this chapter is to ensure that the Smoothed Korenberg Hunter (SKH) parameter estimation method provides an accurate estimate of the parameters of the LNL model. This work needs to be carried out before the LNL model is used to investigate the dynamics and nonlinear responses of FETi (Chapter 7). To this end, investigations into the accuracy and convergence properties of the Korenberg Hunter (KH) based methods with different initialisation schemes were carried out using experimental data (locust FETi data) and data generated from computer simulations. It should be noted that in Chapter 5 the parameters of the LNL model were estimated using the SKH algorithm rather than the standard KH method. The SKH method is a modification of the KH method which has been developed by the current study to reduce high frequency parameter estimation error whilst retaining predictive model performance.

The cost function of the LNL model potentially contains a number of local and a global minimum (multi modal). As KH based methods employ nonlinear local optimisation techniques [74] they require careful parameter initialisation to ensure that they converge to the global rather than a local minimum [15, 27, 29, 33, 79, 107]. An alternative approach is to use a nonlinear global optimisation method such as simulated annealing [71] which has been developed to avoid the problem of local minima. As these methods can suffer from slow convergence and poor local search characteristics their application has often been restricted to finding initial parameter estimates for the nonlinear local optimisation methods [67]. One type of evolutionary algorithm, Differential Evolution (DE), however, has been shown to give fast and robust convergence and good local search performance [112]. It also requires few control parameters and is easy to use and implement [112]. DE has been applied to estimate the parameters of LN and NL models [3] and a modified evolutionary approach to the LNL model [69]. The DE method, however, does not seem to have been applied directly to the LNL model. As the DE method

has been designed to avoid local minima and so should converge to the global minimum it was used to check the convergence of KH based methods.

The parameter estimates produced by both the KH based and the DE methods, however, are sensitive to the properties of the input and output signals. The coloured (low pass filtered) nature of the GWN input signal coupled with the high levels of measurement noise present in the output signal can cause the linear elements of the LNL model to contain high levels of high frequency parameter estimation error and this error can obscure the underlying shape of these elements. The Smoothed Korenberg Hunter (SKH), the Down-Sampled Korenberg Hunter (DKH) and the Down-sampled Differential Evolution methods have been developed by the current study to reduce high frequency parameter estimation error.

6.2 Methods

Section 6.2.1 provides a description of the SKH and DKH parameter estimation methods. The Down-sampled Differential Evolution (DDE) algorithm is described in Section 6.2.2. The performance of the standard KH [74], the SKH, the DKH and the DDE LNL parameter estimation methods were assessed by measuring their predictive performance using experimental data and by visual analysis of their parameters. The sensitivity of the SKH and the DKH methods to parameter initialisation was investigated using experimental data (Section 6.2.3) and computer simulations. Monte Carlo simulations were used to investigate the convergence properties of the methods under controlled experimental conditions (low pass filtered GWN input signal and high levels of additive output noise)(Section 6.2.4).

6.2.1 Korenberg Hunter Based LNL Parameter Estimation

An explanation of the KH method was given in Section 2.4.6; full details can be found in [65, 74]. The SKH and the DKH methods are variants of the KH method and have been developed by the current study to reduce high frequency estimation error in the second linear element of the LNL model. The SKH method reduces this error by applying a smoothing low pass filter to the second linear element in the model $g(\tau)$ (Figure 2.1). As the LNL model is split into a linear element and a NL model $g(\tau)$ is represented by $h(\tau)$ in Algorithm 2. The low pass filter is applied to the inverse of $\hat{h}(\tau)$ ($\hat{h}(\tau)^{-1}$, Step 1, Algorithm 2, the linear element in the Hammerstein (NL) part of the LNL model) and the same filter to the estimate of $\hat{h}(\tau)$ (Step 5, Algorithm 2, Section 2.4.6). The parameters of $\hat{h}(\tau)$ are zero padded before a 4^{th} order low pass Butterworth filter with a cut off frequency of 50 Hz is applied in the forward and reverse direction to avoid introducing any phase delay (zero phase). Any estimation error which occurs at frequencies above 50 Hz (the highest frequency component in the bandlimited GWN input signal) is reduced using this low pass filter.

The DKH method reduces parameter estimation error in the linear elements of the LNL model by down sampling the input and output signals to twice the highest frequency of the input

signal (100 Hz). This increases the whiteness of the input signal, by reducing correlation between successive samples, and improves the condition of the matrix $\mathbf{U}^T\mathbf{U}$ (Section 2.2.2) in the Least Squares estimate of the second linear element of the LNL model. To ensure that the polynomial element does not introduce aliasing errors, the output of the first linear element of the LNL model was up-sampled to twice the order of the polynomial function (5^{th} order) multiplied by the maximum frequency of the input signal which is 50 Hz ($2 \times 5 \times 50 = 500$ Hz). This ensures that the Nyquist sampling condition is satisfied. The output signal from the polynomial element was then down sampled back to the original sampling frequency of 100 Hz.

Given only the input and output signals to the LNL model it is impossible to determine how the gain and delay are distributed between its elements. In the current study the gain of the first $h(\tau)$ and second $g(\tau)$ linear elements of the LNL model were normalised by dividing by the standard deviation of their parameter values. The polynomial coefficients were normalised by multiplying by the standard deviation of the values of the second linear element $g(\tau)$. The optimisation algorithm was left free to split the delay between the two linear elements of the model. It should be noted that to aid comparison of the parameters of the LNL models estimated using different algorithms they have been normalised by dividing by their maximum value before plotting.

6.2.2 Differential Evolution Parameter Estimation

A description of the standard Differential Evolution (DE) algorithm for use with the LNL model follows. The parameters of the LNL model are combined into a single vector

$$\mathbf{x} = \Big(h(1), \ldots, h(T),\ c^0, \ldots, c^Q,\ g(1), \ldots, g(T)\Big) \tag{6.1}$$

which contains D parameters, the total number of linear and nonlinear parameters in the model. Differential Evolution (DE) works with a population P^G of the vectors $\mathbf{x}$. The population contains N_p parameter vectors [112]

$$P^{(G)} = \begin{bmatrix} \mathbf{x}_1^{(G)} \\ \mathbf{x}_2^{(G)} \\ \vdots \\ \mathbf{x}_{N_P}^{(G)} \end{bmatrix} = \begin{bmatrix} x_{1,1}^{(G)} & x_{1,2}^{(G)} & \cdots & x_{1,D}^{(G)} \\ x_{2,1}^{(G)} & x_{2,2}^{(G)} & \cdots & x_{2,D}^{(G)} \\ \vdots & \vdots & \ddots & \vdots \\ x_{N_P,1}^{(G)} & x_{N_P,2}^{(G)} & \cdots & x_{N_P,D}^{(G)} \end{bmatrix} \tag{6.2}$$

Each parameter vector

$$\mathbf{x}_i^{(G)} = \Big(x_{i,1}^{(G)}, x_{i,2}^{(G)}, \ldots, x_{i,D}^{(G)}\Big) \quad i = 1, 2, \ldots, N_P \tag{6.3}$$

represents a possible solution to the optimisation problem. The population is initialised randomly and evolves in generations (iterations), G. With each generation a mutant vector, $\mathbf{v_i}$, is formed from each of the N_P parent vectors, $\mathbf{x_i}$, following

$$\mathbf{v}_i^{(G+1)} = \mathbf{x}_{r_1}^{(G)} + F\left(\mathbf{x}_{r_2}^{(G)} - \mathbf{x}_{r_3}^{(G)}\right) \tag{6.4}$$

with the multiplication factor F set by the user ($F > 0$) and random, mutually different indexes $r_1, r_2, r_3 \in \{1, 2, \ldots, N_P\}$ which are also different from i. The trial vector

$$\mathbf{u}_i^{(G+1)} = \left(u_{i,1}^{(G+1)}, u_{i,2}^{(G+1)}, \ldots, u_{i,D}^{(G+1)}\right) \tag{6.5}$$

is generated using the crossover operator

$$u_{i,j}^{(G+1)} = \begin{cases} v_{i,j}^{(G+1)} & \text{if } (rnd(j) \leq CR) \\ x_{i,j}^{(G)} & \text{if } (rnd(j) > CR) \end{cases} \tag{6.6}$$

where $j = 1, 2, \ldots, D$ and $rnd(j)$ is the j^{th} output from a random number generator with a uniform distribution. The cross over constant CR is set by the user in the range $[0, 1]$ to ensure that at least one of the parameters from $v_{i,j}$ is transferred to $u_{i,j}$. The Mean Square Error (MSE) cost function (Equation 2.3) is used to calculate the predictive performance of the LNL model with the trial ($\mathbf{u}_i$) and parent ($\mathbf{x}_i$) vectors. If predictive performance is most accurate (lowest %MSE) with the trial vector then it replaces the parent vector otherwise the parent vector is retained for the next generation. These steps are repeated until either a certain cost function value is reached or for a specific number of generations. The latter method was used by the current study. The DDE method was set up with $F = 0.5$, $CR = 0.9$ and $N_P = 10 \times D$, the values suggested in [112]. Experiments conducted in this study found that these values resulted in models with predictive performance comparable to the KH based methods and convergence within approximately 300 iterations (Figure 6.6).

The Down-sampled Differential Evolution (DDE) method uses the same approach as the DKH method to reduce parameter estimation error which occurs in the linear elements of the model at frequencies above 50 Hz (Section 6.2.1). Using a lower sampling rate also reduces computation time for this method (it reduces the N_P dimension of the population matrix P^G Equation 6.2).

6.2.3 Modelling with Experimental Data

The performance of the four LNL parameter estimation methods (KH, SKH, DKH and DDE) was measured by calculating the predictive performance of the models on experimental data and by comparison of the estimated model parameters. The aim was to check that the two modifications to the KH method gave similar predictive accuracy and model parameters as the KH method and to investigate if the KH methods converge to the same solution as the DDE method.

The experimental data used in this chapter were the same as those described in Chapter 5. These data were recorded in the FETi motor neuron in six animals by Professor Philip Newland. The predictive performance of the model was measured using the %MSE metric (Equation 2.23) using estimation and validation data. The signal preprocessing methods used in this chapter were the same as those described in Chapter 5. Models were estimated using 3 seconds of estimation data (1500 samples at fs=500 Hz) and validated using 3 seconds of data (1500 samples). This amply satisfies the criterion proposed by Marmarelis [85] that the data length is greater than ten times the number of parameters. The ability of the methods to reduce parameter estimation error and the consistency of the parameter estimates was shown by plotting the parameters of the models.

In Chapter 5 it was determined that the optimum LNL model for representing the response of FETi to GWN stimulation contained a total of 56 linear parameters (28 in each linear element) and a 5^{th} order polynomial element. The KH and SKH methods used an input/output sampling rate of 500 Hz; the DKH and DDE methods reduce this to 100 Hz, decreasing the sampling rate by a factor of 5.

In order to allow comparison of the parameters of the linear elements of the model estimated with different input/output sampling rates, the number of parameters in each linear element was increased to 30 to make it divisible by 5. These changes to the optimum number of linear and polynomial parameters were justified because they only reduced the mean %MSE predictive performance of the model by 0.2% (Figure 5.2). The parameters estimated using the DKH and DDE methods, with a sampling rate of 100 Hz were up sampled to 500 Hz to allow comparison with the parameters generated using the KH and SKH methods. As the gain of the LNL model can be arbitrarily assigned between its elements they were normalised to aid comparison.

The sensitivity of the KH based methods to parameter initialisation was investigated by comparing model performance and estimated model parameters when three different initialisation schemes were used. The first scheme (Init 1) sets the values of the first linear element $h(\tau)$ to $(\frac{1}{fs}, 0, 0, \ldots, 0)$ as these values had been found to give good results (Chapter 5). The second scheme (Init 2) set $h(\tau)$ equal to the first non-zero row of the 2^{nd} order Volterra kernel [123]. The third scheme (Init 3) filled $h(\tau)$ with values taken from MATLAB's random number generator (randn). This random number generator draws its values from a Gaussian distribution with a mean of zero and a standard deviation of one. The predictive performance of the resulting models was calculated using the %MSE metric on both estimation and validation data.

6.2.4 Computer Simulations

The effect that measurement noise has on the SKH and DDE parameter estimation methods was investigated using Monte Carlo (MC) simulations. The input and output signals used in these simulations were tuned to match experimental conditions (low pass filtered GWN input signal and high levels of additive output noise). Models were estimated using 3 seconds of estimation data (1500 samples at fs=500 Hz). MC simulations provide a useful tool for investigating algorithm convergence because they allow the parameters of the known simulated system to be compared with the estimated model parameters. This allows parameter estimation accuracy to be calculated.

A simulated LNL system was created; its parameters were based on those estimated using the SKH method from data measured in Animal 1. A GWN input signal was generated using the MATLAB randn function. This signal was filtered using a 5^{th} order low pass Butterworth filter, with a cut off frequency of 50 Hz, so that its spectrum matched that of the experimental input signal. This signal was applied to the simulated LNL system to generate the output signals. Different realisations of noise signal were added to the output of the simulated LNL system produced when the same realisation of the low pass filtered GWN input signal was applied. This process was repeated 100 times (100 MC trials). The noise signal was produced by filtering different realisations of a GWN signal using a noise model before adding it to the output of the simulated LNL system. The parameters of the noise model, a 24^{th} order autoregressive (AR) model, were estimated from the difference between the predicted model output and the response measured in the respective animal (the residual signal) using the Covariance method [68]. The order of the AR model was selected based on the Minimum Description Length [123].

The parameter bias error was measured by calculating the %MSE difference between the normalised parameters of the simulated system and the mean of the 100 normalised parameter estimates. The variance of the estimated parameters was obtained by calculating the mean (along the number of parameters) of the variance of the normalised estimated parameters. Model parameters were normalised by the maximum absolute parameter value before calculating these metrics. Parameter bias and variance values were calculated for the combined linear element of the LNL model and its polynomial element. The combined linear element was calculated by convolving the two linear elements of the model. Box and whisker plots were used to display the distribution and skewness of the parameter bias (%MSE) and variance of the different methods across the six animals. The central mark (red line) represents the median, the box edges the 25^{th} and the 75^{th} percentiles and hence gives the range of the middle 50% of the data. The Inter-Quartile Range (IQR) is calculated by subtracting the 25^{th} from the 75^{th} percentile. Whiskers extend from each end of the box to values within 1.5 times the Inter-Quartile Range (IQR) from the ends of the box. Outliers which lie more than 1.5 times the IQR from the ends of the box are indicated by the presence of red crosses [26].

6.3 Results

6.3.1 Experimental Data

A Comparison of the KH and DE Methods

The results shown in Figure 6.1 are used to demonstrate the issue of parameter estimation error with the standard KH and DE methods and the ability of low pass filtering to remove this error. LNL models were estimated from experimental data recorded from the 6 animals.

The IRF's of the first linear elements of the LNL models are shown in Figure 6.1A, E, I and M, the IRF of the second linear element in C, G, K and O. The combined linear element of the LNL model is plotted in Figure 6.1D, H, L and P. The input/output response of the polynomial elements are shown in Figure 6.1B, F, J and N. Two standard deviations of the input signal to the polynomial elements are marked by dashed vertical lines and are used to show which range of the polynomial functions response is most relevant. As the gain of the model can be arbitrarily assigned to the elements in the model, the elements have been normalised to make comparison easier. Normalisation was carried out by scaling model parameters by their maximum absolute value.

The first linear ($h(\tau)$), polynomial input/output response, second linear ($g(\tau)$) and the combined linear element of the LNL models with their parameters estimated using the standard KH approach are shown in Figure 6.1A, B, C and D respectively. The estimate of the second linear element of the LNL models (Figure 6.1C), and the combined linear elements (Figure 6.1D), obtained when the standard KH parameter estimation method is used contain high levels of high frequency parameter estimation error. This estimation error is effectively reduced by low pass filtering the second linear elements of the LNL models (Figure 6.1G and H). The filter was a zero phase Butterworth design with a cut off frequency of 50 Hz (Section 6.2). Note how the damping term (Equation 2.62) in the Levenberg Marquardt method reduces parameter estimation error in the first linear element of the LNL model (Figure 6.1A).

The first linear ($h(\tau)$), polynomial input/output response, second linear ($g(\tau)$) and the combined linear element of the LNL models with their parameters estimated using the standard DE approach are shown in Figure 6.1I, J, K and L respectively. Note now that all of the linear elements of the model contain high frequency parameter estimation error (Figure 6.1I, K and L). This estimation error is effectively reduced by applying the low pass filter (zero phase Butterworth design with a cut off frequency of 50 Hz) to the first and second linear elements (Figure 6.1M, O and P). This low pass filtering approach has been incorporated into the KH estimation algorithm and is referred to as the SKH method (Section 2.4.6). The %MSE performance of the LNL models estimated using the KH and SKH algorithms is very similar (Figure 6.4). The null hypothesis that there was no difference in the %MSE predictive performance of the models could not be rejected (Wilcoxon signed-rank test, $p > 0.05$). An alternative approach would be to use the pseudo-inverse method, but experimental work has shown that the low pass filtering method produces very similar IRF estimates (Appendix A) and is simpler and has a much lower

computational cost.

The greater variability found in the polynomial element of the LNL model when the DE method is used (Figure 6.1J and N) probably occurs because of the variability in the estimates of its first linear element (Figure 6.1I and M). It should be noted that the DE method starts with randomly generated LNL model parameters, unlike the KH method where the parameters of the first linear element are fixed (Init 1, Section 6.2.3).

Effect of Parameter Initialisation on the SKH and DKH Methods

The sensitivity of the SKH and DKH parameter estimation methods to different initialisation schemes (Section 6.2.3) was investigated using visual analysis of the models parameter's (Figures 6.2 and 6.3) and by calculating the model's predictive performance (Figure 6.4). It should be noted that these experiments are conducted using experimental data recorded from the six animals and not using simulations.

The IRF's of the first linear elements of the LNL models are shown in Figure 6.2A, E and I, the IRF of the second linear element in C, G and K. The combined linear element of the LNL model is plotted in Figure 6.2D, H and L. The input/output responses of the polynomial elements are shown in Figure 6.2B, F and J. Two standard deviations of the input signal to the polynomial elements are marked by dashed vertical lines and are used to show which range of the polynomial functions response is most relevant. As the gain of the model can be arbitrarily assigned to the elements in the model, the elements have been normalised to make comparison easier. Normalisation was carried out by scaling model parameters by their maximum absolute value.

The effect of Init 1, 2 and 3 on the SKH estimated LNL parameters is shown in Figure 6.2A to D, E to H and I to L respectively. Whilst it is not possible to know that the LNL model with Init 1 has found the true system (the LNL model structure may not be able to represent FETi), this initialisation scheme results in models with relatively stable parameter estimates. The null hypothesis, that there was no difference between the %MSE predictive performance of the SKH method with the three different initialisation schemes was rejected (Kruskal Wallis, $p < 0.05$) (Figure 6.4). A post hoc test (Dunn-Sidak) found that the difference was between the initialisation scheme Init 1 and schemes Init 2 and Init 3, with schemes Init 2 and Init 3 resulting in poor predictive performance (Figure 6.4). The mean (n=6) %MSE predictive performance of the SKH method with initialisation schemes Init 1, Init 2 and Init 3 was 33.0, 83.4 and 80.2% respectively.

The effect of Init 1, 2 and 3 on the DKH estimated LNL parameters is shown in Figure 6.3A to D, E to H and I to L respectively. As with the SKH method, the DKH method with initialisation scheme Init 1 provides models with the most stable parameter estimates. However, the parameter estimates with Init 2 (Figure 6.3E to H) now more closely resemble those obtained when Init 1 is used (Figure 6.3A to D). The null hypothesis, that there was no difference between the %MSE predictive performance of the DKH method with the three different initialisation

schemes was rejected (Kruskal Wallis, $p < 0.05$). A post hoc test (Dunn-Sidak) found that the difference was between the initialisation scheme Init 1 and Init 3, the predictive performance of the model was poor when Init 3 was used (Figure 6.4). The mean (n=6) %MSE predictive performance of the DKH method with initialisation schemes Init 1, Init 2 and Init 3 was 35.6, 32.5 and 60.7% respectively. These results suggest that the convergence of the DKH method may be less affected by the parameter initialisation method used.

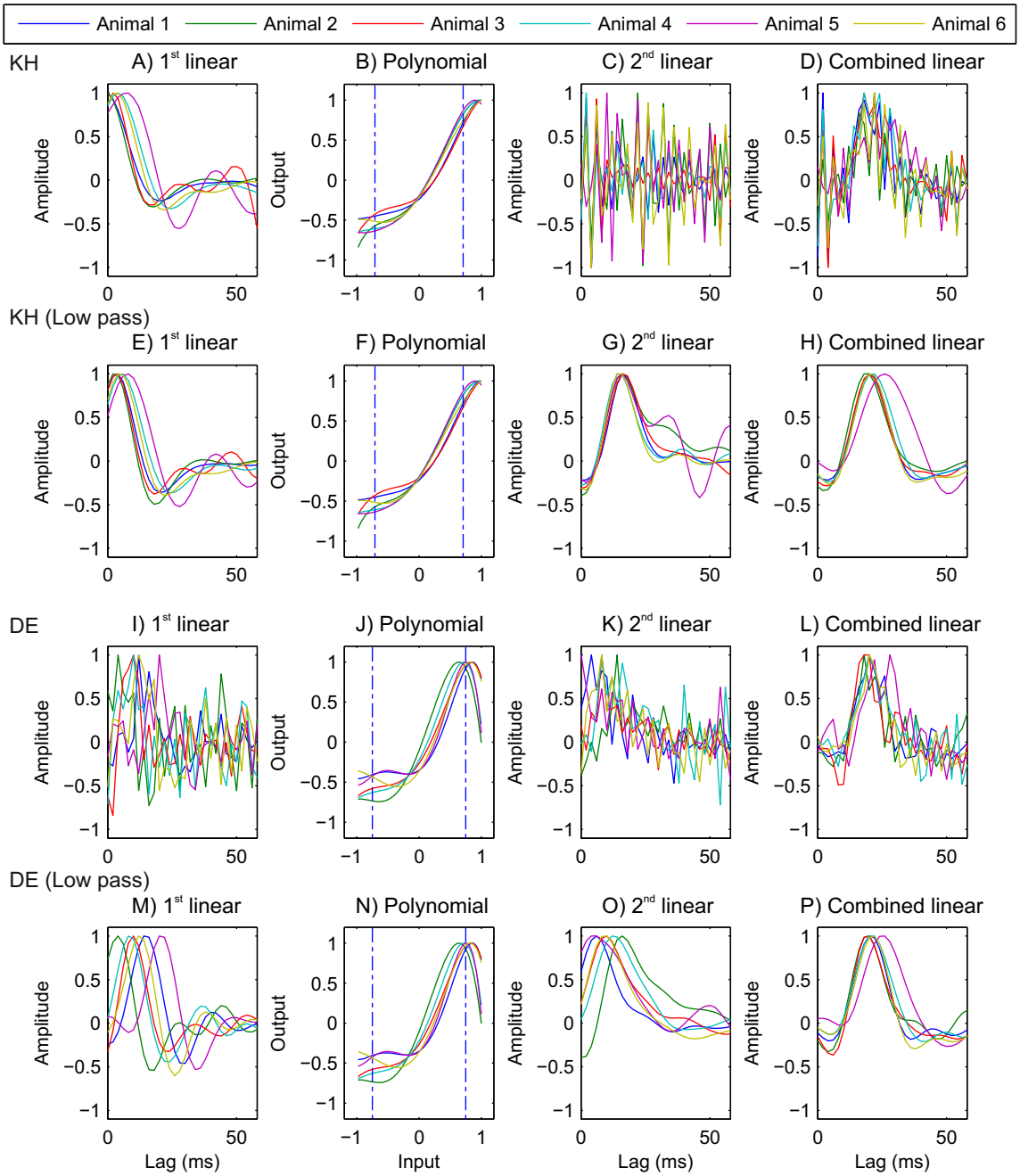

Figure 6.1: (A) - (D) A comparison of the standard Korenberg Hunter (KH) and (I) - (L) Differential Evolution (DE) LNL parameter estimation methods and (E) - (H) and (M) - (P) respectively show the ability of low pass filtering to remove high frequency parameter estimation error. (A), (E), (I), (M) The first linear elements of the LNL models. (B), (F), (J), (N) The input/output responses of the polynomial elements. (C), (G), (K), (O) The second linear elements of the LNL models and (D), (H), (L), (P) show the combined linear elements. An estimate of two standard deviations of the input signal to the polynomial elements are marked by dashed vertical blue lines. As the gain of the model can be arbitrarily assigned to the elements in the model, the elements have been normalised to make comparison easier. Normalisation was carried out by scaling model parameters by their maximum absolute value. (G) The parameters of the second linear element of the LNL model have been low pass filtered (zero phase Butterworth design with a cut off frequency of 50 Hz). (I), (K) The parameters of both the first and second linear elements of the LNL model have been low pass filtered (zero phase Butterworth design with a cut off frequency of 50 Hz).

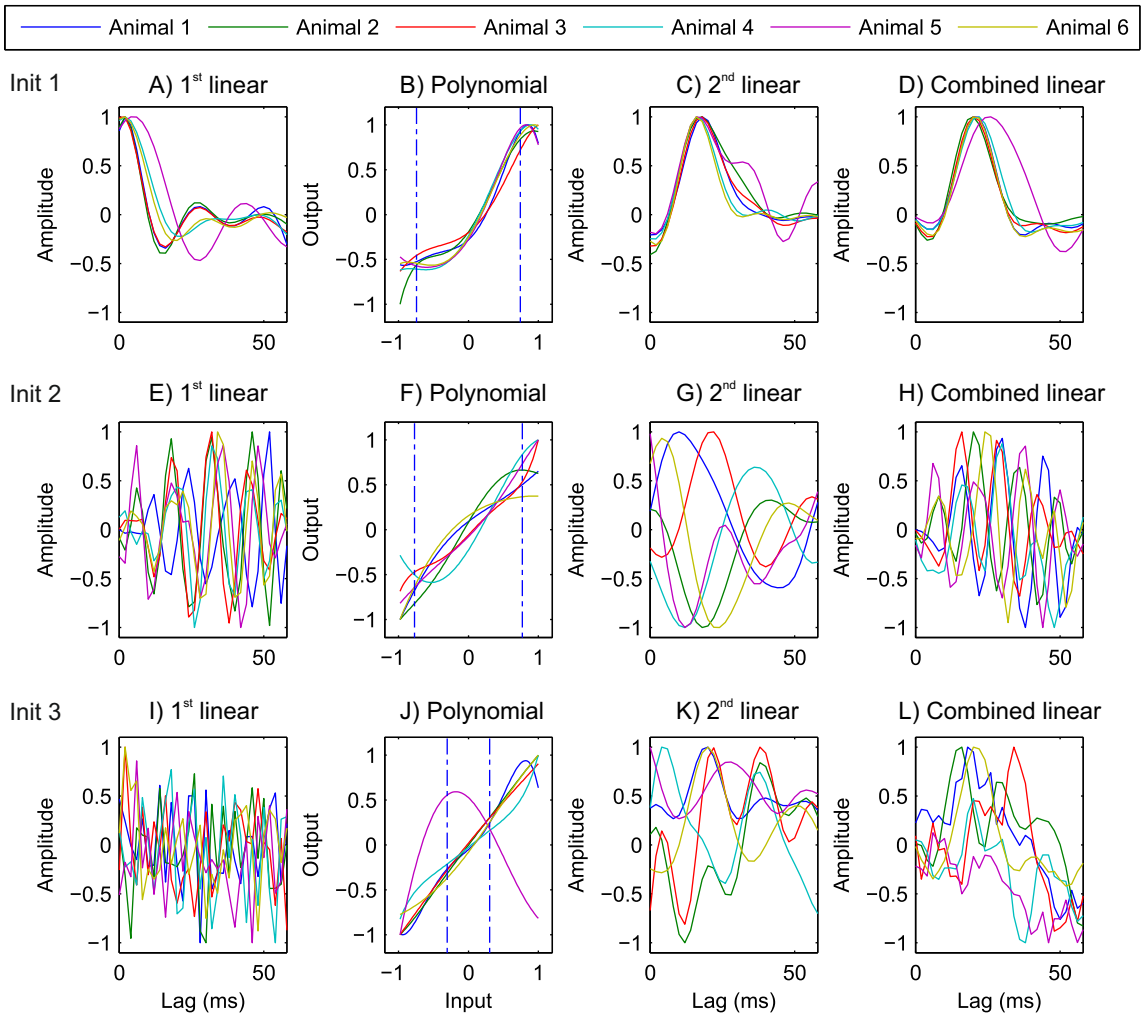

Figure 6.2: The effect that different parameter initialisation schemes have on the parameters of the LNL model. Parameters were estimated using the Smoothed Korenberg Hunter (SKH) estimation method. (A), (E) and (I) The 1^{st} linear elements. (B), (F) and (J) The input/output responses of the polynomial elements. (C), (G), and (K) The 2^{nd} linear elements. (D), (H) and (L) The combined linear elements. An estimate of two standard deviations of the input signal to the polynomial elements are marked by dashed vertical blue lines. As the gain of the model can be arbitrarily assigned to the elements in the model, the elements have been normalised to make comparison easier. Normalisation was carried out by scaling model parameters by their maximum absolute value. The parameters of the model estimated using the SKH method with initialisation scheme Init 1 are shown in (A) to (D), with scheme Init 2 in (E) to (H) and Init 3 in (I) to (L). Init 1 sets the values of the first linear element $h(\tau)$ to $(\frac{1}{fs}, 0, 0, \ldots, 0)$. Init 2 sets $h(\tau)$ equal to the first non-zero row of the 2^{nd} order Volterra kernel [123]. Init 3 fills $h(\tau)$ with values taken from MATLAB's random number generator. This random number generator draws its values from a Gaussian distribution with a mean of zero and a standard deviation of one.

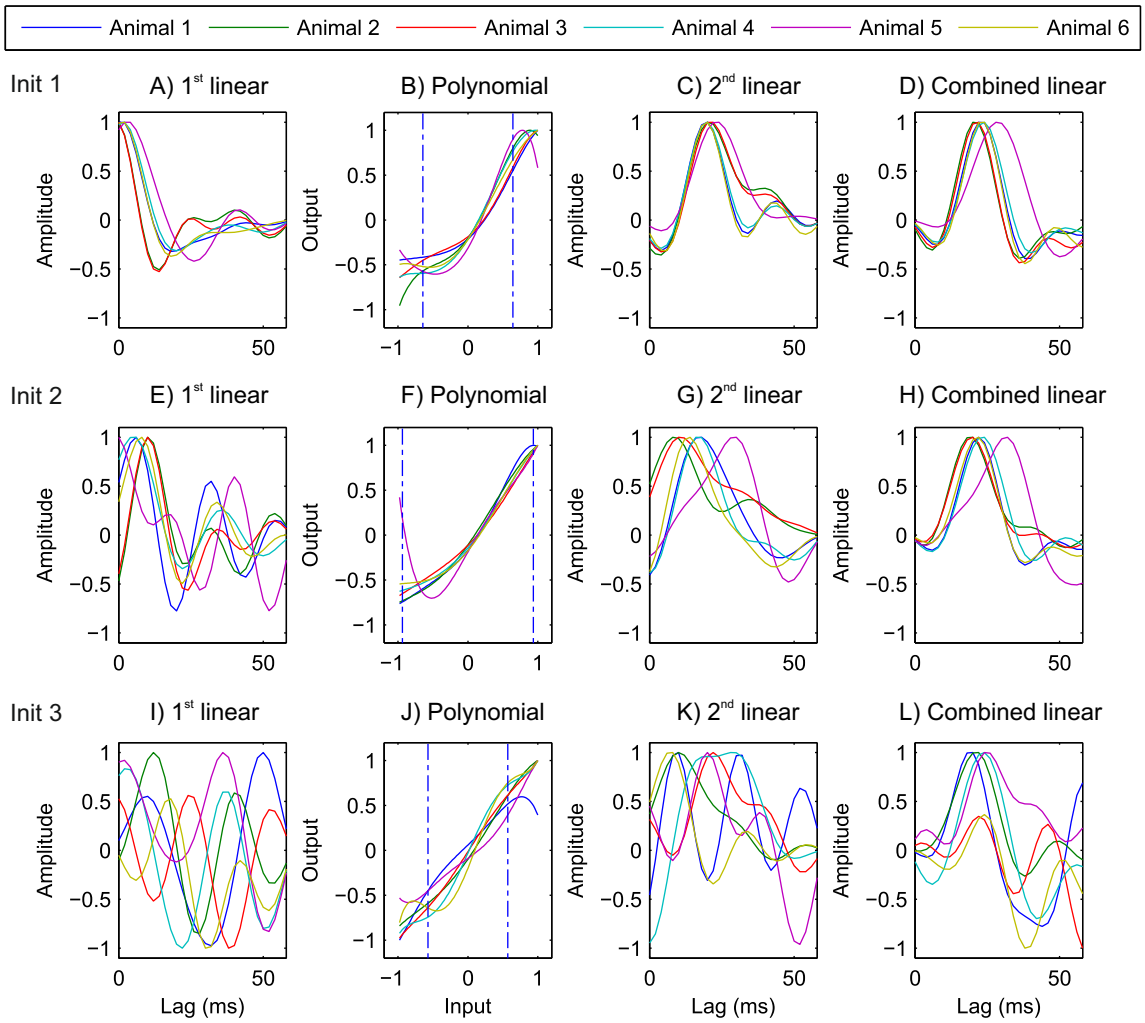

Figure 6.3: The effect that different parameter initialisation schemes have on the parameters of the LNL model. Parameters were estimated using the Down-sampled Korenberg Hunter (DKH) estimation method. (A), (E), (I) The first linear elements of the LNL models. (B), (F), (J) The input/output responses of the polynomial elements. (C), (G), (K) The second linear elements of the LNL models. (D), (H), (L) The combined linear elements. An estimate of two standard deviations of the input signal to the polynomial elements are marked by dashed vertical blue lines. As the gain of the model can be arbitrarily assigned to the elements in the model, the elements have been normalised to make comparison easier. Normalisation was carried out by scaling model parameters by their maximum absolute value. (A) - (D) Show the parameters of the LNL model estimated using the DKH method with initialisation scheme Init 1, (E) - (H) with scheme Init 2 and (I) - (L) Init 3. Init 1 sets the values of the first linear element $h(\tau)$ to $(\frac{1}{fs}, 0, 0, \ldots, 0)$. Init 2 sets $h(\tau)$ equal to the first non-zero row of the 2^{nd} order Volterra kernel [123]. Init 3 fills $h(\tau)$ with values taken from MATLAB's random number generator (randn). This random number generator draws its values from a Gaussian distribution with a mean of zero and a standard deviation of one.

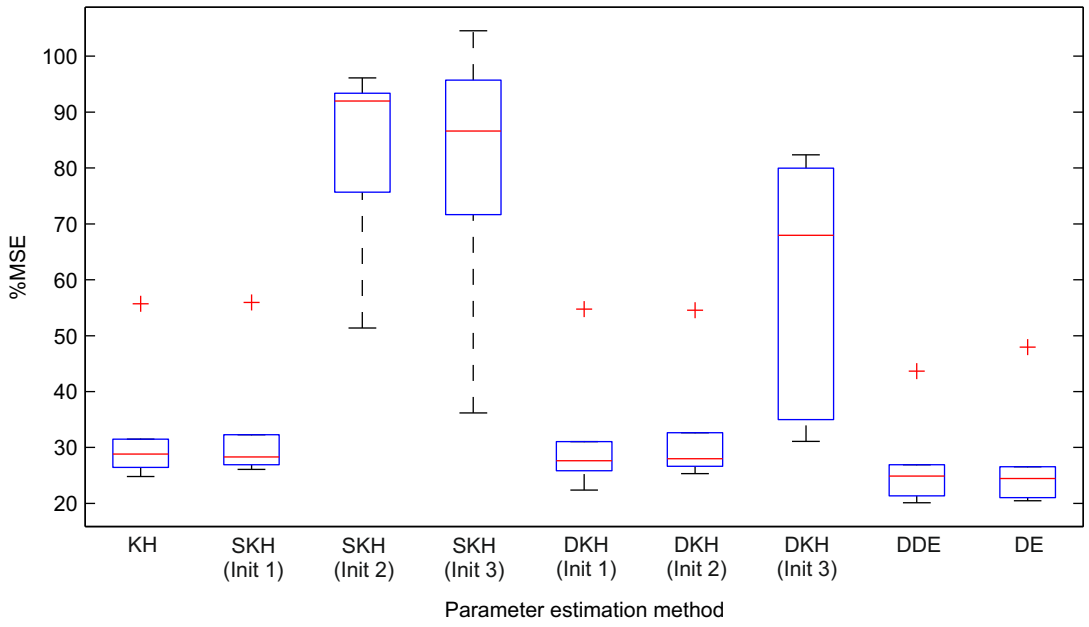

Figure 6.4: The %MSE predictive performance of the LNL model with different parameter estimation methods. Box and whisker plots were used to display the distribution and skewness of the performance (%MSE) of the different methods across the six animals at predicting the response of the system to GWN on estimation data. The central mark (red line) represents the median, the box edges the 25^{th} and the 75^{th} percentiles and hence gives the range of the middle 50% of the data. The Inter-Quartile Range (IQR) is calculated by subtracting the 25^{th} from the 75^{th} percentile. Whiskers extend from each end of the box to values within 1.5 times the Inter-Quartile Range (IQR) from the ends of the box. Outliers which lie more than 1.5 times the IQR from the ends of the box are indicated by the presence of red crosses [26].

LNL Parameter Estimation using the DDE Method

The parameters of the LNL model estimated from experimental data using the DDE method, with random parameter initialisation, are shown in Figure 6.5. This method returns a model with parameters which are very similar to those estimated using the SKH (Figure 6.2A to D) and the DKH methods (Figure 6.3A to D). Furthermore, statistical testing found no significant difference (Kruskall Wallis, $p > 0.05$) between the performance of the DKH, DDE and DE methods.

As the SKH (with initialisation scheme Init 1), the DKH (with initialisation scheme Init 1) and the DDE method effectively reduce parameter estimation error and provide the most consistent and accurate predictions of FETi they were the focus of the rest of this study.

The convergence of the %MSE with each iteration (or generation for the DDE algorithm) for these methods is shown in Figure 6.6. After 260 iterations the %MSE value for all methods plateau at approximately 30%. The initial %MSE values for the DDE method are much larger than those for the SKH and DKH methods. This is probably because the DDE method is initialised with randomly chosen parameters whereas the KH based methods use initialisation scheme Init 1 (Section 6.2.3).

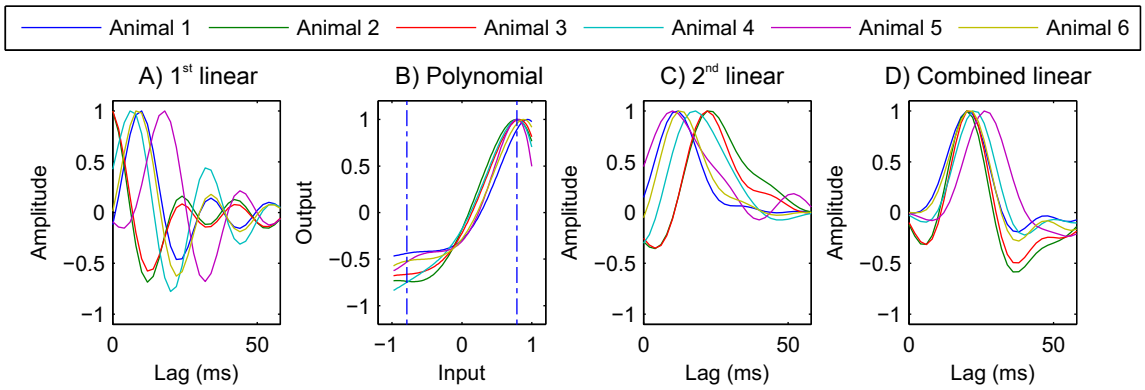

Figure 6.5: The parameters of the model estimated using the Down-sampled Differential Evolution (DDE) method. Note the DDE method uses a random initialisation scheme to set its initial parameter values. (A) The first linear elements of the LNL models. (B) The input/output responses of the polynomial element. (C) The second linear element of the LNL models and (D) the combined linear elements. An estimate of two standard deviations of the input signal to the polynomial elements are marked by dashed vertical blue lines. As the gain of the model can be arbitrarily assigned to the elements in the model, the elements have been normalised to make comparison easier. Normalisation was carried out by scaling model parameters by their maximum absolute value.

6.3.2 Monte Carlo Simulations

MC simulations were used to investigate the convergence properties of the SKH, DKH and the DDE methods. Note that the KH based methods used initialisation scheme Init 1. Simulations used input and output signals which had been generated to match experimental conditions

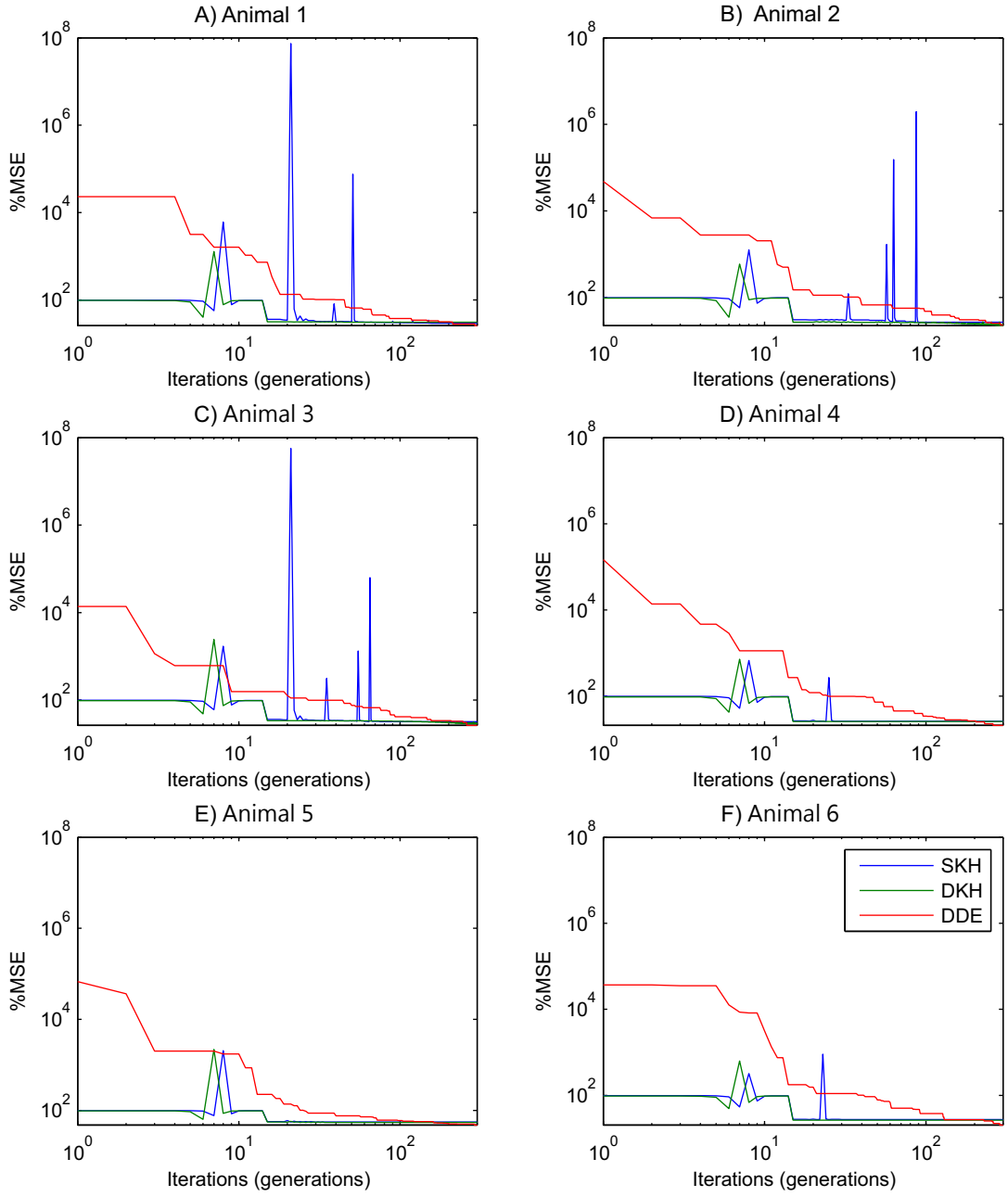

Figure 6.6: The convergence of the Smoothed Korenberg Hunter (SKH), the Down-sampled Korenberg Hunter (DKH) and the Down-sampled Differential Evolution (DDE) algorithms on experimental data. (A) - (F) The results for Animals 1 to 6 respectively.

(low pass filtered GWN input signal and high levels of additive output measurement noise). An example of the results of the MC simulations (100 trials) which used data recorded from Animal 1 to generate the simulated LNL system for the SKH, DKH and the DDE methods is shown in Figure 6.7A to D, E to H and I to L respectively.

The IRF's of the first linear elements of the LNL models are shown in Figure 6.7A, E and I, the IRF of the second linear element in C, G and K. The combined linear element of the LNL model is plotted in Figure 6.7D, H and L. The input/output response of the polynomial elements are shown in Figure 6.7B, F and J. Two standard deviations of the input signal to the polynomial elements are marked by dashed vertical lines and are used to show which range of the polynomial functions response is most relevant. As the gain of the model can be arbitrarily assigned to the elements in the model, the elements have been normalised to make comparison easier. Normalisation was carried out by scaling model parameters by their maximum absolute value.

As the delay of the LNL model can be split arbitrarily between its linear elements (the gain of the linear elements has been normalised for visualisation purposes) the focus of visual analysis of the parameter estimates is on the input/output response of the polynomial element (Figure 6.7B, F and J) and the combined linear response (Figure 6.7D, H and L). For this example, visual analysis of the polynomial elements suggests that the DDE method produces estimates with the smallest bias error but the largest variance (Figure 6.7B, F and J). Visual analysis of the combined linear elements suggests that the SKH method produces estimates with the smallest bias error and variance (Figure 6.7D, H and L).

Parameter bias was quantified by measuring the %MSE difference between the parameters of the simulated system and the mean of the 100 parameter estimates. The variability of the parameter estimates was measured using the mean of the variance of the estimated parameter values. Six simulated systems were generated from the data recorded from Animals 1 to 6. The bias and variance values of the combined linear elements of the LNL models for the SKH, DKH and DDE methods are shown in Figure 6.8A and B respectively. The bias and variance of the input/output response of the polynomial element for the SKH, DKH and DDE methods are shown in Figure 6.8C and D respectively. The box and whisker plots were used to display the distribution and skewness of the parameter bias (%MSE) and variance values across the six animals.

The null hypothesis, that there was no difference between the bias of the linear elements of the model when the SKH, DKH and DDE methods were used was rejected (Kruskal Wallis, $p < 0.05$). A post hoc test (Dunn-Sidak) found that the difference was between the SKH method and the DDE and the DKH methods. The null hypothesis, that there was no difference between the bias of the polynomial elements of the model could not be rejected (Kruskal Wallis, $p > 0.05$).

The null hypothesis, that there was no difference between the variance of the parameters of the linear elements was rejected (Kruskal Wallis, $p < 0.05$); post hoc testing (Dunn-Sidak) found that the difference was between the SKH method and the DKH and DDE methods. The null

hypothesis, that there was no difference between the variance of the polynomial elements was rejected (Kruskal Wallis, $p < 0.05$); post hoc testing (Dunn-Sidak) again found this difference to be between the SKH and DKH methods and the DDE method.

These results suggest that in general the SKH method provides the parameter estimates with the lowest bias and variance error.

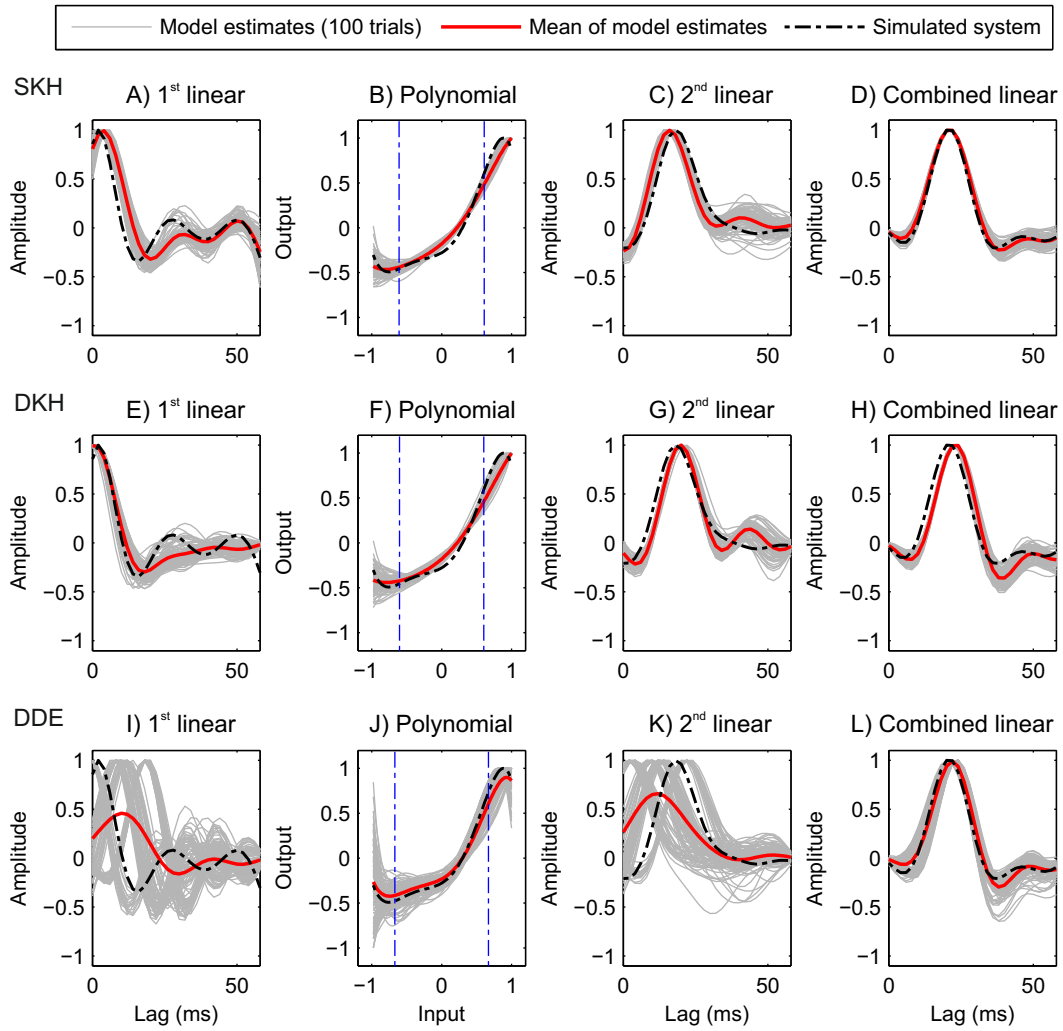

Figure 6.7: MC simulations were used to investigate the convergence properties of the Smoothed Korenberg Hunter (SKH), the Down-sampled Korenberg Hunter (DKH) and the Down-sampled Differential Evolution (DDE) algorithms under experimental conditions (high levels of additive output noise and low pass filtered GWN input signal). The simulated system (dashed black line) was generated from data recorded from Animal 1 and was used to create an input/output data set free from output measurement noise. The input signal was created so that its spectrum matched that of the experimental input signal. Different realisations of noise signal were added to the output of the simulated system produced when the same realisation of low pass filtered GWN input signal was applied. This process was repeated 100 times and resulted in 100 parameter estimates (solid grey lines). The noise signal was produced by filtering different realisations of a GWN signal using a noise model before adding it to the output of the simulated system. (A), (E), (I) The 1^{st} linear elements of the LNL models. (B), (F), (J) The input/output responses of the polynomial elements. (C), (G), (K) The 2^{nd} linear elements of the LNL models. (D), (H), (L) The combined linear elements. An estimate of two standard deviations of the input signal to the polynomial elements are marked by dashed vertical blue lines. As the gain of the model can be arbitrarily assigned to the elements in the model, the elements have been normalised to make comparison easier. Normalisation was carried out by scaling model parameters by their maximum absolute value. (A) - (D) The parameters of the LNL model estimated using the SKH method with initialisation scheme Init 1. (E) - (H) The parameters estimated using the DKH method (Init 1). (I) to (L) The DDE method.

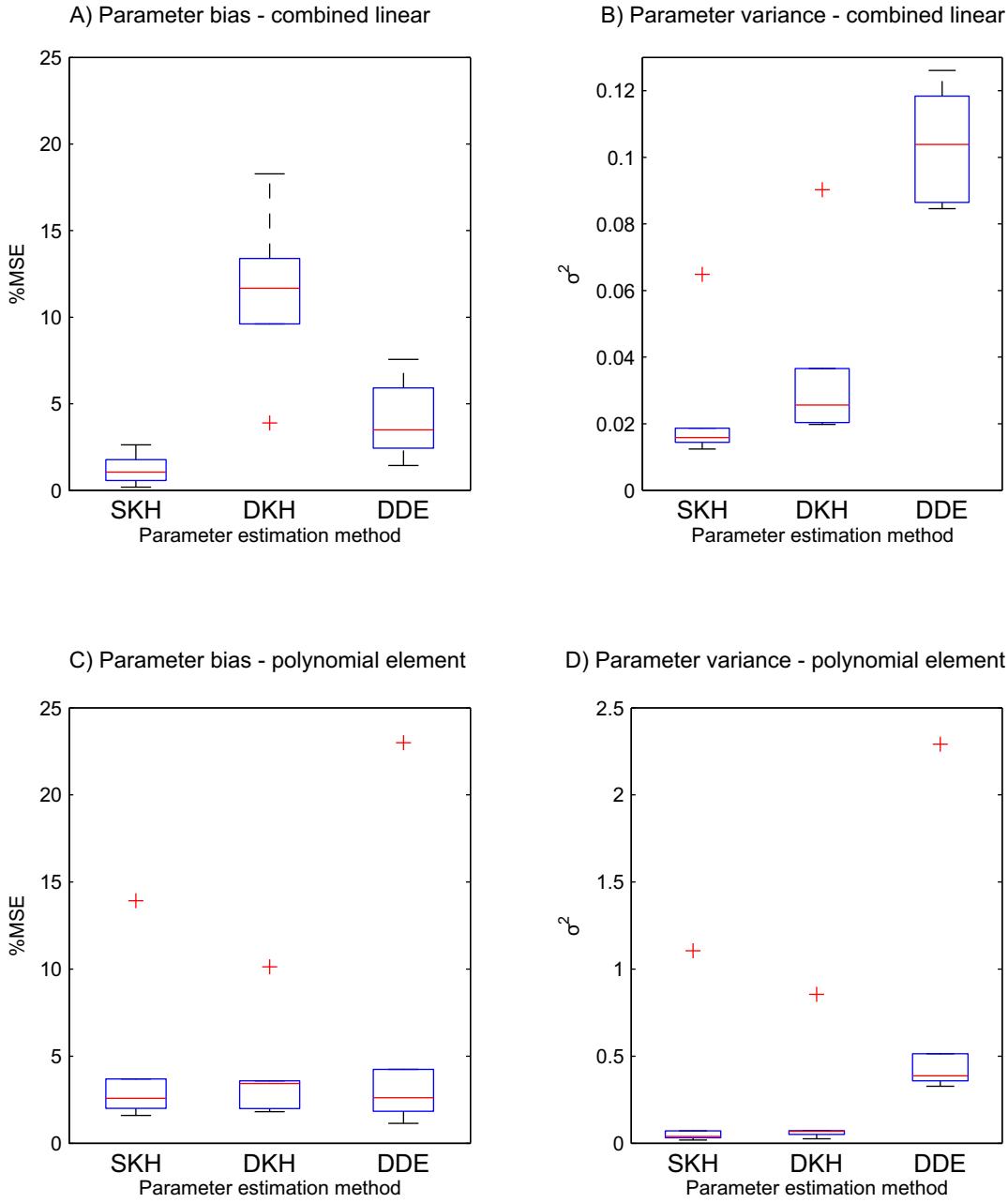

Figure 6.8: LNL model parameter uncertainty calculated from Monte Carlo simulations using the Smoothed Korenberg Hunter (SKH), the Down-sampled Korenberg Hunter (DKH) and the Down-sampled Differential Evolution (DDE) methods. (A) The parameter bias of the combined linear element of the LNL model, (B) the variance of this parameter. (C) The parameter bias of the polynomial element of this model, (D) the variance of this parameter. Box and whisker plots were used to display the distribution and skewness of the parameter bias (%MSE) and variance of the different methods across the six animals. The central mark (red line) represents the median, the box edges the 25^{th} and the 75^{th} percentiles and hence gives the range of the middle 50% of the data. The Inter-Quartile Range (IQR) is calculated by subtracting the 25^{th} from the 75^{th} percentile. Whiskers extend from each end of the box to values within 1.5 times the Inter-Quartile Range (IQR) from the ends of the box. Outliers which lie more than 1.5 times the IQR from the ends of the box are indicated by the presence of red crosses [26].

6.4 Discussion

Investigations into the accuracy and convergence properties of the KH and the DE based parameter estimation methods with different initialisation schemes has been carried out using experimental data and data generated from computer simulations (MC simulations). Methods to estimate the parameters of the Wiener-Hammerstein model have recently received much attention for control applications [106] but not for application to biological systems. KH based methods are those most widely applied to biological applications [74] (Chapter 5). The DE based methods which have been designed to deal with local minimum and so should converge to the global minimum, were used to check the convergence of KH based methods. A key result of the current study is that the KH based algorithms arrive at a solution which is very similar to that reached by the DE based methods suggesting that the KH methods are finding the global minimum.

The SKH and DKH methods have been developed by the current study to reduce high frequency parameter estimation error which occurs in the second linear element of the LNL model when the standard KH method is used. The DDE method has been developed to reduce parameter estimation error in both elements of the LNL model. The results have shown that both the SKH, DKH and DDE methods effectively reduce parameter estimation error whilst retaining accurate %MSE predictive model performance.

Previous work [15, 27, 29, 33, 79, 107] found that gradient based methods (KH based) for estimating the parameters of the LNL model require careful parameter estimation to ensure that they converge to the global rather than suboptimal local minima. This property is common to all gradient based methods working with multi modal error surfaces. The current study has also shown that both the SKH and DKH gradient based methods require careful initialisation to ensure that they converge to the global minimum.

The study by Bali et al. [7] overcame the problem of local minima by simplifying the structure of the LNL model and including a step in their identification algorithm that decomposed the original optimisation problem (four dimensional) into one and two-dimensional problems. As the cost functions could easily be visualised, convergence to the global minimum could be checked [7]. As with the DE approach, the algorithm developed by Bali et al. [7] avoids local minima but this comes at the price of efficiency.

Monte Carlo (MC) simulations have allowed the performance of the parameter estimation methods to be compared under experimental conditions (low pass filtered GWN input and high levels of output measurement noise). In particular, they have allowed the accuracy of the parameter estimates to be compared with the parameters of the simulated system. The DDE method removes the requirement for careful parameter initialisation and has the advantage of a flexible cost function. Tests have been carried out comparing the performance of the DE method with mean and median squared error cost functions on data recorded from neurons in the locust's femur/tibia reflex control loop and no significant difference in performance was found (private communication, Natalia Angarita-James). Furthermore, in the current study, the

DDE method was found to be less accurate, in terms of parameter bias and variance, than the SKH method. In [4] a gradient based optimisation method was found to provide more accurate performance with less deviation than a genetic algorithm. As the DDE method is also computationally more expensive the SKH method was chosen for the experiments described in Chapter 7.

Chapter 7

System Identification Analysis of Adaptation Dynamics and Nonlinear Responses of FETi

7.1 Introduction

The aim of the work presented in this chapter was to test the null hypothesis that FETi dynamics and nonlinear responses are the same during transient and steady state sections.

Spiking and non spiking neurons in the local networks that control limb movements in both the locust and crab are known to adapt their output amplitude or spike firing rate to repetitive stimulation [44, 54]. The focus of previous system identification studies, however, has been on the steady state dynamics and nonlinear responses of such systems [54, 98, 117]. As these studies used Wiener/Volterra series models, which contained many parameters and were estimated from signals which contained high levels of noise, they required large amounts of data (typically 20 s) to obtain robust parameter estimates. Thus, these models are not suitable for application to the dynamics and nonlinearity of the transient response which occurs during the first few seconds of stimulation.

The use of a parsimonious model structure and Monte Carlo simulations has allowed the current study to analyse system dynamics and nonlinear responses while output amplitude adaptation is occurring.

7.2 Methods

In Chapter 6 it was shown how the high levels of measurement noise present in the response of FETi coupled with the short data lengths for model estimation caused the parameters to contain relatively high levels of estimation error. It was desirable to minimise this error, to enable accurate parameter estimation and the null hypothesis to be robustly tested. As the length of the data segments could not be increased, measurement noise was reduced by applying the stimulation signal twice; the output was the average of the two responses.

The method used to optimise the number of model parameters (Section 5.2.3) has been extended to follow the approach described in [95] and data are now split into model estimation, validation and test data sections (Section 7.2.1). Furthermore, estimation and validation data were split into multiple non-contiguous sections to ensure that over training did not occur.

In Chapter 5, it was concluded that the LNL model provided the most suitable Volterra type structure for analysis of FETi dynamics and nonlinear responses during adaptation. The LNL model contains few parameters so it can be fitted to relatively short lengths of data and hence it can be used to represent the system's transient response. The LNL model can also accurately represent the system's complex nonlinear responses to GWN and 5 and 10 Hz sinusoidal stimulation (Chapter 5). Its nonlinear element also remains easy to interpret as, regardless of its order, it remains in two dimensional space. As the methods used in Chapter 5 have been significantly modified, it was necessary to re-compute the optimum number of model parameters for the different model types (2^{nd} and 3^{rd} order Volterra models and the LN, NL and LNL cascade models) and compare their predictive performance (Section 7.2.1). A description of model structures and methods used to estimate their parameters is provided in Chapter 2. It should be noted that the Volterra model parameters were estimated using the Wiener Laguerre method (Section 2.4.4) and those of the cascade models using the SKH method (Section 5.2.2).

7.2.1 Measuring Predictive Performance and Optimising the Number of Model Parameters

Measuring Predictive Performance

Predictive performance was measured by calculating the percentage Mean Square Error (%MSE) difference between the recorded FETi motor neuron output, $z(t)$, and the predicted model output, $\hat{y}(t)$ [123].

$$\%MSE = 100 \times \frac{Var(z - \hat{y})}{Var(z)} \tag{7.1}$$

$Var(x)$ was calculated using

$$Var(x) = \frac{1}{T}\sum_{t=1}^{T} x^2(t) - \left(\frac{1}{T}\sum_{t=1}^{T} x(t)\right)^2 \tag{7.2}$$

where T is the number of samples in the signal x. It should be noted that $z(t)$ is the average of the response of two recordings from the FETi motor neuron to identical GWN stimulation. Signal averaging was carried out in order to reduce measurement noise, to which end the stimulation signal was applied twice. The output was the average of the two FETi responses. The performance of the model improves as the %MSE performance measure decreases.

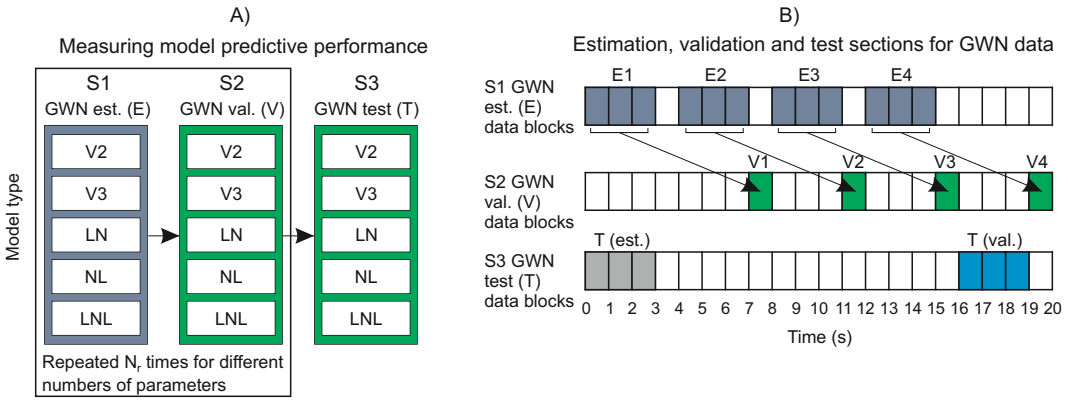

Figure 7.1: Measuring model predictive performance. (A) In S1 and S2 the %MSE predictive performance for each model type was calculated with differing numbers of model parameters (N_r). The optimum number of model parameters was that which gave the most accurate (minimum %MSE) performance on validation data (S2). The average %MSE value from the six animals was used to determine the optimum number of model parameters. The different model structures, containing the optimum number of parameters, were then tested on a previously unused section of GWN data (S3). (B) GWN data sections used for model estimation (E), validation (V) and test (T). The average of the %MSE values calculated from the four data blocks (V1 to V4) was used to represent the performance of the model on GWN data.

The methods used in Section 5.2.3 were extended to take into account the high levels of measurement and background noise which occurs in the recordings prior to the start of stimulation, when the input is constant (Figure 5.1C, s1). As the model cannot predict the random components of this signal an estimate of the Maximum Deterministic Performance (MDP) that could be achieved by the model is calculated. FETi is defined as a deterministic system N whose output $y(t)$ depends only on the input signal $u(t)$, $z(t) = y(t) + \upsilon(t) = N(u(t)) + \upsilon(t)$ where the measured output $z(t)$ depends on the driving input $u(t)$ and measurement noise $v(t)$, which is assumed to be independent of the input. The measurement noise consists of spontaneous background neural activity and electrical measurement noise. Assuming that the model can predict the deterministic response of FETi exactly then Equation 7.1 reduces to the %MDP which can be calculated from the FETi output signal using

$$\%MDP = 100 \times \frac{Var(\upsilon)}{Var(y + \upsilon)} \tag{7.3}$$

Optimising the Number of Model Parameters

Before the performance of the different model types was compared the number of parameters they contained was optimised. As six sets of input/output data were available from individual animals (Animals 1 to 6), for a given model type, six models were estimated (Figure 7.1A S1).

The %MSE performance of each of these models (representing FETi in Animals 1 to 6) with a varying number of parameters (N_r) was then calculated, using validation data (Figure 7.1A S2) not used in estimating model parameters.

This was carried out for the five different model types. For each animal this enabled the %MSE performance of each model type, with varying numbers of parameters, to be calculated and plotted (Figure 7.2). The optimum number of parameters for a given model type was determined from the minimum %MSE value, achieved in each animal, averaged across all animals (Figure 7.2). To reduce the possibility of over training during parameter estimation, validation was carried out on non contiguous blocks of data (E1 to E4, V1 to V4, Figure 7.1B) [95]. Parameters were estimated using four 3 s blocks of data (E1 to E4, Figure 7.1B) and models validated using four 1 s blocks of data (V1 to V4, Figure 7.1B). The overall validation performance, used in stage S2 (Figure 7.1B) to measure model performance when it contained different numbers of parameters, was taken as the average of the %MSE values from the four validation blocks of data. Once the optimum number of model parameters had been determined the predictive performance of the different model structures could be compared. Each model type, containing its optimum number of parameters, was estimated from the first 3 s block of steady state FETi response to GWN stimulation, Figure 7.1B, T (est.). Model testing was carried out on a previously unused 3 s section of GWN response data, Figure 7.1B, T (val.), to provide a more realistic estimate of model performance on fresh data.

The ability of the models to generalise was tested by measuring their %MSE performance to predict the response of FETi to 5 Hz sinusoidal stimulation. As with GWN response data, for each animal, the average of two recordings of the response of FETi to identical sinusoidal input stimulation was taken to reduce measurement noise. Models, with their parameters estimated from GWN input/output data, were evaluated by calculating the %MSE difference (3 s sections of data) between the average measured output of FETi to sinusoidal stimulation and the predicted model output to the same sinusoidal stimulation. Whilst it would have been ideal to use more natural walking stimulation signals for model validation it was found (Chapter 5) that the LNL model could not accurately predict the system's response to such low (<2 Hz) frequency stimulation. A 5 Hz frequency, however, is functionally relevant as it matches the stepping frequency of 5.1 Hz ± 0.56 Hz observed in other work [13], from ten animals.

7.2.2 Measuring FETi Dynamics and Nonlinear Responses

Block wise LNL models were estimated from 3 s non overlapping blocks of input/output data recorded from the onset of GWN stimulation until the end of the steady state section. The first block wise model, therefore, corresponds to the transient response of FETi. The dynamics of the FETi motor neuron, its sensitivity to position, velocity or acceleration, were characterised through analysis of the combined linear element of the block wise LNL models [35, 54, 73, 97, 98, 117].

A position sensitive model was identified by a linear element (kernel) with a monophasic im-

pulse response and flat frequency response; a velocity sensitive model by a biphasic kernel and a frequency response with a linear increase in the frequency response (20dB/decade) and an acceleration sensitive model by a triphasic impulse response (40dB/decade increase in the frequency response) [35, 117]. The dynamics of each block wise model was measured by fitting a regression line to the frequency response (magnitude only) of the combined linear element of the LNL model. The regression line was fitted between 2 and 15 Hz [35] and its gradient was used to quantify the dynamics of FETi for each 3 s block.

The nonlinear response of FETi was represented using the input/output response of the polynomial nonlinear element of the block wise LNL models.

7.2.3 Parameter Estimation Error

Monte Carlo (MC) simulations [38] were used to assess the accuracy of the gradient estimates and the nonlinear responses of the block wise LNL models. For each recording the block wise LNL model was used as a simulated system model (SSM) to create an input/output data set free from output measurement noise. The input signal was created by filtering a GWN signal using a 5^{th} order low pass Butterworth filter, with a cut off frequency of 50 Hz, so that its spectrum matched that of the experimental input signal. Different realisations of noise signal were added to the output of the SSM produced when the same realisation of low pass filtered GWN input signal was applied. This process was repeated 100 times (100 MC trials). The noise signal was produced by filtering different realisations of a GWN signal using a noise model before adding it to the output of the SSM. The parameters of the noise model, a 24^{th} order autoregressive (AR) model, were estimated from the difference between the predicted model output and the response measured in the respective animal (the residual signal) using the Covariance method [68]. The order of the AR model was selected based on the Minimum Description Length [123].

7.2.4 Null Hypothesis Testing

The null hypothesis, that FETi dynamics are the same during transient and steady state response sections, was tested using the Wilcoxon signed rank test. The analysis was extended to consider the accuracy of the gradient estimates, obtained using MC simulations, and changes in FETi dynamics with time in each individual animal. If the confidence limits given by the 2.5 and 97.5% percentiles from the 100 MC trials of the transient gradient estimate fell outside the mean of the gradient values calculated from the steady state response of the recording this would strongly suggest that differences existed between transient and steady state dynamics. If they included the mean then differences were probably due to parameter estimation error.

A similar approach was applied to investigate the nonlinear response of FETi and its response to 5 Hz sinusoidal stimulation.

7.3 Results

7.3.1 Model Structure Comparison and Selection

Optimisation of the Number of Model Parameters

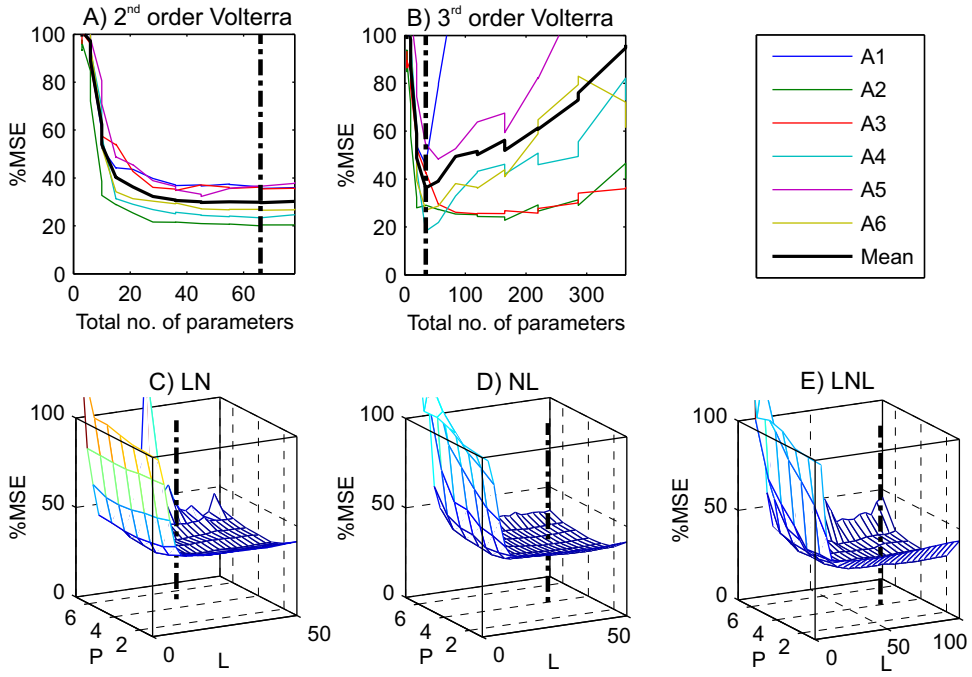

Figure 7.2: Variation of %MSE predictive performance for the different model structures with the number of parameters they contain. The panel shown top right defines the traces, for example A1 represents the result obtained from Animal 1. (A) - (E) The %MSE variation for the 2^{nd} and 3^{rd} order Volterra models and the mean (n=6) %MSE for the LN, NL and LNL cascade models. The mean %MSE value is marked using the thick solid black line, the minimum mean %MSE value by the dotted thick black line. L and P represent the total number of linear parameters and the polynomial order respectively. Note that model performance improves as the %MSE value decreases and that model accuracy was calculated using validation data. In general there is a plateau in the %MSE curves (A), (C), (D) and (E) and once this area has been reached a change in the number of parameters has little effect on model performance.

The number of parameters each model contained was optimised before the predictive performance of the different model structures was compared. The variation in the %MSE predictive performance of the 2^{nd} and 3^{rd} order Volterra and the LN, NL and LNL cascade models is shown in Figure 7.2A to E respectively. Note that model performance improves as the %MSE value decreases (Equation 7.1). Model accuracy was calculated using validation data (Section 7.2.1 and Figure 7.1A and B) and parameters were estimated from 3 s blocks of steady state responses. In general there is a plateau in the %MSE curves (Figure 7.2A, C, D and E) and once this flat area has been reached an increase in the number of parameters has little effect on performance. For the 2^{nd} order Volterra and cascade models the exact choice of the number of model parameters is therefore not critical provided that the plateau is reached. The exception is the %MSE curve for the 3^{rd} order Volterra model (Figure 7.2B). The number of parameters in

this model type can have a considerable effect on model performance (Figure 7.2B) indicating over training.

The minimum %MSE performance of the 2^{nd} order Volterra model of 29.6% (Figure 7.2A) occurs when it contains a total of 66 parameters. It should be noted that this is the number of the reduced set of parameters used in the regression matrix of the Wiener Laguerre method. The total number of parameters M is given by

$$M = \frac{(J+Q)!}{J!Q!} \tag{7.4}$$

where J is the number of functions in the decomposition (J=6), Equation 2.42, and Q is the order of the Volterra series. The minimum %MSE performance of the 3^{rd} order Volterra model of 36.1% (Figure 7.2B) occurs when it contains 35 parameters. As the cascade models contain dynamic linear and static nonlinear elements it was necessary to determine the variation in %MSE performance across both of these variables to enable the optimum number of parameters to be found. The mean %MSE performance for the LN, NL and LNL models with the number of linear parameters they contain (L) and polynomial order (P) is plotted in Figure 7.2C, D and E. These results show that the optimum LN cascade model had a mean %MSE performance of 33.1% and contained 26 linear parameters and 6 polynomial coefficients (5^{th} order polynomial) (Figure 7.2C). The optimum NL cascade model had a mean %MSE performance of 32.2% and contained 36 linear parameters and 5 polynomial coefficients (4^{th} order polynomial) (Figure 7.2D). The optimum LNL model had a mean %MSE performance of 26.9% and contained 36 parameters in each linear element and 5 polynomial coefficients (4^{th} order) (Figure 7.2E).

Predictive Performance of the GWN Models

Having found the optimum number of parameters for each model structure it was possible to compare their performance. To provide a more realistic estimate of model performance on fresh data, predictive performance was calculated on a previously unused 3 s section of steady state data (Figure 7.1B). Model parameters were estimated using the first 3 s of steady state response (Figure 7.1B). The mean (n=6) performance on test data for the 2^{nd} and 3^{rd} order Volterra models and the LN, NL and LNL cascade models was 28.0, 38.4, 35.2, 31.5 and 29.1 %MSE respectively. Statistical analysis of these data using the Kruskal Wallis test [77] found no significant difference ($p > 0.05$) between the predictive performance of the models.

Model Structure Choice

As performance of the different model types was similar the cascade model structure was chosen for use in the current study. This was because the cascade model structure was more suitable, as unlike the Volterra series models, its nonlinearity remains in two dimensional space, regardless of its order.

Measurement noise was reduced by taking the average of two recordings of the response of

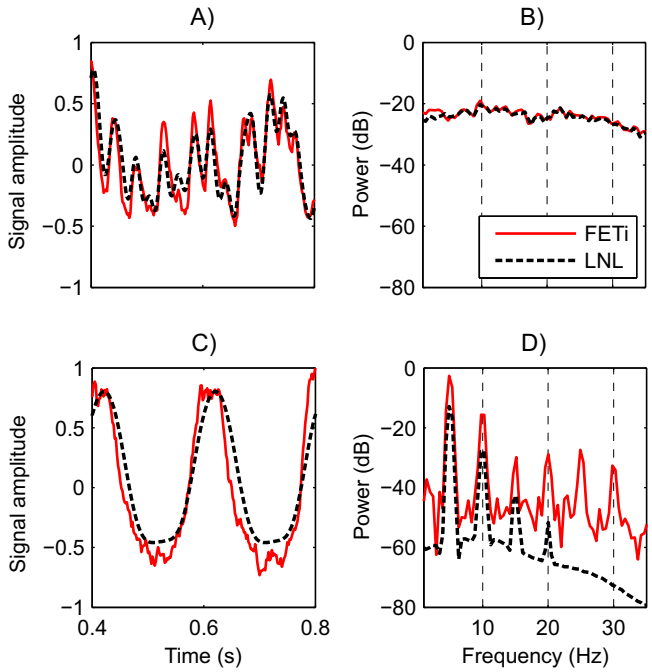

Figure 7.3: LNL model validation with GWN and sinusoidal stimulation. Note that the LNL model parameters are estimated using GWN estimation data and validation is carried out using GWN test data and the response of FETi to 5 Hz sinusoidal stimulation of the FeCO. The examples are generated using data recorded from Animal 4. (A) The response of FETi to GWN stimulation of the FeCO and the signal predicted by the LNL model (test data). (B) The spectrum of these signals. (C) The response of FETi to 5 Hz sinusoidal stimulation of the FeCO and the signal predicted by the LNL model. (D) The spectrum of these signals. The LNL model, with its 4^{th} order nonlinear element can successfully capture the higher order dynamics in the response of FETi.

FETi to the same sinusoidal input signal. Models, with their parameters estimated from GWN input/output data, were evaluated by calculating the %MSE between the average measured output of FETi to sinusoidal stimulation and the predicted model output to sinusoidal input on a 3 s section of data.

The mean (n=6) performance on test data for the LN, NL and LNL cascade models was 38.2, 34.1 and 20.4 %MSE respectively. As statistical analysis of these data using the Kruskal Wallis test [77] found a significant difference ($p < 0.05$) between the predictive performance of the LNL and the LN and NL models, the LNL structure was chosen to represent FETi. It should be noted that the predictive performance of the 2^{nd} and 3^{rd} order Volterra models was 66.7 and >100 %MSE respectively, and they are thus clearly inferior in their ability to generalise.

An example of the typical response of FETi to GWN and 5 Hz sinusoidal stimulation and the LNL model predictions are shown in the time and frequency domain in Figure 7.3. Analysis of the response of FETi to 5 Hz sinusoidal stimulation shows how the LNL model with its 4^{th} order polynomial element is able to capture the half wave rectifying dynamics of this system (Figure 7.3C). The ability of the model to represent the higher order harmonics present in the response of FETi can be clearly seen by plotting its spectrum (Figure 7.3D). The relatively high %MSE performance of the LNL model (around 30% for GWN stimulation), suggests

that it provides quite a poor fit to the system (similar performance was also obtained in [98]). However, the mean %MDP which could be expected from a LNL model which provides an exact fit to FETi (GWN stimulation) was estimated to be 20.8%.

7.3.2 Interpretation of Model Parameters

The parameters of the LNL models of FETi estimated from data from animals 1 to 6 are plotted in the time domain in Figure 7.4A, B, C and G. The impulse response of the first $h(\tau)$ and second $g(\tau)$ linear elements of the model are shown in Figure 7.4A and C respectively. The input/output responses of the polynomial elements are shown in Figure 7.4B and are approximately half wave rectifying in nature. Two standard deviations of the input signal to the polynomial elements are marked by dashed vertical lines. The Gaussian distribution of the input signal causes parameter estimation error to be greatest in the tails of the polynomial elements as fewer data points are available at large amplitude values [50]. The combined linear element $c_{hg}(\tau)$, the convolution of $h(\tau)$ with $g(\tau)$, is plotted in Figure 7.4G. The frequency responses of the linear elements are plotted in Figure 7.4D, F and H. The range between DC and the upper stimulus frequency of the GWN input signal (50 Hz) is of main interest.

As the LNL model is a subset of the Volterra series, its parameters can be transformed directly into Volterra form. This allows the parameters of the LNL model of FETi estimated in the current study to be compared with those of the 2^{nd} order Volterra models used in the study by Newland and Kondoh [98]. In the current study the 2^{nd} order Volterra kernels were calculated directly from the mean (n=6) parameters of the LNL model using

$$\mathbf{h}_n(\tau_1, \ldots, \tau_n) = c^n \sum_{\sigma=0}^{T-1} g(\sigma) h(\tau_1 - \sigma) h(\tau_2 - \sigma) \tag{7.5}$$

The 1^{st} order Volterra kernel is created by convolving the two linear elements of the LNL model and scaling the result by the $c^{(1)}$ polynomial coefficient, Equation 7.5. It is equivalent to the combined linear elements of the LNL model. The 2^{nd} order Volterra kernel is the convolution of the second linear element, $g(\tau)$, with two copies of the first linear element, $h(\tau)$, for different lags τ_1 and τ_2. The result of this convolution is scaled by the $c^{(2)}$ polynomial coefficient.

As the gain and delay of the LNL model can be split arbitrarily between its linear elements its combined linear response is considered. The peak position of the combined linear element of the LNL model estimated from Animal 5, which occurs at 26 ms is slightly inconsistent with that of the other elements (Figure 7.4G). Its shape, however, is very similar to that of the other elements (Figure 7.4G) and a similar peak position spread was found by Newland and Kondoh [98] over a larger number of recordings (n=17). The mean (n=6) combined linear parameters of the LNL model have a monophasic kernel (Figure 7.4G) which has a bandpass frequency response (Figure 7.4H). Its mean (n=6) gain increases from approximately 12.4dB at 1 Hz to a maximum of 17.2dB at 15.1 Hz and then drops to 4.4dB at 50 Hz (Figure 7.4H). FETi has been classified as mainly position sensitive but with some velocity sensitivity due to the small

increase in its frequency response (Figure 7.4H) [35, 54, 98, 117] (Section 7.2.2). A similar conclusion was also reached in a study which used narrow band (triangular) stimulus signals at frequencies between 0.1 and 20 Hz [44].

The half wave rectifying function (Figure 7.4B) represents the directional sensitivity of FETi. The inputs to the FETi motor neuron are excitatory (polynomial output values between 0 and 1, Figure 7.4B); the extensor reflex system responds to extension movements. A similar conclusion was reached by Newland and Kondoh [98] but from analysis of the 2^{nd} order Volterra kernel. The 2^{nd} order Volterra kernel of the LNL model (Figure 7.4E) is very similar to that of their 2^{nd} order kernel estimated directly from input/output data [98]. Their mean 2^{nd} order kernel parameter values had a positive elongated peak on the diagonal at $\tau_1 = \tau_2 = 15 - 30$ ms and two smaller negative off diagonal peaks (Figure 5.6). In the current study a positive elongated peak was found on the diagonal at $\tau_1 = \tau_2 = 14 - 34$ ms along with two smaller negative off diagonal peaks (Figure 7.4E).

7.3.3 Transient and Steady State Dynamics and Nonlinear Responses

FETi Frequency Response Changes with Time

Block wise LNL models were estimated from 3 s non overlapping blocks of data recorded from FETi when GWN stimulation was applied. The frequency response (magnitude only) of the combined linear element of the LNL model was estimated from each block (block wise (BW), Figure 7.5). The frequency responses shown in Figure 7.5A are calculated from the model estimated from the transient response of FETi and those in Figure 7.5D to H from its steady state response. Parameter estimation error is also considered and represented by the 2.5 and 97.5% percentiles (Figure 7.5, BW ± pctl) calculated from MC trials (100). The average model frequency response from the steady state section is represented by SSμ (Figure 7.5). This example also illustrates how little the frequency response of the block wise model changes with time (Figure 7.5A to H). It also demonstrates how the dynamics of FETi (Dyn, Figure 7.5) can be represented by the gradient of a regression line fitted to the model's frequency response (magnitude only) between 2 and 15 Hz (Figure 7.5). Comparison of FETi dynamics with that of ideal position (IP) and ideal velocity (IV) sensitive models reinforces the classification of FETi in Section 7.3.2 as being mainly position sensitive but with some velocity sensitivity.

FETi Dynamics

In this section a null hypothesis that FETi dynamics are the same in the transient and the steady state response sections is tested.

LNL model parameters were estimated from 3 s long non overlapping blocks of input/output data recorded from FETi. Models were fitted to the data from the onset of GWN stimulation until the end of the steady state section. Six LNL models were estimated from the six different

animals (A1 to A6) (Figure 7.6A to F respectively). The first LNL model corresponds to the transient response of FETi. A regression line was fitted to the frequency response (magnitude only) of the combined linear element of each block wise model. The regression line was fitted between 2 and 15 Hz [35] and its gradient was used as a measure of the dynamics of FETi for each 3 s block (Figure 7.6 BW). For reference, the gradient of a regression line, fitted to the frequency response (magnitude only) of ideal position and velocity sensitive LNL models, was also calculated (Figure 7.6 IP and IV respectively). Comparison of FETi dynamics with that of ideal position and velocity sensitive models reinforces the classification of FETi (Section 7.3.2) as being position sensitive but with some velocity sensitivity. MC simulations were used to provide an estimate of LNL parameter estimation error for each block wise model (Section 7.2.3). Parameter estimation error was represented by plotting the 2.5 and 97.5% percentiles of these values around the gradient value estimated from input/output data (Figure 7.6 BW ± pctl).

Firstly the null hypothesis was tested using the Wilcoxon signed rank test. There were two nominal values, time (transient and steady state) and individual animals (A1 to A6) and one measurement variable, the gradient value [92]. The median change between the transient and average steady state gradient values was not significantly different from zero ($p > 0.05$).

Secondly the analysis was extended to consider the accuracy of the gradient estimates, obtained using MC simulations, and changes in FETi dynamics with time in each individual animal. It was used to assess whether differences existed between transient and steady state dynamics or if they were due to parameter estimation error caused by noise. As the transient gradient value ± the parameter estimation error (Figure 7.6 BW ± pctl) falls on the average of the steady state gradient values (Figure 7.6, SSμ) in each animal it was concluded that any differences between transient and steady state dynamics could be explained by parameter estimation error caused by noise.

It should be noted, however, that there were four cases, in two animals (Figure 7.6B and F, marked in bold black), when gradient values and their parameter estimation error did not fall on to the average steady state gradient values (Figure 7.6, SSμ). In order to investigate these exceptions and to test for the possibility of a general trend in the dynamics of FETi further statistical analysis was carried out using the Kruskal Wallis test. There was one nominal value, time (blocks 1 to 8) and one measurement variable, the gradient value [92]. As the results were not significant ($p > 0.05$) the null hypothesis that the dynamics of FETi in each 3 s block are the same could not be rejected.

These results lead to the conclusion that the dynamics of FETi in its transient and steady state sections do not change significantly.

FETi Nonlinear Responses

In this section a null hypothesis that FETi nonlinear responses are the same in the transient and the steady state response sections is tested. The nonlinear response of FETi to GWN

stimulation was represented using the input/output response of the polynomial element of the block wise models estimated from the six different animals (Figure 7.7A to F).

As in Section 7.3.3, LNL model parameters were estimated from 3 s long non overlapping blocks of data. The input/output response of the polynomial element of the LNL model estimated from the first 3 s block of data corresponds to the transient nonlinear response of FETi (TR, Figure 7.7). The steady state nonlinear response of FETi is represented by the average of the block wise polynomial input/output responses estimated from the steady state section of data (SSμ, Figure 7.7). MC simulations were used to provide an estimate of LNL parameter estimation error (Section 7.2.3) for the transient polynomial input/output response and represented by plotting the 2.5 and 97.5% percentiles of the 100 MC simulations (TR ± pctl, Figure 7.7). Transient polynomial and parameter estimation error values which do not overlap the steady state response values are coloured in black and marked in bold (Figure 7.7).

The null hypothesis that FETi nonlinear responses are the same in the transient and steady state response sections was tested using the Wilcoxon signed rank test. For each input value there were two nominal values, time (transient and steady state) and individual animals. There was also one measurement variable, the output of the polynomial function [92]. This test was repeated for each input value. Unlike the results for system dynamics (Section 7.3.3), the null hypothesis was rejected for some input values. The median change between states for polynomial input values between -0.44 and -0.8 were significantly different from zero ($p < 0.05$). These values are marked in Figure 7.7 using a shaded blue patch. Whilst a significant difference existed between transient and steady state nonlinear responses, this effect was small and also near the tail of the polynomial. This is a region of the nonlinearity with high estimation errors. Furthermore, the change was not significant in any individual as the parameter estimation error values from the transient response (TR ± pctl, Figure 7.7) overlap the average steady state response values (SSμ, Figure 7.7).

These results lead to the conclusion that while there are significant differences between transient and steady state nonlinear responses the differences are small and the shape of the non linearity remains very similar. Furthermore, these small differences would not change the description of FETi behaviour.

Sinusoidal Stimulation

In this section the null hypothesis that FETi response to 5 Hz sinusoidal stimulation remains the same in the transient and steady state sections is tested.

The transient response coherent average (TRCA) and the steady state response coherent average mean (SSCAμ) of FETi across six animals (A1 to A6), are shown in Figure 7.8A to F respectively. The output signal recorded from FETi was split into 3 s long non overlapping blocks of data. The first block represents the transient response of FETi and blocks 4 to 8 its steady state response. In each block the coherent average was formed by splitting the output signal of FETi into segments corresponding to one cycle of the input signal (0.2 s long) and

then averaging. The average of these coherent averages from blocks 4 to 8 were used to calculate SSCAμ. In addition, the variability of the response of FETi was represented by plotting the 2.5 and 97.5% percentiles (TR ± pctl and SSCAμ± pctl, Figure 7.8) of the transient and the average steady state cycle values.

The null hypothesis was tested using the Wilcoxon signed rank test. For each time point (Figure 7.8, x axis) there were two nominal values, response section (transient and steady state) and individual animals. There was also one measurement variable, the normalised signal amplitude [92]. This test was repeated for each time point. As no significant differences were found ($p > 0.05$) this result provides further evidence that system dynamics and nonlinear responses in the transient and steady state section are similar.

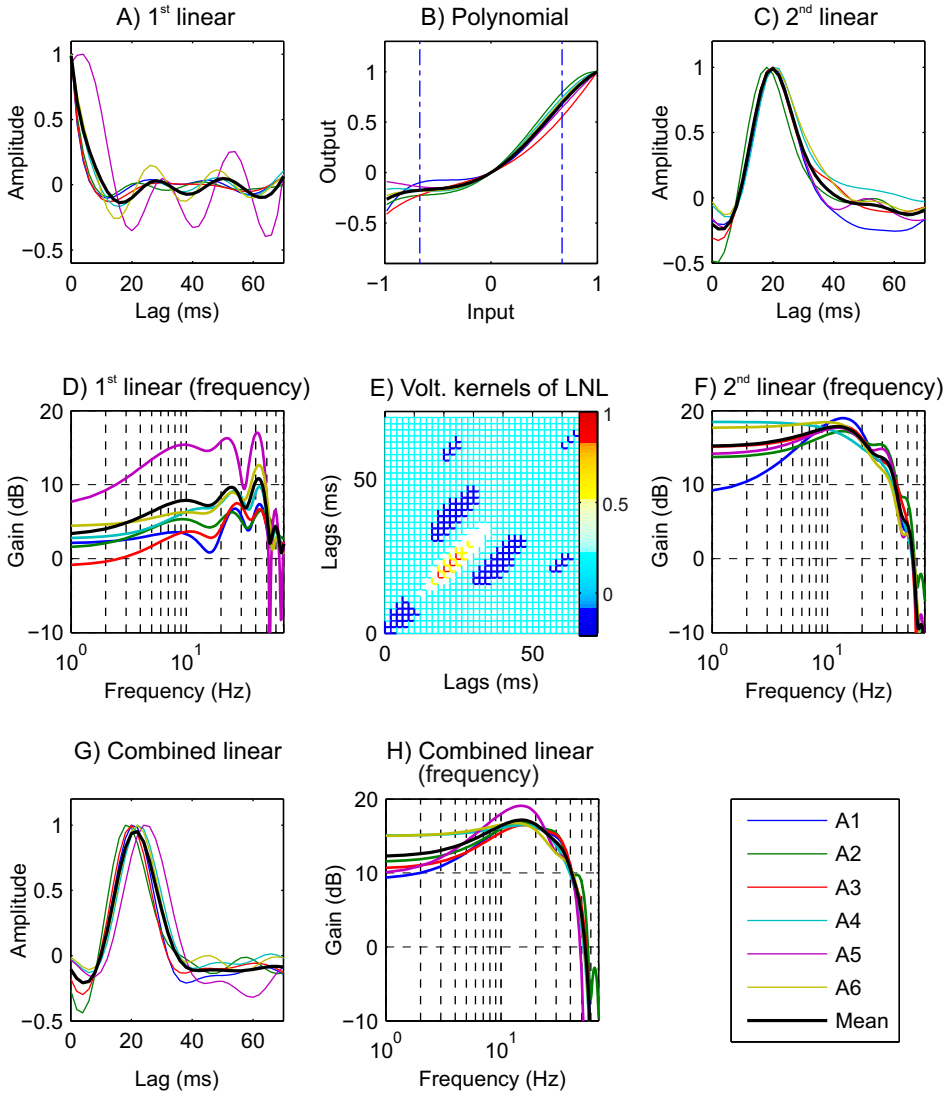

Figure 7.4: The parameters of LNL models of FETi. The bottom right panel defines the traces, for example A1 represents the results obtained from Animal 1. (A) The first linear element $h(\tau)$. (B) The input/output response of the polynomial element resembles a half wave rectifier and the directional sensitivity of FETi. Leg flexion occurs when the input signal is between 0 and 1 and extension between 0 and -1. Excitatory inputs to the FETi motor neuron occur when the output signal is between 0 and 1, inhibitory inputs to the FETi motor neuron occur when it is between 0 and -1. Two standard deviations of the input signal to the polynomial elements are marked by dashed blue lines. (C) The second linear element $g(\tau)$. (D) The frequency response (magnitude) of $h(\tau)$. (E) The 2^{nd} order Volterra kernel calculated directly from the mean (n=6) parameters of the LNL model. (F) The frequency response (magnitude) of $g(\tau)$. (G) The combined linear element $c_{hg}(\tau)$. (H) The combined linear parameters (the convolution of the parameters of the linear elements) have a bandpass frequency response. This led to the classification of FETi as mainly position sensitive but with velocity sensitivity.

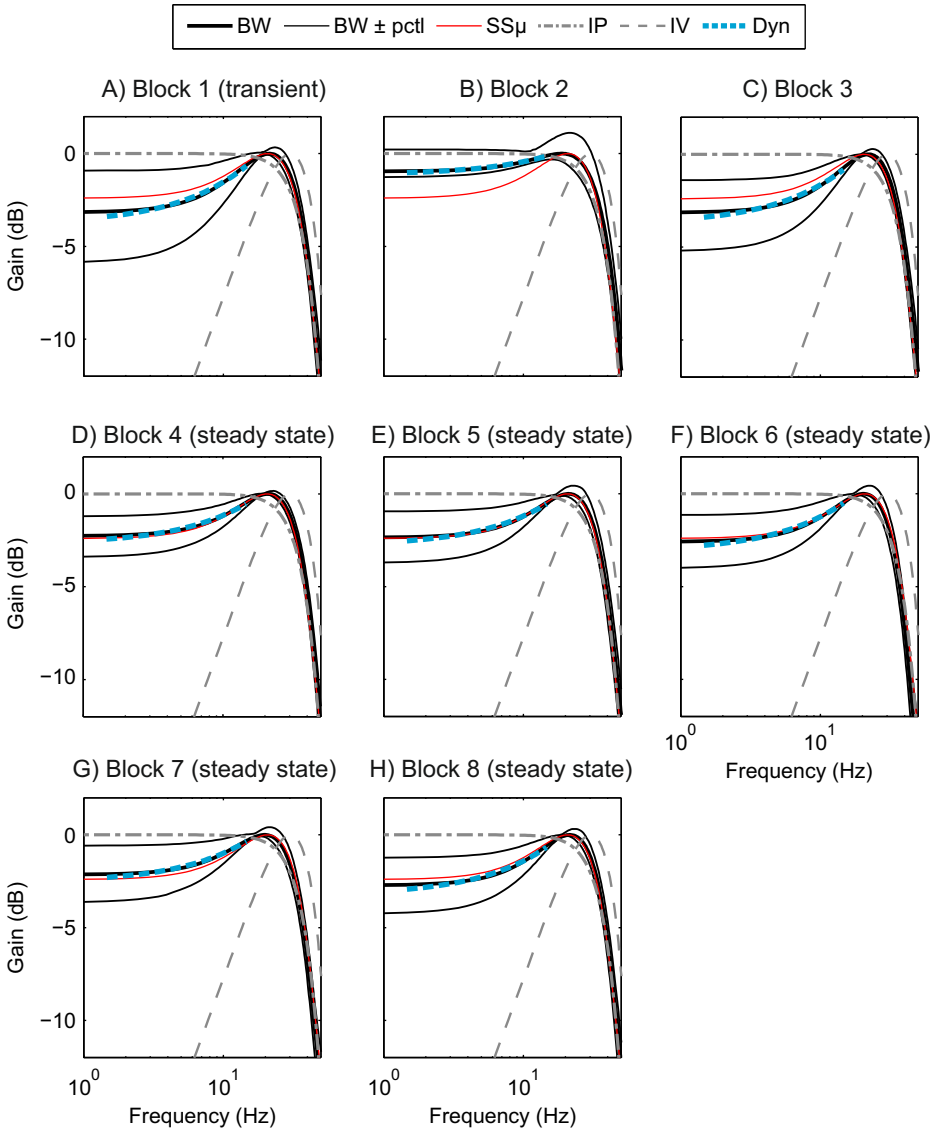

Figure 7.5: Changes in the frequency response (magnitude only) of the combined linear elements of block wise LNL models of FETi with time. This example was generated from data from Animal 3. (A) - (H) Block wise LNL models were estimated from 3 s non overlapping blocks of data recorded when GWN stimulation was applied. The frequency response (magnitude only) of the combined linear element of the LNL model was estimated from each block (BW). (A) The frequency response was estimated from the transient response of FETi and in (D) - (H) its steady state response. Parameter estimation error is also considered and represented by the 2.5 and 97.5% percentiles (BW ± pctl) calculated from MC trials (100). SSμ is the average model frequency response from the steady state section. This example illustrates how little the frequency response of the block wise model changes with time. It also demonstrates how the dynamics of FETi (Dyn) can be represented by the gradient of a regression line fitted to the model's frequency response (magnitude only) between 2 and 15 Hz. Comparison of FETi dynamics with that of ideal position (IP) and velocity sensitive (IV) models reinforces the classification of FETi in Section 7.3.2 as being mainly position sensitive but with some velocity sensitivity.

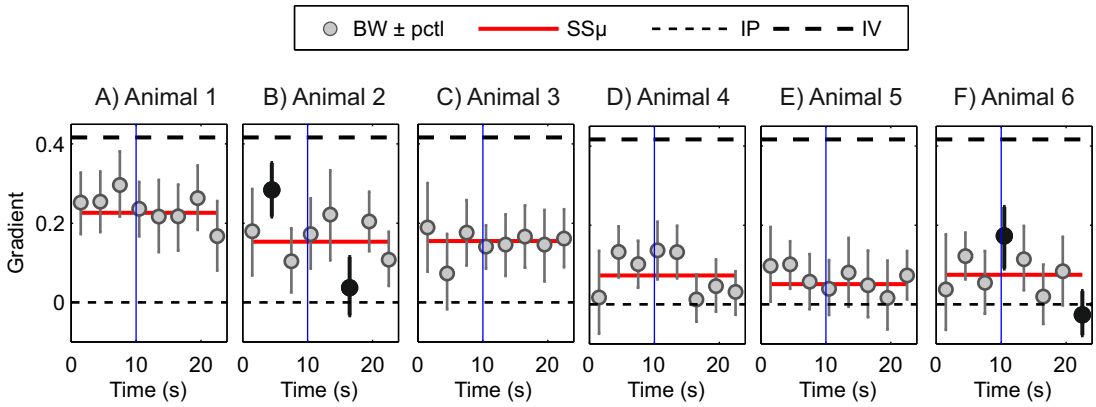

Figure 7.6: Changes in the dynamics of LNL models of FETi with time. Block wise LNL models were estimated from 3 s non overlapping blocks of data recorded from FETi when GWN stimulation was applied. The results obtained from animals 1 to 6 are shown in (A) to (F) respectively. The dynamics of FETi was represented by the gradient of a regression line (Figure 7.5), fitted to the frequency response (magnitude only) of the combined linear element of the LNL models between 2 and 15 Hz (BW). The vertical blue line marks the start of the steady state section. The average of the gradient values estimated from the steady state section is marked using a horizontal red line (SSμ). The first gradient value represents the dynamics of the transient response of FETi. Parameter estimation accuracy is represented by the 2.5 and 97.5% percentiles (BW ± pctl) of the gradient values from MC trials for each block. Cases where the gradient values and parameter estimation error (BW ± pctl) do not fall on SSμ are marked in black. The null hypothesis, that FETi dynamics are the same during transient and steady state response sections, could not be rejected (Wilcoxon signed rank, $p > 0.05$). This suggests that the dynamics of the transient and steady state responses of FETi are the same. The gradient of a regression line fitted to the frequency response (magnitude only) of ideal position (IP) and velocity (IV) sensitive models is also shown. Comparison of FETi dynamics with that of ideal position and velocity sensitive models reinforces the classification of FETi in Section 7.3.2 as being mainly position sensitive but with some velocity sensitivity.

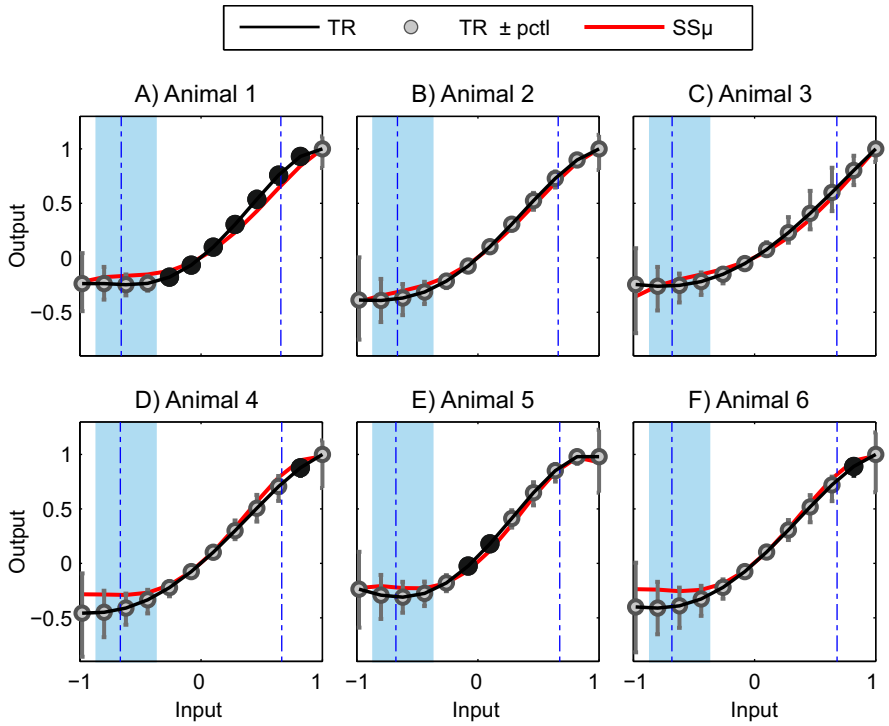

Figure 7.7: The transient and steady state nonlinear responses of FETi. The nonlinear response of FETi was represented by the nonlinear input/output response of the polynomial element of LNL models. Block wise LNL models were estimated from 3 s non overlapping blocks of data recorded from FETi when GWN stimulation was applied. (A) - (F) The results obtained from animals 1 to 6 respectively. Two standard deviations of the input to the polynomial elements are marked by dashed blue lines. A null hypothesis that the nonlinear response of FETi is the same during transient (TR) and mean steady state (SSμ) response section was tested. Parameter estimation error is also considered and represented by the 2.5 and 97.5% percentiles (TR ± pctl) calculated from MC trials (100). TR ± pctl values which do not overlap the SSμ values are coloured in black and marked in bold. The blue shaded area highlights parameter values which are significantly different from zero (Wilcoxon signed rank, $p < 0.05$).

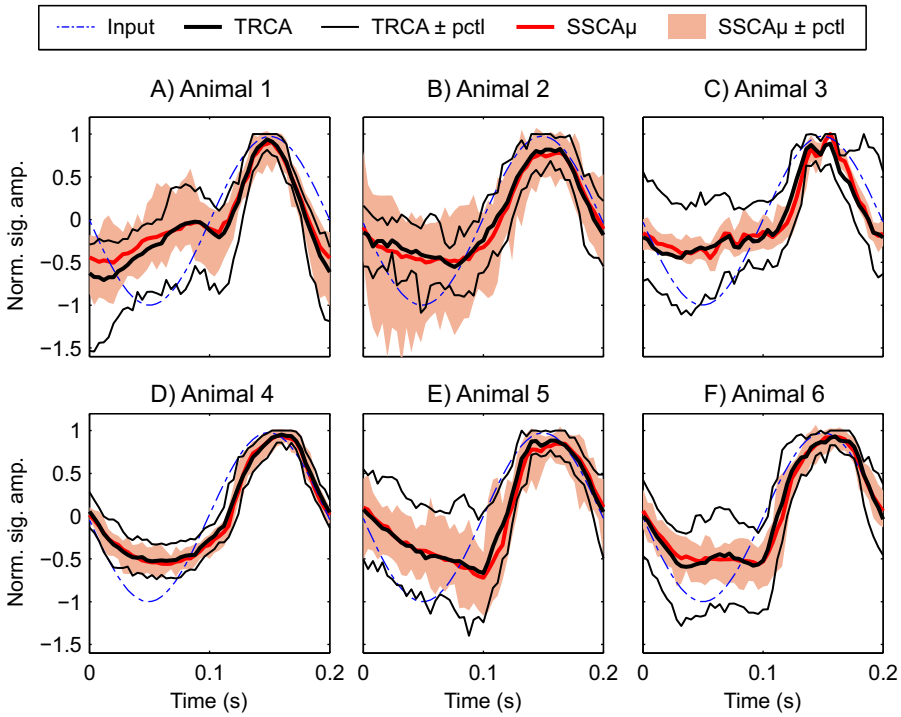

Figure 7.8: The transient and steady state response of FETi to 5 Hz stimulation. FETi transient response coherent average (TRCA) and steady state response coherent average mean SSCAμ are shown. Coherent averages are calculated from 3 s long non overlapping blocks of data. (A) - (F) The results obtained from animals 1 to 6 respectively. The variability of the response of FETi was represented by plotting the 2.5 and 97.5% percentiles (TR ± pctl and SSCAμ± pctl) of the transient and average steady state cycle values. Response variability is greater in the transient response of FETi. It is also greater in both transient and steady state sections for negative input values (leg in extension). Leg flexion occurs when the normalised amplitude of the input signal is between 0 and 1 and extension between 0 and -1. Excitatory and inhibitory inputs to FETi are represented by positive and negative values respectively. The null hypothesis, that FETi responses are the same during transient and steady state response sections, could not be rejected (Wilcoxon signed rank, $p > 0.05$).

7.4 Discussion

7.4.1 Methodological Considerations

The aim of this study was to apply the LNL model (Chapter 5) in a quasi stationary fashion to enable adaptation and steady state dynamics and nonlinear responses of an invertebrate neuromuscular reflex limb control system to be investigated.

It was identified (Chapter 6) that the high levels of measurement noise present in the response of FETi and the short data lengths for model estimation resulted in relatively high levels of parameter estimation error. As it was desirable to reduce this error, to allow the null hypothesis to be robustly tested, measurement noise in the output signal was reduced in the current study by applying the stimulation signal twice. The average of the two responses was taken as the output signal for model estimation. Averaging over just two runs only reduces measurement noise by a small amount and ideally multiple runs would have been used [83]. However, given the experimental protocol and the duration over which recordings could be made in the preparation, this was not feasible.

The methods described in Chapter 5 to validate and select the optimum number of model parameters have been extended in the current study. Data were now split into estimation, validation and test sections with the estimation and validation data being split into multiple non-contiguous sections to ensure that over training did not occur [95]. Whilst the system identification methods used in the study (described in Chapter 5 and in the current chapter) differ, the results obtained from both of the studies were very similar. For example, the parameters of the LNL models are very similar (compare Figure 5.11D and B with Figure 7.4G and B). Furthermore, model parameter optimisation gave similar results. In Chapter 5 the optimum LNL model had a %MSE performance of 32.8% (estimation data) and contained 28 linear parameters, in each linear element, and 6 polynomial coefficients (5^{th}order). In the current chapter, the optimum LNL model had a %MSE performance of 26.9% (estimation data) and contained 36 linear parameters, in each linear element, and 5 polynomial coefficients (4^{th}order).

In Chapter 5 the %MSE predictive performance of the LNL model was 29.9% (GWN stimulation and predictive performance measured using validation data). In the current chapter, using the averaging approach, the %MSE predictive performance of the LNL model was 26.9% (GWN stimulation and predictive performance measured using validation data). It should be noted that the work described in Chapter 5 and in this chapter used different segments of data for model estimation and validation. Whilst it has been assumed that the system's response is deterministic and that measurement noise is stationary, it is possible that this is not the case. It is, therefore, not possible to determine if this improvement in %MSE predictive performance is solely due to signal averaging. The method used to optimise the number of model parameters (Chapter 5, Section 5.2.3) was extended in the current study and data are now split into model estimation, validation and test data sections. The performance of the LNL model when validated using test data was found to be 29.1%. This suggests that, as has been found in other work [95], using the same data for validation and test may provide an overly optimistic estimate

of the model's predictive performance.

In Chapter 5 the rather high %MSE performance of the LNL model (around 30%) was noted. It was concluded in Section 5.4 that the high %MSE value was due to the low SNR ratio of the output signal recorded from FETi rather than poor model fit. The consistency of the estimated kernels across and within animals (Figures 5.4, 5.7 and 7.4) also suggests that the model provides robust characterisation of the system [87] and that predictive performance of the model is due to the high level of activity unrelated to the input. This conclusion has been reinforced in the current chapter as the mean %Maximum Deterministic Performance (MDP) which could be expected from a model which provides an exact fit to FETi (GWN stimulation) was estimated to be 20.8%.

7.4.2 Adaptation in Reflex Limb Control

The neural elements of both vertebrate and invertebrate reflex limb control systems are known to adapt their responses to constant stimulation [102]. Neurons have been found to either change their firing frequency [49] or the amplitude (power) of their synaptic response [44]. Adaptation provides numerous benefits, for example facilitating stable but reactive limb control [72]. Adaptation to repetitive stimulation over a time scale of seconds has been shown to occur in locust tactile hair afferents [96], locust hind leg flexor tibia motor neurons [44], the stick insect's femur-tibia feedback system [10] and non spiking and spiking crab limb proprioceptors [54].

The locust's local circuit is composed of sensory neurons [20] located in the FeCO stretch receptor [46], spiking [117] and non spiking interneurons [35]. The sensory neurons synapse directly on to FETi, and connect indirectly through the spiking and local non spiking interneurons via multiple parallel paths [20]. Previous work has shown that there is considerable variation in the sensitivity of the neurons in this network to position, velocity and acceleration and also to range and direction [35, 46, 73, 117] but has only considered steady state responses. Output power adaptation could occur in any of these elements, for example through presynaptic inhibition of the sensory neurons [24] or changes in the weighting of the excitatory or inhibitory pathways via the interneurons with the potential to change the dynamics and nonlinear responses of this system. In the current study, the null hypothesis that FETi dynamics and nonlinear responses are the same during transient and steady state sections has been tested using a model based approach. It has been assumed that FETi can be represented over 3 s as a time invariant model and that measurement/background noise is stationary. Shorter blocks would be desirable to study faster changes but that would require different models and experimental procedures. MC simulations have been used to make the problem tractable.

Whilst this system identification study of adaptation has provided some evidence of significant nonlinear changes between transient and steady state sections the effect was small and only found in the tail of the polynomial nonlinearity. This change would not affect the way in which the neural circuits behaviour might be described and can thus probably be ignored for practical

purposes. The use of biologically more relevant 5 Hz sinusoidal stimulation reinforces this conclusion. The methodological implication is that either transient or steady state response data combined with a parsimonious LNL model structure can be used to represent the dynamics and nonlinear responses of the mechanical and neural elements of locust reflex limb control systems.

The functional/physiological implication is that whilst the power in the response of the control system adapts with time its dynamic and nonlinear responses remain similar.

Chapter 8

Summary, Discussion and Suggestions for Further Work

8.1 Summary

The system identification approach, coupled with GWN stimulation, has provided a useful tool for investigating and categorising the function of both human [33, 122, 123] and invertebrate [73, 97, 98, 117] limb control systems. The aim of these system identification studies has been to increase understanding of how these systems function. This knowledge has the potential for improving treatment of patients with neuromuscular dysfunction and to enhance the design of engineering control systems used for robotic applications. As the response of the majority of such biological control systems is nonlinear, nonlinear system identification methods have therefore been required. Nonlinear Volterra or Wiener series models have been the structure of choice used in previous investigations. GWN stimulation, band limited to cover the operating range of interest, provides a computationally convenient input signal which is information rich, covering a wide range of amplitudes and frequencies. These desirable properties simplify the computation and allow the parameters of the Volterra/Wiener models to be estimated from as little as 20-30 seconds of data.

The literature review in Chapter 3 revealed two established approaches for investigating invertebrate reflex limb control systems. The first approach used by investigators was to excite these systems with physiological input signals and use simple analysis methods to link the resulting nerve impulses to system function. The second approach, applied in more recent investigations, has used system identification techniques coupled with GWN stimulation. The literature review has identified a more recently emerging trend which uses the system identification approach but with natural input signals to excite the biological system. It has also identified that whilst the local networks that control limb movements in both the locust and crab are known to adapt their output amplitude or spike firing rate to repetitive stimulation [44, 54] little work has been carried out to investigate this property. Furthermore, no previous studies appear to have applied the GWN system identification technique to investigate adaptation of the dynamics and

nonlinear responses of such systems.

Given the potential benefits of understanding invertebrate reflex limb control under natural operating conditions and during its transient (adapting) and steady state responses the objectives of this study were:

1. To refine the experimental methods used to prepare, measure and analyse the reflex response of neuromuscular elements in invertebrate limb control systems.

2. To find a parsimonious nonlinear (Volterra type) model which allows robust parameter estimation from short data lengths and gives accurate predictive performance.

3. To extend previous studies to probe the limitations of the parsimonious model by measuring its accuracy at predicting the response of the system to sinusoidal and more natural walking inputs.

4. To investigate and, if required, improve the robustness of the parameter estimation methods to the properties of the experimental signals.

5. To determine the suitability of the parsimonious model as a tool for modelling the dynamics and nonlinear responses of the neuromuscular elements in invertebrate limb control systems during both transient and steady state response sections. This was carried out by applying the model to test the null hypothesis that FETi dynamics and nonlinear responses are the same during transient and steady state sections.

6. To recommend experimental and data analysis methods for further model based studies of invertebrate neurophysiology.

The equipment and methods used by previous studies to investigate invertebrate neuromuscular limb control systems have been improved (Chapter 4). The impact of the shaker amplifier, shaker, new forceps mount and forceps (input stage) was assessed using a system identification approach. Having removed the resonance caused by the old forceps mount it was concluded that the properties of the input stage could now be ignored. Dissections were carried out to reveal the location of the loop structure in the apodeme and ensure that it was not damaged during experiments. These dissections revealed a previously unreported bifurcation of the flexor strand. The adaptation rate (power) of the FETi motor neuron to GWN and sinusoidal stimulation has been shown in general to be similar and this has aided the definition of transient and steady state response sections. The consistency of the response of FETi to sinusoidal and walking stimulation both in each animal and across animals has been shown using a coherent averaging approach combined with statistical analysis. This result strongly suggests that the experimental protocol produces robust and repeatable results. It should be noted that, as was found in other investigations which used a similar experimental set-up and input signals [44, 98] to stimulate the FeCO as the current study, only synaptic inputs were recorded in FETi.

The system identification methods used by previous studies have been extended and developed. The aim was to find a parsimonious model which could be applied in a quasi stationary fashion to enable the effect of adaptation on the dynamics and nonlinear responses of FETi to be in-

vestigated. To enable this, the performance of five parametric model structures were compared (Chapter 5). The model structures used were: the 2^{nd} and 3^{rd} order nonlinear Volterra models and three cascade models (the Linear Nonlinear (LN), the Nonlinear Linear (NL) and the Linear Nonlinear Linear (LNL)). The number of parameters a model contains can affect its predictive performance and the computational cost to calculate its parameters [81, 130] but many studies do not state how the number of parameters in the model are chosen [54, 73, 93, 97, 98]. The current study has developed a method for optimising the number of parameters in nonlinear Volterra type system identification models. Results have shown that once a plateau in performance is reached, change in model order has little effect on its performance. Exact choice of model order, therefore, is not critical provided that this plateau is reached. The parsimonious nonlinear LNL model was found to provide the most suitable structure for testing the null hypothesis as its parameters could be accurately estimated from short data lengths and therefore allowed its application in a quasi stationary fashion. Furthermore, unlike the Volterra models, the nonlinear polynomial element of the LNL model is simpler to interpret as it remains in two dimensional space regardless of model order. The LNL structure was, therefore, chosen for use in the current study to investigate the transient and steady state dynamics and nonlinear responses of FETi. A LNL model containing 62 parameters, 28 in each linear element and a 5^{th} order polynomial (6 parameters) for the nonlinear element, was shown to give the most accurate mean (n=6) %MSE predictive performance on the steady state response of FETi. As the LNL model is a subset of the Volterra series its parameters can be transformed into Volterra form. This will allow the LNL models to be used with the classification approach used by previous work [73, 97, 98, 117].

The system identification models obtained using GWN stimulation have been validated with the use of more biologically realistic sinusoidal and walking stimulation signals to determine where the model performs well and to identify its limitations. The current study has found that, as in previous work [53], the model fails to accurately predict the output of FETi to the 1 and 2 Hz sinusoidal and the walking stimulation. However, unlike previous work [53], the model could predict the output of FETi to 5 and 10 Hz sinusoidal stimulation as accurately as it could predict its response to GWN. A 5 Hz frequency is functionally relevant as it matches the stepping frequency of 5.1 Hz ± 0.56 Hz observed in other work [13] from ten animals.

The robustness of the LNL parameter estimation methods to the properties of the experimental signals (low pass filtered GWN input and high levels of output measurement noise) was described in Chapter 6. The performance of different KH based LNL parameter estimation methods was compared using experimental data and computer simulations. As was found in previous work [15, 27, 29, 33, 79, 107] and in the current study, such gradient based methods require careful parameter initialisation to ensure that they converge to the global rather than suboptimal local minima. This is a property common to all gradient based methods working with multi modal error surfaces. The DE based methods which have been designed to deal with local minimum and so should converge to the global minimum, were therefore used to check the convergence of KH based methods. The DE and DDE methods were found to remove the requirement for careful parameter initialisation and have the advantage of a flexible cost func-

tion. The SKH, DKH and DDE methods were developed by the current study to reduce high frequency parameter estimation error which occurs in the second linear element of the LNL model when the standard KH or DE methods are used. The results have shown that all methods effectively reduce parameter estimation error whilst retaining accurate %MSE predictive model performance. Through the use of Monte Carlo simulations, the DDE and the DKH methods were found to be less accurate, in terms of parameter bias and variance, than the SKH method. The DDE method is also computationally more expensive. The SKH method was therefore chosen for use by the current study (Chapter 7).

The use of the parsimonious cascade model structure applied in a quasi stationary fashion coupled with Monte Carlo (MC) simulations has been shown to provide a useful tool for the characterisation of the dynamics and nonlinear responses of the neuromuscular elements in an invertebrate limb control system during both transient and steady state response sections. This method has allowed the null hypothesis that FETi dynamics and nonlinear responses are the same during transient and steady state sections to be tested (Chapter 7). It has shown that key FETi dynamics remain relatively unchanged during repetitive stimulation while output amplitude adaptation is occurring. Whilst it has also revealed evidence of significant changes between nonlinear responses in transient and steady state sections the effect was small and only found in the tail of the polynomial nonlinearity. This change would not affect the way in which the neural circuits behaviour might be described and can thus probably be ignored for practical purposes. The use of biologically more relevant 5 Hz sinusoidal stimulation reinforces this conclusion.

8.2 Discussion

The main aim of the current study, to find a parsimonious model which could be applied in a quasi stationary fashion to enable the dynamics and nonlinear responses of the neuromuscular elements in invertebrate limb control systems during both transient and steady state response sections to be investigated has been achieved (Chapter 7). This method has been applied to test the null hypothesis that FETi dynamics and nonlinear responses are the same during transient and steady state sections.

The quasi stationary approach used in this study, however, assumes that FETi can be represented as a time invariant model over the 3 s window and that measurement noise is stationary. Shorter data windows are required to enable faster changes to be studied but that would require different models and experimental procedures (Section 8.3). The quasi stationary approach may not fully capture underlying parameter changes as it makes a compromise between time resolution and parameter estimation accuracy. This, however, is also the case with other parameter tracking methods. The quasi stationary approach is a commonly used and well established method of dealing with time varying systems and importantly it does not require any complex methodological or mathematical formulations [42, 87].

Adaptive filtering [124] methods can be used to estimate model parameters in a more contin-

uous fashion and have the potential to increase the accuracy of the parameters of successive model estimates [14, 87]. In the unpublished work by Natalia Angarita-Jaimes the parameter estimation accuracy of the quasi stationary and adaptive filtering approaches with a linear FIR model structure were compared. This study used data recorded from the non spiking interneurons in the locust femur/tibia reflex control loop and both Least Mean Squares (LMS) and Recursive Least Squares (RLS) adaptive algorithms were tested [124]. However, no benefit was found between the use of the quasi stationary approach and an adaptive filtering approach (private communication, Natalia Angarita-Jaimes).

Because of the low sample size (6 animals) non parametric rather than parametric statistical tests were chosen for use in the current study. However, given that the data were also noisy, caution was required when interpreting the results of these test and wherever possible MC testing was also carried out [64]. Further work should increase the sample size and also consider the use of Bayesian analysis [119]. It should also be noted that as in a previous study [44], given that the apodeme to tibial insertion is composed of hard rather than soft tissue, it was assumed that the steady state displacement angle relationship (Figure 4.7) holds for dynamic excitation signals. Further work is required to test this assumption.

The current study and the majority of previous system identification studies of neuromuscular invertebrate reflex control [54, 73, 97, 98, 117] have so far only used the linear element of nonlinear Volterra or cascade model structures to characterise the dynamics of the neural elements (sensitivity to position, velocity or acceleration). This is probably because the interpretation of the 1^{st} order Wiener/Volterra kernels, which represent the linear IRF of a system, is relatively straightforward whilst that of the 2^{nd} order kernels is very complex. A disadvantage with this approach is that the nonlinear frequency response of the model, and hence the system, is not used for system classification. It should be noted that the inclusion of the nonlinear 2^{nd} order Volterra kernel improves the mean predictive performance of the model by $\sim 15\%$MSE [98]. Methods which cluster the responses of neurons based on their linear and nonlinear responses to physiologically realistic inputs have been developed and applied to the non spiking interneurons responsible for reflex control of the locust's hind leg [5, 35]. The great diversity of response types found in [5] was clearly the result of strong nonlinear responses in some of the non spiking interneurons. Further work, therefore, is required to extend previous analysis of sensory, spiking inter and motor neurons [73, 97, 98, 117] to consider the model's overall (linear and nonlinear) responses.

System identification models generated using GWN stimulation signals are commonly validated by calculating their performance at predicting the response of the system to further GWN stimulation [87, 123]. This approach is also often commonly employed by studies of invertebrate reflex limb control systems [54, 73, 97, 98, 117]. As the inputs to the FeCO in a freely moving locust are very different from those of GWN stimulation it is important to evaluate the ability of the models to predict the responses to natural stimulation. A previous study by French et al. [53] validated 3^{rd} order Volterra models of spider sensory neurons, with their parameters estimated using a GWN input signal, with step inputs. Their models could predict the response of the system to GWN with "...reasonable fidelity" [53]. The mean predictive performance of

the 3^{rd} order Volterra model of the Type A neuron was 33%MSE, and was 37%MSE for the model of the Type B neuron (n = 10; performance was calculated using validation data). It is interesting to note that very similar levels of %MSE accuracy (on GWN validation data) were provided by the LNL models of FETi developed in the current study. The Volterra models of the spider sensory neurons, however, failed to predict the response of the two neurons to step input stimulation [53]. French et al. [53] suggest two reasons for this failure. The first was that the model structure is not flexible or powerful enough to capture the underlying neural process; the second, that wide-band stimuli may change the response of the neurons and so models generated using this input signal will not be able to predict the response of the system to narrow or band limited stimulation. The fact that the properties of the stimulus signal can alter the response of sensory neurons has also been found by other investigators [70, 115, 126, 127].

In the current study, as in the work by French et al. [53], the LNL model (generated using GWN stimulation) could not accurately predict the output of FETi to 1 and 2 Hz sinusoidal stimulation and the walking stimulation. The LNL model, however, could predict the output of FETi to 5 and 10 Hz sinusoidal stimulation with the same level of accuracy as its response to GWN stimulation. With hindsight, it may have been optimistic to expect a model estimated from the response of the system to band limited GWN over the frequency range from 0-50 Hz to be able to accurately predict the response of the system to narrow band signals covering the frequency range from 0-2 Hz. Ljung [81] suggests that models should be limited to representing a maximum of three decades of frequency range. Because of the nonlinear nature of the system, new experiments to measure and record its response to GWN stimulation, band limited over a narrower range, need to be carried out. Care needs to be taken to ensure that the amplitude range of the GWN stimulus signal covers that of the sinusoidal and walking signals. These data need to be collected before the ability of the system identification models to generalise can be properly and fairly tested. However, it should be noted that the study by Angarita-Jaimes et al. [5] found that nonlinear Volterra models (generated using GWN stimulation) could predict the response of non spiking interneurons to walking stimulation with at least the same level of accuracy as they could predict their responses to GWN stimulation. However, model predictive performance in the study by Angarita-Jaimes et al. [5] (~80%MSE) was generally less accurate than the in current study (~30%MSE).

Whilst use of more natural sinusoidal and walking stimulation signals for model validation has allowed the limitations of the model to be determined it raises the question, what is the best input for increasing understanding of the neural elements of reflex limb control systems? Furthermore, is a walking input the most intelligent choice for probing a reflex system?

The current study and that by Angarita-Jaimes et al. [5] have made much progress in the application and evaluation of system identification methods. However, additional work is required before a full understanding of how reflex control operates and is integrated into the locust's robust and adaptive locomotor control system.

The non parametric system identification approach with Volterra type models has been shown to be a useful tool which has improved understanding of both invertebrate [53, 54, 98, 117] and

human [33, 122, 123] systems. It is, therefore, hoped that the methods developed in the current study have the potential to generalise to other invertebrate and vertebrate systems.

8.3 Suggestions for Further Work

Further work remains in terms of the development and validation of system identification methods and their application and interpretation to improve understanding of the locust's local hind leg reflex control system. This section provides a number of suggestions for future work.

Given the parsimonious LNL model structure and Monte Carlo simulations developed in this study it is now possible to quantify the dynamics and nonlinear responses of the sensory, inter and motor neurons in the locust local hind leg reflex control system. As the transient response of the system may be more important than its steady state response this investigation could provide key information regarding system function. As the spiking output signal produced by some of the neurons in this system is a discrete sequence of events, rather than the continuously varying function of time measured in the FETi system, modifications to the model structure, parameter estimation method and predictive performance measurement will be required [99].

Further insight into locust local hind leg reflex control system function may be gained through the application of methods from the field of information theory [37]. Such methods should, for example, make it possible to determine if the system is tuned to behaviourally relevant features or codes a wide range of different stimuli [82]. Such methods may also help to map connections between the sensory, inter and motor neurons in the locust reflex limb control system [118].

The analysis of the rate of power adaptation in the response of the FETi motor neuron to GWN stimulation has already been extended to consider the Posterior Intermediate Flexor Tibiae (PIFlTi) and the slow and extensor tibia (SETi) motor neurons in the study by Dewhirst et al. [34]. In that study, the adaptation rate of the two extensor (SETi and FETi) and one flexor (PlFITi) motor neuron to 27 Hz band limited GWN stimulation of the FeCO were found to be the same. Further work is required, using both GWN and more natural stimulation signals, to map the adaptation rates of the sensory, inter and motor neurons in the network responsible for reflex hind limb control in the locust.

8.3.1 General Experimental and Signal Processing Work

A number of experimental and system identification issues have arisen throughout this study, many of which have been resolved but some require further attention and refinement. Models of the FETi system, for instance, contain the properties of the shaker amplifier, shaker, forceps mount and forceps. The frequency response of these components has been shown by the current study to be flat within 2dB and to have an approximately linear phase response over the 0-50 Hz frequency range. Further work, however, should be carried out to determine the frequency response of the glass electrode and the amplifier used to measure the signal produced by the

FETi system, as their properties will also be included in the system identification models.

The failure of the model (GWN estimated parameters) to generalise at lower frequencies could occur because the FETi system responds differently to low frequency GWN, sinusoidal and walking input signals. An approach could be taken which compares models estimated from synthetic or GWN stimulus and stimuli with their properties based on natural inputs [31, 113, 114]. The Least Squares parameter estimation method, used in the current study, does not require an input signal with a white spectrum. It should, therefore be possible to fit models to the response of the FETi system when natural stimuli (ensemble of walking inputs) are applied. Comparison of the parameters of these models with those obtained from GWN stimulation may provide an insight into how the system changes its response to different input signal types.

In the current study, in order to obtain natural stimulation signals, locusts were filmed using a single camera and the position of tibia relative to the femur was tracked by using software. This method requires the locust to be moving along a line perpendicular to the single camera. If the locust deviates from this line then substantial errors could be introduced. Further work, therefore, should be carried out to improve the video tracking system. A multi camera system similar to that developed by Zakotnik et al. [129] should provide more accurate results.

The DDE LNL parameter estimation method has been shown to be insensitive to parameter initialisation and it has a flexible cost function. Further work, however, is required to reduce the uncertainty in the parameter estimates produced by this method and also to reduce computation time. Utilising feedback from the search procedure to guide parameter adaptation may help to improve performance [103]. It would also be interesting to test the very recently developed algorithm for initialising and estimating LNL models [111] which potentially overcomes the problem of local minima.

The number of parameters in the model and the SNR of the output signal are two factors which determine the length of data required to achieve accurate parameter estimates [87]. For accurate parameter estimates the number of model parameters should be small compared with the number of samples in the data. Ideally the data length should be more than ten times the model length [87]. In the current study, analysis of transient dynamics sacrificed time resolution, by estimating the parameters of the block wise LNL models from 3 s lengths of data (no overlap), to provide more accurate parameter estimates. It may be possible to modify the methods developed over the last decade for tracking heart rate variability [84] to allow faster changes in the locust's limb control system to be tracked.

The current work was limited to Volterra type models, including cascade models with polynomial nonlinear elements, because such models have been extensively applied in related work [54, 98, 117, 126]. However, many different model types exist, for example Auto Regressive Moving Average with exogenous inputs (NARMAX) and Neural Networks [95]. Whether such models would provide improved performance in the study of FETi responses and their transient behaviour requires further investigation.

Bibliography

[1] A.M.H.J. Aertsen and P.I.M. Johannesma. The spectro-temporal receptive field. *Biological Cybernetics*, 42:133–143, 1981.

[2] H. Akaike. A new look at the statistical model identification. *IEEE Transactions on Automatic Control*, 19(6):716–723, 1974.

[3] H.N. Al-Duwaish. A genetic approach to the identification of linear dynamical systems with static nonlinearities. *International Journal of Systems Science*, 31(3):307–313, 2000.

[4] S.H. Alavi, J. Jassbi, P.J.A. Serra, and R.A. Ribeiro. Comparison of genetic and gradient descent algorithms for determining fuzzy measures. In *IEEE 10th International Conference on Intelligent Engineering Systems (INES 06), London (UK), 2006*, pages 139–144, 2006.

[5] N. Angarita-Jaimes, O.P. Dewhirst, D.M. Simpson, Y. Kondoh, R. Allen, and P.L. Newland. The dynamics of analogue signalling in local networks controlling limb movement. *European Journal of Neuroscience*, In Press.

[6] R.C. Aster, B. Borchers, and C.H. Thurber. *Parameter estimation and inverse problems*. Elsevier Academic Press, first edition, 2005.

[7] E.-W. Bai, Z. Cai, S. Dudley-Javorosk, and R. K. Shields. Identification of a modified wienerhammerstein system and its application in electrically stimulated paralyzed skeletal muscle modeling. *Automatica*, 45(3):736–743, 2009.

[8] Y. Bar-Cohen. Biomimetics using nature to inspire human innovation. *Bioinspired Biomimetics*, 1(1):1–12, 2006.

[9] J.F. Barrett. The use of functionals in the analysis of non-linear physical systems. *This paper was written in April 1955 as a Cambridge University Engineering Laboratory Report and distributed in 1956 by the Ministry of Supply. It was also published December 1963 in the Journal of Electronics and Control*, 1955.

[10] U. Bassler. The femur-tibia control system of stick insects – a model system for the study of the neural basis of joint control. *Brain Research Reviews*, 18(2):207 – 226, 1993.

[11] J. Benda, L. Maler, and A. Longtin. Linear versus nonlinear signal transmission in neu-

ron models with adaptation currents or dynamic thresholds. *Journal of Neurophysiology*, 104(5):2806–2820, 2010.

[12] R.M. Berne, M.N Levy, B.M. Koeppen, and B.A. Stanton. *Physiology*. Mosby, fourth edition, 1998.

[13] L. M. Blackburn, S. R. Ott, T. Matheson, M. Burrows, and S. M. Rogers. Motor neurone responses during a postural reflex in solitarious and gregarious desert locusts. *Journal of Insect Physiology*, 56(8):902–910, 2010.

[14] A. Blasi, J. Jo, E. Valladares, B.J. Morgan, J.B. Skatrud, and M.C.K. Khoo. Cardiovascular variability after arousal from sleep: time-varying spectral analysis. *Journal of Applied Physiology*, 95(4):1394–1404, 2003.

[15] H. Boutayeb and M. Darouach. Recursive identification method for miso wiener-hammerstein model. *IEEE Transactions on Automatic Control*, 40(2):287–291, 1995.

[16] N. Brenner, W. Bialek, and S. de Ruyter van Steveninck. Adaptive rescaling maximizes information transmission. *Neuron*, 26(3):695–702, 2000.

[17] M.D. Burns. The control of walking in orthoptera: I. leg movements in normal walking. *Journal of Experimental Biology*, 58:45–58, 1973.

[18] M.D. Burns and P.N.R. Usherwood. The control of walking in orthoptera: Ii. motor neurone activity in normal free-walking animals. *Journal of Experimental Biology*, 79(1):69–98, 1979.

[19] M. Burrows. Motor patterns during kicking movements in the locust. *Journal of Computational Physiology*, 176(3):289–305, 1995.

[20] M. Burrows. *The neurobiology of an insect brain*. Oxford University Press, first edition, 1996.

[21] M. Burrows and M. Genevieve. The kinematics and neural control of high-speed kicking movements in the locust. *Journal of Experimental Biology*, 204(20):3471–3481, 2001.

[22] M. Burrows and G. Hoyle. Neural mechanism underlying behaviour in the locust Schistocerca gregaria III. Topography of limb motorneurons in the metathoracic ganglion. *Journal of Neurobiology*, 4(2):167–186, 1973.

[23] M. Burrows and G. Laurent. Synaptic potentials in the central terminals of locust proprioceptive afferents generated by other afferents from the same sense organ. *Journal of Neuroscience*, 13(2):808–819, 1993.

[24] M. Burrows and T. Matheson. A presynaptic gain control mechanism among sensory neurons of a locust leg proprioceptor. *Journal of Neuroscience*, 12(1):272–282, 1994.

[25] A. Buschges. The physiology of sensory cells in the ventral scoloparium of the stick insect femoral chordotonal organ. *Journal of Experimental Biology*, 189(1):285–292, 1994.

[26] M.J. Campbell and D. Machin. *Medical statistics: a commonsense approach*. Wiley, third edition, 1999.

[27] C. H. Chen and S. D. Fassois. Maximum likelihood identification of stochastic weiner-hammerstein-type non-linear systems. *Mechanical Systems and Signal Processing*, 6(2):135–153, 1992.

[28] F. Clarac, D. Cattaert, and D. Le Ray. Central control components of a "simple" stretch reflex. *Trends in Neuroscience*, 23(5):199–208, 2000.

[29] P. Crama and J. Schoukens. Wiener-hammerstein system estimator initialisation using a random multisine excitation. In *ARFTG Conference Digest-Fall, 58th*, pages 1–6, 2001.

[30] H. Cruse. Which parameters control the leg movement of a walking insect?: I. velocity control during the stance phase. *Journal of Experimental Biology*, 116:343–355, 1985.

[31] S. V. David, W. E. Vinje, and J. L. Gallant. Natural stimulus statistics alter the receptive field structure of v1 neurons. *Journal of Neuroscience*, 24(31):6991–7006, 2004.

[32] F. Delcomyn. *Foundations of neurobiology*. W.H. Freeman and Company, first edition, 1997.

[33] E.J. Dempsey and D.T. Westwick. Identification of Hammerstein models with cubic spline nonlinearities. *IEEE Transactions on Biomedical Engineering*, 51(2):237–245, 2004.

[34] O.P. Dewhirst, N. Angarita-James, D. Simpson, R. Allen, C.D. Maciel, and P. Newland. Neural adaptation in local reflex control of limb movements. In *Proceedings of Biosignals 2012 International Conference on Bio-inspired Systems and Signal Processing, Vilamoura, Algarve, Portugal*, pages 398–401, 2012.

[35] O.P. Dewhirst, N. Angarita-James, D. Simpson, R. Allen, and P. Newland. The dynamics of locust non-spiking local interneurons, responses to imposed limb movements. In *Proceedings of Biosignals 2011 International Conference on Bio-inspired Systems and Signal Processing, Rome, Italy*, pages 270–275, 2011.

[36] O.P. Dewhirst, D.M. Simpson, R. Allen, and P.L. Newland. Neuromuscular reflex control of limb movement - validating models of the locust's hind leg control system using physiological input signals. In *Proceedings of the 4th International IEEE EMBS Conference on Neural Engineering, Antalya, Turkey*, pages 689–692, 2009.

[37] A. G. Dimitrov, A. A. Lazar, and J. D. Victor. Information theory in neuroscience. *Journal of Computational Neuroscience*, 30:1–5, 2011.

[38] A. Doucet, N. De Freitas, and N. Gordon. *Sequential Monte Carlo methods in practice*. Springer, first edition, 2001.

[39] J. Duysens, F. Clarac, and H. Cruse. Load-regulating mechanisms in gait and posture: comparative aspects. *Physiological Review*, 80(1):83–133, 2000.

[40] J.J. Eggermont. Wiener and volterra analyses applied to the auditory system. *Hearing Research*, 66(2):177–201, 1993.

[41] A. A. Faisal and T. Matheson. Coordinated righting behaviour in locusts. *Journal of experimental biology*, 204(3):637–648, 2001.

[42] T.W. Fawcett and A.D. Higginson. Heavy use of equations impedes communication among biologists. *Proceedings of the National Academy of Sciences*, 2012.

[43] G. Felson and Y. Dan. A natural approach to studying vision. *Nature Neuroscience*, 8(12):1819–1828, December 2005.

[44] L.H. Field and M. Burrows. Reflex effects of the Femoral Chordotonal Organ upon leg motor neurones of the locust. *Journal of Experimental Biology*, 101(1):265–285, 1982.

[45] L.H. Field and M.M.L. Coles. The position-dependent nature of postural resistance reflexes in the locust. *Journal of Experimental Biology*, 188(1):65–88, 1994.

[46] L.H. Field and T. Matheson. Chordotonal organs of insects. *Advances in Insect Physiology*, 27(27):1–228, 1998.

[47] M.O. Franz and B. Scholkopf. Implicit estimation of wiener series. In *Machine Learning for Signal Processing, 2004. Proceedings of the 2004 14th IEEE Signal Processing Society Workshop*, pages 735–744, 2004.

[48] A.S. French. Practical nonlinear system analysis by wiener kernel estimation in the frequency domain. *Biological Cybernetics*, 24(2):111–119, 1976.

[49] A.S. French. The role of calcium in the rapid adaptation of an insect mechanoreceptor. *Journal of Neuroscience*, 6(8):2322–2326, 1986.

[50] A.S. French and M.J. Korenberg. A nonlinear cascade model for action potential encoding in an insect sensory neuron. *Biophysical Journal*, 55(4):655–661, 1989.

[51] A.S. French and M.J. Korenberg. Dissection of a nonlinear cascade model for sensory encoding. *Annals of Biomedical Engineering*, 19(4):473–484, 1991.

[52] A.S. French, M.J. Korenberg, M. Jarvilehto, E. Kouvalainen, M. Juusola, and M. Weckstrom. The dynamic nonlinear behavior of fly photoreceptors evoked by a wide range of light intensities. *Biophysical Journal*, 65(2):832–839, 1993.

[53] A.S. French, S. Sekizawa, U. Hger, and P.H. Torkkeli. Predicting the responses of mechanoreceptor neurons to physiological inputs by nonlinear system identification. *Annals of Biomedical Engineering*, 29(3):187–194, 2001.

[54] E.R. Gamble and R.A. DiCaprio. Nonspiking and spiking proprioceptors in the crab: white noise analysis of spiking cb-chordotonal organ afferents. *Journal of Neurophysiology*, 89(4):1815–1825, 2003.

[55] G.H. Golub and C.F. Van Loan. *Matrix computations*. Oxford: North Oxford Academic, first edition, 1983.

[56] M. G. Hall, A. V. Oppenheim, and A. S. Willsky. Time-varying parametric modeling of speech. *Signal Processing*, 5(3):267–285, 1983.

[57] S. Haykin. *Adaptive filter theory*. Prentice Hall International Editions, third edition, 1996.

[58] K.J. Hildebrandt, J. Benda, and R.M. Hennig. The origin of adaptation in the auditory pathway of locusts is specific to cell type and function. *Journal of Neuroscience*, 29(8):2626–2636, 2009.

[59] A.L. Hodgkin and A.F. Huxley. A quantitative description of membrane current and its application to conduction and excitation in nerve. *Journal of Physiology*, 117(4):500–544, 1952.

[60] T. Hofmann, U.T. Koch, and U. Bassler. Physiology of the femoral chordotonal organ in the stick insect cuniculina impigra. *Journal of Experimental Biology*, 114:207–223, 1985.

[61] G. Hoyle. The anatomy and innervation of locust skeletal muscle. *Proceedings of the Royal Society of London. Series B - Biological Sciences*, 143(911):281–292, 1955.

[62] G. Hoyle and M. Burrows. Neural mechanism underlying behavior in the locust schistocerca gregaria i. physiology of identified motorneurons in the metathoracic ganglion. *Journal of Neurobiology*, 4(1):3–41, 1973.

[63] M. Hoyle. Potassium ions and insect nerve muscle. *Journal of Experimental Biology*, 30(1):121–135, 1953.

[64] R. Hubbard and R. M. Lindsay. Why p values are not a useful measure of evidence in statistical significance testing. *Theory and Psychology*, 198(1):69–88, 2008.

[65] I.W. Hunter and M.J. Korenberg. The identification of nonlinear biological systems: Wiener and Hammerstein cascade models. *Biological Cybernetics*, 55(2):135–144, 1986.

[66] I.P. Jaaskelainen, J. Ahveninen, G. Bonmassar, A.M. Dale, R.J. Ilmoniemi, S. Levnen, F. Lin, P. May, J. Melcher, S. Stufflebeam, H. Tiitinen, and J.W. Belliveau. Human posterior auditory cortex gates novel sounds to consciousness. *Proceedings of the National Academy of Sciences of the United States of America*, 101(17):6809–6814, 2004.

[67] M. Juusola, J.E. Niven, and A.S. French. Shaker K+ channels contribute early nonlinear amplification to the light response in Drosophila photoreceptors. *Journal of Neurophysiology*, 90(3):2014–2021, 2003.

[68] S.M. Kay. *Modern spectral estimation: theory and application*. Prentice-Hall, 1988.

[69] J. Ke, C. Zhang, and Y. Qiao. Modified evolution strategy based identification of multi-input single-output wiener-hammerstein model. In *ICNC 2007. Third International Conference on Natural Computation, 2007*, pages 251–255, 2007.

[70] J. Kean, P. Reinagel, R. C. Reid, and M. Meister. Predicting every spike: a model for the responses of visual neurons. *Neuron*, 30(3):803–817, 2001.

[71] S. Kirkpatrick, C. D. Gelatt, and M. P. Vecchi. Optimization by simulated annealing. *Science*, 220(4598):671–680, 1983.

[72] R. Kittmann. Neural mechanisms of adaptive gain control in a joint control loop: muscle force and motorneuronal activity. *Journal of Experimental Biology*, 200:1383–1402, 1997.

[73] Y. Kondoh, J. Okuma, and P.L. Newland. Dynamics of neurons controlling movements of a locust hind leg: Wiener kernel analysis of the responses of the proprioceptive afferents. *Journal of Neurophysiology*, 73(5):1829–1842, May 1995.

[74] M.J. Korenberg and I.W. Hunter. The identification of nonlinear biological systems: LNL cascade models. *Biological Cybernetics*, 50(2):125–134, 1986.

[75] M.J. Korenberg and I.W. Hunter. The identification of nonlinear biological systems: wiener kernel approaches. *Annals of Biomedical Engineering*, 18:629–654, 1990.

[76] F. B. Krasne and D. L. Glanzman. What we can learn from invertebrate learning. *Annual Review of Psychology*, 46(1):585–624, 1995.

[77] W.H. Kruskal and W.A. Wallis. Use of ranks in one-criterion variance analysis. *Journal of the American Statistical Association*, 47(260):583–621, 1952.

[78] S. B. Laughlin. The role of sensory adaptation in the retina. *Journal of Experimental Biology*, 146(1):39–62, 1989.

[79] L. Lauwers, J. Schoukens, and R. Pintelon. Initial estimates for wiener-hammerstein models using the best linear approximation. In *IMTC 2008. IEEE Instrumentation and Measurement Technology Conference Proceedings, 2008*, pages 928–932, 2008.

[80] Y.W. Lee and M. Schetzen. Measurement of the wiener kernels of a nonlinear system by cross-correlation. *International Journal of Control*, 2:237–254, 1965.

[81] L. Ljung. *System identification: theory for the user*. Prentice-Hall, second edition, 1998.

[82] C.K. Machens, M.B. Stemmler, P. Prinz, R. Krahe, B. Ronacher, and A.V.M. Herz. Representation of acoustic communication signals by insect auditory receptor neurons. *Journal of Neuroscience*, 21(9):3215–3227, 2001.

[83] J.B. MacNeil, R.E. Kearney, and I.W. Hunter. Identification of time-varying biological systems from ensemble data. *IEEE Transactions on Biomedical Engineering*, 39(12):1213–1225, 1992.

[84] L.T. Mainardi. On the quantification of heart rate variability spectral parameters using timefrequency and time-varying methods. *Philosophical Transactions of the Royal Society A: Mathematical, Physical and Engineering Sciences*, 367(1887):255–275, 2009.

[85] P.Z. Marmarelis and V.Z. Marmarelis. *Analysis of physiological systems: the white-noise approach*. New York: Plenum, first edition, 1978.

[86] V.Z. Marmarelis. Identification of nonlinear biological systems using laguerre expansions of kernels. *Annals of Biomedical Engineering*, 21:573–589, 1993.

[87] V.Z. Marmarelis. *Nonlinear dynamic modeling of physiological systems*. Wiley-IEEE Press, first edition, 2004.

[88] D. W. Marquardt. An algorithm for Least-Squares estimation of nonlinear parameters. *SIAM Journal on Applied Mathematics*, 11(2):431–441, 1963.

[89] T. Matheson. Innervation of the metathoracic femoral chordotonal organ of locusta migratoria. *Cell and Tissue Research*, 259(3):551–560, 1990.

[90] T. Matheson. Responses and locations of neurones in the locust metathoracic femoral chordotonal organ. *Journal of Comparative Physiology A*, 166:915–927, 1990.

[91] T. Matheson. Range fractionation in the locust metathoracic femoral chordotonal organ. *Journal of Comparative Physiology*, 170:509–520, 1992.

[92] J.H. McDonald. *Handbook of biological statistics*. Sparky House Publishing, second edition, 2009.

[93] G.D. Mitsis, A.S. French, U. Hger, S. Courellis, and V.Z. Marmarelis. Principal dynamic mode analysis of action potential firing in a spider mechanoreceptor. *Biological Cybernetics*, 96(1):113–127, 2007.

[94] J. A. Nelder and R. Mead. A simplex method for function minimization. *Computer Journal*, 7:308–313, 1965.

[95] O. Nelles. *Nonlinear system identification*. Springer-Verlag, first edition, 2001.

[96] P.L. Newland. Physiological properties of afferents from tactile hairs on the hind legs of the locust. *Journal of Experimental Biology*, 155:487–503, 1991.

[97] P.L. Newland and Y. Kondoh. Dynamics of neurons controlling movements of a locust hind leg ii: flexor tibiae motor neurons. *Journal of Neurophysiology*, 77(4):1731–1746, April 1997.

[98] P.L. Newland and Y. Kondoh. Dynamics of neurons controlling movements of a locust hind leg iii: extensor tibiae motor neurons. *Journal of Neurophysiology*, 77(5):3297–3310, June 1997.

[99] S. Ostojic and N. Brunel. From spiking neuron models to linear-nonlinear models. *PLoS Computational Biology*, 7:e1001056, January 2011.

[100] K. L. Page, J. Zakotnik, V. Durr, and T. Matheson. Motor control of aimed limb movements in an insect. *Journal of Neurophysiology*, 99(2):484–499, 2008.

[101] K. G. Pearson. Common principles of motor control in vertebrates and invertebrates. *Annual Review of Neuroscience*, 16:265–297, 1993.

[102] S.A. Prescott and T.J. Sejnowski. Spike-rate coding and spike-time coding are affected oppositely by different adaptation mechanisms. *Journal of Neuroscience*, 28(50):13649–13661, 2008.

[103] A.K. Qin, V.L. Huang, and P.N. Suganthan. Differential evolution algorithm with strategy adaptation for global numerical optimization. *IEEE Transactions on Evolutionary Computation*, 13(2):398–417, 2009.

[104] W.J. Rugh. *Nonlinear system theory. The Volterra/Wiener approach*. Originally published by The Johns Hopkins University Press, 1981, web version edition, 2002.

[105] M. Schetzen. Nonlinear system modeling based on the wiener theory. *Proceedings of the IEEE*, 69(12):1557–1573, 1981.

[106] J. Schoukens, J. Suykens, and L. Ljung. Wiener-hammerstein benchmark. In *15th IFAC Symposium on System Identification (SYSID 2009)*, 2009.

[107] J. Schoukens, W. D. Widanage, K. R. Godfrey, and R. Pintelon. Initial estimates for the dynamics of a Hammerstein system. *Automatica*, 43(7):1296–1301, 2007.

[108] J. Schwarzenbach and R. Allen. Modelling of physiological receptors using on line data acquisition. In *Proceedings of 5th IFAC Symposium on Identification and System Parameter Estimation, Darmstadt, Fed. Rep. Germany, 24 to 28 Sept. 1979, Published by Pergamon Press, Oxford, Isermann, R. Ed., 1980, Vol. 2*, pages 817–826, 1980.

[109] P.M.J. Shelton, R.O. Stephen, J.J.A. Scott, and A.R. Tindall. The apodeme complex of the femoral chordotonal organ in the metathoracic leg of the locust schistocerca gregaria. *Journal of Experimental Biology*, 163(1):345–358, 1992.

[110] M. A. Simon and B. A. Trimmer. Movement encoding by a stretch receptor in the soft-bodied caterpillar, manduca sexta. *J Exp Biol*, 212(7):1021–1031, 2009.

[111] J. Sjberg and J. Schoukens. Initializing wienerhammerstein models based on partitioning of the best linear approximation. *Automatica*, 48(2):353–359, 2012.

[112] R. Storn and K. Price. Differential evolution a simple and efficient heuristic for global optimization over continuous spaces. *Journal of Global Optimization*, 11(7):341–359, 1997.

[113] F. E. Theunissen, S. V. David, N. C. Singh, A. Hsu, W. E. Vinje, and J. L. Gallant. Estimating spatio-temporal receptive fields of auditory and visual neurons from their responses to natural stimuli. *Network*, 12(3):289–316, 2001.

[114] F. E. Theunissen, K. Sen, and A. J. Doupe. Spectral-temporal receptive fields of nonlinear auditory neurons obtained using natural sounds. *Journal of Neuroscience*, 20(6):2315–2331, 2000.

[115] J. Touryan, G. Felson, and Y. Dan. Spatial structure of complex cell receptive fields measured with natural images. *Neuron*, 45(5):781–791, March 2005.

[116] P.N.R Usherwood, H.I. Runion, and J.I. Campbell. Structure and physiology of a chordotonal organ in the locust leg. *Journal of Experimental Biology*, 48(2):305–323, 1968.

[117] A. G. Vidal-Gadea, X. Jing, D. Simpson, O. P. Dewhirst, Y. Kondoh, R. Allen, and P.L. Newland. Coding characteristics of spiking local interneurons during imposed limb movements in the locust. 103:603–615, 2010.

[118] R. Vincente, M. Wibral, M. Lindner, and G. Pipa. Transfer entropy - a model-free measure of effective connectivity for the neurosciences. *Journal of Computational Neuroscience*, 30:45–67, 2011.

[119] E. Wagenmakers. A practical solution to the pervasive problems of p values. *Psychonomic Bulletin and Review*, 14(5):779–804, 2007.

[120] D.T. Westwick. *Methods for the identification of multiple-input nonlinear systems*. PhD thesis, Department of Electrical Engineering and Biomedical Engineering Department, McGill University, Montreal, 2005.

[121] D.T. Westwick and R.E. Kearney. Nonparametric identification of nonlinear biomedical systems, part i: theory. *Critical Reviews in Biomedical Engineering*, 26(3):153–226, 1998.

[122] D.T. Westwick and R.E. Kearney. Separable Least Squares identification of nonlinear Hammerstein models: application to stretch reflex dynamics. *Annals of Biomedical Engineering*, 29:707–718, 2001.

[123] D.T. Westwick and R.E. Kearney. *Identification of nonlinear physiological systems*. IEEE Press, first edition, 2006.

[124] B. Widrow and S. D. Stearns. *Adaptive Signal Processing*. Prentice Hall, first edition, 1985.

[125] N. Wiener. *Nonlinear problems in random theory*. The MIT Press, first edition, 1958.

[126] M. C.-K. Wu, S.V. David, and J.L. Gallant. Complete functional characterization of sensory neurons by system identification. *Annual Review of Neuroscience*, 29(1):477–505, 2006.

[127] Y. Yu and T. S. Lee. Adaptation of the transfer function of the hodgkin-huxley (hh) neuronal model. *Neurocomputing*, 52-54:441–445, 2003.

[128] L.A. Zadeh. On the representation of nonlinear operators. *IRE Weston Conv.*, 2:105–113, 1957.

[129] J. Zakotnik, T. Matheson, and V. Drr. A posture optimization algorithm for model-based motion capture of movement sequences. *Journal of neuroscience methods*, 135(1-2):43–54, 2004.

[130] Q. Zhang, B Suki, D.T. Westwick, and K.R. Lutchen. Factors affecting volterra kernel estimation: emphasis on lung tissue viscoelasticity. *Annals of Biomedical Engineering*, 26:103–116, 1998.

[131] S. Zhang, Y. Li, X. Li, Z. Yang, and L. Zhao. System of synchronous averaging denoising based on labview. In *Proceedings of the 2008 International Conference on MultiMedia and Information Technology MMIT, Three Gorges, China, December 30-31, 2008*, pages 446–448, 2008.

[132] S.N. Zill. Plasticity and proprioception in insects. i. responses and cellular properties of individual receptors of the locust metathoracic femoral chordotonal organ. *Journal of Experimental Biology*, 116(1):435–461, 1985.

[133] S.N. Zill. Plasticity and proprioception in insects. ii. modes of reflex action of the locust metathoracic femoral chordotonal organ. *Journal of Experimental Biology*, 116(1):463–480, 1985.

Appendix A

Computer Simulation to Investigate Two Parameter Estimation Error Reduction Methods

The results of a computer simulation to compare the performance of two methods for reducing parameter estimation error from the parameters of a linear FIR filter are shown in Figure A.1. The properties of the input and output signals in the 'low pass + noise' data set causes the Least Squares model to contain high levels of parameter estimation error (Figure A.1 A, B and C). Parameter estimation error completely obscures the underlying shape of the example system's IRF (Figure A.1 A). The frequency response of this IRF (Figure A.1 B and C) shows that the parameter estimation error which obscures the IRF occurs at frequencies above the highest frequency in the input signal (50Hz).

The results of using the low pass filtering methods are shown in Figure A.1 D, E and F along with the example system for comparison. The results of estimating the FIR model using the pseudo-inverse algorithm are shown in Figure A.1 G, H and I. The %MSE difference between the parameters of the example low pass system and the parameters estimated using the smoothed Least Squares method is 0.18%. The difference between the parameters of the low pass system and the parameters estimated using the pseudo-inverse method is 0.22%. By reducing estimation error, both methods reduce the predictive performance of the models but this reduction is less than 0.01%. As the smoothed Least Squares method is simpler to implement this method will be used in the current study.

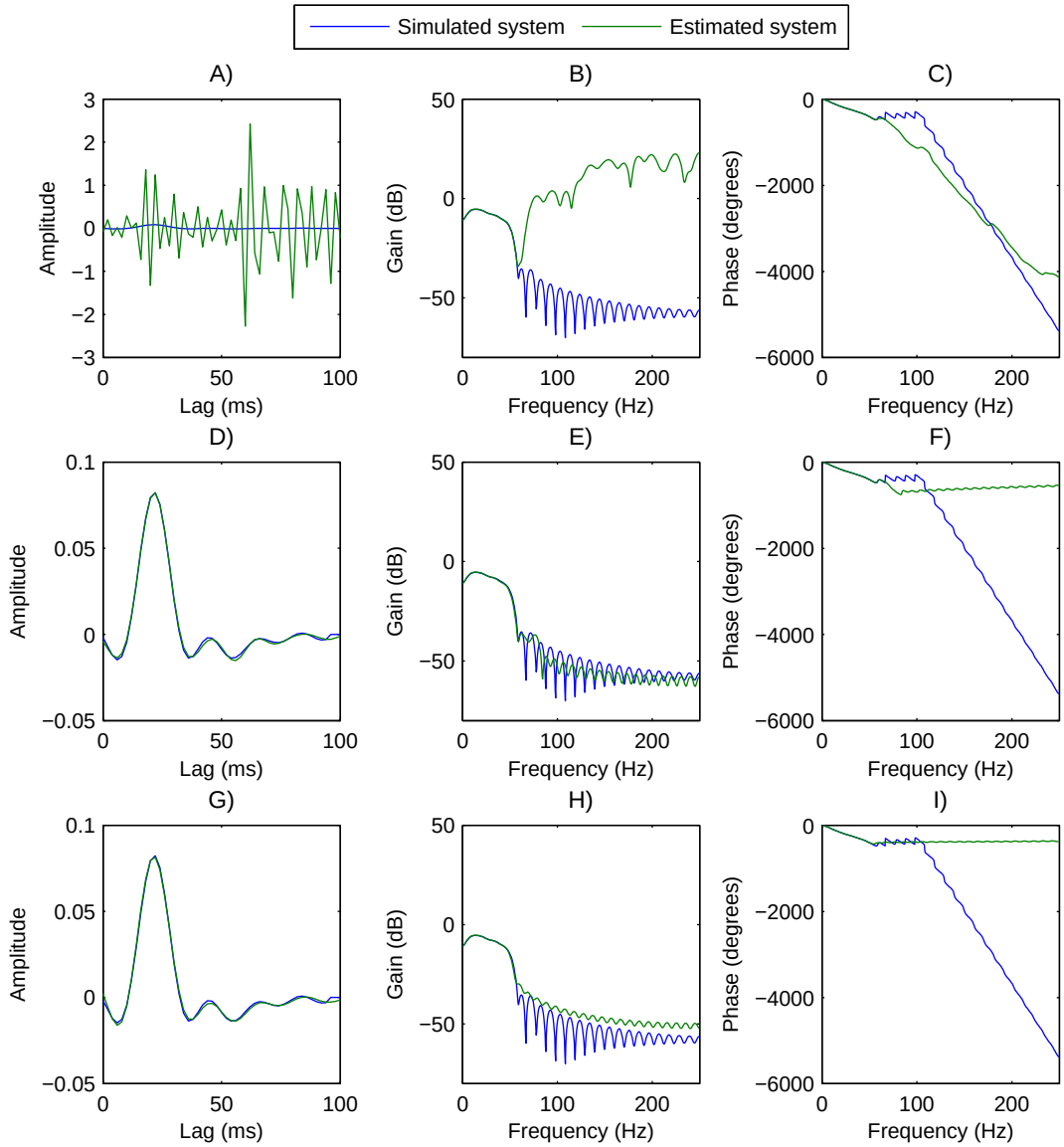

Figure A.1: Linear FIR model parameter estimation error reduction. The Least Squares estimate of the simulated system obtained using the 'low pass + noise' data set. (A) Plot of the IRF. (B), (C) The frequency response of the IRF. (D), (E) and (F) The IRF and frequency response of the smoothed Least Squares estimate. (G), (H) and (I) The IRF and frequency response obtained using the pseudo-inverse method [123].

Appendix B

Derivation of the Normal Equations

A derivation of the normal equations, starting from Equation 2.8 in Section 2.2.2 is given below.

$$\begin{aligned} \mathrm{J} &= \frac{1}{N}(\mathbf{z}-\mathbf{U}\mathbf{h})^T(\mathbf{z}-\mathbf{U}\mathbf{h}) && \text{(B.1)} \\ &= \frac{1}{N}\left(\mathbf{z}^T\mathbf{z}-\mathbf{z}^T\mathbf{U}\mathbf{h}-(\mathbf{U}\mathbf{h})^T\mathbf{z}+(\mathbf{U}\mathbf{h})^T\mathbf{U}\mathbf{h}\right) && \text{(B.2)} \end{aligned}$$

As $-\mathbf{z}^T\mathbf{U}\mathbf{h}$ and $(\mathbf{U}\mathbf{h})^T\mathbf{z}$ produce scalars they can be combined as $-2\mathbf{h}^T\mathbf{U}^T\mathbf{z}$ and using the standard result that $(\mathbf{A}\mathbf{B})^T = \mathbf{B}^T\mathbf{A}^T$ gives

$$\mathrm{J} = \frac{1}{N}\left(\mathbf{z}^T\mathbf{z}-2\mathbf{h}^T\mathbf{U}^T\mathbf{z}+\mathbf{h}^T\mathbf{U}^T\mathbf{U}\mathbf{h}\right) \quad \text{(B.3)}$$

Differentiating J with respect to the parameter vector $\mathbf{h}$ to find the gradient:

$$\frac{\partial \mathrm{J}}{\partial \mathbf{h}}\left(\mathbf{z}^T\mathbf{z}\right) = 0 \quad \text{(B.4)}$$

using the standard result that $\frac{\partial[y^T x]}{\partial \mathbf{x}} = \frac{\partial[x^T y]}{\partial \mathbf{x}} = y$ and letting $y = -2\mathbf{U}^T\mathbf{z}$

$$\frac{\partial \mathrm{J}}{\partial \mathbf{h}}\left(-2\mathbf{h}^T\mathbf{U}^T\mathbf{z}\right) = -2\mathbf{U}^T\mathbf{z} \quad \text{(B.5)}$$

and using the result that $\frac{\partial}{\partial \mathbf{x}}\left[\mathbf{x}^t\mathbf{M}\mathbf{x}\right] = \left[\mathbf{M}+\mathbf{M}^T\right]\mathbf{x}$ and letting $M = \mathbf{U}^T\mathbf{U}$

$$\begin{aligned} \frac{\partial \mathrm{J}}{\partial \mathbf{h}}\left(\mathbf{h}^T\mathbf{U}^T\mathbf{U}\mathbf{h}\right) &= \left[\mathbf{U}^T\mathbf{U}+\left(\mathbf{U}^T\mathbf{U}\right)^T\right]\mathbf{h} && \text{(B.6)} \\ &= \mathbf{U}^T\mathbf{U}\mathbf{h}+\mathbf{U}^T\mathbf{U}\mathbf{h} = 2\mathbf{U}^T\mathbf{U}\mathbf{h} && \text{(B.7)} \end{aligned}$$

the minimum of J is found by setting its gradient to zero:

$$\frac{\partial \mathrm{J}}{\partial \mathbf{h}} = -2\mathbf{U}^T\mathbf{z}+2\mathbf{U}^T\mathbf{U}\mathbf{h} = 0 \quad \text{(B.8)}$$

which can be rearranged to give the normal equations.

$$\left(\mathbf{U}^T\mathbf{U}\right)\mathbf{h} = \mathbf{U}^T\mathbf{z} \tag{B.9}$$